An Investigation of Dielectric Thermoplastic Elastomers for Civil Infrastructural and Energy Harvesting Applications

By

Anup Poudel (B.E., M.Sc.)

Submitted in Fulfilment for the Requirements for Doctorate in Engineering Technology

Waterford Institute *of* Technology
INSTITIÚID TEICNEOLAÍOCHTA PHORT LÁIRGE

School of Engineering

Waterford Institute of Technology

Research Supervisors: Prof. Austin Coffey

Dr. Philip Walsh

Dr. James Kennedy

Dr. Ken Thomas

Submitted to Waterford Institute of Technology

June 2017

Declaration of Authorship

I, Anup Poudel, certify that this thesis is all my own work and contains no plagiarism. By submitting this work, I agree to the following terms:

- Any text, diagrams or other material copied from other sources (including, but not limited to, books, journals and the internet) have been clearly acknowledged and referenced. These details are then confirmed by a fuller reference in the bibliography.
- I have read the sections on referencing and plagiarism in the handbook or in the WIT Plagiarism policy and I understand that only assignments which are free of plagiarism will be awarded marks. I further understand that WIT has a plagiarism policy which can lead to the suspension or permanent expulsion of students in serious cases.
- I have read the relevant institutional regulations and hereby declare that this thesis is in line with these requirements.

Signed:

_____

Date:

_____

Abstract

Poly(styrene-ethylene/butylene-styrene) [SEBS] and poly(styrene-ethylene/butylene-styrene)-grafted-maleic anhydride [SEBS-g-MA] triblocks have been shown to have superior mechanical performance relative to conventional dielectric elastomers with better morphology. However, historically their use in capacitive energy harvesting, and stress/strain sensing have been constrained by (i) the dearth of knowledge about thermal, mechanical, thermo-mechanical and thermo-electrical properties of elastomers and their nanocomposites, (ii) low dielectric constant of elastomers, and (iii) poor dispersion of high dielectric materials in elastomers.

Dielectric filler (barium titanate [BT]) and conductive fillers (carbon black [CB]) based elastomeric composites were successfully manufactured using twin screw extrusion process with/without supercritical fluid carbon-dioxide ($scCO_2$). Thermal, mechanical, morphological, dielectric and conducting properties of dielectric thermoplastic composites (DTC) were studied.

Dielectric analysis and dynamic mechanical analysis showed CB composites (below the percolation threshold) manufactured using $scCO_2$ assisted twin screw extrusion were found to have low dielectric loss at low frequency (0.0001 Vs 0.006 dielectric loss at 1Hz for SEBS/CB 1 wt.%), low mechanical losses (0.034 and 0.043 Vs 0.046 and 0.051 value of tan delta in transverse and parallel direction to extrusion respectively at 30℃ of SEBS/CB 1 wt %) and improved dielectric permittivity (30% Vs 15% increase upon addition of 1% CB on SEBS) compared to those composites manufactured without $scCO_2$. Similar results were obtained for BT filler based composites. In addition, the composites manufactured with an assistance of $scCO_2$ showed highly conductive behaviour and low mechanical losses at 5 wt. % of CB in SEBS making them sensitive under strain conditions. This result is far superior compared to conventional processing for similar materials. Similarly, chemical, thermal and morphological analysis showed improved interaction and dispersion of both CB and BT in all phases of elastomers when elastomers were extruded with $scCO_2$. Thermoelectric analysis confirms the BT fillers based composites manufactured using $scCO_2$ have highly stable dielectric permittivity over a range of temperatures (40-120℃) and frequencies (1kHz-1MHz) compared to composites manufactured without $scCO_2$. TEM images showed that composites manufactured using

$scCO_2$ have uniformly dispersed additives (CB as well as BT) in elastomers compared to composites manufactured without $scCO_2$.

Finally, dielectric measurement of CB and BT composites manufactured with $scCO_2$ presented high sensitivity to uniaxial strain making them highly suitable for stress/strain sensing and energy harvesting applications

Acknowledgements

I would like to thank all, who gave their valuable time and support during the course of my project. This thesis would not have been possible without the support of my supervisors, Prof. Austin Coffey, Dr. Philip Walsh, Dr. James Kennedy and Dr. Ken Thomas.

Their advice and suggestions were always valuable to me, for which I am extremely grateful. I would also like to thank the following people in particular:

Dr. Siobhan Matthews, SCF Processing Ltd., Drogheda

Dr. John J. Lyons, Applied Polymer Technology, Athlone Institute of Technology, Ireland and all of the staff at W.I.T.

I would especially like to thank my wife, brother, sisters, and my parents for all of their help, support and understanding over the entire course of this Ph.D. Last but not least, I would like to thank Convergent Technologies Research Group (WIT), SCF Processing Ltd (Drogheda), Pharmaceutical and Molecular Biotechnology Research Centre (WIT) and Applied Polymer Technology (AIT) for materials and technical support.

Contents

List of Figures

List of Tables

Abbreviations

AC:	Alternating current
ASTM:	American Society of Testing and Materials
ATR-FTIR:	Attenuated total reflection-Fourier transform infrared
BT:	Barium titanate ($BaTiO_3$)
CB:	Carbon Black
CNTs:	Carbon nanotubes
SWCNTs:	Single wall carbon nanotubes
MWCNTs:	Multiwall Carbon Nanotubes
DC:	Direct current
DMA:	Dynamical Thermal Mechanical Analysis
DSC:	Differential Scanning Calorimetry
DTE:	Dielectric thermoplastic elastomer
EAPs:	Electroactive polymers
EPDM:	Ethylene propylene diene monomer
EB:	Ethylene/butylene
LCE:	Liquid crystal elastomer
MDSC:	Modulated Differential Scanning Calorimetry
MEMS:	Micromechanical Systems
MWS:	Maxwell-Wanger-Sillar
NMR:	Nuclear magnetic resonance
P(VDF-TrFE):	Poly(vinylidenefluoride-co-trifluoroethylene)

PEBAX:	Polyether block amide
PPE:	Poly (2,6-dimethyl-1,4-phenylene ether)
PS:	Polystyrene
PTBA:	Poly(tert-butyl-acrylate)
PU:	Polyurethane
PVC:	Polyvinyl chloride
PVDF:	Polyvinylidene difluoride
PZT:	Lead-zirconate-titanate
SAXS:	Small angle X-ray scattering
SCF:	Supercritical Fluid
SEBS SCF:	Poly(styrene-ethylene/butylene- styrene) triblock extruded with Supercritical fluid carbon dioxide
SEBS-g-MA SCF:	Poly(styrene-ethylene/butylene-styrene)-grafted-maleic anhydride extruded with Supercritical fluid carbon dioxide
SEBS-g-MA:	Poly(styrene-ethylene/butylene-styrene)-grafted-maleic anhydride
SEBS:	Poly(styrene-ethylene/butylene- styrene) triblock
SHM:	Structural health care monitoring
S:	Styrene
TA:	Thermal analysis
sSEBS:	Sulfonated poly(styrene-ethylene/butylene-styrene)
$scCO_2$:	Supercritical fluid carbon dioxide

List of Symbols

ε_r : Total relative dielectric permittivity

ε' : Real relative dielectric permittivity

j : Imaginary unit

ε'' : Imaginary relative dielectric permittivity

$\tan \partial_e$: Relative dielectric loss of the material

M^* : Total electric modulus

M' : Real electric modulus

M'' : Imaginary electric modulus

D : The charge density at the electrode of a capacitor (C/m^2)

D_0 : The charge density at the electrode of a capacitor at vacuum condition

E : Electric Field (kV/m)

P : Polarization of a material (C/m^2)

ε_o : Electrical permittivity of free space (F/m)

C : Capacitance of a capacitor (F)

A : Surface area of an electrode (m^2)

d : Thickness of an electrode (m)

ΔA Change in surface area of an electrode under strain condition (m^2)

C_s : Capacitance of a capacitor under stretched condition (F)

A_s : Surface area of an electrode under stretched condition (m^2)

d_s : Thickness of an electrode under stretched condition (m)

R_m :	Maxwell stress (Pa)
Υ	Compressive modulus (Pa)
S_m	Total thickness change due to Maxwell stress (m)
C_r :	Capacitance of a capacitor under relaxed condition (F)
A_r :	Surface area of an electrode under relaxed condition (m^2)
d_r :	Thickness of an electrode under relaxed condition (m)
U	Total amount of energy harvested (J)
U_s	Total energy at stretched state (J)
U_r	Total energy at relaxed state (J)
V_b	Biasing voltage of a capacitor (V)
Z_m	Total thickness change due to mechanical stress (m)
M :	Apparent electro-restrictive coefficient
$\tan \partial_m$	Mechanical loss tangent of the material
∇	Del operator
$\bar{H}$	Magnetic field strength (Wb/m^2)
J	The current density (A/m^2)
ω	Angular frequency (rad)
J_i	Impressed electric current density due to application of electric field (A/m^2)
J_c	Conduction current density due to application of electric field (A/m^2)
ε_s	Real dielectric permittivity under stretched condition

λ	Elongation (m)
k	Ratio of dielectric permittivity under stretched and relaxed condition

Chapter 1

1 Background and Introduction

Energy harvesting or power harvesting is a process of capturing energy from external sources such as solar energy, mechanical or vibration forces, ocean tides, piezoelectricity, thermoelectricity, and magnetoelectricity. Mechanical energy can be harvested either from large sources, such as seawaves, or from small sources like the vibration of machines or speaker present in mobile phones. Conventional motors and generators tend to get heated with time, thereby wasting most of the energy which could be harvested in the form of heat. This major issue from conventional generators has garnered the interest of engineers and scientists for further research in materials science for energy harvesting applications. Piezoelectric harvesters, electrostatic or capacitive harvesters, electrostatic harvesters and magnetostrictive harvesters are some of the most commonly used and described efficient technologies for capturing mechanical energy from different sources. The high potential of scavenging energy for renewable energy sources has brought major changes in wireless technology and low power electronics, such as micromechanical systems (MEMS) devices.

Like energy harvesting technology, development of technologically and economically attractive materials/composites for strain/stress sensitivity with flexibility, affordability, durability and compatibility for structural health monitoring (SHM) has led to a novel research field for dielectric/conductive nanocomposites, as it can give alarm warnings about the structural change in civil infrastructure with disaster notification. Continuous SHM of civil infrastructure gives information about the time scale and the severity of change in civil infrastructures which is crucial for saving both lives and properties. The primary conventional sensors deployed in SHM applications are typically of optical, strain gauge and a piezoelectric type. Conventional sensors used in SHM applications are deficient due to bond sensitivity issues (piezoelectric type), loss of accuracy with increased number of cracks (optical type) and measurement inefficiencies (strain-gauge type). Therefore, there is an unmet need for the development of materials suitable for the development of stress and strain sensors with optimized chemical, electrical, thermal and mechanical properties.

Electroactive polymers (EAPs) are types of polymers which tend to respond to the electric field with structural, mechanical or rheological change. Dielectric polymers/composites are one of the classes of EAPs which show large mechanical deformation on the

application of electric voltage. Due to high mechanical deformation activity on the application of electricity coupled with flexibility and vice versa, these polymers/composites have the ability to be used as superior actuators and energy harvesters. Dielectric composites/polymers have potential to be used as sensors for SHM of civil infrastructure. Conductive nanocomposites derived from dielectric elstomers around percolation threshold changes their DC/AC conductivity under stress/strain condition show their high sensitivity for sensing application. The functional performance of capacitive energy harvesters, soft actuators and strain/strain sensors fabricated from dielectric elastomers/composites is also dependent on elastic compliance, actuating pressures under electric field and sensitivity to AC frequency. Dielectric generators and sensors work on the principle of relative change in capacitance under different strain/stress conditions. Ease of processing, low manufacturing cost as well as superior properties in the context of elongation, energy density and electromechanical coupling efficiency of dielectric thermoplastic elastomers over piezoelectric, electrostatic and magnetostrictive energy harvesting materials make them suitable for such smart applications. Silicone is one of the most commonly researched dielectric elastomers for these applications. However, with silicone being thermoset in nature, tailoring mechanical and electrical properties of it using sophisticated manufacturing procedures has always been an issue. In addition, silicone requires high voltage (1-2 kV/μm) for actuation uses. Dielectric thermoplastic elastomers (DTEs) such as polyurethanes are also widely researched for such applications. Although DTEs are lightweight, flexible, have a low production cost as well as easy moulding capabilities in any shape and size, the phase size of each block in DTEs are in micro-meter range. For optimized performance, the phase size of such DTEs should be as small (nm) as possible for obtaining high mechanical flexibility. Moreover, small phase size produces low hysteresis loss, low molecular heating effects during mechanical loading and unloading conditions.

Even though DTEs and DTEs based composites are widely studied for their mechanical actuation under electric field due to their morphology (they consist of hard and soft blocks in small phase sizes), their study in relation to the effect of manufacturing processes and additives types in mechanical, thermal and electrical properties (crucial for electromechanical performance) of individual thermoplastic elastomers are highly neglected and poorly understood in scientific communities. In addition, thermoplastic elastomer composites manufactured using standard solvent casting method lacks

scalability and are limited to laboratory test prototypes. Furthermore, composites manufactured using different modifiers tend to have highly altered morphology. The morphological changes, in turn, cause significant changes in the thermal, mechanical, and electrical properties, thereby potentially making a new class of materials. Because of the above-stated problems, their production as actuators, energy harvesters, and strain/ stress sensors in large scale and their applications are very much limited.

This work aims to investigate the potential of dielectric thermoplastic elastomers based conductive and dielectric composites manufactured using highly scalable techniques like extrusion with/without the assistance of supercritical fluid carbon dioxide ($scCO_2$). The $scCO_2$ was used as an exfoliator of additives in polymer matrices to enhanced the sensitivity of elastomer under stress/strain conditions for civil infrastructural and energy harvesting applications. Thermal, mechanical, morphological, and electrical properties of thermoplastic elastomers and their nanocomposites were investigated under different temperature, frequency and strain/strain conditions to know their suitability for different strain sensing and capacitive energy harvesting applications. In addition, this work further aims to explore the effect of a supercritical fluid assisted extrusion on additive dispersion, dielectric properties and morphological change of different thermoplastic elastomers and their composites.

1.1 Thesis Organization

This thesis is organized as follows.

Chapter 2 focuses on a literature review of different dielectric elastomers and nanocomposites. It addresses (i) manufacturing procedures of elastomeric nanocomposites for making elastomers highly smart materials for sensing and energy harvesting applications, (ii) mechanical, thermal and electric properties of such nanocomposites and (iii) mechanism of capacitive energy harvesters, strain/strain sensors and actuators manufactured using different thermoplastic elastomers. In addition, it also describes the different techniques to measure thermal, mechanical and electrical properties of nanocomposites. Chapter 2 ends with aims and objectives to address the current research gap which exists in scientific and engineering communities about thermal, mechanical and electrical properties of thermoplastic elastomers and their nanocomposites for electroactive applications.

Chapter 3 details materials and methods used in the study in order to address and fulfill the knowledge gap with the aims and objectives proposed in Chapter 2. The chapter highlights include: (i) basic properties of thermoplastic materials and additives selected (ii) methods used for manufacturing different composites (iii) detailed experimental matrix of thermal, mechanical and electrical characterization performed on different thermoplastic elastomers and their different composites.

Chapter 4 analyses, compares and discusses the electrical behavior of different types of thermoplastic elastomers, followed by a further selection of two elastomers best suited for capacitive energy harvesting with the dielectric loss, improved morphology, large scale manufacturing feasibility and the economically low-cost elastomers.

Chapter 5 argues the feasibility of using twin screw extrusion for manufacturing dielectric filler based elastomeric composites for energy harvesting applications and strain/stress sensing applications. Conductive fillers (CB-carbon black) used for production of conductive composites for SHM applications were discussed. The morphological, thermal, electrical, and mechanical changes on thermoplastic elastomers are presented along with the probable application as well as the issue related to dispersion of CB in thermoplastic elastomers using twin screw extruder. Similarly, the morphological, thermal, electrical and mechanical changes in these thermoplastic elastomers with dielectric filler (barium titanate-BT) is also documented in the chapter. The chapter also includes issues associated with polymer-additive interaction, the dispersion of additives in the polymer matrix and their uses in capacitive energy harvesting applications.

Chapter 6 introduces a novel supercritical fluid assisted extrusion process for manufacturing of electrically active elastomers for a wide number of applications. In Section 6.2 of Chapter 6, a detailed investigation into the mechanical, thermal, morphological and electrical enhancement caused due to supercritical fluid assisted extrusion on thermoplastic elastomer like SEBS is illustrated. Similarly, Section 6.3 and Section 6.5 details the morphological, thermal, electrical and mechanical enhancement in thermoplastic elastomers (SEBS and SEBS-g-MA) with the addition of conductive fillers with supercritical fluid assisted extrusion mainly due to the dispersion of CB on different phases of polymers making them highly conductive as well as mechanically elastic under large extension at low % of carbon black. Finally, in Section 6.4, the morphological, thermal, electrical and mechanical properties of thermoplastic elastomer (SEBS-g-

MA)/barium titanate composites manufactured with/without the assistance of supercritical fluid carbon dioxide are discussed. These results were compared with SEBS-g-MA/BT composites manufactured without an assistance of supercritical fluid carbon dioxide in terms of mechanical and electrical performance over the range of temperature.

Chapter 7 describes the thermoelectric behavior of elastomers/composites manufactured with/without the assistance of supercritical fluid. It is further divided into two sections. In Section 7.1, the thermoelectric behavior of SEBS-g-MA /BT manufactured with/without an assistance of supercritical fluid is described. Similarly, in Section 7.2, the dielectric behavior and the relaxation phenomena of SEBS-g-MA /CB composites near the percolation threshold at different temperature range is also discussed in this section.

The conduction behavior, as well as dielectric relaxation phenomenon of various conductive and dielectric thermoplastic elastomers/composites under tensile strain conditions, is discussed and the amount of energy harvested under small strain condition for DTEs/ composites is estimated in Chapter 8. The relative change in conduction behavior of conductive DTEs composites under strain condition is also illustrated to the possibility of conductive composites for SHM applications.

Chapter 9 summarizes the conclusions from the work thus far achieved and finally, outlines the further work based on investigations done.

Chapter 2

2 Literature Review

A polymer, which is defined as a number of repetitive units of monomers, has gained huge importance in many commercial products because of their attractive characteristics including but not limited to flexibility, processibility, affordability, and lightweights. Polymers could be in either liquid, gel-liquid or solid states, which are broadly classified into different types based on thermal characteristics, types of monomers, and source of extraction. In the early 1990s, a new class of polymers known as electroactive polymers (EAPs) emerged that respond to an electrical field. Since then these polymers have garnered the attentions of scientists and engineers for a wide range of smart applications such as actuation, sensing, and energy harvesting.

2.1 Electroactive Polymers

Different biological systems found in nature are perfect examples of smart materials, which tend to respond to different stimuli (Such as optical energy, pH, temperature, etc.) resulting in changes in the morphological, structural, mechanical, electrical, optical, and chemical properties. Mimicking biological systems and replicating them in an engineering device is very challenging, but still a good opportunity to make environmentally active transducers.

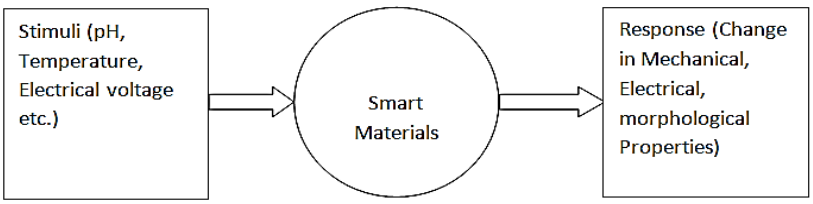

Figure 2.1 Response of smart materials to different stimuli

Electroactive polymer technologies are captivating the interest of a number of multidisciplinary research groups and institutions because of their abilities to be used in many smart applications like artificial muscles, capacitive sensors, and energy harvesters. Electroactive polymers are broadly classified as ionic and field active as shown in Figure 2.2 [1-3]. Although both classes of electroactive polymers (ionic and field activated) respond to electrical fields, they differ in their working principles and environments; particularly their mechanical and electrical activation properties. Field activated polymers

require a high actuation voltage for mechanical deformation compared to ionic polymers, but their actuation processes are fast and actuation is constant upon application of a DC voltage. Moreover, ionic polymers must be wet in order for actuation to take place, whereas field activated polymers do not [1-8].

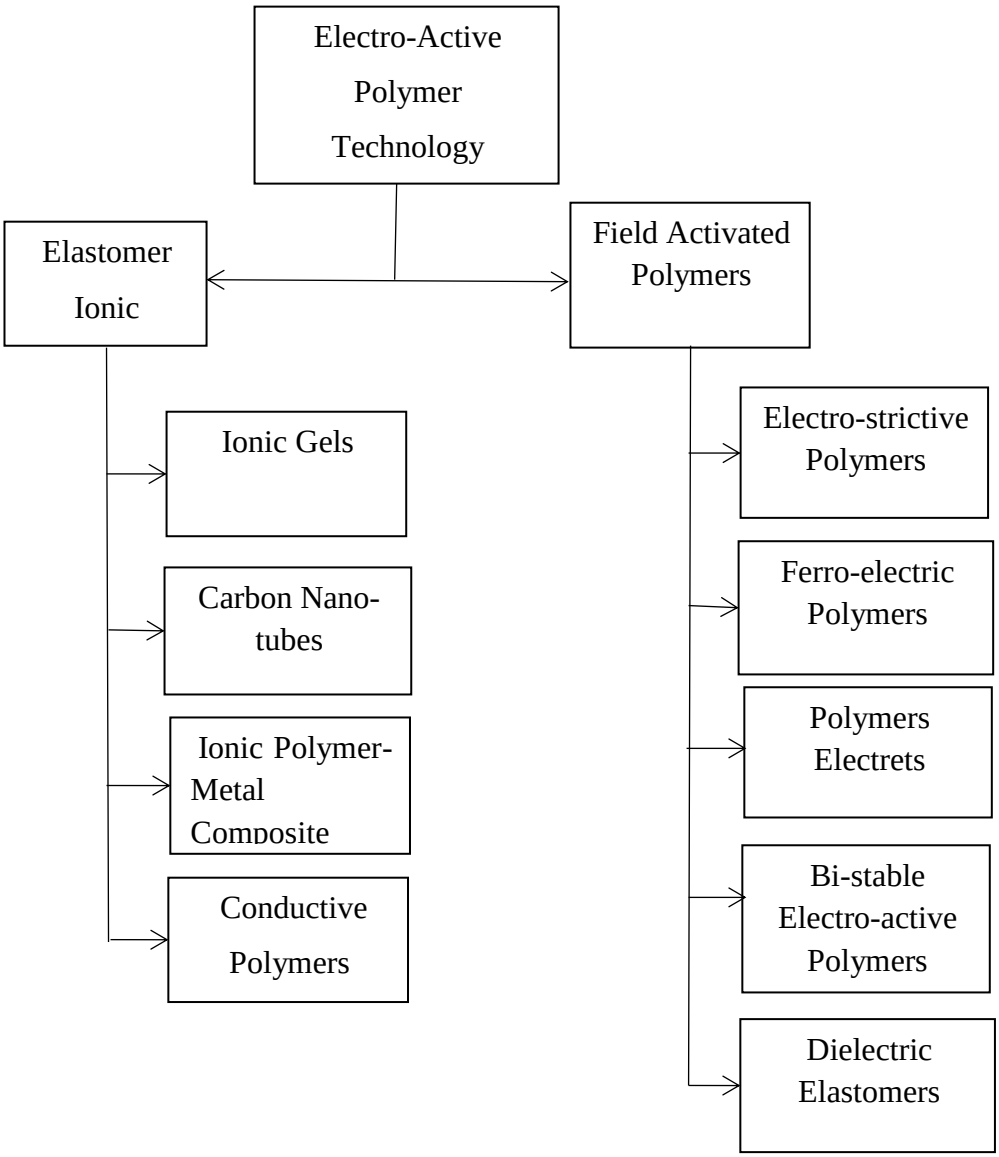

Figure 2.2 Types of electroactive polymers [1-8]

2.1.1 Ionic Polymers

Ionic EAPs involve deformation due to the involvement of mobility or diffusion of ions inside the polymer matrix driven by electrical forces [1,2], as shown in Figure 2.3

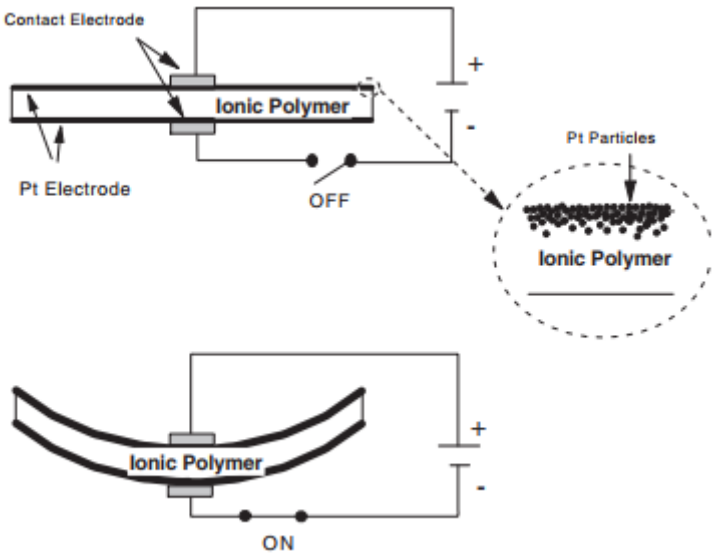

Figure 2.3 Ionic polymer under electric field [2]

The deformation of ionic electroactive polymers can be bi-directional depending on the polarity of the voltage applied. The voltage required for the activation of the ionic polymer can be small as 1-2V, but the deformation is not constant on the application of a DC voltage (with the exception of conductive polymers) and the deformation process is very slow [1-3]. Moreover, the resultant stress due to electrical activation of ionic polymers is low and not stable. In addition to these demerits, hydrolysis takes place in these types of EAPs in aqueous conditions (>5volt) [4-7]. Ionic polymers are further divided into carbon nanotubes (they are a class of EAPs, even though, they are non-polymeric macromolecular materials)[8], conductive polymers, ionic polymer gels, and ionic polymer metal composites. Merits, demerits along with working principles of these types of polymers are highlighted in Table 2.1. Conductive polymers and ionic polymer metal composites have shown huge potential as mechanical actuators in smart valves, pumps, and mechanical catheters because of their high electro-mechanical pressure [5-26]. However, these EAPs are speed limited and possess low electro-mechanical coupling efficiencies. Ionic gels are used for artificial muscles because of their softness and very slow response time (similar to biological muscles) [5,9,10]. Carbon nanotubes have shown promising results in actuation and fast response time, but issues related to electromechanical coupling efficiency and high production cost still hinder their applications in many commercial products [26-28].

2.1.2 Electronic or Field Activated EAPs

Electronic EAPs are types of electroactive polymers which deform or actuate on the application of high electric field due to polarization phenomena, as shown in Figure 2.4. Depending on the polarization phenomena, they can further be divided into ferroelectric, polymer electrets, dielectric elastomers, electrostrictive polymers and bistable electroactive polymers [29-47].

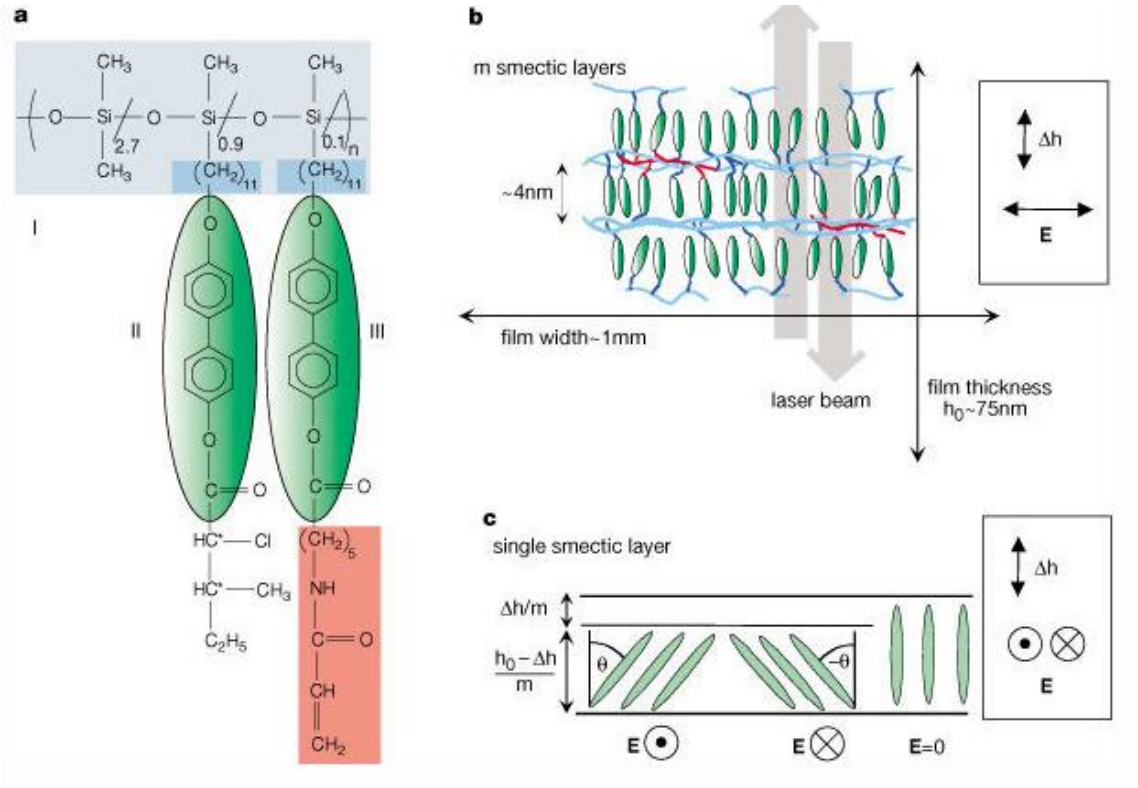

Figure 2.4 Field activated Electroactive Polymer [39]

Table 2.2 illustrates the different merits, demerits, and applications of different types of electronic EAPs. Bi-stable and dielectric EAPs tend to have a high electromechanical strain, low production cost, and fast electric response [18, 36-38]. Hence, these EAPs have garnered attention in capacitive energy harvesters, capacitive sensors, and artificial muscles. Similarly, ferroelectric, electrostrictive and polymer electrets have limited strain under electrical field, however, have profound potential in energy harvesting applications [31, 32, 36-47].

Table 2.1 Merits and Demerits of Ionic Electroactive Polymer Types

Ionic EAP Type	Working Principle	Merits	Demerits	Applications
Ionic Gels (IG)	• Hydrogels placed in liquid solution changes its shape due to polymer liquid interaction. • Application of a voltage causes movement of hydrogen ions in or out of the gel causing the change in pH [5, 9, 10]. • Bending is produced due to the difference in ion diffusion rate between electrolyte and polymer solution [11]. • Hydrogels of Polyvinyl alcohol, Polyacrylonitrile are examples of ionic gel EAPS	• Requires very low voltage (1-2 volt).	• Very long response time (operates slowly).	• Artificial muscles [12]
Ionic Polymer Metal Composite	• Ionic polymer-metal comprises of solvent swollen ionic polymer membrane with a mobile facility of positive ions and negative ions in respect to the applied potential between two flexible metal electrodes (gold and platinum) [7, 10]. • Actuation or bending moment is controlled by using the difference in voltage [5]. • Membrane materials may be sulfonated tetrafluoroethylene (nafion) or perfluoro carboxylated polymer (felmion) with anionic groups. sSEBS (Sulfonated poly(styrene-b-ethylene-butylene-b-styrene)) has shown promising results in the case of bending capability and harmonic responses.	• Require low voltage (1–5 V) • Strain is greater than 3% and stress is around 33 MPa [2, 13-15]	• Highly sensitive to hydration. • DC causes permanent deformation • Undergoes hydrolysis if the supplied voltage is above 1.23V. • IPMC has very low-frequency response (in the range of 1 Hz).	• Actuators in Mechanical grippers, Metering valves, Micropumps etc. [3, 7, 13, 16] and sensors
Conductive Polymers (CP)	• Conductive polymers actuate in response to applied voltage as a result of oxidation or reduction [17]. • Change in oxidation state along polymer chain causes the charge to flux along the polymer chain. • Migration of electrolytes occurs to balance charge of oxidized polymer resulting in actuation or bending of the polymer [7, 18-21] [22] • Examples of this type of EAPs include Polypyrrole, Polyaniline, Polythiophenes etc. [5].	• Require relatively low voltage (1-2 volts). • Strain range from 1-40% with relatively large force around 100MPa to 45 MPa • These materials are generally biologically compatible	• Very low electromechanical coupling efficiencies (around 1%) and very low operating efficiency (1%) [18, 22, 23]. • Suffer fatigue after repeated activation. • Speed limited (<40 Hz)	• Blood vessels connections, dynamic Braille, valves, smart catheters etc. [24, 25]
Carbon Nanotubes	• The carbon-carbon bond of nanotubes suspended in an electrolyte changes length due to charge injection affecting the ionic charge balance between the nanotubes and electrolyte [5]. • Examples: Single- and multi-walled carbon nanotubes	• High tensile stresses (20 - 40 GPa) [26] • Low actuation voltage (1V), high thermal stability(<1000°C) and fast (in millisecond) speed [27]. • A novel super-elastic CNTs aerogel can produce anisotropic linear elongations of 220 % and strain rates 3.7x104 %/s at between 80 to 1900 K [28]	• Expensive and difficult for mass produce • Low strain % (around 2%), low electromechanical coupling.	• Artificial muscles

Table 2.2 Different types of field activated EAPs with their working principle, merits, demerits, and applications

Types	Working Principle	Merits	Demerits	Applications
Ferroelectric EAPs	• Maintains permanent polarization of dipole having a non-centro-symmetric structure on application of electric field. • Reverse field or temperature above Curie temperature is required to remove the polarization. It means ferroelectric EAPS have high hysteresis loss. • Examples of such EAPs include PVDF (polyvinylidene difluoride) as well as odd number nylon (nylon 7 and nylon11) and their blends [29, 30]	• 10% strain capability and high electromechanical coupling efficiency [31, 32].	• Require high voltage (~150 MV/m). • Limited applications at high temperature	• As piezoelectric materials.
Dielectric EAPs	• Maxwell force (force developed by the polarization of molecules) squeezes the material. • Expansion or contraction of material is normal to apply electrical force [33]. • Thin films can stretch between 200-380% [5]. • Examples: Silicone, Polyurethane [5].	• Large electromechanical strain (200–380%) high pressure (7.2 MPa) [18, 34, 35] • Fast response in msec. • Inexpensive to produce.	• Require high voltage (~150 MV/m) and pre-strain • Large displacements compromise the actuation force.	• Artificial muscles for robotic applications[34], soft actuators and compliant variable capacitors [34, 36]
Electrostrictive EAPs	• Those EAPs which show very fast response to electric field are known as electro-restrictive EAPs • Ferroelectric Polymers (eg. P(VDF-TrFE) copolymer), Electrostrictive Graft-Copolymers (eg. graft copolymer consisting of chlorofluoroethylene and trifluoroethylene backbone with P(VDF-TrFE) side chains[7], and Liquid Crystal Elastomers (LCE) are three types of electro-restrictive EAPs • Liquid crystal elastomers are further divided into nematic and smetic. • Mesogens (a unit incorporated in a backbone structure of LCE) coil when nematic LCE chain relaxes and align when chain elongate.[37]. • Electrical and thermal stimuli affect in orientation [38-42] and polarization phenomena of electrostrictive EAPs	• (P(VDF-TrFE)) can produce 4.6% strain and 334 MPa of Maxwell pressure. • Thermally activated LCEs display strain of 400% with limited speed response [43] • Electrically active LCEs show a fast response (10 ms) and require low electric field for actuation (1.5-25 MV/m) compare to other filed activated EAPs technology [39]. • Very fast response to electrical field	• Strain is very much limited compared to other artificial muscles	• Actuators and capacitive energy harvester
Bistable EAPS	• These types of polymers have both the properties of shape memory alloys as well as dielectric elastomers. Example of bistable EAPs is Poly(tert-butyl-acrylate) (PTBA) [44]	• They can produce 335 % of electromechanical strain and 3.2 MPa of electromechanical pressure [36] • It can be locked in different positions and can also be reversibly actuated.	• No leakage current. • High voltage requirement	• Below Tg, these materials behave as a capacitor. Above Tg, they have compliant elastomeric structure behaving as compliant capacitor[36]. • Artificial muscles
Polymers Electrects	• Non-uniform charge distribution results into piezoelectric effects and acts as a sensor as well as transducer [45]. • The highly porous polymer may be with highly polarizing gas in pores. • Examples includes poly(vinlychloride) (PVC), polystyrene (PS), poly(2,6-dimethyl-1,4-phenylene ether) (PPE) [46].	• High piezoelectric transfer coefficient [45, 47].	• Low electromechanical response • High voltage requirement	• Microphones, sensors, transducers, filters, energy harvesting Ionic exchange membrane

2.2 Dielectric Electroactive Polymers

Impedance and dielectric are basic electrical properties of plastic materials. Impedance is generally considered as a resistance to a flow of electric current at a specified frequency, whereas, the dielectric property is the function of electric polarization when a material is kept under an electric field. The word 'Dielectric' refers to an insulating material, in which no flow of current occurs on application of direct current, instead, polarization occurs in the material [48]

Insulators (do not allow the direct current to pass through, where conductivity is zero and impedance is infinite) possess the electric dipole structure which allows materials to displace their negative charge and positive charge inside the material with the application of electric field This type of material can be modeled as different combinations of capacitors, resistors, and inductors [49]. The total dielectric permittivity of the material can further be classified into two types as shown in Equation 2.1

$$\varepsilon_r = \varepsilon' + j\varepsilon'' \qquad \text{Equation 2.1}$$

Where, ε' is the real value of the dielectric constant which defines the polarization capability of the material, ε'' is the imaginary part of the dielectric constant defining the loss of the material and the conducting behavior of the polymer. The relative loss of the material is given by Equation 2.2

$$\tan \partial_e = \varepsilon' / \varepsilon'' \qquad \text{Equation 2.2}$$

$\tan \partial_e$ of different polymers is generally used to explore different relaxation phenomena in polymers

The dielectric properties of the material are dependent on the following parameters.

- Frequency

Dielectric permittivity of a material is dependent on the polarization of dipole present in a material. The polarization of dipoles is dependent on frequency as they require some interval to orient in the direction of electric field. Therefore, at a higher frequency, dipole shows low polarization and vice versa.

- Temperature

The high thermal energy of molecules provided by an increase in temperature increases the amplitude of thermal motion providing a deviation from the perfect alignment of molecules. However, this does not mean that dielectric permittivity increases as the temperature lowers. Discontinuities are widely seen in the dielectric constant of a material with its phase change.

- Orientation

Highly oriented dipoles have a high dielectric permittivity and vice versa.

- Mixture

A mixture of different percentages of different materials with different dielectric permittivity gives rise to different dielectric constant.

- Pressure

Like temperature, pressure also affects the orientation of materials giving rise to different dielectric constant.

- Molecular structure of the material

The highly polar molecular material has high dielectric constant and vice versa.

Choosing a correct dielectric measurement technique for a dielectric material differs with the type of material as well as test frequencies at which the material is tested. Figure 2.5 depicts the different measurement techniques used, based on the range of frequencies at which dielectric properties are measured.

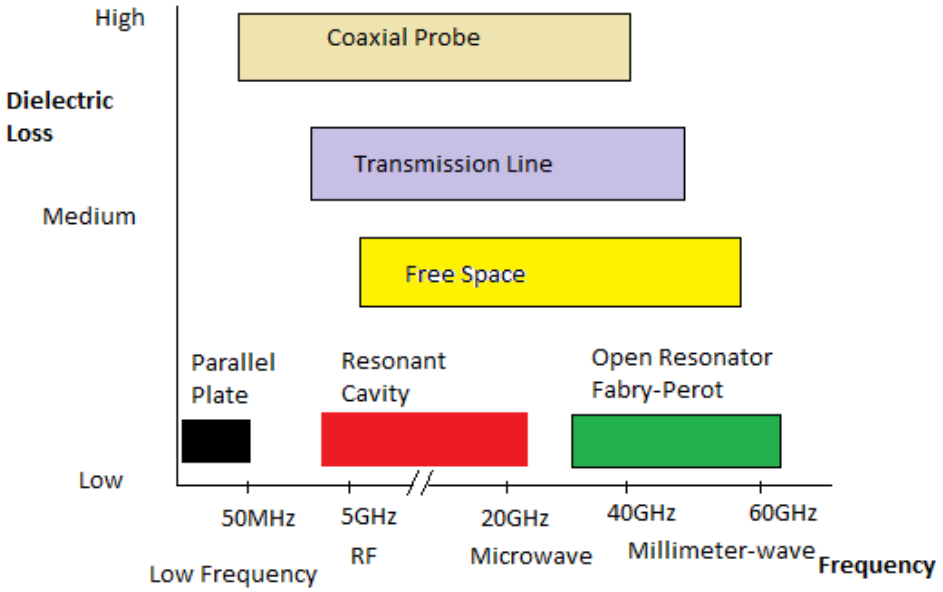

Figure 2.5 Measurement techniques and their dependency with frequency [50]

The dielectric measurement technique used differs with the dielectric loss and test frequencies, as illustrated in Figure 2.5. For most strain/strain sensing, mechanical energy harvesting, actuation, and artificial muscles applications, low test frequency between 0.1 Hz to 1MHz is used. In addition, a capacitive measurement technique at low frequency is often used to understand polymer-additive interaction, molecular relaxation phenomena on the application of external stimuli such as temperature, frequency and strain/stress. In this technique, the material under test (MUT) is placed between electrodes making direct contact with the electrode. Figure 2.6 shows the capacitive measurement method at low frequency. This method is generally used for low loss media with a low frequency of interest, as illustrated in Figure 2.5.

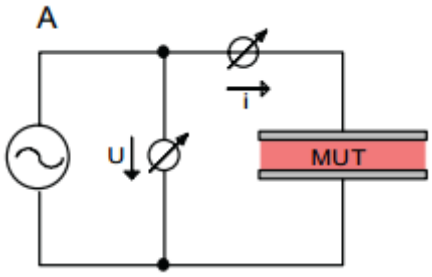

Figure 2.6 Capacitive approach of electrical parameters measurement

Hence, dielectric spectroscopy has become a major tool for investigation, not only for conducting behavior of different polymers, liquids, and other solid samples, but also the relaxation phenomena of different molecules [51]. Relaxation phenomena of materials is crucial for understanding change in the electric behavior of polymers under different frequencies and temperature conditions. At a molecular dynamics level, dielectric spectroscopy has proven to be a more improved technique compared to other measurement techniques including Nuclear Magnetic Resonance (NMR), Small angle X-ray scattering (SAXS), Dynamic Mechanical Analysis (DMA), Quasi-elastic light scattering and neutron scattering [52]. Cooperative relaxation, crystalline relaxation, and Maxwell-Wanger-Sillar (MWS) polarization are the three types of relaxation phenomena that are commonly found in thermoplastic elastomers and thermoplastic elastomeric based nanocomposites. Cooperative relaxation occurs due to the relaxation of the backbone chain of polymers and is generally termed as glass transition relaxation. Crystalline relaxation occurs in the crystalline part of thermoplastic elastomers. MWS relaxation generally occurs at a very low frequency with the conducting polymers or conducting composites due to charge trapping at the interface of materials having different permittivity. Frequency based MWS and crystalline relaxation phenomena in thermoplastic elastomers are hard to find using imaginary dielectric permittivity. However, electric modulus, M^*, an inverse of dielectric permittivity, can be used to define different relaxation especially MWS and crystalline loss in polymer and nanocomposites. Mathematically, it is presented by Equation 2.3

$$M^* = 1/\varepsilon_r = 1/(\varepsilon' - i\varepsilon'') = \varepsilon'/(\varepsilon'^2 + \varepsilon''^2) + j\varepsilon''/(\varepsilon'^2 + \varepsilon''^2) = M' + jM'' \qquad \text{Equation 2.3}$$

Where M' and M'' are the real and imaginary component of electric modulus, which is analogous to the shear modulus.

All the above mentioned relaxation phenomena are crucially important to understand the behavior phase transition of polymers under different strain/strain, temperature, frequency conditions, for a specific application such as energy harvesters, strain/stress sensors, artificial muscles and other electroactive applications.

In a dielectric material, when an electric field is applied to a material possessing negative (-Q) and positive (+Q) dipoles of distance d', a dipole moment is produced given by 'Q_d'.

For an applied voltage of V at the surface of the electrode, the charge density D at the surface is given by Equation 2.4

$$D = D_0 E + P \qquad \text{Equation 2.4}$$

Where the polarization P is given by Equation 2.5

$$P = \varepsilon_o(\varepsilon' - 1)E \qquad \text{Equation 2.5}$$

Where D is the total charge density at the surface of electrodes with applied electric field E to a material, D_0 is the charge density at the electrode at vacuum conditions with permittivity(ε_o). From Equation 2.5, it is clear that the dielectric permittivity measurement gives valuable information about the polarization of molecules within the material [51].

The discovery of polarization phenomena of dielectric elastomers opened the door to varieties of smart electroactive applications such as sensors and transducers. Dielectric elastomeric materials are also promising groups of polymers which have a broad range of applications based on the dielectric values. Specifically, low dielectric constant materials are generally used as insulators for insulating wires, signal-carrying wires, interlayer dielectric, crosstalk and power dissipation materials, etc. Whereas, high dielectric constant materials are used as polarizing capacitors, media for propagation and reflection of electromagnetic waves and various other semiconductor devices [52]. Polymers with low polarization ability can also be transformed into high dielectric constant materials by incorporating additives into them, thereby tailoring various properties that are not found in virgin materials [49]**.**

Dielectric elastomers are a most widely studied research area, targeting the application of actuation, stress/strain sensors, and energy generators. However, these materials can only be used for such smart applications if the materials have optimum mechanical and electrical properties [35]. Understanding of dielectric phenomena, dielectric tangent loss, mechanical tangent loss, mechanical flexibility and thermal properties are crucial to maximize the output in terms of frequency of operation, temperature and thermal conditions. Potential novel and innovative applications of electroactive dielectric elastomers technologies with their working principles are highlighted in the following sections.

2.3 Energy Harvesting Technology

Energy harvesting is the process of capturing energy from ambient sources and converting it to electrical energy for powering different electrical and electronic equipment [48]. Different types of energy sources available in the environment include solar energy, mechanical energy from the wind, sea etc., vibration energy, acoustic energy, thermal energy with temperature gradient, etc. [53]. However mechanical energy has garnered special interest from both scientific research and industries due to its ubiquity [54].

Mechanical energy can be harvested from large sources like sea waves or from small sources like the vibration of machines. Technologies for harvesting mechanical energy from different mechanical sources are relatively common; some of the most common techniques of mechanical energy harvesting include

(i) Piezoelectric harvester - These induce an electrical charge when a mechanical force is applied; as shown in Figure 2.7 (a). Polycrystalline materials like lead-zirconate-titanate (PZT) are commonly used in energy harvesting applications [55]

(ii) Capacitive harvesters - These devices function via capacitive energy harvesting mechanisms. Applied mechanical forces cause changes in the capacitance of the capacitor held between two plates harvesting energy, as depicted in Figure 2.7 (b). However, they require an external energy source [54].

(iii) Electromagnetic harvesters - These devices work on the principle of electromagnetic induction or Lenz's law. When a magnetic field is changed around the coil, it generates electrical energy, as in Figure 2.7 (c). The energy harvested using this technology is very low (0.1V) compared to piezoelectric and electrostatic harvesters (2-10V) [56]

(iv) Magnetostrictive harvesters - In such materials, when a force is applied to a magnetostrictive material, the microstructural configuration tends to align such that a magnetic field is produced; hence electrical energy is generated when the material is kept inside the coil, as shown in Figure 2.7 (d) [56, 57].

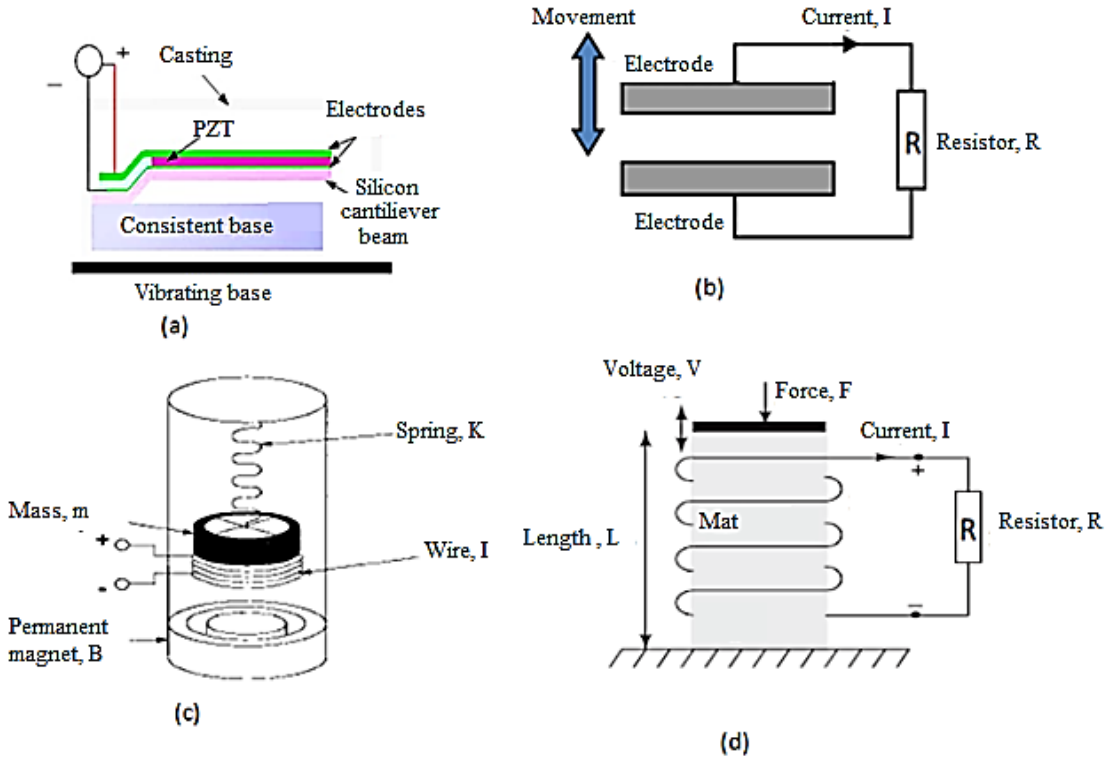

Figure 2.7 (a)Piezoelectric harvester (b) Capacitive Harvester (c) Electromagnetic harvester and (d) Magnetostrictive harvesters [56, 58].

Table 2.3 compares different material properties. Although piezoelectric, and magnetorestricitive materials act as an electric generator without the requirement of biasing voltage [59], dielectric elastomeric materials, which work on the principle of changing capacitance, exhibit superior properties in the context of elongation, energy density (energy stored per unit volume), and electromechanical coupling efficiency (numerical value representing an electrical energy to mechanical energy conversion efficiency).

Table 2.3 Comparison of material properties for energy harvesting applications [60-62].

Material Features	Piezoelectric Materials (PZT)	Magnetostrictive Material (Terfenol-D)	Shape Memory Alloys	Thermoplastic Dielectric Material (SEB-30% polymer faction)
Elongation (%)	0.1	0.15- 0.2	5	47
Energy Density (kJ/m^3)	2.5	20	10^{-3}	139
Electromechanical Coupling Efficiency	0.5-0.6	0.7	0.5	0.85

2.4 Sensor Technologies

A device that detects and measures physical, chemical and biological change within its environment is known as a sensor Based on their operational principles, sensor technologies can be broadly classified into different types; which include optoelectronic sensors, mechanical sensors, thermal sensors, magnetic sensors and multimodal sensors. Engel *et al*. [63] combined polymers and thin film metals for the design of a sensor similar to that of skin with the help of MEMS technology. MEMS technology is the miniaturization of mechanical and electromechanical elements manufactured using microfabrication techniques. The designed sensor demonstrated a response to different stimuli similar to that of skin, however, effective wiring systems remains a challenge [63].

The primary sensors deployed in SHM are typical of optical, strain gauge and a piezoelectric type. Table 2.4 highlights the advantages and disadvantages of these sensors in the context of SHM of civil infrastructural applications. From Table 2.4, conventional sensors used in SHM applications are deficient due to problems which include bond sensitivity (piezoelectric type), loss of accuracy with increased number of cracks (optical type) and measurement inefficiencies (strain-gauge type) [64-66].

Table 2.4 Comparison of different sensors used in civil structural monitoring [64-66]

Types	Advantages	Disadvantages
Piezoelectric Sensors	• Do not require external power source, small size and can be connected without another embedded system	• Requires embedded system for SHM, less immunity to electrical interference, costly process, and weakened at certain levels and sensitive of bond at applied surface
Optical Sensors	• Immunity to electrical interference, small size, and light weight	• Requires embedded system, costly process weakened at certain levels and loss of accuracy with increased number of crack
Strain gauge	• Small size, easy to install, and inexpensive compared to optical sensors	• Not efficient to measure concrete structures, needs embedded system for SHM and expensive installation process and weakened at certain levels

From Table 2.4, conventional sensors used in SHM applications are deficient due to problems which include bond sensitivity (piezoelectric type), loss of accuracy with

increased number of cracks (optical type) and measurement inefficiencies (strain-gauge type) [64-66]. To overcome the drawbacks associated with these sensors, mechanical and electrical efficient stress/strain sensors with optimized material properties compatible with structural infrastructure are prerequisite; especially for deployment in SHM applications.

2.5 Artificial Muscle Technology in Robotics or Prosthetics

When an electric field is applied to a thin film, it stretches due to Maxwell stress. These materials can be used as artificial muscles for robotic applications for locomotion, small pressure generation and so on.

Several attempts were made to make prosthetics from (i) ***Conventional actuators*** which include (a) D-C motors (coreless and brushless) - Linear motion to rotational motion for finger control in prosthetics [67, 68], (b) Hydraulic system - An artificial micro muscle for gentle movement [69], and (c) Servo motors - For the movement of artificial finger [70], (ii) ***Non-conventional actuators*** which include (a) Piezoelectric motors for mechanical displacement [71], (b) Ultrasonic motors for elliptical movement [72, 73], (c) Shape memory alloys for finger with 4 degrees of freedom made up of aluminium [74] and (d) Smart polymers which can act like muscles [75-77] and can move the joint of artificial prosthetics [78]. Use of smart polymers sufficiently reduces the weight of the smart prosthesis and has enormous potential for biomedical prosthesis.

2.6 Smart Catheter Technology

The concept of smart catheters has recently emerged with the advancement in electroactive polymer technology. The principle of operation is the actuation of the catheter on the application of electric field. Especially sulfonated polyetherimide [79] a well proven biocompatible material, which can undergo bending on the application of very low electric field (starts with 1V), has the potential to be used as catheters for medical diagnostic as well as health care applications. However, research reported by Rajagopalan *et al*. [79] does not fully explain the mechanical efficiency of such actuators, as heat energy was found increasing with increasing voltage. Therefore, a comprehensive study is essential for the use of such materials in smart catheter technology.

2.7 Dielectric Thermoplastic Materials as Energy Harvesters, Sensors and Artificial Muscles

Among the field of activated electro-active materials, dielectric EAPs (electro-active polymers) are most promising for energy harvesting and sensing applications because of their high actuation pressure (0.1-100MPa), high strain (up to 100%) and fast response time (>1ms) [77]. Actuation pressure represents the maximum pressure exerted by the elastomer under electric field when elastomers actuates. Conventional dielectrics, such as acrylics, are considered superior when compared to conventional piezoelectrics as they exhibit high energy density (>3MJ/m^{-3}) and are lightweight (1/7th the density of a piezoelectric equivalent) [78, 80]. These unique properties show that dielectrics are a superior class of materials for use as actuators in energy harvesting applications [35, 81].

2.7.1 Working Principle

The basic working principle of the dielectric elastomer as a sensor is dependent on its relative change in capacitance or impedance of dielectric elastomers upon application of an external force. However, the working principle of the dielectric elastomer as artificial muscle depends upon the mechanical deformation on application of electrical field. Finally, both working principles are combined to describe the working principle of elastomers for energy harvesting application.

2.7.1.1 Sensors for Civil Infrastructure Monitoring Applications

With dielectric materials, it is always possible to measure the material's capacitance. Moreover, the capacitance of the dielectric material changes with a change in its dimensions i.e. area, thickness, and other parameters. For a material to be suitable for use as a sensor, it must be attached to the structure with a compliant electrode; as shown in Figure 2.8.

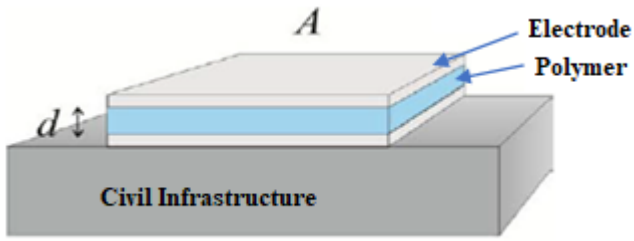

Figure 2.8 Sensor in original shape [82]

When the material is in its original shape, the capacitance C is given by Equation 2.6:

$$C = \varepsilon_r \varepsilon_0 \mathrm{A} / d \qquad \text{Equation 2.6}$$

Where, C is the original capacitance of the dielectric elastomer, A is the original cross section area of a capacitor, d is the thickness of the dielectric elastomers, ε_r is the relative dielectric constant of the elastomer and ε_0 is the dielectric permittivity of free space

However, when there is a crack in the structure, the material tends to stretch causing a change in its area as shown in Figure 2.9.

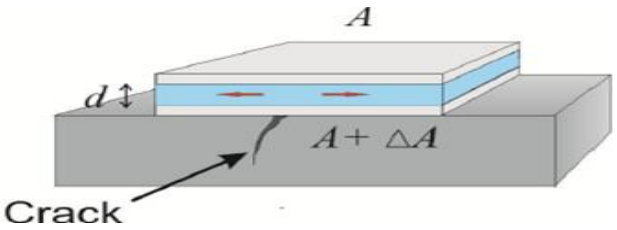

Figure 2.9 Change in dimension with change in structure of sensors with change in structure of civil infrastructure [82]

When the shape of the sensor changes, the capacitance of the material is given by Equation 2.7

$$C = \varepsilon_o \varepsilon_r (\mathrm{A} + \Delta A) / d \qquad \text{Equation 2.7}$$

Where, ΔA is the relative change in cross section area.

Therefore, by measuring the change in capacitance, it is possible to measure structural changes thereby overcoming some of the outlined difficulties including; the need for embedded systems, lack of sensitivity, lack of efficiency with increased crack number etc. Moreover, these types of sensors are very promising due to their small size, low-cost processing and other additional features such as sensitivity.

Furthermore, conductive elastomeric nanocomposites are more promising for SHM application as they tend to change the DC/AC conductivity or total dielectric permittivity upon application of small strain/stress. Good dispersion of conductive fillers in an insulating elastomer results in conductive elastomeric nanocomposites. The conduction

mechanism in such nanocomposites depends on interconnecting networks formed by conductive particles through electron tunnelling effect. The minimum amount of particle concentration required for the formation of interconnecting networks is called the percolation threshold. Change in interconnected networks upon application of stress/strain give rise to piezo-resistivity (change of resistance upon application of strain/stress) and tenso-resistivity in such conductive nanocomposites. Tenso-resistivity/piezo-resistivity of such nanocomposites affords a novelty and feasibility for the measurement of tensile stress/strain in more economical ways than conventional systems (example strain gauge).

2.7.1.2 Energy Harvesting

The use of a dielectric polymer as an energy harvester involves four main steps; as shown in Figure 2.10.

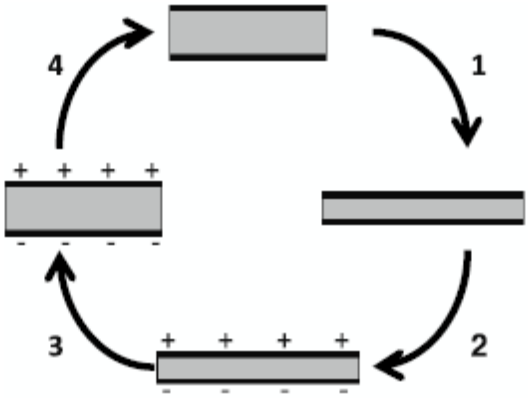

Figure 2.10 Energy harvesting process from dielectric materials 1. Stretching of the material 2. Injection of charge 3. Relaxation 4. Energy harvested [83]

From Figure 2.10, the four main steps involved in energy harvesting from the capacitive approach which is described is as follows;

i. Stretching

Fundamentally, the material is stretched by applying a mechanical force. In an ideal situation, the material used should be able to stretch to its maximum capacity without any volume change.

Let C_s be the capacitance of stretch polymer, which is given by Equation 2.8

$$C_s = \varepsilon_o \varepsilon_r (\mathrm{A}_s) / d_s \qquad \text{Equation 2.8}$$

Where A_s is the cross-section area under stretched condition and d_s is thickness of dielectric material under stretched condition.

ii. Injection of charge

After stretching of the material, the charge is embedded on to it by applying a constant voltage, constant electric field or constant charge through an electrode. During this process, like charges are separated wide apart because of the high columbic force of interaction between like charges. Two deformations forces, mechanical and field activated (sometimes referred to as the stress produced by columbic force) are thus present in the energy harvester. The stress produced by like charges due to the columbic force of interaction is known as Maxwell stress. Maxwell stress is given by the Equation 2.9.

$$R_m = -\varepsilon_o \varepsilon_r / 2\Upsilon \qquad \text{Equation 2.9}$$

Where; R_m is the Maxwell stress and Υ is the compressive modulus of the material.

The negative sign in the equation signifies the decrease in thickness of the structure when an electric field is applied. So, the total thickness change, S_m , in a material with applied electric field, *E*, is applied is given by Equation 2.10

$$S_m = R_m E^2 \qquad \text{Equation 2.10}$$

For energy harvesting application, the Maxwell stress must be smaller than that of the mechanical stress. Hence high Young's modulus material with high elastic compliance under large extension in preferred for energy harvesting applications

iii. Relaxation

During relaxation, the material can relax completely when the applied mechanical force is removed. During this process like charges come close to each other thereby generating a voltage which is higher than the applied voltage. Conversion of mechanical to electrical energy takes place at this stage. The capacitance of the material changes from C_s to C_r which is given by Equation 2.11

$$C_r = \varepsilon_r \varepsilon_0 (\mathrm{A}_r)/d_r \qquad \text{Equation 2.11}$$

Where A_r is the cross-section area during relaxed condition and d_r is the thickness of dielectric thin film after relaxation.

iv. Energy Harvested

During this process, a voltage is generated and subsequently harvested by some form of electrical or electronic appliance. If U_r and U_s is the total energy at relaxed and stretched state, and V_b is the biasing voltage then, the total amount of energy harvested U will be given by the Equation 2.12

$$U = U_s - U_r \qquad \text{Equation 2.12}$$

$$U = 0.5 C_r V_b^2 (C_r / C_s - 1) \qquad \text{Equation 2.13}$$

If a dielectric elastomer is considered volumetrically incompressible, the volume always remains constant, as shown in Equation 2.14;

$$\mathrm{A}_r d_r = \mathrm{A}_s d_s \qquad \text{Equation 2.14}$$

Then,

$$U = 0.5 C_s V_b^2 (Z_m^2 - 1) \qquad \text{Equation 2.15}$$

where Z_m is the change in thickness between stretch and relaxed state and is dependent on the force applied and elastic compliance of the material.

It is generally understood that the softer/deformable materials (with high dielectric constant and low dielectric loss tangent) can be easily used for energy harvesting applications using the capacitive method with very small applied force. Even though the low Young's modulus materials with high mechanical performance and high dielectric characteristics are considered most suitable for actuation and capacitive sensors applications [35], energy harvesting applications using capacitive technique is considered difficult to achieve from very soft materials as they tend to deform easily on the application of biasing voltage.

In addition, the dielectric permittivity along with dielectric loss is a crucial factor required for capacitive energy harvesters. The dielectric permittivity can be highly enhanced by the use of different fillers types if the polymer has high mechanical and electrical tailoring properties, as suggested by different authors [84, 85], however, authors fail to explain the effect of exfoliation, distributive/dispersive dispersion of fillers on dielectric properties and dielectric loss of thermoplastic elastomers. In addition, dielectric fillers tend to increase the dielectric loss of the elastomer due to agglomeration of fillers in elastomer. Dielectric tangent loss decreases the efficiency of the material as the result of thermal losses when biasing voltage is applied during the capacitive energy harvesting technique. An additional crucial factor that determines the energy harvesting capability of a material is the apparent electro-restrictive coefficient which is directly proportional to the ratio of dielectric permittivity to Young's modulus of the material. as given by the Equation 2.16

$$M\alpha \frac{\varepsilon_o(\varepsilon_r - 1)^2}{(\varepsilon_r Y)} \qquad \text{Equation 2.16}$$

The amount of energy harvested from an elastomer is directly proportional to the electro-restrictive coefficient of the elastomer.

Both thermoset and thermoplastic dielectric elastomers are activated by electric fields. Most thermosets used in smart applications in the past were conventional elastomers. Conventional dielectric elastomers like silicones are widely studied for their potential applications as actuators for artificial muscles [86], wearable hardware and physiological sensors, smart surfaces, animatronics and humanoids etc [87, 88]. However, several materials related problems such as material mechanical/thermal strength failure, dielectric breakdown failure, pull in failure is related to thermal failure due to cyclic loading of

electric field (occurs as the result of high domain sizes and also related to high dielectric loss), the requirement of high biased voltage, creep, long relaxation time, high hysteresis loss and difficult processing etc. still persists as shortcoming [61, 89-91]. Among these limitations, high creep and hysteresis losses due to the viscoelastic properties of the materials are considered to be most significant issues

Recent advancements in materials science and technological development make it possible to tailor the properties of thermoplastic elastomers to match the prerequisites of application specific properties, such as mechanical and superior electrical performance. Lately, there have been many influential developments in the field of dielectric thermoplastic elastomers (DTEs) which possess the ability to change shape and size under applied electric fields [92]. In addition, mechano-electrical conversion is also one of the featured possibility under the application of specific biased voltage. Such exciting new classes of materials differ from conventional materials in many different ways; which are highlighted in Table 2.5

Table 2.5 Comparison between nano-dielectric elastomers (thermoplastic) and conventional dielectric elastomers [61]

Properties	**Nanostructure Dielectric Elastomers (Thermoplastic)**	**Conventional Dielectric Elastomers**
Morphology	Soft middle block and hard end blocks in regular fashion	Homopolymers of soft and hard block
Cross-linking	Physical	Chemical
Processing	Simple even after cross-linking	Difficult due to chemical links
Hysteresis loss	Very low	High compared to nanostructure
Actuation properties	High even at low electric field	Low at low electric field
Dielectric constant	low (2-3)	Comparatively high (3-5)
Example	poly(styrene-*b*-ethylbutylene-*b*-styrene) triblock copolymers	Acrylics, silicones

Thermoplastic materials consist of soft/amorphous blocks in between the hard crystalline blocks. Thermoplastic copolymers may be of styrene block copolymers, copolyesters, thermoplastic polyurethanes and/or co-polyamides. Thermoplastic elastomers are formed by blending rubber and a thermoplastic polymer, where the thermoplastic polymer and rubber exist in different phases, for example, thermoplastic olefin formed by polypropylene with ethylene propylene diene monomer (EPDM) or ethylene polypropylene copolymer [93]. In thermoplastic olefins, polymers are in different phases. In most cases, the EPDM phase exists as discrete particles as shown in Figure 2.11, but, in some cases, the rubber phase is a co-continuous phase. Hence, in thermoplastic olefins, the morphology is not clear. The elastic performance of these polymers is time dependent and does not show elastic behavior above the crystallization temperature as there is no locking in these copolymers [93]. The rubber particle size varies from 0.2 to 5 μm [94].

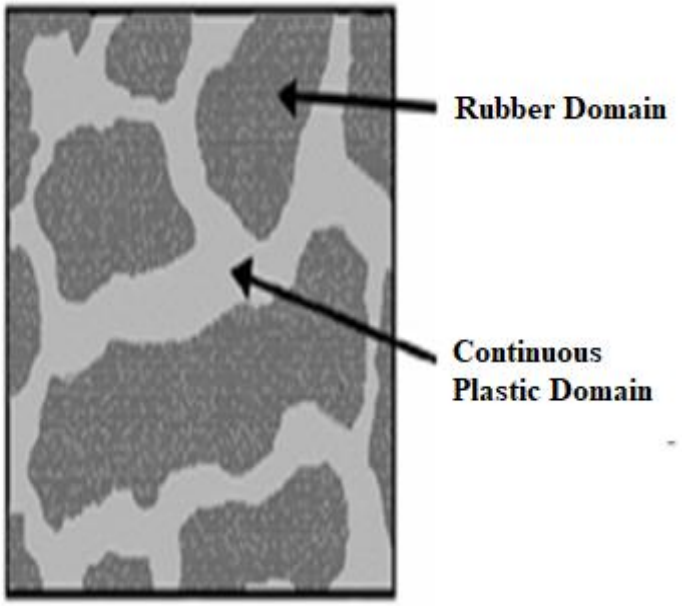

Figure 2.11 Thermoplastic olefins rubber plastic technology [93]

Due to the improved mechanical performance of dielectric thermoplastic elastomers over conventional dielectric elastomers (as illustrated in Table 2.5), thermoplastic dielectric materials are believed to be more suitable for energy harvesting applications and for deployment as sensors in SHM applications. However, their electrical properties need to be improved without affecting their mechanical performance based upon their applications. For capacitive energy harvesting application, high dielectric material with

very low dielectric loss is preferred whereas, for sensors in SHM applications, conductive nanocomposites are preferred.

According to Rajagopalan *et al*.[95], thermoplastic elastomers made from polyetherimide by attaching sulphonic groups show maximum displacement of thin film under DC excitation at 5V around 0.1Hz. However, material actuation was due to the movement of cations of materials to water molecules. Moreover, the materials dissipate electrical energy. Hence, this material may not be suitable for energy harvesting and other flexible capacitive applications.

Similarly, thermoplastic polyurethane (PU) based elastomers are also widely investigated for actuation as well as energy harvesting applications [96, 97]. However the low strain capability of PU based elastomers, when compared with styrene based rubbers, hinders their application for actuation and energy harvesting applications.

Some of the thermoplastic copolymers based on styrene have a rubbery like character and are found to be activated by application of an electric field. Polystyrene butylene rubber [SBR] and poly(styrene-ethylene/butylene-styrene)) [SEBS] are of some of the potential materials that can be used as an actuator as well as energy harvesting materials due to their chemical make-up, mechanical, thermal and electrical properties. Thermoplastic dielectric elastomers like SEBS are found to be better than conventional elastomers in the context of nanostructure morphology, smartness and electrical actuation [98], but their low relative permittivity (dielectric constant) remains very dubious for application in energy harvesting applications. Unlike conventional elastomers, dielectric thermoplastic elastomers consist of a micro-phase separated multiphase structure as shown in Figure 2.12 to give high shape memory (rubber-like-elasticity) properties suitable for electroactive applications like actuators, energy harvesters, and stress and strain sensors. The size of the domain is within several tens of nanometers. In Figure 2.12, the black spheres consist of a hard block of polystyrene and bright spheres consist of a soft block of poly(ethylene-butylene).

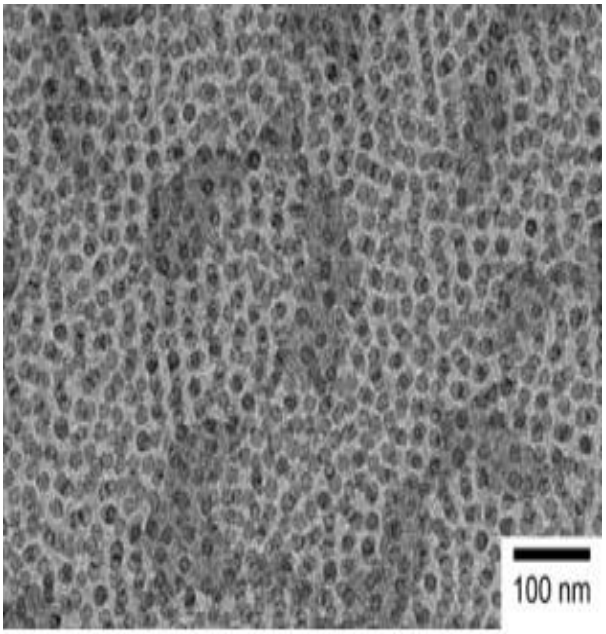

Figure 2.12 TEM images of SEBS swollen in 80% of paraffin oil [98]

Kim et al [99] found that thermoplastic elastomer (SEBS and SEBS–g-MA [poly(styrene-ethylene/butylene-styrene)-grafted maleic-anhydride]) shows a deflection on the application of electric field. In addition, the authors also reported that the dielectric constant and tan delta of SEBS were independent of frequency. It is suggested that such behaviour may be due to lack of polar bonds in SEBS [100].The loss tangent of SEBS was less than 0.03 over a range of frequencies [99]. For applications like an artificial muscle, the electric strain of SEBS-g-MA has higher electric strain than that of SEBS [99]. A possible explanation might be due to the polarized group (MA) being attached to SEBS. Shankar et al. [101] described that when SEBS is mixed with a low volatile aliphatic solvent, it yields a high displacement on the application of low electric field (200 % strain rate with less than 27 volts per µm). Moreover, recent research also reports that unlike conventional elastomers, the electrical activation of thermoplastic elastomers like SEBS does not need any pre-strain of the materials [101].

For the electrical characterisation of polymers with polar molecules from µHz to GHz, the electrical response with polarization function group changes with frequency, but non-polar polymers don't change their electrical response with change in frequency [102]. Palakodeti and Kessler [103] carried out an experiment of dielectric elastomers in between 5 to 20 Hz and suggested that the actuation and energy conversion is higher at low

frequency with low loss tangent. According to Kornbluh et al.[35], the electrical efficiency (η_e) of an elastomer for actuation application is dependent on the dielectric loss tangent ($\tan\partial_e$)given by Equation 2.17

$$\eta_e = \frac{1}{1+\Pi\tan\partial_e} \qquad \text{Equation 2.17}$$

Equation 2.17 should hold true for capacitive energy harvesting condition as charges on the surface of the capacitor decay as the value of tangent loss increases.

In addition, Kornbluh et al.[35] also explained that the mechanical actuation efficiency (η_m) of an elastomer depends on mechanical tangent loss ($\tan\partial_m$) measured under tan delta using dynamic mechanical analysis and is given by Equation 2.18

$$\eta_m = \frac{1}{1+\Pi\tan\partial_m} \qquad \text{Equation 2.18}$$

However, they failed to explain the instrumental limitations of measuring tan delta under large strain conditions. The tangent loss measurement for mechanical performance of such elastomers remains still questionable due to the instrument limitations. However, the hysteresis loss measured using cyclic loading can provide information about the lossy nature of the elastomer at different strain conditions. Materials with high hysteresis loss provides low mechanical efficiency during cyclic loading and vice versa.

Van den Berg, et al. [102] also suggests that the dielectric constant of SEBS elastomer remains constant over the range of frequencies after a slight decrease of dielectric constant at low frequency (up to 1 Hz). It is likely that the slight decrease in initial stage frequency might be due to the polarization of electrodes rather than a polymer response. In addition, the higher polymer concentration in solvent increases the dielectric constant by a negligible amount, however, it also depends on the type of solvent (polar Vs non-polar) used. Molberg [104] performed a dielectric measurement of acrylate adhesive film, silicone and styrene block copolymer from 0.5 mHZ to 1 MHz . He observed that the dielectric constant of silicon (dielectric constant=2.5) and styrene block copolymer (dielectric constant=2) remained the same over the frequency range, but the dielectric constant (4.7 below 1 kHz) of acrylate film tends to decrease above 1 kHz. The authors

also suggest that the dielectric constant of the material is independent of the electric field applied.

Even though low polarization of thermoplastic elastomers compared to conventional dielectric elastomers can be considered as a hindrance, this issue can be solved by adding either highly polarizing materials or by adding highly conductive materials. Putson et al [55] investigated the use of polyurethanes with copper nano-fillers for energy harvesting applications and reported that use of nanofillers tends to increase the energy harvesting capabilities of the materials, but (when compared with elastomers) did not undergo large rubbery deformation. The same group [105] also evaluated the dielectric constant of polyurethanes (PU) with copper (Cu) fillers at the frequency range of 1 Hz to 1 MHz and found that the dielectric constant decreases with an increase in frequency due to the presence of the polar bond in PU. In addition, the addition of nano-sized Cu fillers increases the dielectric constant irrespective of frequency. Furthermore, the authors also hold the view that the value of loss tangent is much less for PU at around 100 Hz. On the other hand, for capacitive and energy harvesting applications from natural mechanical sources, these types of elastomers suggest having a number of shortcomings due to high energy loss at low frequency. Impregnation of additives (metallic fillers like Cu, metal oxides like TiO_2, nanoparticles like carbon black) into polar as well as non-polar molecules causes a change in polymer electrical properties [55].

Even though the addition of certain additives tend to increase polarity in materials, they also tend to increase the mechanical stiffness thereby lowering the electrical output [106] Poly(vinylidene fluoride) fibers show high output power compared to poly(vinylidene fluoride tetrafluoroethylene) (P(VDF-TrFE) (70/30), from Solvay) with barium titanate ($BaTiO_3$ nanoparticles), but the output power is dependent on nanoparticle sizes (decrease with increase in the size of nanoparticles). Moreover, the output power is independent of the frequency in the polymer composite. The addition of additives like high permittivity titanium oxide nanoparticles to soft dielectric polymers like silicone increase the mechanical performance and enhance the permittivity [107]. The high parasitic loss in low energy density materials occurs due to viscosity and electrode resistance. Similarly, the relative permittivity (dielectric constant) is increased from 2.5 to 6.3, when TiO_2 is mixed with SEBS copolymers but this decreases the mechanical performance of the material [108]. The experiment performed by Zulfiqar, et al. [109] and other authors [110] suggest that the addition of nano-sized silica to SEBS-g-MA polymer enhances the

mechanical performance of the polymer significantly by lowering loss modulus and increasing tensile strength, but the experiment performed did not include any measurement of electrical performance and mechanical compliance. Ghallabi et al.[111] found that the three-phase composite made up of polyvinylidene fluoride, carbon nanotubes and barium nanotubes showed an excellent dielectric constant and a very low dielectric loss over the different frequency range. In general, virgin soft dielectric elastomers without additives have low dielectric constant and vice versa, but the realization of material with optimized mechanical and electrical properties has always been an issue.

Sensors have already been made and tested by using soft capacitors made up of conventional dielectric and thermoplastic dielectric elastomers (SEBS-g-MA) and are found to be effective enough for monitoring the health structure of civil infrastructure. Kollosche et al. [112] observed the accuracy of a sensor increases with an increase in capacitance of the thin film or dielectric constant of the material. For higher sensitivity in stress and strain sensing applications, thermoplastic materials also should have higher dielectric constant which can be achieved by using highly polarizing additives or conductive fillers. Section 2.8 highlights different fillers used to enhance the electrical performance of thermoplastic for such applications.

2.8 Conductive Fillers and High Dielectric Based Thermoplastic Elastomer Composites

The ease of processing of thermoplastic elastomers using extrusion with the addition of different filler types (conductive fillers such as CB and dielectric fillers such as barium titanate) to tailor their dielectric properties makes them more suitable for artificial muscles, capacitive sensors and capacitive energy harvesters [53, 113]. Conductive fillers tend to change the dielectric permittivity of polymer matrices several fold [114] He and Tjong [114] reported the dielectric permittivity of polyvinylidene difluoride (PVDF) increased by 15 times with the addition of 0.5% of reduced graphene sheets. However, they also tend to increase the dielectric permittivity loss of nanocomposites leading such manufactured nanocomposites to have low dielectric breakdown strength [115]. In addition, Kim [116] noticed the low deformation of thermoplastic elastomers on the application of an electric field even with the addition of a higher percentage of carbon black. This may be due to a higher relative stiffness change on the polymer nanocomposite

matrix, rather than its relative dielectric permittivity increase due to the high reinforcing effect of carbon black. It has also been reported that the high dielectric loss (six times increase in dielectric loss of polymer matrix upon addition of 4% volume concentration of carbon black), low dielectric breakdown strength (less than 3 V/ μm upon addition of 2.5% volume concentration of CB in SEBS versus 50 V/μm of virgin SEBS), and high reinforcing effects (40% increase in Young's modulus with the addition of 0.5 wt. % of graphene-carbon nanotubes particles) of conductive fillers such as carbon black, carbon nanotubes and graphene. These issues limit applications of elastomer based nanocomposites for many electroactive applications such as energy harvesting generators and charge storing flexible supercapacitors [84], [117]. However, conductive fillers based nanocomposites have good piezo-resistive properties making them highly sensitive to stress and strain conditions and making them suitable of SHM applications. This sensitivity is very high near the conductive threshold percolation

The dielectric enhancement of dielectric fillers such as barium titanate is very low when compared to conductive fillers. However, the increase in dielectric strength, low reinforcement effects (better shape memory properties with low hysteresis loss) and low change in dielectric loss makes them more suitable for energy harvesting generators and charge storing flexible capacitors. However, literature still report the dielectric loss which defines the electrical efficiency of dielectric based composites at low frequency needs serious attention for their use for capacitive energy harvesting and flexible capacitor applications [35, 84].

In addition, most of the methods used in manufacturing such elastomers/composites in lab scale environment involve the solvent casting method. As a result, the large part of work carried out fail to address the question of not only reproducibility and repeatability but also the processing parameters and their effect on electrical and mechanical behavior of materials processed [90, 112]. Hence, the unmet need of manufacturing such polymers/ composites can only be resolved using industrial standard processing techniques such as extrusion system and novel scalable systems.

2.9 Supercritical Fluid Carbon Dioxide Assisted Extrusion Technology for Processing of Thermoplastic Elastomers and Their Composites

Many standard methods are defined for manufacturing of carbon based conductive thermoplastic elastomeric composites [118-122]. However, manufacturing using solvent technique methods is always limited to laboratory efforts because of their low potential for scalability, high processing time duration, and low-cost efficiency. Twin screw hot melt extrusion is the most commonly used industrial standard compounding machine which has a huge potential for cost effectiveness, scalability and better dispersion of additives for making composites for wide applications. Rauwendaal defined melt extrusion as the process of transforming raw materials into an artifact of uniform shape and density under controlled conditions by forcing the material through a restricted orifice, called a die [121-123]. Production of composites using scalable machines such as extrusion is limited because of the high concentration requirement of conductive and dielectric fillers to produced enough change in electrical properties of the materials [122, 124, 125]. However, supercritical assisted extrusion has huge potential for better dispersion of these fillers in several polymers making them electrically useful for many applications [126].

Supercritical fluid carbon dioxide ($scCO_2$) assisted extrusion has been found to be a most promising solution for the processing of different thermoplastic nanocomposites. The use of $scCO_2$ technology has been limited to extraction for years due to high initial investment requirements as well as a dearth of combined knowledge of high shear force machines such as extrusion; high-pressure chamber equipment used for $scCO_2$ processing and advanced polymer processing techniques.

Supercritical fluid (SCF) is defined as any substance with both pressure and temperature above its critical values. Researchers have reported that SCF offers unique characteristics such as gas-like diffusivity, liquid-like density, low viscosity and surface tension when compared to conventional organic solvents [125, 126]. Among SCFs, it is well known that supercritical carbon dioxide ($scCO_2$) provides good solubility in molten polymers and acts as a plasticizer resulting in a decrease in the viscosity of the molten polymer, the melting point, and the glass transition temperature [126-128]. These changes, in turn, result in the fractionation of polymer, modifying the mechanical, as well as physical properties of the polymer [126, 128-131]. Although a plethora of work exists in scientific

and industrial communities using SCF batch processing technique, a lack of knowledge still persists on the use of SCF for continuous industrial standard polymer manufacturing process such as hot melt extrusion. In addition, lack of scientific understanding on how SCF affects the thermal, mechanical, electrical, and morphological properties of phase separated thermoplastic elastomers (TPEs) using hot melt extrusion still persists. Furthermore, complete use of $scCO_2$ assisted extrusion of TPEs is limited for commercial applications. Therefore, it is highly likely that combination of the extrusion process and $scCO_2$ would benefit processing of polymers with lower processing temperatures and/or act as a foaming agent during expansion through the die [126, 128, 131]. Moreover, the supercritical conditions for CO_2 are easily achieved (Tc = 304.15 K, Pc = 7.38 MPa) and can be removed from the system by simple depressurization [126, 130, 132-136]. It is a general representation that CO_2 solubility in a polymer is a function of pressure and temperature [126, 128, 137], yet, the specific molecular interaction between CO_2 and polymer holds has considerable impact in terms of solubility and diffusivity.

Sameer *et al.*[130], Kazarian [137] and other researchers have reported that CO_2 has the potential to act as both a weak Lewis acid and Lewis base due to its quadrupole moment, indicating that CO_2 may solubilise dipolar and non-dipolar molecular structures through site-specific solute–solvent interactions [137, 138]. However, the solubility and diffusivity of CO_2 in polymers is not only subjective to the interaction between molecular chains but also in the crystalline or amorphous nature relating to the free volume of the polymers [130, 137, 138]. In the case of SEBS, weak Lewis acid-base interaction with CO_2 is initiated due to the phenyl ring in PS, resulting in sorption and swelling of SEBS [126, 128, 130, 138].

Processing of polymers using supercritical fluid CO_2 ($scCO_2$) has gained importance in scientific and engineering communities because of its non-toxicity, non-flammability, zero-ozone layer depletion effect and cheap costs [126]. However, the advantages of using $scCO_2$ are not limited to the above mentioned properties. $scCO_2$ is a proven technology for tailoring mechanical, thermal, morphological, and viscoelastic properties of polymer and polymer blends [126, 139, 140]. In addition, the low surface tension and high diffusibility of $scCO_2$ in polymers have enhanced its importance in the drying of polymers with solute and purifying of different types of polymers from unreacted residues, unreacted species, and harmful chemicals [126, 141]. Furthermore, $scCO_2$ is also widely used for the making of better polymer blends as well as for impregnation of different additives into different polymer matrices [126, 139, 142].

Recent development of graphene and graphene-based oxide has shown great potential for the improvement of electrical properties of different polymers and composites making them superior for solar cells [143, 144], water purification [145], supercapacitors [146-149], sensors [150-152], tissue engineering [153], electromagnetic interference [154], gas absorption [155], fuel cell [146, 149, 156], antibacterial [157] and thermal insulation applications. However, production of graphene from graphite is a costly and time-consuming process. Sasikala *et al.* [158] showed that $scCO_2$ has huge potential for processing of graphene directly from graphite as an easy and convenient process for particle formation. In addition, $scCO_2$ can be used for assistance for the manufacturing different graphene-based devices and composites at different stages of manufacturing and fabrication process of different devices. Literature [158] reports that uniform dispersion of additives in polymer composites or manufacturing of polymer blends using this technique show materials with superior mechanical and thermal properties thereby enhancing polymer–additives or polymer-polymer interactions respectively.

Thermal, morphological, mechanical and electrical properties of materials play an important role in determining the electrical and mechanical performance of dielectric thermoplastic elastomers and composites for their specific applications**.** Thermal properties like crystallization temperature, glass transition temperature, melting point and degradation profile give information about the softness, hardness, amorphous, and crystallinity over temperature [159, 160]. These materials, in turn, play an important role in mechanical, as well as electrical properties of materials. For example, highly crystalline materials tend to have higher stiffness resulting in higher force required to deform the materials and vice versa. Similarly, dielectric permittivity enhancement due to different fillers depends on the different processing parameters as well as viscoelastic properties of the polymers [161]

The addition of additives in elastomers and different manufacturing procedures highly affects their mechanical properties of elastomers [162, 163]. In addition, viscoelastic properties of elastomers are also highly affected due to the addition of additives due to polymer additive interaction as well as different processing conditions such as extrusion with/without the assistance of supercritical fluid. The viscoelastic properties are crucial for processing as well as for determining the stability and elastic properties of elastomeric composites under different environmental conditions. In addition, alteration in viscoelastic properties, in turn, changes dielectric (including dielectric relaxation under

different stress/ strain, temperature, and frequency condition) as well as mechanical properties of elastomers and nanocomposites.

Mechanical properties and dielectric properties at a specific frequency, temperature and stress and strain condition affect the performance of elastomeric composites in different ways, resulting in different electromechanical coupling efficiency. Electro-mechanical coupling efficiency is measured by using the mechano-electrical coupling coefficient given by Equation 2.19.

$$K = \sqrt{\chi} \qquad \text{Equation 2.19}$$

Where χ = Energy converted per input energy

Measurement of polarization ability gives information about the potential application of dielectric elastomers in different applications as energy harvesters, actuators, and capacitive sensors. However, the conduction capability and polarization ability of different composites are highly dependent on processing parameters and test variables. Tang *et al.* [164] presented a change in conduction behavior of polyethylene/carbon black composites over the range of temperature. Similarly, Moreno [165] showed the difference in conduction behavior of SEBS based conductive composites under different stress/strain conditions. Hence, more and more research has been carried out to enhance as well as understand the dielectric parameters as well as relaxation phenomena of such triblock based highly dielectric/ conductive composites which differ with processing parameters, chemical and physical additive-polymer interaction, the morphology of thermoplastic composites and viscoelastic properties of composites. In addition, the frequency of conduction, dielectric crystallization relaxation and dielectric backbone relaxation of such thermoplastic elastomer based composites differs with temperature and strain/strain applied. The relaxation phenomenon of conductive and dielectric triblock composites is hard to interpret because of the presence of multiphase within an SEBS-g-MA triblock where styrene acts as hard block, ethylene-butylene acts as a soft phase and many interphases are present in between the hard phase and the soft phase [166]. Because of these different phases present in SEBS and SEBS-g-MA, the relative change in dielectric permittivity over the range of temperature and stress/strain applied differs due to different swelling behavior and relaxation of the hard and soft block at different temperature and strain conditions respectively.

2.10 Problem Definition

Dielectric thermoplastic elastomeric nanocomposites have the potential for deployment across a diverse application space as sensors, actuators, and energy harvesters. However, at present, production of very low dielectric loss nanocomposites with highly responsive characteristics to electrical and/or mechanical stimuli is poorly understood, particularly in relation to the electrical behaviour change on application of mechanical forces and vice versa. Insufficient documentation of these operational mechanisms exist for mapping and validation of material characterization data obtained from experimentation. Subsequently, their commercial exploitation and industrial uptake have been stifled. Factors which promote this lack of scientific understanding include (i) a scarcity of research into the electrical and mechanical characteristics of DTEs, their composites and their potential applications (which include but are not limited to SHM and energy harvesting applications) based on different manufacturing processes, (ii) deficiencies in research on variation in electrical and mechanical properties because of additive-polymer interactions, viscoelastic properties and scalable processing conditions using extrusion with/without assistance of $scCO_2$, (iii) deficiencies in understanding the conduction and dielectric relaxation frequencies of such elastomeric composites over temperature and stress/ strain conditions for the deployment of thermoplastic composites for sensors, actuators and energy harvesters applications and (iv) challenges in coupling to other energy sources and high level circuitry requirements.

2.11 Aims and Objectives

The purpose of this research is to address this paucity of scientific understanding of thermoplastic elastomers for smart applications such as stress/stress sensors and energy harvesters. In doing so this work will seek to develop a comprehensive understanding of the physical, chemical, electrical and mechanical properties of DTEs nanocomposite based on sophisticated manufacturing processes for large volume production, and the interdependent constraints that dictate their performance characteristics. This research will also address novel ways for in-depth analysis of thermal, mechanical and electrical behavior of different nanocomposites based on the compatibility and miscibility of additives of a number of dielectric polymer matrices making them suitable for various sensors and energy harvesting applications. Definition and parameterization of these

issues will build on prior research, and in doing so will provide a springboard from which the advantages, limitations and application-specific suitability of DTEs can be evaluated.

The main objectives of this work are to;

i. Develop a comprehensive physical understanding of the different stages of production of dielectric thermoplastic elastomers (DTEs) (i.e. synthesis, polarization process and polarization enhancement) and their nanocomposites using scalable production process such as extrusion. This objective is addressed in Chapter 2.

ii. Identification, selection, and production of DTEs and nanocomposites of nano-structured thermoplastic elastomers with nano-additives based on elastic compliance, dielectric constant, dielectric loss tangent, and electro-restrictive properties. Chapter 2, Chapter 3 and Chapter 4 address this objective.

iii. To develop and evaluate the thermal, mechanical, electrical and morphological modifications of thermoplastic elastomers upon addition of different types of additives using conventional industrial standard processing methods, such as extrusion. This objective is addressed in Chapter 5.

iv. Use of supercritical fluid assisted extrusion methods for the enhancement of conductive as well as dielectric permittivity of thermoplastic elastomers with conductive fillers or high dielectric fillers. This novel processing system along with detailed analysis of thermal, mechanical, morphological and electrical characteristics for electroactive application is highlighted in Chapter 6. The main objective is to enhance the dielectric permittivity at least by 100% with a maximum dielectric loss of 0.02 at low frequency (below 1 Hz) as well as to make thermoplastic elastomers conductive at very low percentage of CB (below 5 wt. %) using this novel extrusion method. However, the literature suggests that the minimum dielectric loss achievable for the thermoplastic elastomers is greater than 0.02; when dielectric permittivity of SEBS was increased by 100% with the addition of conductive or dielectric fillers at 1 Hz [84].Similarly, the percolation

threshold of CB in an elastomeric polymer like SEBS using extrusion was detailed quite high (well above 5 wt. %) in the literature.

v. Understanding and enhancement of electrical and mechanical properties of dielectric and conductive fillers based thermoplastic elastomers processed with/without $scCO_2$ as a function of polymer-additive interaction, viscoelastic properties and dispersion of additives. This objective is achieved comparing the results of with and without $ScCO_2$ assisted extrusion in Chapter 7 and Chapter 8

vi. Improvement of electrical and mechanical properties of thermoplastic composites by using an enhanced dispersion of dielectric as well as conductive fillers as well as reducing the particle size of dielectric and conductive fillers by using scalable $scCO_2$ assisted extrusion manufacturing process compared to conventional solvent casting methods for dispersion. The significance of dispersion function, additive particle size reduction, and polymer interaction is highlighted in Chapter 7 and Chapter 8.

vii. Evaluate and enhance the scientific understanding of conduction and dielectric relaxation of different conductive and dielectric fillers thermoplastic composites thereby making suitable for different electroactive and sensing applications. This objective is addressed in Chapter 9 by a detailed evaluation of the relaxation processes as well as a change in conductivity and dielectric permittivity (along with tangent loss) under different strain condition.

To achieve the stated objectives a comprehensive research methodology was developed around a number of core areas outlined as follows;

- Investigation into the physics of manufacturing of DTE materials and production of a comprehensive process roadmap in which manufacturing/processing interdependencies and constraints can be examined
- Identification and selection of suitable materials for the production of DTEs including synthesis and formulation methods for same.

- Identification and application of appropriate characterisation methods to samples produced in-house to accurately define intrinsic material properties (e.g. mechanical, chemical, thermal, morphological, etc.). Subsequently, optimal materials determined from characterisation will be selected for further investigation.
- Identify a suitable manufacturing procedure and produce highly enhanced thermoplastic nanocomposites to enhance charge induction and polarization in DTE composites.
- Investigate and modify a variety of DTE composites for the electrical and mechanical response, and operational performance characteristics with higher sensitivity for energy harvesting and sensors applications.

The achievement of the outlined aims and objectives is expected to contribute significantly to scientific knowledge in the field thereby providing a research platform which will allow end users within the industry to optimize formulations and response behaviors of DTEs for specific applications.

Chapter 3

3 Materials and Methods

Figure 3.1 describes the research methodologies used for this research. It consists of four phases. In the first phase, different dielectric elastomers and additives were selected. In the second phase, nanocomposites were produced using different manufacturing techniques. Electrical, thermal and mechanical characterization of different types of nanocomposites produced using different processing techniques were carried out in the third phase. Finally, in the fourth phase, mechanical, mechano-electrical, thermal and electrical analysis were performed to determine the suitability of nanocomposite for energy harvesting and sensing application. Finally, dielectric tests under strain of selected composites samples were carried for the final estimation of energy harvested under different strain conditions.

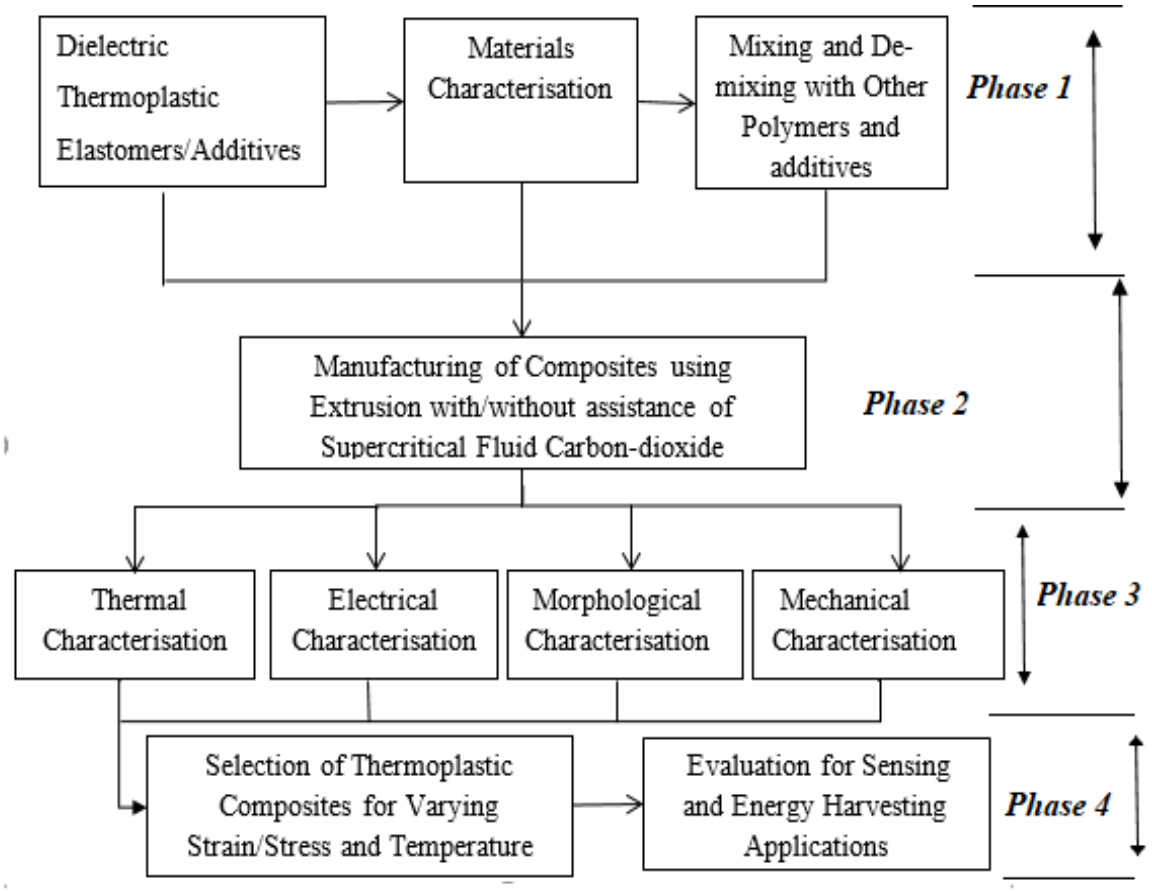

Figure 3.1 Research Methodology

3.1 Material Selection

Polymer matrices were selected based on mechanical compliance, ease of manufacturing, shape memory property (highly elastic under large strain) and thermal stability. A range of thermoplastic elastomers was selected as tabulated in Table 3.1 and their dielectric properties were analyzed thoroughly in Chapter 4. The suitability to tailor the mechanical and electrical properties of thermoplastic elastomers especially SEBS and SEBS-g-MA enables us to produce materials with a high electro-restrictive coefficient and high energy density with good shape memory property. Dispersion of additives into these polymers can be achieved by simple manufacturing processes like an extrusion system as a function of shear force. Moreover, these materials have degradation temperature around 400 °C and mechanical stability up to 60 °C. High thermal stability enables these elastomers processable even at high temperatures. Mechanical and electrical properties can directly be enhanced using swelling of the polymers in solvent and addition of additives respectively.

Table 3.1 Materials with their commercial names

Materials	**Brand-name**
PEBAX (polyether block amide)	PEBAX 7233
Polyurethanes	Pellethane® 2363-75D TPU
Poly (styrene-b-ethylene-butylene –b-styrene) (SEBS)	KRATON® G1652 E Polymer
Poly (styrene-b-ethylene-butylene –b-styrene) grafted maleic anhydride (SEBS-g-MA)	KRATON® FG1901 G

Poly(ether-block-amide) (PEBAX 7233)

Poly (ether-block-amide) – PEBAX 7233 used in this work was procured from Arkema, France. PEBAX 7233 is composed of Polyamide 12 (Nylon 12) as the hard segment and poly(tetramethylene oxide) as the soft segment. The percentage of hard segments and soft segments are 80% and 20% respectively. The density of grade 7233 series Pebax is around 1.01g/cm3 by ISO 1183.

Polyurethane (PU) (PELLETHANE® 2363-75D Elastomer)

Aromatic polyether polyurethane (PELLETHANE® 2363-75D elastomer) used in this work is based on 4,4'-diphenylmethane diisocyanate (MDI), poly(tetramethylene glycol) (PTMG), and 1,4-butanediol. In pellethane 75 D, MDI acts as a hard segment and PTMG acts as a soft segment. PELLETHANE® 2363-75D used in this work was procured from Arkema, France.

Poly(styrene-ethylene/butylene-styrene) (SEBS) (KRATON® G1652 E Polymer)

SEBS triblock is a type of styrene block copolymer which consists of polystyrene as end hard blocks and ethylene-butylene as mid soft blocks. Synthesis of SEBS triblock is done by the hydrogenation of the double bond present on poly (styrene- butadiene- styrene) (SBS) triblock. The commercial production of SBS is done by a living anionic process. The anionic polymerization mechanism takes place with a number of steps, which are described below

a. Initiation

During initiation, there is an activation reaction between the organometallic catalyst and styrene leading to an active radical bi-product known as poly(styryl)-lithium. This living bi-product initiates the polymerization of styrene and is illustrated in Figure 3.2.

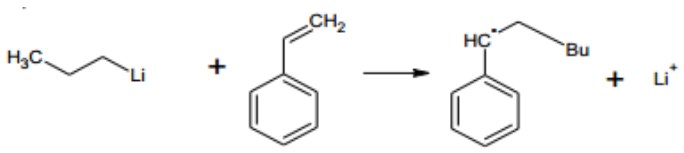

Figure 3.2 Initiation of styrene chain [108]

b. Propagation

Propagation starts with the addition of new styrene monomers leading to a new living end in the polymer chains and lengthening the existing chains. Due to the presence of non-terminating living end polymer chain, the polymerization process can be controlled in a precise manner. After all the styrene monomer is consumed,

diene monomers are chemically bonded leading to soft mid-blocks. At the end, styrene monomers are added again to the process forming a second hard segment. When the reaction is complete, a protonating species such as alcohol is used to inactivate the final product $S - B - S - Li^{+}$. This mechanism is given in Figure 3.3.

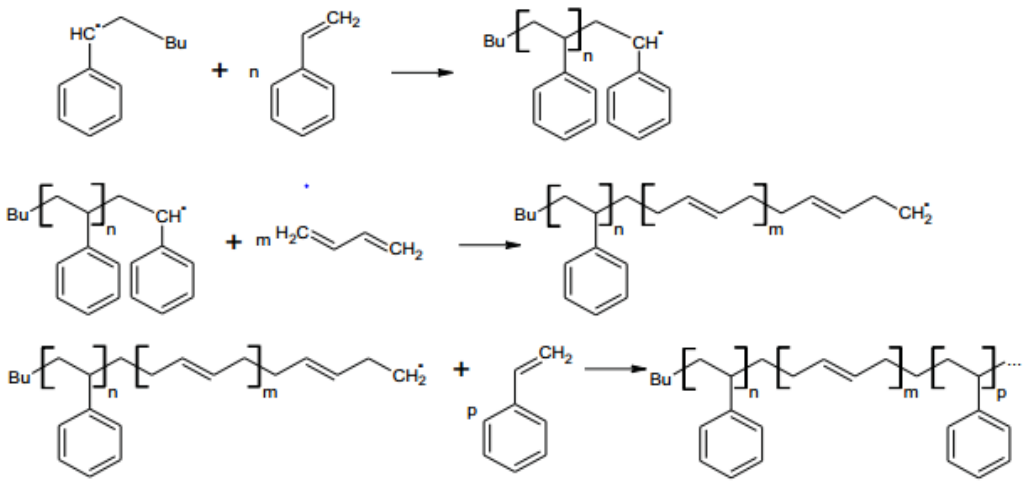

Figure 3.3 Propagation of styrene monomers, followed by chemical bonding of diene monomers and final addition of styrene end block [108]

Finally, the hydrogenation of butadiene group of SBS is done to obtain the SEBS, which is a more stable compound to form chemical resistance, weather resistance, and heat aging resistance compound.

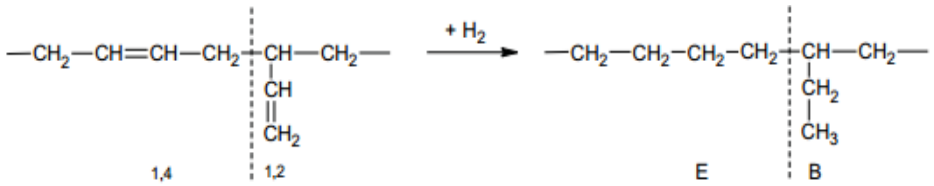

Figure 3.4 Hydrogenation of butadiene [108]

The final structure of SEBS is shown below

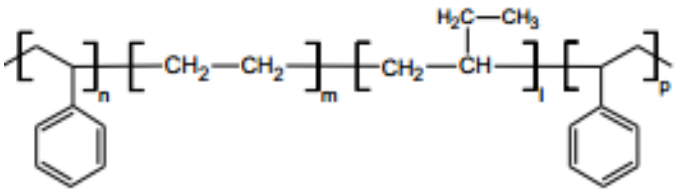

Figure 3.5 Structure of SEBS [108]

The general properties of SEBS triblock polymer obtained for this research is highlighted in Table 3.2 as provided by manufacturer

Table 3.2 General properties of SEBS Triblock KRATON® G1652 EH Polymer

Property	Test Method	Units	Typical Value
Specific gravity	ASTM D4025	gm/cc	0.91
300% Modulus	ASTM D-412	MPa	4.8
Melt index 230°C	n/a	gms/10 min.	5
Hardness	ASTM 2240	Shore A (10s)	69
Tensile strength	ASTM D-412	MPa	31
Styrene/Rubber ratio	n/a	n/a	30/70
Elongation at break	ASTM D-412	%	500

Poly (styrene-ethylene/butylene -styrene)-grafted maleic anhydride (SEBS-g-MA) KRATON® FG1901 G

When SEBS is functionalized with maleic anhydride, a polar thermoplastic elastomer is formed. The general structure of SEBS-g-MA is shown in

Figure 3.6.

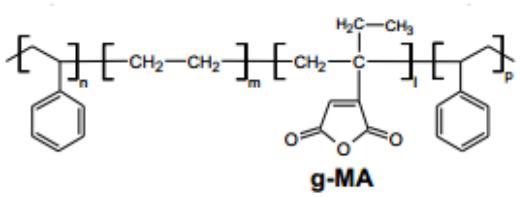

Figure 3.6 General structure of SEBS-g-MA

The general properties of SEBS-g-MA obtained for this research is highlighted in Table 3.3

Table 3.3 General properties of SEBS-g-MA Kraton FG 1901G

Property	Test Method	Units	Typical Value
Tensile Strength	ASTM D 412	MPa	34.5
Specific gravity	ASTM D4025	gm/cc	0.91
Melt index 230°C	n/a	gms/10 min.	22
Styrene/Rubber ratio	n/a	n/a	30/70
Elongation at break	ASTM D-412	%	500

3.2 Additives

Various material additives were explored to augment mechanical properties and bulk surface chemistry with a view to subsequent optimization of the materials polarization ability, and subsequent electro-mechanical performance characteristics. This process includes the embedding of polar or conductive additives to optimize the materials actuation properties and electromechanical conversion efficiency.

Additives were selected based on their effects on dielectric permittivity, ease of working in the lab and the ability to disperse in the polymer matrix, as shown in Table 3.4. Carbon black (CB) was chosen as the first additive. General properties of selected CB are highlighted in Table 3.5. CB has got high dispersion ability in polymer matrices under high shear and longitudinal flow. The dispersion ability of CB in polymers makes nano/micro-composites polarisable when homogenously mixed other with the polymer matrix. Another type of additive chosen was barium titanate (BT) because of its high dielectric permittivity and ease of working in the lab. However, this dielectric filler has very poor dispersion ability in elastomers. General properties of selected BT are highlighted in Table 3.5 as provided by the manufacturer. Brunauer-Emmett-Teller Theory (BET) surface used in Table 3.5 is the specific surface area of the additive measured using N_2 sorption technique as stated by the manufacturer. New manufacturing procedures under high shear force and longitudinal flow was used for the dispersion of this filler in polymer matrices.

Table 3.4 Additives selection matrix

Additives	Dielectric permittivity	Ease of working in lab	Dispersion ability in polymer matrix
Carbon black **(Ketjenblack EC 600JD)**	Conductive properties and has the ability to polarized when homogeneously mixed with the polymer matrix.	Non-toxic Less of health and safety requirement at working temperature.	Has the ability to disperse under high shear and longitudinal flow.
Barium titanate	High (500-2500) - temperature dependent	Non-toxic Less health and safety requirement at working temperature	Very low– but new mixing process will be used

Table 3.5 Additives details

Additives	Size of particles	BET Surface Area (m^2/g)	Molecular Weight (amu)	Structure	Purity (%)	Suppliers
CB **(Ketjenblack EC-600 JD)**	Pellets (10-100 mm). Easily broken down by high shear forces into µm. 30-100nm (basic carbonic particles)	1400	12	Highly branched and fibroid like	99.4	Akzo Nobel, Inc
BT	100 nm	10	233.91	Cubic	99.9	IoLi Tec., Germany

Barium Titanate ($BaTiO_3$)

Barium titanate, $BaTiO_3$, [BT] is a well-known ferroelectric material with very high dielectric constant. Due to high permittivity and ferroelectric behavior, this additive has gained importance in a wide range of applications in electronics and electro-optical devices like thermistors, capacitors, microwave absorbers and many transducers. $BaTiO_3$ occurs in different forms. Among different forms, $BaTiO_3$ is widely used and investigated in tetragonal and cubical phases [167]. Properties of $BaTiO_3$ are highly dependent on particle size, purity and different phases of the material.

For the production or synthesis of $BaTiO_3$, both in the laboratory as well as in industry, there is involvement of an organic compound. An organic compound is usually introduced as chelating agent. $BaCO_3$ is formed during the process of formation of $BaTiO_3$ which may remain as an incomplete reaction [168] and make $BaTiO_3$ impure.

$$BaCO_3 + TiO_2 = BaTiO_3 + CO_2$$

$BaTiO_3$ with tetragonal distortion of the cubic perovskite structure was the first material used for a transducer. The presence of the very large Ba cation provides the ferroelectric distortion by replacing O_2^- ions in the anion lattice and Ti^{4+} occupies the octahedral interstices surrounded by O_2^-ions [169].

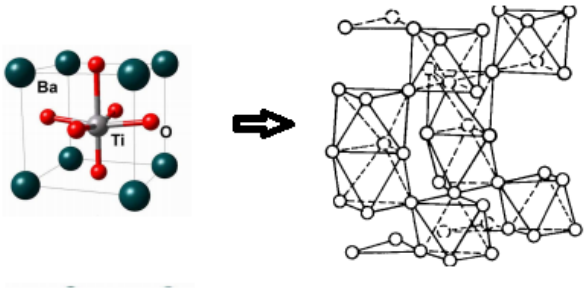

Figure 3.7 Hexagonal structure of $BaTiO_3$ [169]

$BaTiO_3$ has been used as an additive for different plastics for the improvement of dielectric permittivity [170]. For increasing the permittivity of polymer, it alone or in combination with other fillers can be used for the improving the dielectric properties of polymer composite [171].In this research, $BaTiO_3$ was mixed with other polymers under

different manufacturing conditions. The mechanical, morphological and electrical properties of prepared nanocomposite then investigated.

Carbon Black (CB)

Carbon black (CB) is an elemental carbon which might take a different form like a diamond, coke charcoal and graphite produced by incomplete combustion or thermal decomposition of hydrocarbon gases and liquids. During the process, aromatic oil or natural gas, (C_xH_y), undergoes incomplete combustion with oxygen (O_2) to produce fine particles of carbon (C) and other biproducts gases such as carbon monoxide (CO), hydrogen (H_2), carbon dioxide (CO_2) and water (H_2O).

$$C_xH_y + O_2 \longrightarrow C + CH_4 + CO + H_2 + CO_2 + H_2O$$

Material properties are dependent on particle size, porosity, surface area, and structure. CB may be of different types such as lamp black, channel black, furnace black, thermal black and acetylene black. Lamp black, channel black, and furnace black are produced by the incomplete combustion of hydrocarbons, whereas, the thermal decomposition technique is used for the production of thermal and acetylene black

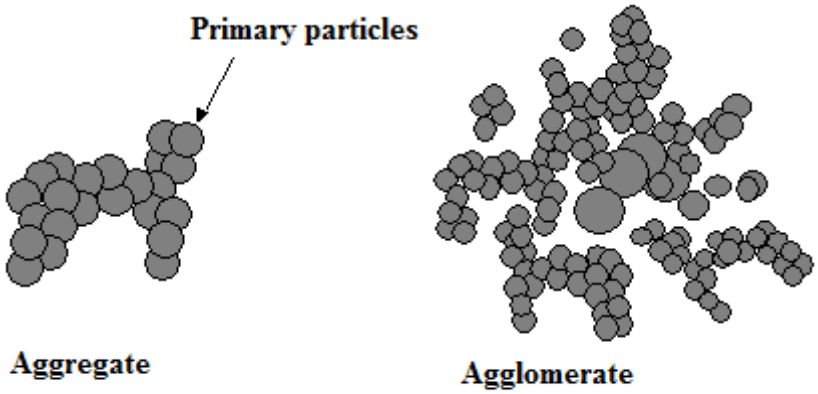

Figure 3.8 Structural unit of carbon black

Properties of CB are highly dependent on the manufacturing process. For example, CB manufactured by the acetylene black process due to thermal decomposition of acetylene has high crystalline structure and high conductivity. CB manufactured by this process can

be used for electrical conductive purposes. However, CB produced by lamp black process (by collecting carbon generated by burning oils) is used for ink sticks [172].

The primary unit of CB is called aggregate. Aggregates are held together by very small amount of force to form an agglomerate as presented in Figure 3.8. These agglomerates can easily be broken down by shear or compression forces or ultrasonic forces. CB is widely used as a conductive, reinforcement or dyeing filler material in different plastics, elastomers, adhesives, and paints. The conduction of CB is due to the hexagonal arrangement of the carbon atoms with sp^2 double bonding resulting in a delocalized pi system.

When a conductive filler like CB is added into the elastomeric matrix, the material does not conduct electricity up to the threshold amount which is determined by percolation theory [173]. Below the percolation threshold, composites manufactured are only able to form a dipole with some amount of leakage current. After percolation threshold, composites manufactured become conductive to direct current (DC). Moreover, this threshold amount is dependent on electrical properties of CB which in turn depends on shape orientation and dispersion of CB [174]. CB with elongated particle size requires a higher threshold and vice versa.

Various material additives were explored in order to augment mechanical properties and bulk surface chemistry with a view to subsequent optimization of the materials' polarization ability, and subsequent electro-mechanical performance characteristics. This process may include the embedding of polar polymers (e.g. poly anhydride) to optimize polarization ability, together with additional additives to optimize the materials actuation properties and electro-mechanical conversion efficiency; carbon nanopowder being one possibility. Selection of additives were concentrated on those materials which demonstrate an ability to enhance electrical, mechanical and electro-mechanical properties but which can be processed by conventional polymer processing methods.

3.3 Preparation for Composites

For the preparation of nano/micro-composite of SEBS and SEBS-g-MA with CB and BaTiO3, hot melt compounding was used because of its ability to provide high shear forces for homogenous mixing of additives with thermoplastic elastomers and better

mixing ability than solvent casting method. Table 3.6 provides the details for nano/micro-composite selection matrix.

Table 3.6 Experimental matrix for extrusion of different polymers/composites under different conditions

Experiment Number	**Polymers used**	**Additives used (wt. %)**	**Stage 1 processing – hot melt extrusion**		**Stage 2 processing Hot melt extrusion with haul off system without $scCO_2$**	**Associated Section in results and discussion**
			With $scCO_2$	**Without $scCO_2$**		
1	SEBS, SEBS-g-MA, PU and PEBAX	n/a	×	√	×	4
2	SEBS	CB (0%, 1%, 5%, 10%)	×	√	√	5.2
3	SEBS	BT ((0%, 1%, 5%, 10%)	×	√	√	5.3
4	SEBS-g-MA	CB (0%, 1%, 5%, 10%)	×	√	√	5.2
5	SEBS-g-MA	BT ((0%, 1%, 5%, 10%)	×	√	√	5.3 and 7.2
6	SEBS	n/a	√	×	×	6.2
7	SEBS	CB (0%, 1%, 2%, 5%, 10%)	√	×	√	6.3, and 8
8	SEBS-g-MA	CB (0%, 1%, 5%,)	√	×	√	6.5 and 7.3
9	SEBS-g-MA	BT ((0%, 1%, 2%, 5%, 10%)	√	×	√	6.4, 7.2 and 8

Extrusion of different composites was completed in series of processes which are described in detail in the following sections;

1. Materials Drying

Materials like SEBS-g-MA tend to absorb moisture because of the polarity of maleic anhydride (MA). Similarly, PEBAX and PU also tend to absorb moisture because of highly polar molecule present in them. So, prior to compounding it is essential to dry the materials due to the hygroscopic nature of polar molecules. Hygroscopic polymers tend to absorb moisture leading to degradation and processing difficulties. The drying conditions are shown in Table 3.7. These processing conditions are determined as suggested by the suppliers.

Table 3.7 Drying conditions of SEBS-g-MA related composite

Materials	Drying time	Temperature (°C)	Drying Type
PEBAX 7733	12 hours	60	Desiccant
Pellethane 75D	12 hours	110	Desiccant
SEBS-g-MA	12 hours	50	Desiccant
SEBS-g-MA+ CB	12 hours	50	Desiccant
SEBS-g-MA+ BT	12 hours	50	Desiccant

2. Twin screw compounding

Material blending was carried out in a corotating twin-screw extruder (extruder 1) with L/D ratio of 25:1. Samples of SEBS and SEBS-g-MA with different percentages of $BaTiO_3$ (1%, 5%, and 10%) and CB (1%, 5%, and 10%) were subsequently produced. Extrusion was carried out at a screw speed of 70 revs/min, torque between 15 to 10 Nm, die pressure between 34.5-69 kPa. The temperature profile was maintained from 176 to 240 °C, 140 to 200 °C, 140 to 180 °C and 180 to 210 °C over 6 zones for all SEBS composites, SEBS-g-MA composites, PEBAX and PU respectively.

For all supercritical assisted extrusion from experiment 6-10, during the extrusion process, the supercritical fluid carbon dioxide was passed through the mixing section. For experiment 6, the processing was carried out at a pressure of 5.50, 6.90 and 8.27 MPa and flow rate at 2.5 ml/min. For all other experiment, the pressure and CO_2 flow rate were maintained at 8.27 MPa and 2.5ml/min respectively. All other parameters were remained constant.

Some fraction of polymer processed from experiment 6 was directly used for characterization to know the direct effect of $scCO_2$ on polymer properties as highlighted in Chapter 6.1 whereas all other composites were further processed using extruder 2 before characterisation.

For both cases (with or without supercritical fluid), the extruded material from extruder 1 was chopped into pieces and fed into a separate corotating twin screw extrusion machine

(extruder 2) of L/D of 25:1 with haul off technique using a gravimetric feeder. The extrudate was then passed through a roller system running at a constant speed of 0.5rev/min in order to produce a constant thickness sheet. Processing was carried out with a screw speed of 70 rev/min, torque between 25% to 50% and die pressure between 27.5-48.3 kPa. The temperature profile was maintained from 176 to 240 °C over 6 zones for all SEBS composites and 140 to 200 °C over 6 zones for all SEBS-g-MA composites.

3.4 Materials Characterisation

Thermal, mechanical, morphological and electrical characteristics differ from one thermoplastic elastomer to another based on structure, crystallization properties, the presence of polar and non-polar groups and the ratio of soft and hard blocks within thermoplastic copolymers.

Thermogravimetric and differential scanning calorimetry were performed to see the thermal changes, morphological changes, microphase separation, the interaction of additives with polymers and degradation changes in elastomers/composites during different processing conditions.

Mechanical properties such as tensile and cyclic tests were carried out to observe the mechanical changes as well as hysteresis losses upon addition of fillers as well as processing conditions to elastomers/composites. Dynamic mechanical analysis was performed to analyze the viscoelastic behavior, structural change, and polymer additive interaction under different processing conditions.

Morphological characterization such as Fourier transform infrared spectroscopy was carried out to identify chemical changes and polymer additive interaction. In addition to identifying the dispersion of additives in polymer matrices, scanning electron microscopy and transmission electron microscopy were performed.

Finally, dielectric analysis was performed to observed polarization phenomena, dielectric loss behavior, conduction behavior, and relaxation phenomena

3.4.1 Thermogravimetric Analysis

Thermal degradation profile and filler contents in different composites were studied using thermogravimetric analysis (TGA) using TA instrument Q50. The sample was heated

from 25 °C at 10 °C/min up to 500 °C in a nitrogen atmosphere. Change in mass over temperature was analyzed based on the curve obtained from the TGA instrument for different nanocomposites.

3.4.2 Modulated Differential Scanning Calorimetry

Modulated differential scanning calorimetry (MDSC) of all composites were carried with TA instrument 2000. The heat capacity was calibrated using sapphire, while the temperature and baseline were calibrated using indium. An oscillation period of 60 seconds and amplitude of ±0.47 °C was used in modulated heating and cooling experiments. About 10 mg of sample was encapsulated and hermetically sealed in Aluminium pans for all sample types. Sample was then subjected to equilibration from 35 to –80 ºC followed by heating at 3 °C/min to 180 ºC. At the beginning of each heating run, materials were held isothermally for 3 min to obtain thermal stabilization between the reference pan and sample pan. TA software for MDSC was used for recording, analysis, and deconvolution of the signals. The least square method was used to smooth all the curves for better analysis. The level of smoothing was selected within the range of 3 ºC to give minimum distortion and no shift of peaks. Thermal analysis of each composite type was performed using the total heat flow curve and the derivative of reversible specific heat capacity curve. The temperature derivative of reversible specific heat capacity was used to measure glass transition because it is reported to show high sensitivity to the process of heat flow during glass transition [175, 176].

3.5 Mechanical Characterization

Mechanical characterization was performed to evaluate the mechanical performance of thermoplastic elastomers and their composites to find the mechanical performance of elastomers/composites including but not limited to flexibility under the large extension, viscoelastic properties, and mechanical loss tangent over temperature and structural changes of polymers upon addition of fillers. In this work, tensile testing and dynamical mechanical analysis are the two major mechanical characterization techniques used.

3.5.1 Tensile Testing

The mechanical analysis was carried out using a Zwick Tensile Machine (Z005) with 2.5 kN capacity load cell. ASTM D638 type I tensile bars from all composites were cut from the sample extruded from a roller system and tensile and cyclic testing was carried out. During the test, the grip speed was held constant at 500mm/min. In both cyclic and tensile testing, samples are extended till 200% strain. Different parameters like average Young's modulus, hysteresis loss, total energy etc. were calculated from five specimens of each sample types unless stated to find the mechanical compliance, the stiffness of nanocomposites as well as compatibility of additives to polymers

Cyclic testing was performed on all composite samples. Figure 3.9 shows the first cyclic curve of the thermoplastic elastomer. The extension and relaxation of the elastomer occurs with combination of sliding and non-sliding action between hard and soft block is shown in Figure 3.9. Similarly, Figure 3.10 shows the typical cyclic test for five cycles of thermoplastic elastomers (SEBS) measured at an extension of 200%.

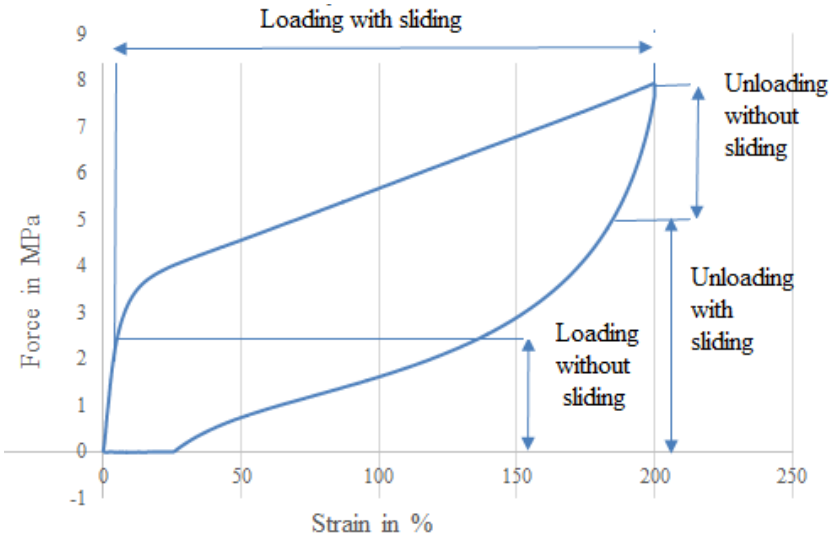

Figure 3.9 Loading and unloading cycle of thermoplastic elastomer.

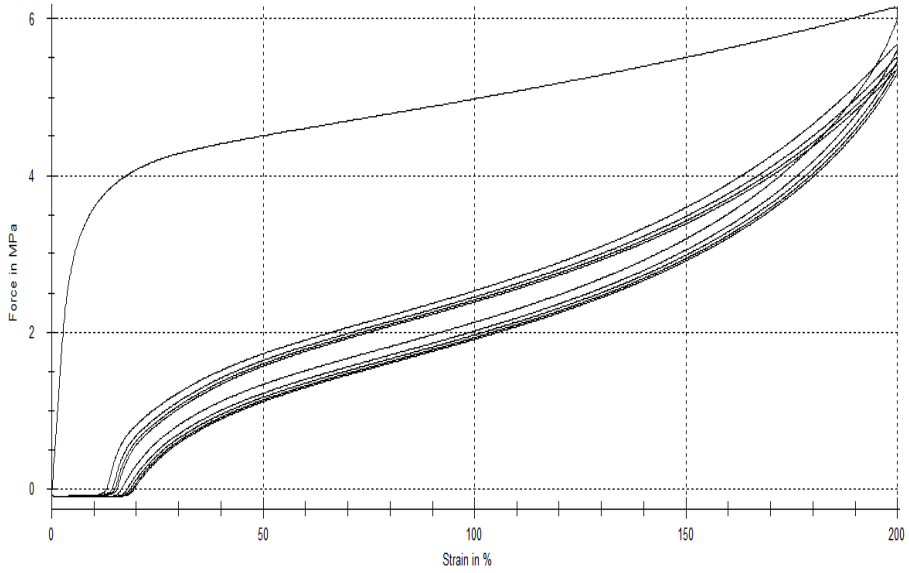

Figure 3.10 Typical hysteresis curve of thermoplastic elastomer (SEBS)

Total hysteresis loss (area under the hysteresis loss curve as shown in Figure 3.9) and total elastic energy (area under the curve during extension minus area under the hysteresis loss curve as shown in Figure 3.9) present were measured using work curves for each cycle. The total amount of energy required for the composite to extend by 200% was divided into two types of energy; (i) elastic energy and (ii) loss energy as shown in Figure 3.11.

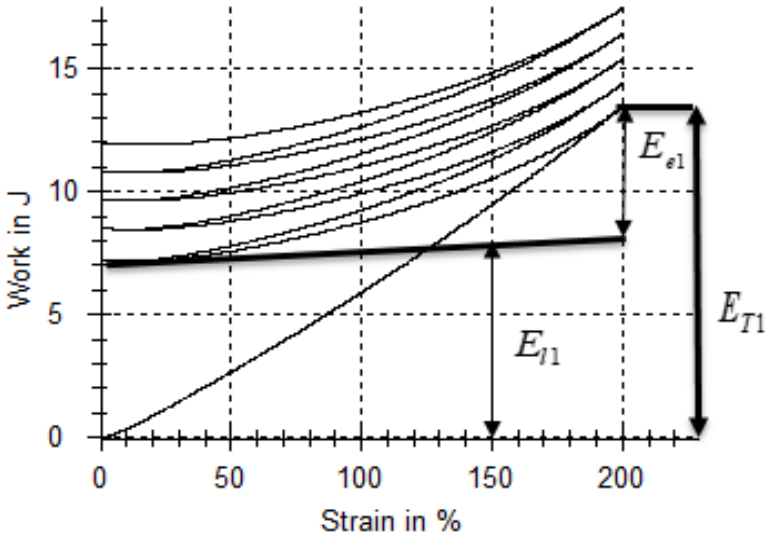

Figure 3.11 Total energy (E_{T1}) divided into elastic energy (E_{el}) and loss energy (E_{l1}) for SEBS

$$E_{Ti} = E_{ei} + E_{li}$$ Equation 3.1

Where, E_{Ti}, E_{ei} and E_{li} are total energy applied, elastic energy present in the material after reloading and loss energy or hysteresis loss of thermoplastic elastomer respectively for the cycle i.

The term loss factor was used to measure the shape memory properties of nanocomposites under large extension. The loss factor can be directly defined as presented in Equation 3.2.

$$LF_i = E_{li} / E_{ei}$$ Equation 3.2

3.5.2 Dynamic Thermal Mechanical Analysis

Dynamic mechanical analysis (DMA) was carried out on a TA Instruments DMA 800 to evaluate the viscoelastic properties of the composite. The experiment was carried out in a ramp temp/multi frequency mode at 16 μm extension in the range of 25 to 140 °C at a 1Hz frequency and a heating ramp of 3 °C/min. Samples were prepared by cutting in perpendicular as well as parallel directions to an extruded sheet to the axis of rotation of extruder screw.

3.6 Dielectric Measurement

Dielectric characterization of flat samples of thickness 1-2 mm was carried out using a Solartron 1260 impedance analyzer with a 1296 2A dielectric interface. The Solartron 1260 impedance analyzer is a fast, accurate and repeatable impedance measurement technique which gives information about the electrical characteristics for a wide range of materials including plastics, ceramics, ion conductors, dielectric, piezo/ferroelectrics and other materials with an impedance range of more than 10^{14} TΩ across a frequency range of 10 μHz to 10 MHz. In addition, a Solartron 1296 2A sample holder was used to facilitate measurement of the solid samples; which consisted of two parallel electrodes, both of 40 mm diameters, between which the material was placed and a 5 Vrms alternating voltage applied. A standard procedure as stated in datasheet of Solartron 1296 dielectric interface was applied for finding all electrical parameters unless stated in results and discussion. A different but complimentary procedure was used for Chapter 5.

Dielectric measurement over a range of temperatures for selected samples of thickness between 1-2 mm was carried out using an HP 3652-50 LCR Hitester impedance analyser from 40 °C to 120 °C. In addition, a custom-made sample holder was used to facilitate the measurement of the solid samples; which consisted of two parallel electrodes, both of 2 cm diameter, between which the material was placed and a 1 Vrms alternating voltage from 1 kHz to 1 MHz applied. For this experiment, samples were stored at room temperature for 2 months and measurement was carried out. The results carried out using this technique are presented in Chapter 7.

3.7 Morphological Analysis

3.7.1 Scanning Electron Microscopy

Extruded samples (SEBS, SEBS and SEBS-g-MA with 10 wt.% of BT) were submerged in liquid nitrogen and were cryo-fractured to visualize the distribution of additives in polymer matrix along the thickness (traverse cross section area). Morphological studies were carried out in TECAN scanning electron microscopy (SEM) at 20 kV. Different regions were selected and element mapping was performed to get the information about the filler distribution profile. Similarly, SEBS extruded under supercritical fluid pressure were analyzed without reprocessing to see the porosity affects.

3.7.2 Transmission Electron Microscopy

Different composite samples were carefully sliced and very thin samples obtained by slicing were transferred to copper grids of 400 mesh sizes. Then, 200 kV FEI-Tecnai G2 20 S-TWIN High-resolution Transmission Electron Microscope was used for the analysis of additive dispersion in thermoplastic composites processed under different conditions. Bright-field transmission electron microscopy (TEM) images of composites were obtained at different magnification from 1.7kx-19kx at 80 kV. ImagJ software was used for further analysis to enhance the desired region of the sample where required.

3.7.3 Attenuated Total Reflectance-Fourier Transfer Infrared Spectroscopy Studies

Polymer-additive interaction in the different composites was studied using attenuated total reflectance-fourier transfer infrared spectroscopy (ATR-FTIR). Infrared spectra of all composites were obtained with a VARIAN 600 ATR-FTIR. ATR-FTIR spectroscopy was carried out at room temperature on clean solid extruded flat samples with a resolution of 4 cm^{-1}. All data was collected between 600 cm^{-1} and 4000 cm^{-1} with an average of 32 scans.

3.8 Dielectric Analysis under Uniaxial Strain

Dielectric polarization, loss tangent and relaxation phenomena under various uniaxial strain conditions of different thermoplastic composites were measured using the set up as shown in Figure 3.12. A Solartron 1260 impedance analyzer with a 1926 A dielectric interface was used to provide the AC electrical signal from 0.1Hz to 1 MHz and measure the response of the sample under 0.25%, 0.5%, 1%, 2.5% and 5% uniaxial strain provided by Zwick Roell Z005 tensile test machine. The strain of sample was carefully controlled using Text Expert II software.

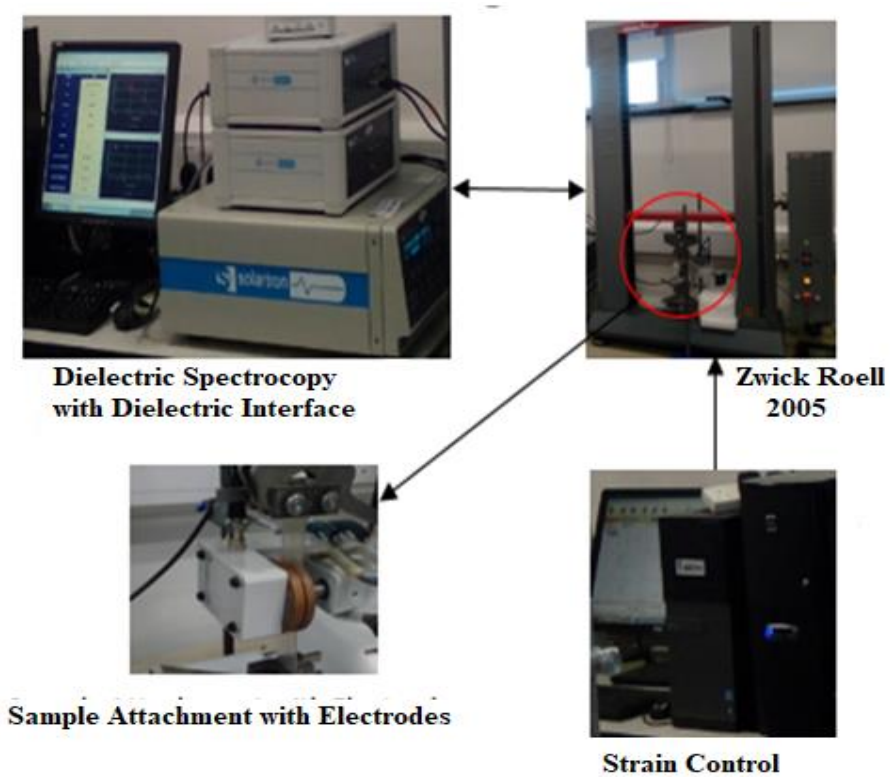

Figure 3.12 Dielectric analysis set-up under strain condition.

Chapter 4

4 Dielectric Analysis of Suitability of Selected Dielectric Thermoplastic Elastomers for Energy Harvesting and Civil Infrastructural Applications

4.1 Introduction

A primary objective (described in Chapter 2) of understanding polarization phenomena of different thermoplastic elastomers manufactured using the extrusion technique is highlighted in this chapter. A number of thermoplastic elastomers were selected for further analysis to evaluate the suitability of dielectric elastomers for capacitive energy harvesting applications and stress/strain sensing applications. These selected thermoplastic elastomers are well known for their flexibility because of their morphology. The morphology of these polymers consists of the hard and soft domain. The glass transition of the soft domain is lower than room temperature, whereas glass transition temperature of the hard block is higher than room temperature. Hence, the hard block can easily slide over the soft domain at room temperature. For flexible capacitive energy harvesting and stress/strain sensing applications, the operating temperature is always higher than the glass transition of a soft block of thermoplastic elastomers to maintain the flexibility of these polymers. However, in some elastomers, the movement of unreacted ions, movement of rubbery phases as well as DC bulk conductivity within an elastomer at low frequency hinder their application as capacitive energy harvesters.

Dielectric analysis involving dielectric permittivity, relaxation processes, conduction behavior of polyurethanes (PU), polyether amide block copolymer (PEBAX), poly(styrene-ethylene/butylene-styrene) (SEBS), and poly(styrene-ethylene/butylene-styrene)-grafted -maleic anhydride (SEBS-g-MA) is presented in this chapter.

4.1.1 Dielectric Studies

The real dielectric permittivity, loss tangent, real electric modulus and imaginary loss modulus of different thermoplastic elastomers measured at 20℃ is presented in Figure 4.1 The dielectric relaxation process is highly influenced by the temperature of measurement and the glass transition temperature.[177] At 0.2 Hz, the real dielectric permittivity of PU and PEBAX is very high and found to be 12.3 and 22.57 respectively. This high real dielectric permittivity of these two polymers is attributed to highly polar segmental

rotation of cyanate, diol, and oxide groups in PU [178, 179] and oxide and amide group (with bounded water) in PEBAX

However, the value decreases exponentially with increase in frequency and reaches 8.6 and 6.78 at 10 Hz for PU and PEBAX, respectively. This exponential decrease of real dielectric permittivity is the relaxation of dielectric permittivity of the crystalline structure within a polymer and can be represented by the real electric modulus. This behavior is found to relax at 1 Hz and 10 Hz for PU and PEBAX respectively. The dielectric permittivity measured for SEBS and SEBS-g-MA remains constant over 1 Hz to 10^6Hz and is found to be around 2.7 for both thermoplastic elastomers.

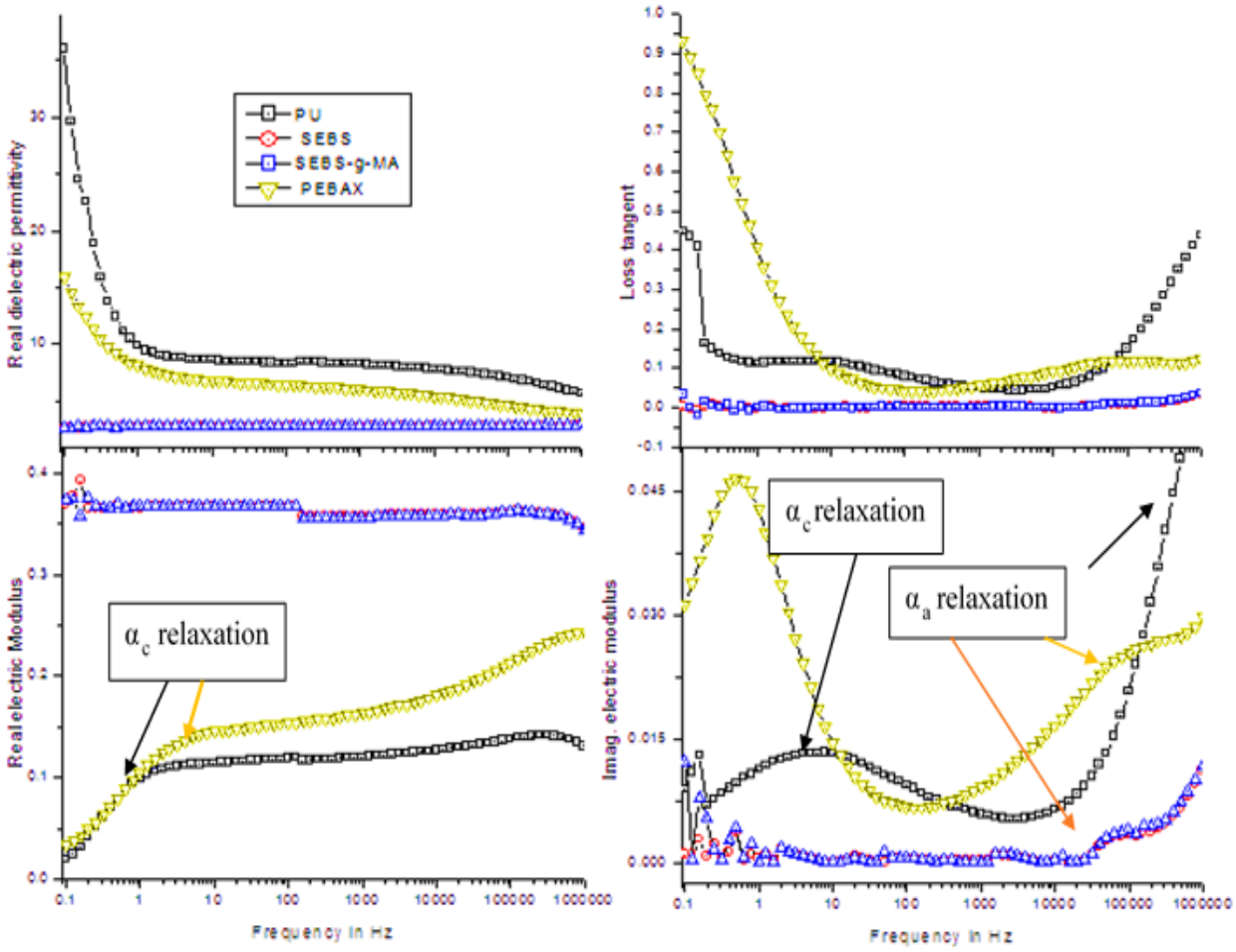

Figure 4.1 Real dielectric permittivity, Dielectric loss, real electric Modulus and Imaginary electric modulus of polyurethanes, SEBS, SEBS-g-MA, and PEBAX

From the dielectric loss graphs observed from Figure 4.1, PU and PEBAX show a high dielectric loss tangent at low frequency making them unstable for energy harvesting and other capacitive applications. For capacitive applications, materials should have a dielectric loss below 0.1. However, PU and PEBAX have a dielectric loss tangent of above 0.2 and 0.8 at low frequency (<1Hz) respectively making them unstable for such applications. This high dielectric loss is attributed to mobile unreacted species, bounded water, bulk ion conductivity of elastomers increased due to presence of polar soft blocks), and microstructural crystalline phases present in PU and PEBAX [179] Styrene-based thermoplastic elastomers, on the other hand, SEBS and SEBS-g-MA possess very low dielectric loss tangent at all frequency range from 0.1 Hz to 10^6 Hz due to lack of nanostructured domains, and highly nonpolar and hydrophobic ethylene-butylene (EB) soft blocks. In addition, high tangent loss of the material also signifies energy loss due to heating effects as well as the fast transfer of charges in polymers making them inappropriate for capacitive energy harvesting applications from mechanical sources under DC biased conditions. Many authors state that different mechanical energy sources such as sea waves involve a low complex frequency (<0.5Hz) profile [180, 181].

A broad crystallization relaxation of PU was observed from 1 Hz to 100 Hz as also shown in imaginary electric modulus of Figure 4.1. However, a sharp peak around 0.5 Hz was observed in PEBAX which is also similar to Maxwell-Wagner-Sillar (MWS) polarization. This might be due to the zwitterion effect of the N-H bond present in the imide group as well as the mobile oxide group which occurs specifically due to low glass transition (ca. -75℃) of a soft block present in PEBAX. Similar results have been reported by several authors when the experiment was carried out above the glass transition temperature of polar molecules present in polyurethane and nylon polymers [179, 182]. The zwitterion effect of N-H bonds in PEBAX leads to conduction of charges at low frequency under humid conditions. The MWS effect is also the result of the separation of charge carriers between amorphous and crystalline structures at the mesoscopic scale [182]. The MWS relaxing frequency (0.5 Hz) is also considered as the AC conduction set frequency in most disordered solids. A slight difference in electric loss modulus was observed between SEBS-g-MA and SEBS. Around 0.2 Hz, like PU, a slight loss modulus relaxation was observed in SEBS-g-MA because of the presence of a highly polar group MA. This effect of MWS polarization is completely absent in SEBS. The absence of MWS relaxation and

crystalline peaks on SEBS based triblocks was attributed to low crystallinity and lack of mobile polar chains compared to PU and PEBAX [183].

At high frequency, around 10^5 Hz, cooperative relaxation occurs in SEBS and SEBS-g-MA. This relaxation behavior starts much earlier around 1000 Hz for PEBAX and 20000 Hz for PU. The difference in glass transition temperature of soft blocks present in these elastomers has led to different relaxation frequencies between these elastomers [177]. In addition, the electric modulus (M") showed relaxation of PU and PEBAX chains with some conductivity as well as crystal relaxation at low frequency due to the polar nature of molecules and large crystal sizes present in PU and PEBAX. These relaxations are completely absent in non-conducting polymers like SEBS and SEBS-g-MA due to low conductive behaviour and small domain sizes. This result was found similar to other literature [176].

4.1.2 Conclusion

In this work, the total dielectric investigation of extruded PU, PEBAX, SEBS and SEBS-g-MA was carried out to evaluate the feasibility of these polymers as capacitive energy harvesters at 20℃ for different low-frequency mechanical sources. Results show that PU and PEBAX have high real dielectric permittivity at low a frequency (<1Hz) because of their high polarization capability compared to low polarizing thermoplastic elastomers like SEBS and SEBS-g-MA. However, the high loss tangent (>0.2) at low-frequency conditions (<1Hz) present in PU and PEBAX does not allow them to be used as capacitive energy harvesting applications and flexible capacitors. In addition, high imaginary electric modulus confirms PEBAX has DC conducting characteristics at very low frequency making them lossy materials for energy harvesting application. Hence, the characteristics of these polymers (PU and PEBAX) need additional studies for their uses in energy harvesting applications. However, based on the dielectric nature, PU and PEBAX show an advantage over SEBS and SEBS-g-MA for strain/stress sensors for civil infrastructure. On the other hand, SEBS- SEBS-g-MA are highly flexible because of their superior morphology and addition of conductive fillers in SEBS and SEBS-g-MA will easily overcome the limitation of their conductivity for stress/strain sensing applications Similarly, the low loss tangent of SEBS and SEBS-g-MA makes them suitable for capacitive energy generators if the dielectric permittivity of these thermoplastic

elastomers remains constant or increases on stretching. The low dielectric permittivity of these polymers must be enhanced for improved power generation using capacitive methods. Permittivity enhancement also adds to advantages for strain sensing of civil infrastructure.

Chapter 5

5 Conventional Extrusion Manufacturing and Characterization of Dielectric Thermoplastic Composites for Electromechanical Applications

5.1 Introduction

A detailed scientific understanding and evaluation of the thermal, mechanical, electrical and morphological modifications of various additive types in selected thermoplastic elastomers based on results of Chapter 4 are discussed in this chapter. A conventional industrial standard processing method (such as extrusion) was used for the manufacturing of different composites types with the criteria that the aims and objectives of this work are accomplished. Two types of fillers (conductive and dielectric) were used in this study.

5.2 Conductive Filler (CB) Based Thermoplastic Composites

5.2.1 Introduction

For SHM of civil infrastructure as well for artificial muscle applications, conductive composites were widely studied. Most of the interesting characteristics of these composites present for stress/strain sensing and artificial muscle applications are mainly due to superior electrical conductivity and dielectric around the percolation threshold. However, in addition to electrical changes, mechanical changes (stiffness, shape memory properties), thermal changes and morphological changes also play an important role for the composites that caters for the needs of stress/strain sensing applications. This section describes the detailed understanding of the electrical, thermal, morphological and mechanical behavior of polymers with the addition of conductive fillers like carbon black (CB) manufactured using twin screw extruder.

5.2.2 Dielectric Studies

The real and imaginary dielectric permittivity calculated without using any correction factor for SEBS and SEBS-g-MA composites from the Solartron 1296 at a frequency of 1 kHz is shown Table 5.1. These results have not been computed using a correction factor. The dielectric permittivity obtained from polymer composites was systematically smaller by a factor of approximately 100 compared to that reported in the literature [84]. A

correction factor was therefore applied by measuring the permittivity of the air at a distance of 1.5-2 mm (depending on thickness of the sample) between two electrodes which is believed to have an absolute value of 1 from 1 Hz to 1 MHz. The correction factor calculation for 1 Hz was calculated to be 72. This correction factor is used to calculate a reference of permittivity of air which is further modified from 72 to 82 for curve smoothing in Figure 5.1 and Figure 5.2

Table 5.1 Dielectric permittivity of SEBS and SEBS-g-MA measured Solartron 1296 at a frequency of 1 Hz without using a correction factor

Additives	**Dielectric constant of SEBS**		**Dielectric constant of SEBS-g-MA**	
	Real ε' (10^{-2})	**Imaginary ε'' (10^{-2})**	**Real ε' (10^{-2})**	**Imaginary ε'' (10^{-2})**
Pure	3.47	0.017	4.5	0.025
CB-1%	4.17	0.024	5.37	0.044
CB-5%	6.22	0.075	6.65	0.076
CB -10%	8.30	0.86	9.71	0.34

The dielectric permittivity calculated for SEBS and SEBS-g-MA composites from the Solartron 1296 at a frequency of 1 Hz at room temperature corrected with correction factor of 72 is shown in Table 5.2. Similarly, the real dielectric permittivity and imaginary dielectric permittivity of SEBS and SEBS-g-MA composites over a range of frequencies corrected with correction factor of 82 is shown in Figure 5.1 and Figure 5.2 respectively.

Table 5.2 Dielectric permittivity of SEBS with Carbon black (CB) using a correction factor

Additives	**Dielectric constant of SEBS**		**Dielectric constant of SEBS-g-MA**	
	Real ε'	**Imaginary ε''**	**Real ε'**	**Imaginary ε''**
Pure	2.5	0.012	3.24	0.018
CB-1%	2.99	0.017	4.45	0.032
CB-5%	4.47	0.054	5.45	0.055
CB -10%	6.82	0.706	7.00	0.250

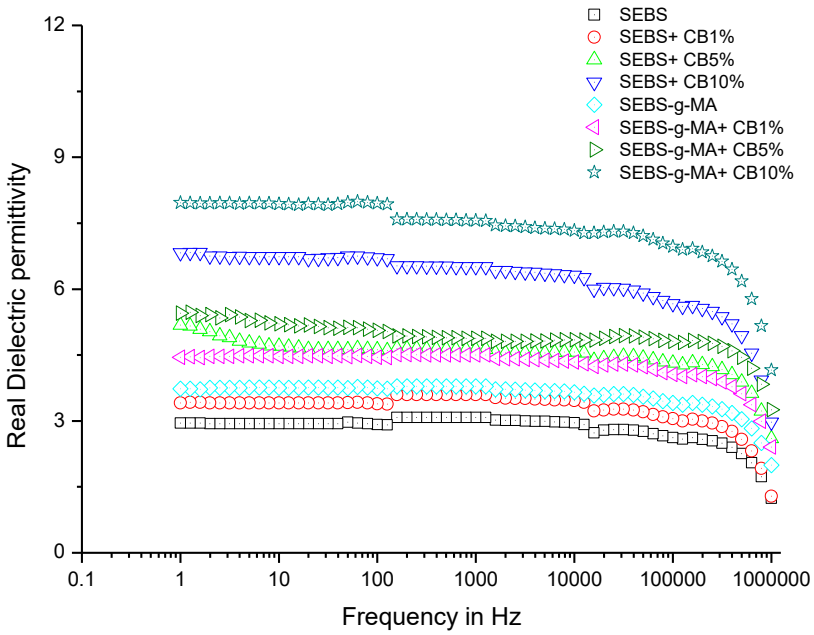

Figure 5.1 Real dielectric permittivity of SEBS and SEBS-g-MA composite with different percentages of CB

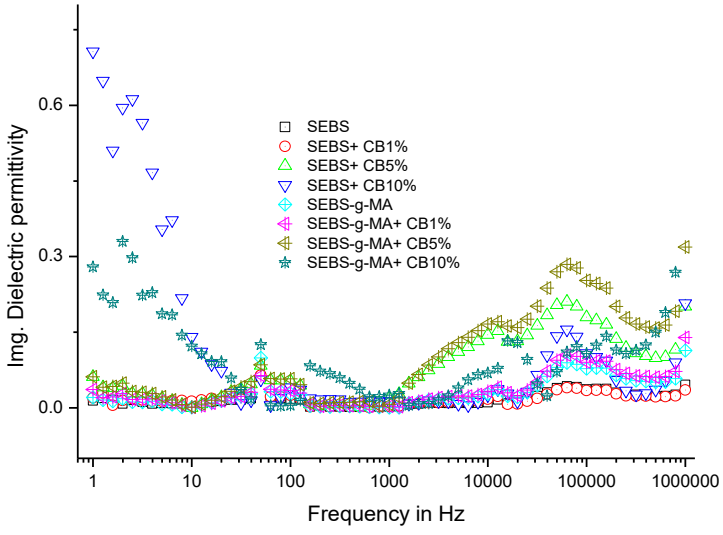

Figure 5.2 Imaginary dielectric permittivity of SEBS and SEBS-g-MA composites with different wt .% of CB

The real dielectric permittivity graphs for SEBS-CB and SEBS-g-MA-CB composites are comparable to the work of Stoyanov [84]. However, the difference in manufacturing technique of composites preparation (hot melt extrusion Vs. solvent casting method), the dielectric measurement techniques, and samples thickness lead to the relative change in permittivity from the addition of CB is found to be different than in Stoyanov's work. Stoyanov reported the dielectric permittivity of SEBS to be 27 at 100 Hz upon addition of 4 vol % (7.6 wt. %) of carbon black, whereas, the dielectric permittivity of SEBS was found to be only 7.5 at 100 Hz upon addition of 10 wt. % CB in this work.

As is self-evident, CB tends to improve the dielectric permittivity of the polymer matrix to some threshold as predicted by percolation theory [173]. Orientation and dispersion of CB in the polymer matrix, including the shape of CB, defines the threshold value of nanocomposite required for conduction [174]. When the amount of CB is below the percolation threshold, primary particles of CB are separated from each other. In this case, the nanocomposite becomes highly resistive to direct current; interfacial polarization exists between the polymer matrix and carbon nanoparticles resulting in an increase in dielectric permittivity with an increase in the amount of CB [184-187]

The imaginary dielectric constant of nanocomposite increases drastically with increase in higher filler materials even at low frequency. This phenomenon can further be analyzed using the time-harmonic Maxwell's equation as shown in Equation 5.1,

$$\nabla \times \bar{H} = J + j\omega D \qquad \text{Equation 5.1}$$

Where ∇ is the del operator, D is the electric flux density, $\bar{H}$ is magnetic field strength, J is the current density. J can further be divided into two parts, impressed electric current density J_i and aforementioned conduction current densities J_c due to the application of electric field.

$$\nabla \times \bar{H} = J_i + J_c + j\omega D \qquad \text{Equation 5.2}$$

If σ_s is the conductivity of nanocomposites, then the J_c can be written as

$$J_c = \sigma_s E \qquad \text{Equation 5.3}$$

Then, Equation 5.3 can be written as

$$\nabla \times \bar{H} = J_i + j\omega\varepsilon^{'}(1 - j\frac{\sigma_S}{\omega\varepsilon^{'}} - j\frac{\varepsilon^{'}}{\varepsilon^{''}})\bar{E} \qquad \text{Equation 5.4}$$

The last two terms in Equation 5.4 contribute to total loss of nanocomposites and the total imaginary dielectric permittivity of nanocomposites during measurement. The first term, $\sigma_s/\omega\varepsilon^{'}$, describes the loss of energy due to the collision of electrons, highly dominant in conductor and semiconductors. Moreover, it is more prominent in low-frequency conditions. The significant imaginary dielectric value obtained from an experiment at the high amount of CB (10 wt. %) suggests that CB nanocomposites have high dielectric permittivity near its percolation threshold, but it comes at the expense of a high dielectric loss. This phenomenon can be directly compared with semiconductor materials. In semiconductors, the leakage current increases with increase in temperature as the result of more electrons present in the valance band. However, this phenomenon will not remain the same when the frequency is increased [188]. Due to this conduction mechanism present in nanocomposites with conductive fillers, they tend to have very low dielectric strength when compared with nanocomposites with dielectric fillers [115]. In addition, high dielectric loss at a low frequency of nanocomposite at high CB content also suggests fast discharge of charges present in the materials in the form of conduction or heat. The high dieelctric loss property further imparts the issue related to such materials for charge storage devices applications such as supercapacitors and capacitive energy generators from mechanical sources at low frequency.

The last term, $\varepsilon^{'}/\varepsilon^{''}$, is dominant in all CB based dielectric elastomers, which describes high dielectric nature of such nanocomposites. In addition, it also demonstrates that the conduction behaviour is dependent of frequency or AC current with no actual movement of electrons (as in DC current) above 1Hz. The conductivity of CB based dielectric elastomers is shown in Figure 5.3. The total AC conductivity is the result of electrons movement (DC conductivity) and dielectric polarization. However, in the case for all composites, the DC current is much less resulting only polarization effect with the addition of CB. This result confirms elastomer needs further addition of CB (>10 wt. %) to attend its percolation threshold.

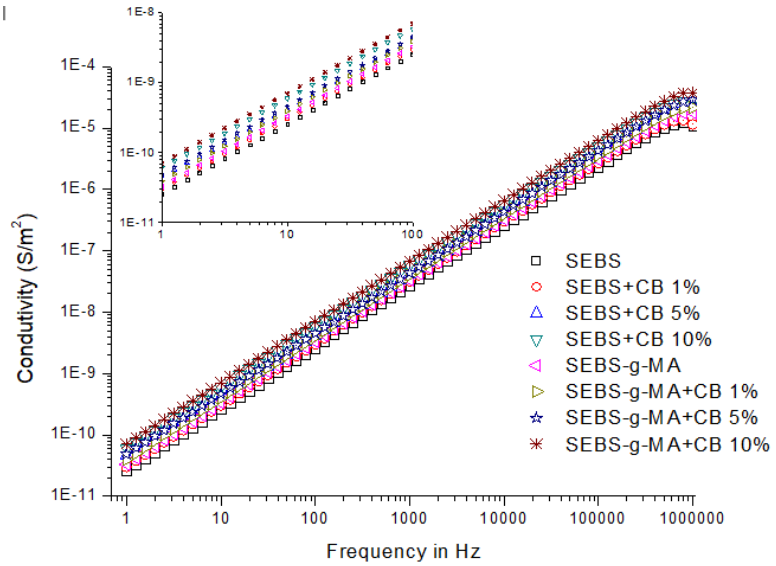

Figure 5.3 Conductivity of SEBS and SEBS-g-MA with different wt. % of CB

Furthermore, at high frequency, dipoles of dielectric materials will not have sufficient time for polarization and depolarization. This phenomenon leads to a loss in the dielectric as heat and motion at high frequency. Such behavior was also observed in CB nanocomposites at all concentration due to imbalance charge distribution on CB and polymer interface which are also known as space charge of interfacial polarization.

5.2.3 Mechanical Properties

Figure 5.4 and Figure 5.5 show the tensile profile of SEBS and SEBS-g-MA with CB in the parallel direction to extrusion respectively. The stress was measured up to 200 % strain for all samples. No breakage occurred until 200% for all samples. In all-composite types, curves consist of a linear region or elastic region, necking point, drawing region, and the again linear region for all concentrations of modifiers. The stretching of the necking region is also known as natural draw ratio, it is hardly seen in both composite types in this work. However, it prevails in most experiments as suggested in the literature [189]. The observation of the necking region of an elastomer in the tensile graph is a function of processing parameter and prevails depending on the process used to manufacture the samples. Unlike glassy materials, in most of the thermoplastic elastomers, the sample does not break after necking but continues to extend. It is due to this fact that necking produces

a stronger microstructure leading to the higher amount of energy or stress required for breakage [189].

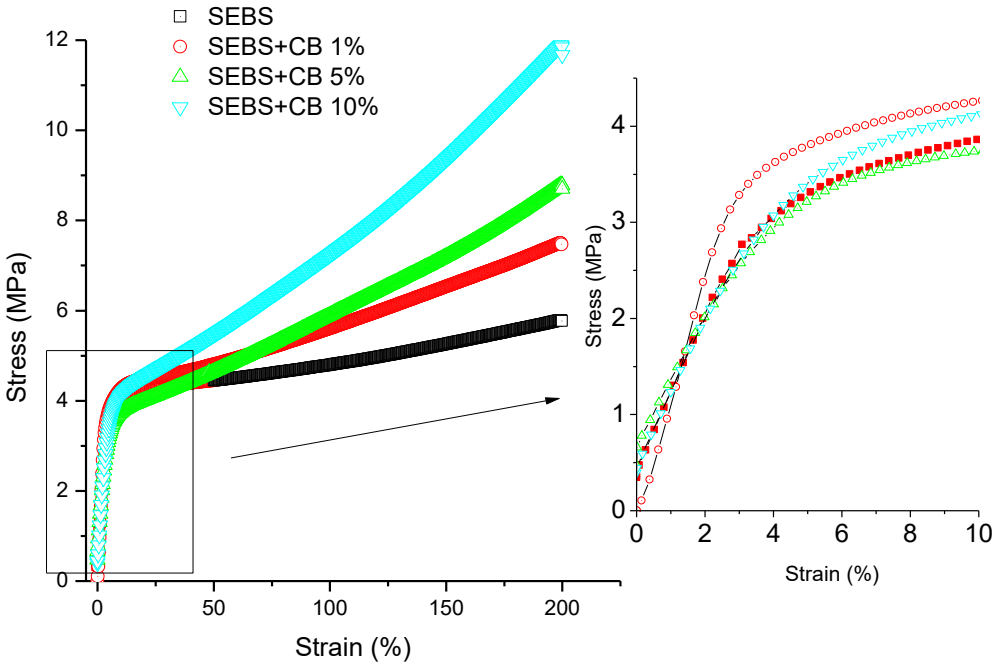

Figure 5.4 Tensile properties of SEBS/CB composites measured in the parallel to extrusion

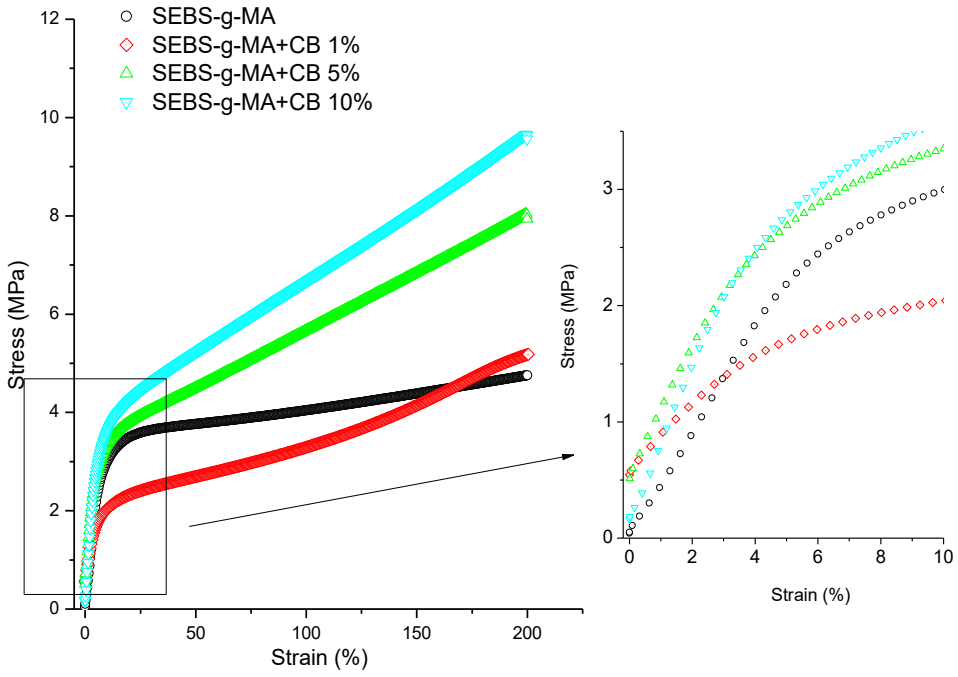

Figure 5.5 Tensile properties of SEBS-g-MA/CB composites measured in the parallel to extrusion.

The modulus of resilience is defined as the energy absorbed by the material below its yield point. The result showed negligible difference in resilience with the addition of CB in SEBS, however, the modulus of resilience was found to be decreased upon addition of 1% of CB in SEBS-g-MA, as shown in Table 5.3.

Table 5.3 Average modulus of resilience and modulus of roughness for five samples of each composite type.

Composite	**In Parallel direction to the extrusion**	
	Average modulus of resilience (MPa)	**Average modulus of toughness at 200 % strain (MPa)**
SEBS	44.83	912.76
SEBS+CB 1%	50.44	1074.86
SEBS+CB 5%	41.57	1144.87
SEBS+ CB 10%	48.93	1434.4
SEBS-g-MA	47.79	748.35
SEBS-g-MA+CB 1%	34.56	649.28
SEBS-g-MA+CB 5%	57.35	1066.23
SEBS-g-MA +CB 10%	59.11	1257.92

The energy observed between yield point and breakage defines the modulus of toughness of the material. Table 5.3 depicts the modulus of toughness which increases with an increase in the amount of CB for both polymer matrices when measured to 200% strain. The relative change in modulus of toughness can also be observed from Figure 5.4 and Figure 5.5. From Figure 5.5 and Table 5.3, SEBS-g-MA with 1 wt.% of CB showed low toughness compared to pure SEBS-g-MA, but the result might be different if these nanocomposites are extended up to the breakage point as the slope gradient of SEBS-g-MA with 1 wt. % of CB are higher after yield point of virgin SEBS-g-MA which is illustrated in Table 5.4.

Table 5.4 Young's modulus of SEBS and SEBS-g-MA with different percentage of CB

Polymer matrix with wt. % of additives	Secant Young's modulus (Y) of nanocomposite different strain (MPa)							
	1%		50%		100%		150%	
	Y	% Δ	Y	% Δ	Y	% Δ	Y	% Δ
SEBS	110.0±17.7	NA	8.8±0.44	NA	4.8±0.26	NA	3.5±0.22	NA
SEBS + CB 1%	118.5 ±26.7	9.6	9.6 ±1.54	9.0	5.6±0.57	16.7	4.4±0.23	25.7
SEBS + CB 5%	124.0±20.7	12.7	9.3±1.82	5.7	5.9 ±0.47	22.9	4.8±0.29	37.1
SEBS +CB 10%	108.0±26.09	-1.8	10.9±1.98	23.9	7.2±0.56	50.0	6.2 ±0.46	77.1
SEBS-g-MA	45.0±8.8	NA	7.5±0.49	NA	4.0±0.29	NA	2.9±0.23	NA
SEBS-g-MA + CB 1%	68.0±18.0	47.9	5.4 ±1.9	-28	3.3 ±1.5	-17.5	2.8±.45	-3.4
SEBS-g-MA + CB 5%	93.0±19.2	97.9	9.0 ±1.59	20	5.7 ±1.5	42.5	4.6±0.45	58.9-
SEBS-g-MA + CB 10%	78.o±18.6	73	10.4 ±1.8	38.7	6.7±1.39	67.5	5.4±.95	5.4

Table 5.4 shows Young's modulus of SEBS and SEBS-g-MA with CB. No significant difference was observed in Young's modulus in SEBS with the addition of additives within the region at which stress is directly proportional to stress, but the modulus of SEBS increases with an increase in the percentage of CB at the high extension. The reinforcement effect of CB in SEBS-g-MA at which stress is directly proportional to strain is highly enhanced. This is attributed to greater interaction between SEBS-g-MA with CB compared to SEBS with CB. Slight change in Young's modulus within a region where stress is directly proportional to stress and an increase in dielectric permittivity with the addition of CB in SEBS composites give high electro-restrictive coefficient and Maxwell stress during electrical actuation under an electric field. High electro-restrictive coefficient and high Maxwell stress induced under electric field suggest the suitability of these composites manufactured for robotic muscles like applications. However, the high dielectric loss (ca. 0.7 with real dielectric permittivity of 6.5) at low frequency (ca. 1 Hz) at higher CB concentration (10 wt. %) suggests a faster loss of charges when stored as a capacitor. This is also an issue for these composites to be used as capacitive energy

harvesters from low-frequency mechanical energy sources. In addition, very low conductivity (low imaginary dielectric permittivity) even at a high percentage of CB (10 wt. %) suggests low electrical sensitivity under small stress and strain conditions making this manufacturing system inappropriate for stress/strain sensing applications.

5.2.4 Dynamic Mechanical Analysis

Table 5.5 shows storage modulus, loss modulus and tan delta of SEBS and SEBS-g-MA with different wt. % of CB measured at a test frequency of 1Hz and 31°C. The measurements of extrudates were taken parallel and transverse to the direction of extrusion to observe the reinforcement effect of additives in different directions.

Table 5.5 Storage modulus, Loss modulus and Tan delta of nanocomposites measured at a test frequency of 1 Hz and 31 ^{o}C temperature

Additives	**In transverse direction to extrusion**			**In parallel direction to extrusion**		
	Storage modulus (E')	**Loss Modulus. (E")**	**Tan Delta**	**Storage Modulus (E')**	**Loss Modulus (E")**	**Tan Delta**
	MPa (% Δ)	**MPa (% Δ)**	**NA (% Δ)**	**MPa (% Δ)**	**MPa (% Δ)**	**NA (% Δ)**
SEBS	5.16	0.20	0.039	104.27	5.19	0.049
SEBS+CB1%	6.50 (25.9)	0.30 (50.0)	0.046 (17.9)	66.39 (-36.3)	3.14 (-39.5)	0.047 (4.1)
SEBS+CB5%	15.84 (206.9)	1.54 (670.0)	0.097(148.7)	80.20 (-22.1)	4.10 (-21.0)	0.051 (4.1)
SEBS+ CB10%	45.79 (787.0)	2.88 (1340)	0.063 (61.53)	91.97 (-11.8)	4.35 (16.2)	0.047(4.1)
SEBS-g-MA	4.12	0.39	0.095	70.70	6.34	0.047
SEBS-g-MA+CB1%	4.86 (17)	0.43 (10.2)	0.089 (-6.3)	47.64 (-3)	3.94 (-37.8)	0.082 (74.4)
SEBS-g-MA+CB5%	13.65 (231.1)	1.45 (271.8)	0.080 (-15.7)	78.62 (11.2)	6.84 (7.9)	0.087 (85.1)
SEBS-g-MA +CB10%	17.78 (313.6)	1.45 (271.8)	0.081 (-14.7)	76.95 (8.8)	6.25 (-1.4)	0.081 (72.3)

In the transverse direction of extrusion, CB addition with SEBS and SEBS-g-MA tends to increase the value of both moduli. The increase in the tan delta was also observed in

SEBS upon addition of CB, however, not much difference in the tan delta was observed with SEBS-g-MA. The increase in moduli for both polymer matrices is directly proportional to the amount of additive present in the polymer.

Unlike the slight increase in storage modulus observed in SEBS-g-MA upon addition of 5 and 10 wt. % of CB observed in a parallel direction to the extrusion, CB decreases storage and loss moduli of SEBS nanocomposites as shown in Table 5.5. The decrease in both moduli of SEBS and a slight increase in both moduli of SEBS-g-MA is due to the presence of low shear stress along the axis of screw rotation and high draw ratio of rollers during extrusion, however, the reinforcing effect increases with an increase in the amount of CB with SEBS and SEBS-g-MA. The value of tan delta obtained from samples parallel to extrusion almost remains constant in all cases for SEBS. Such behavior is attributed to a negative change in storage modulus. High tan delta change was observed in SEBS-g-MA when the positive change in storage modulus was observed. Figure 5.6 and Figure 5.7 show the storage modulus of SEBS-CB and SEBS-g-MA-CB composites respectively.

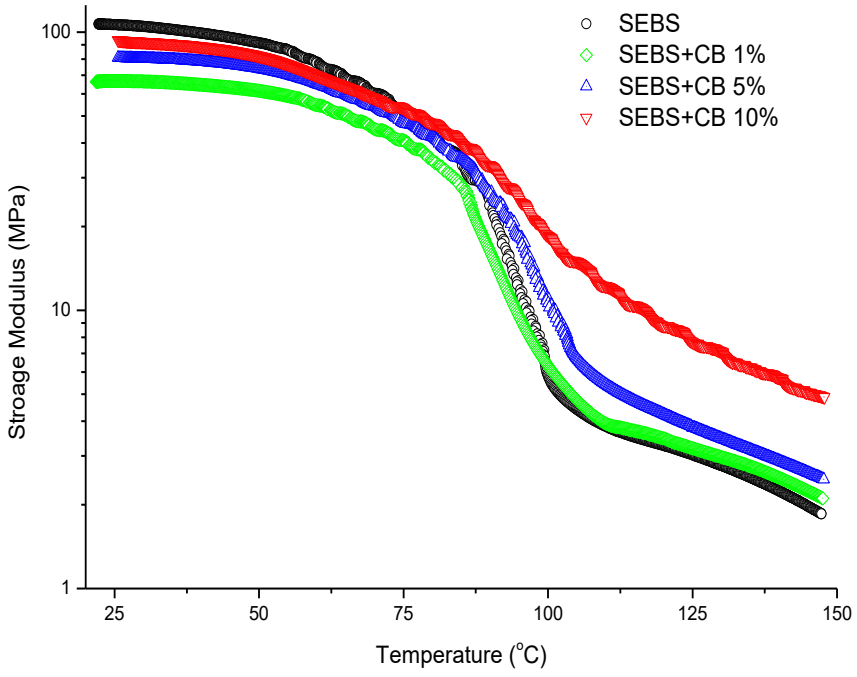

Figure 5.6 Storage modulus of SEBS/CB composites measured in the parallel direction to extrusion

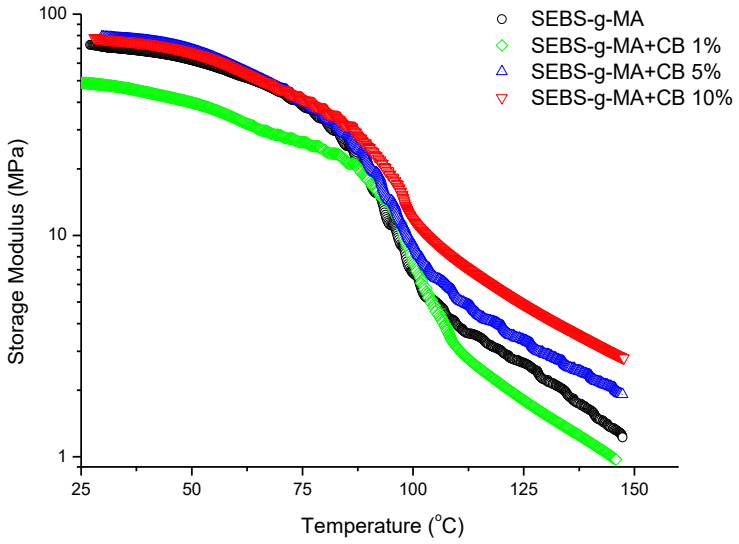

Figure 5.7 Storage modulus of SEBS-g-MA/CB composites measured in the parallel direction to extrusion.

The stability or elastic property of composites was increased with an increase in CB content at a higher temperature making them more thermally resistive. Loss modulus, a representation of the molecular motion of polymer segment, is only slightly affected by the addition of CB as shown in Figure 5.8 and Figure 5.9.

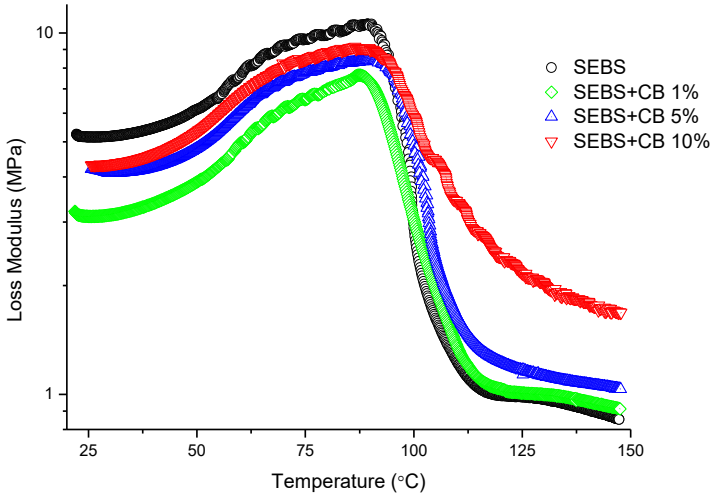

Figure 5.8 Loss Modulus of SEBS/CB composites measured in the parallel direction to extrusion

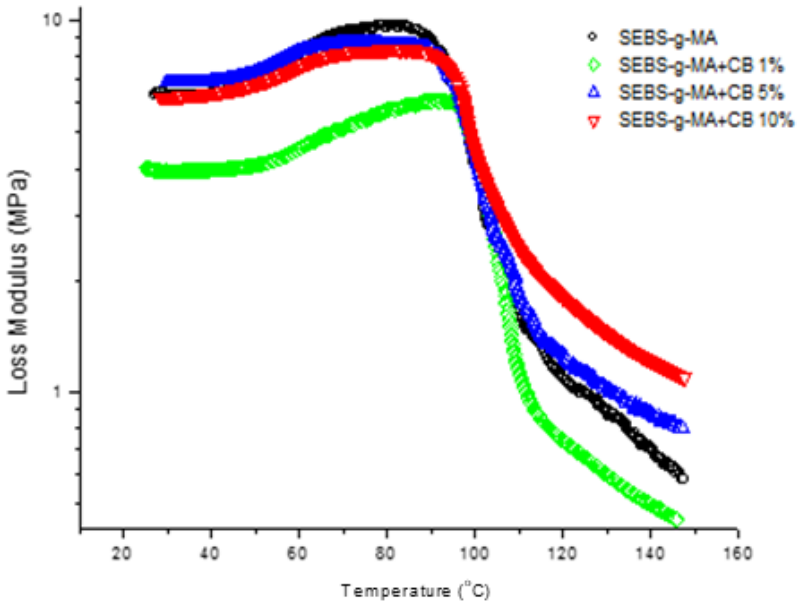

Figure 5.9 Loss modulus of SEBS-g-MA/CB composites measured in the parallel direction to extrusion

These absolute changes in storage and loss moduli result in a change in the peak of the tan delta. The relative changes in this peak were observed with a varied carbon content as shown in Figure 5.10 and Figure 5.11. Some authors suggest these changes are as the result of a change in glass transition due to the addition of CB [190], whereas other literature suggest that they are due to a change in time-dependent relaxation of polymers molecules due to the effect of CB [191]. The virgin SEBS, as well as SEBS-g-MA, shows a sharp peak in tan delta compared to their composites. As the level of CB increases in thermoplastic elastomers, the broadness of peak of tan delta also increases. This is suggested that the formation of different phase separated domains results in the heterogeneous mixture of thermoplastic elastomer with carbon black. In addition, CB restricts the mobility of different segments of an elastomer by reinforcement effect and lowers the peak of the tan delta. The broad peak of the tan delta is also the indication of a structurally heterogeneous network of elastomer-CB composite [192].

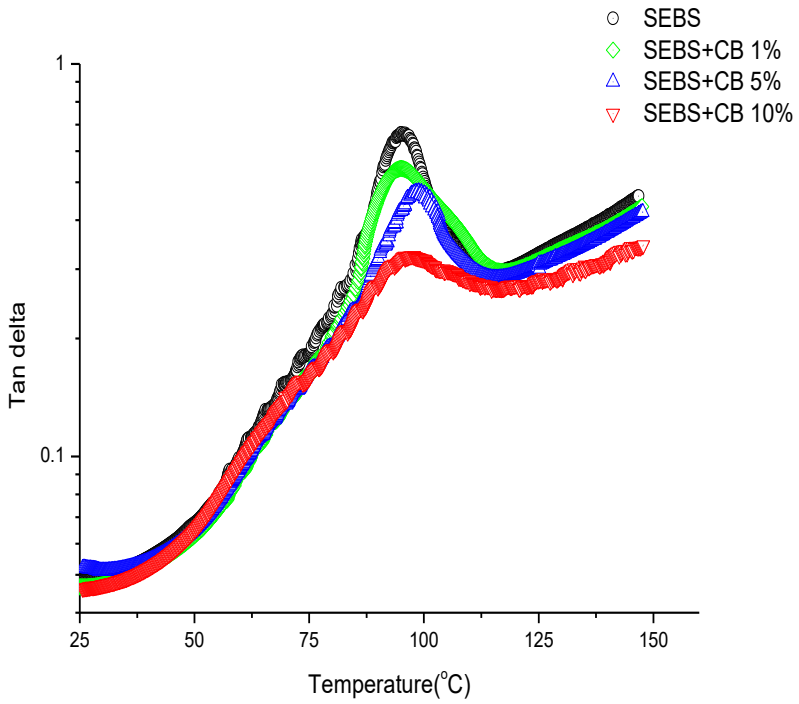

Figure 5.10 Tan delta of SEBS/CB composites measured in the parallel direction to extrusion

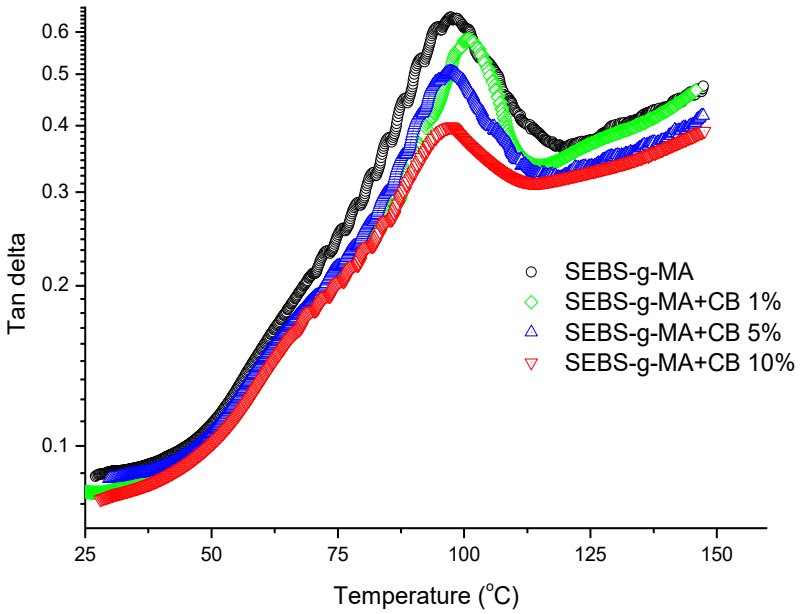

Figure 5.11 Tan delta of SEBS-g-MA/CB composites measured in the parallel to extrusion

The continuous changes in moduli of composites over the range of temperatures suggest temperature dependency behaviour of different composites. It also suggests that high compliance can be easily achieved at high temperature. However, the continuous rise in tan delta suggests that nanocomposite increases its viscous nature with an increase in temperature making nanocomposite non-elastic. It is also due to continuous changes in the microstructure changes observed within a polymer

When the amount of filler is sufficient high, these additives form a reinforcing effect overcoming the hydrodynamic effects of polymers. This network is only broken down by a high percentage of strain (generally above 0.1% strain range) which is best defined by the Payne effect [193-196]. This effect is not seen when strain % is very low as used in this work. The reinforcing factors have a more pronounced effect above the Tg of polystyrene causing an increase in both storage and loss moduli, but the former is affected. The reinforcing effect of additives is dependent on the dispersion of additives in elastomers. Wang [197] used a concept of surface energy to describe additives dispersion in the rubber matrix either in the form of aggregates or agglomerates. He used a kinetic model as described by Equation 5.5.

$$\Delta w = w_{aa} + w_{pp} - 2w_{ap} \qquad \text{Equation 5.5}$$

Where, Δw is a change in adhesion energy, w_{aa} is the adhesive energy between additive-additive particles, w_{pp} is the adhesive energy between the polymer-polymer molecule and w_{ap} is the adhesion energy between additive and polymer. According to Wang's model, when Δw=0, additives, once dispersed, do not form agglomerates. If Δw>0, the aggregates form agglomerates once they are totally dispersed in thermoplastic elastomers. Finally, if Δw<0, the aggregates have high tendency to disperse in the polymer matrix [194].

5.2.5 Modulated Differential Scanning Calorimetry

Figure 5.12 and Figure 5.13 show the heat flow curve, and temperature derivative of reversible specific heat capacity respectively for different CB/polymer matrices. The region T_{s1} and T_{s2} in Figure 5.12 represent the enthalpic relaxation of soft EB block in SEBS and SEBS-g-MA respectively. Different molecular micro-phase structures in both

polymer matrices (SEBS and SEBS-g-MA) include two pure microphases because of polystyrene and poly(ethylene-butylene) block and other interphases between these domains. The continuous change in heat flow upon annealing is the result of continuous molecular movement of complex structure present between hard and soft blocks [198-200].

From Figure 5.12, it is observed that the total heat enthalpy of the soft block in both polymer matrices shows negligible change with the addition of CB at all concentration levels. This confirms that interaction of CB with both polymer matrices is negligible. However, on both triblock, rearrangement of this peak due to densification of aromatic structure (T_{r1} and T_{r2} in SEBS-g-MA and SEBS, respectively) forming multiple interphases with soft block soon after the endothermic peak enthalpy was found to be affected upon addition of CB. This effect is more prominent in SEBS-g-MA than SEBS triblock due to the slightly higher interaction of the polar MA molecule attached to the soft block with CB.

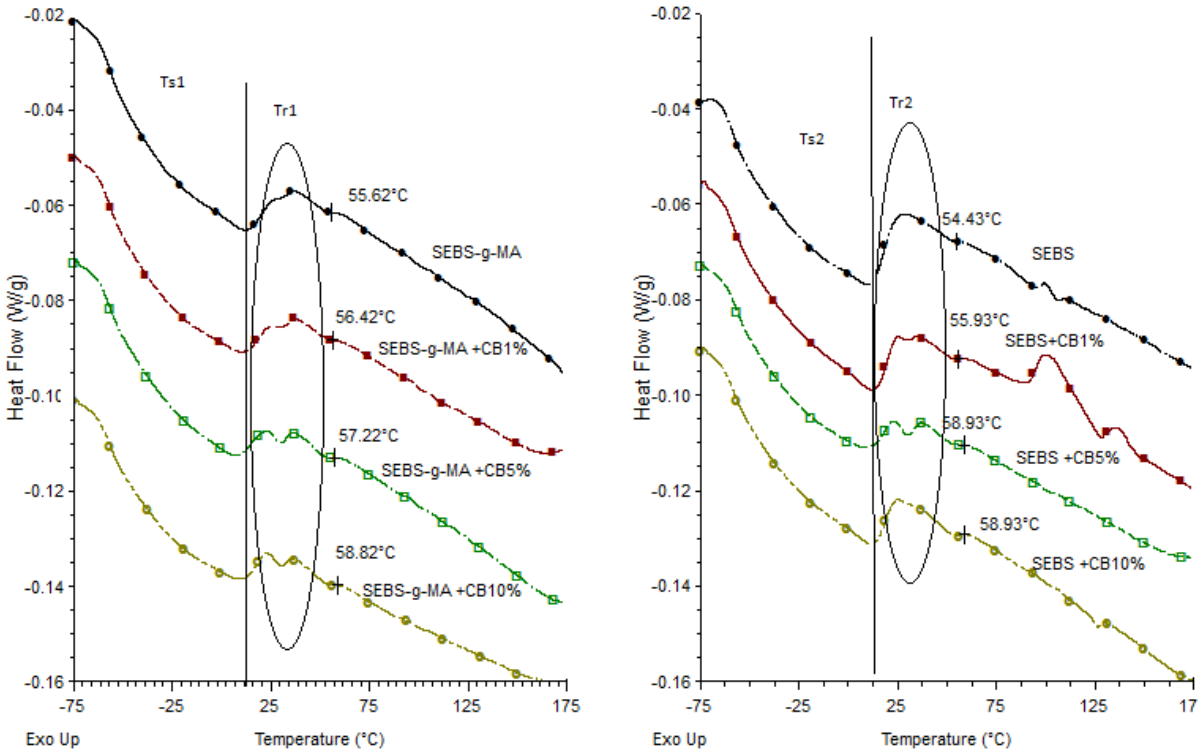

Figure 5.12 Total heat flow of SEBS-g-MA/CB (left) and SEBS/CB composites

P. Claudy *et al.* reported that the heat flow, Q, can be converted to heat capacity Cp, by dividing by the underlying heating rate [201, 202]. During glass transition, the long polymer chains are oriented randomly and have more freedom to move which results in a change in the microstructure of the material [203, 204]. In glassy materials like polystyrene, heat capacity does not change suddenly in the glass transition region. The total change in heat capacity is not a delta function of the change in temperature, however, it shows sensitivity to the process of glass transition due to change in molecular movements [204-207]. Hence, B. Wunderlich *et al.* mathematically described the change in heat capacity at Tg by its derivative as shown in Equation 5.6

$$\Delta Cp = \int \frac{dC_p}{dT} dT \qquad \text{Equation 5.6}$$

, Where, ΔCp is the change in heat capacity within the interval of initial temperature and final temperature during the heating process [205, 208-211]. The glass transition temperature of different composites (ca. -53°C for SEBS-g-MA composites and -56°C for SEBS composites) calculated by temperature derivative of reversible specific heat capacity in Figure 5.13 were found almost to be constant with the addition of a different amount of CB additives. A slight difference in the glass transition of the soft block was observed between SEBS-g-MA and SEBS triblock because of the presence of MA, a bulkier molecule, in an ethylene/butylene molecule in SEBS-g-MA. A significant difference can be observed in the derivative of reversible Cp graph of both polymer matrices upon addition of CB due to the formation of different microphase domains between the soft phase and the interphase domains between soft and hard block.

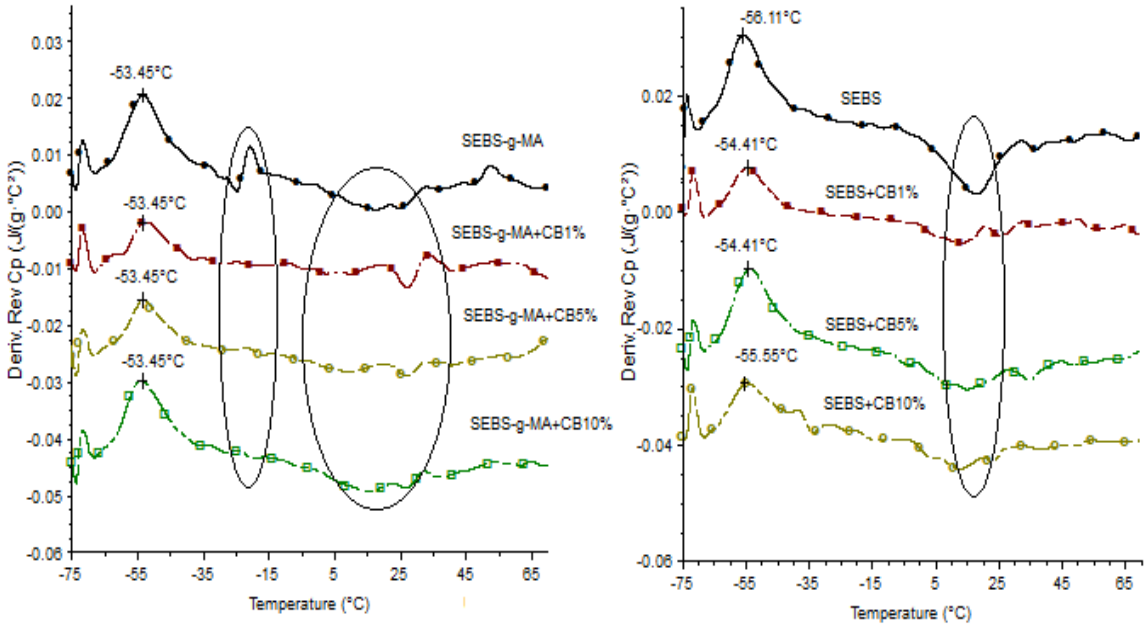

Figure 5.13 Temperature derivative of reversible specific heat capacity of SEBS-g-MA/CB (left) and SEBS/CB composites

5.2.6 Attenuated Total Reflectance-Fourier Transfer Infrared Spectroscopy Studies

Figure 5.14 and Table 5.6 shows the ATR-FTIR spectra of SEBS and SEBS-g-MA triblock, and their different frequencies of bands observed respectively [212-214]. Generally, anhydride shows two FTIR bands due to vibration coupling of C=O groups. In succinic anhydride, these two bands are seen at 1871 cm^{-1} and 1793 cm^{-1} for asymmetric and symmetric vibration of C=O groups respectively [212]. Extruded SEBS-g-MA did not show any strong bands at those fingerprint regions, however, two strong peaks were observed at 1735 cm^{-1} and 1715 cm^{-1}. The strong band present at 1715 cm^{-1} shows C=O dimers present in COOH dimers [212, 213]. It may be due to the ring opening of MA by hydrolysis phenomenon due to prolonged storage of SEBS-g-MA leading to hydrolysis of 95% of Maleic anhydride. However, the presence of 1310 cm^{-1}-1210 cm^{-1} bands observed by C-O-C stretching of anhydride group suggests that some anhydride groups were still unaltered during extrusion or prolonged storage [213]. In addition, observation of 1776 cm^{-1} band peak along with other peaks in between 1776 cm^{-1} and 1735 cm^{-1} concludes esterification of maleic anhydride due to prolonged storage of SEBS-g-MA

elastomer [215]. Moreover, the formation of other groups like alcohol during the process can also be confirmed due to the presence of a strong band at 1045 cm^{-1} and 1017 cm^{-1} [212]. The peak shown at 1601 cm^{-1} confirms the presence of C=C bond of benzene ring [216].

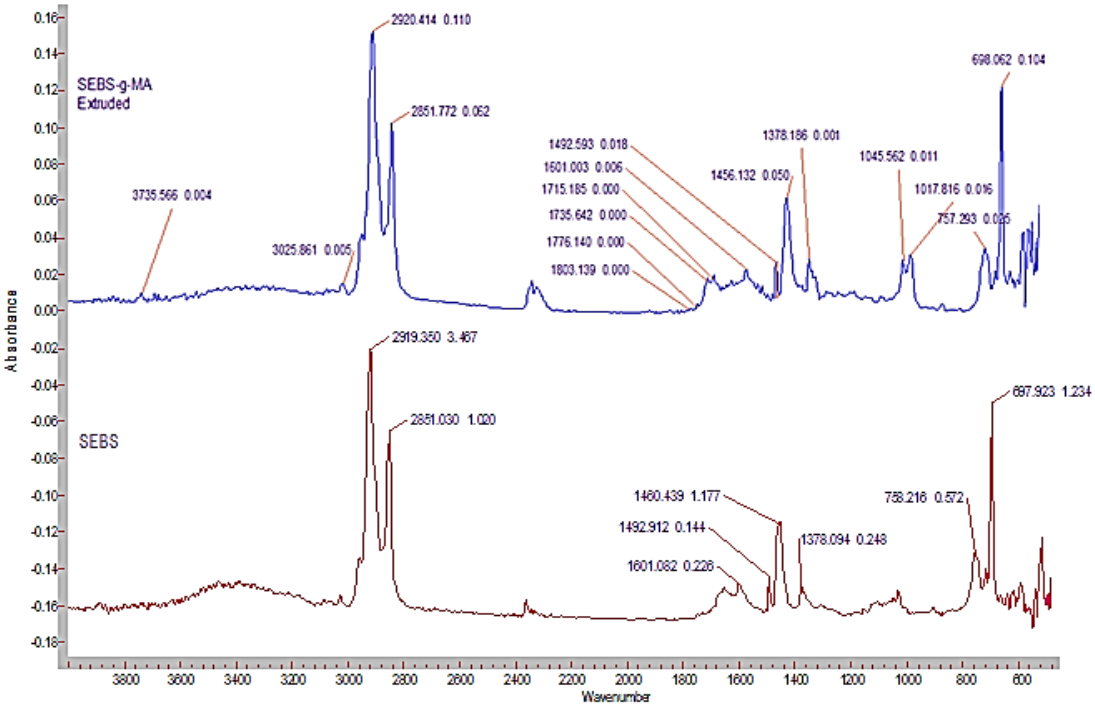

Figure 5.14 ATR- FTIR Spectra of SEBS and SEBS-g-MA

Table 5.6 Different frequency bands of SEBS and SEBS-g-MA observed in FTIR spectra [212-214]

Wavenumber (cm^{-1})	**Assignment and observations**
2919	Asymmetrical stretching vibration of CH_2 in EB units
2851	Symmetrical stretching vibration of CH_2 in EB units
1601, 1492, 1460	Assigned for stretching vibration of carbons in aromatic ring
1715	Assigned for stretching of C=O dimers present in COOH dimers
1378	Wagging of CH_2 in EB units of SEBS
758	Deformation vibration of CH groups in aromatic ring in PS units
697	Out of plan bending of CH groups in aromatic ring in PS units

The FTIR spectra of SEBS-CB composites are presented in Figure 5.15.

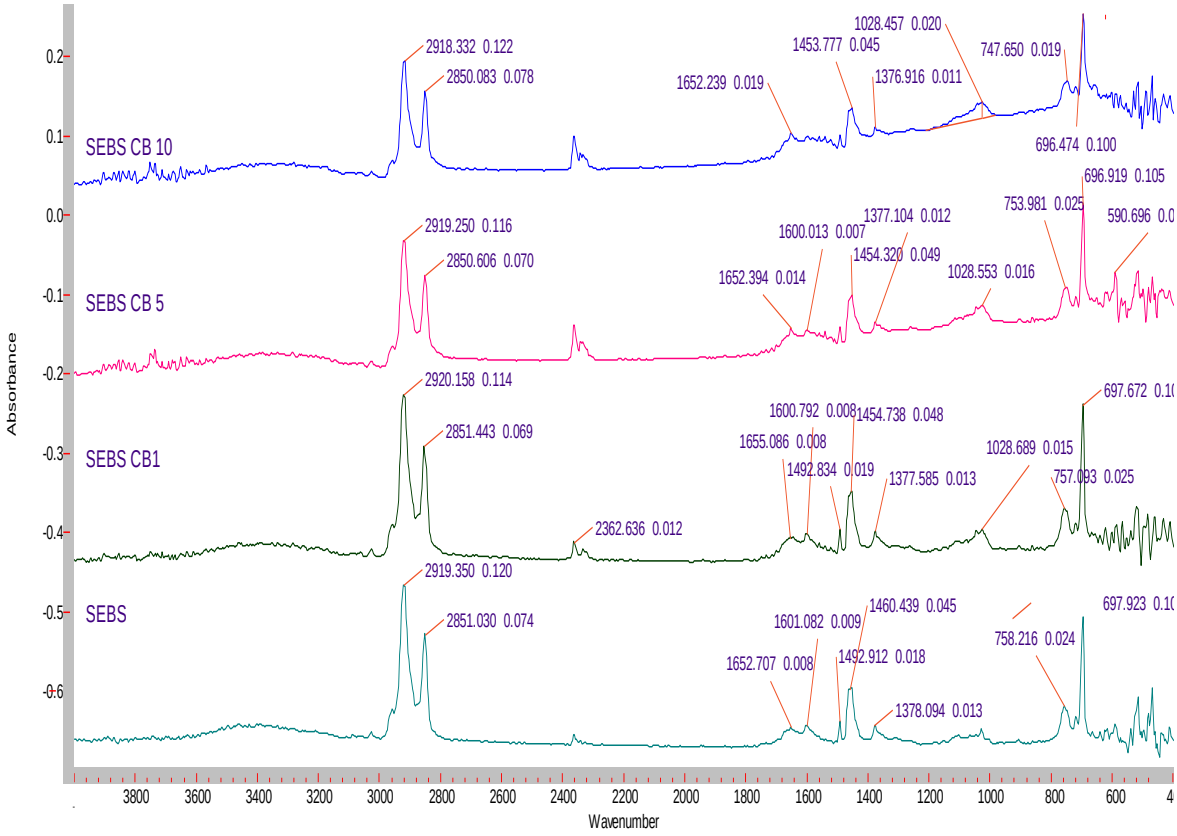

Figure 5.15 FTIR-spectra of SEBS/CB composites

It can be observed that bending of the C=C bond present in the benzene ring has the high interaction with CB. C=C bond bending vibration was observed at 1601 cm^{-1} wavenumber in virgin SEBS, which shows a change in absorbance intensity and wavenumber upon addition of CB. Similarly, a maximum wavenumber shift of 6.6 cm^{-1} from 1460.4 cm^{-1} to 1453.77 cm^{-1} was observed upon addition of 10 wt. % CB. The vibration observed at 697 cm^{-1} and 758 cm^{-1} shows the rocking effects of the benzene ring. The rocking effect of benzene ring at 758 cm^{-1} wavenumber was also shifted to 747.69 cm^{-1} wavenumber upon addition of 10% of carbon black. A negligible interaction was observed between C-H and CB with a minimum wavenumber shift in C-H asymmetric and symmetric stretching (observed in 2919 cm^{-1} and 2851 cm^{-1} respectively) of around 1 cm^{-1} wave number.

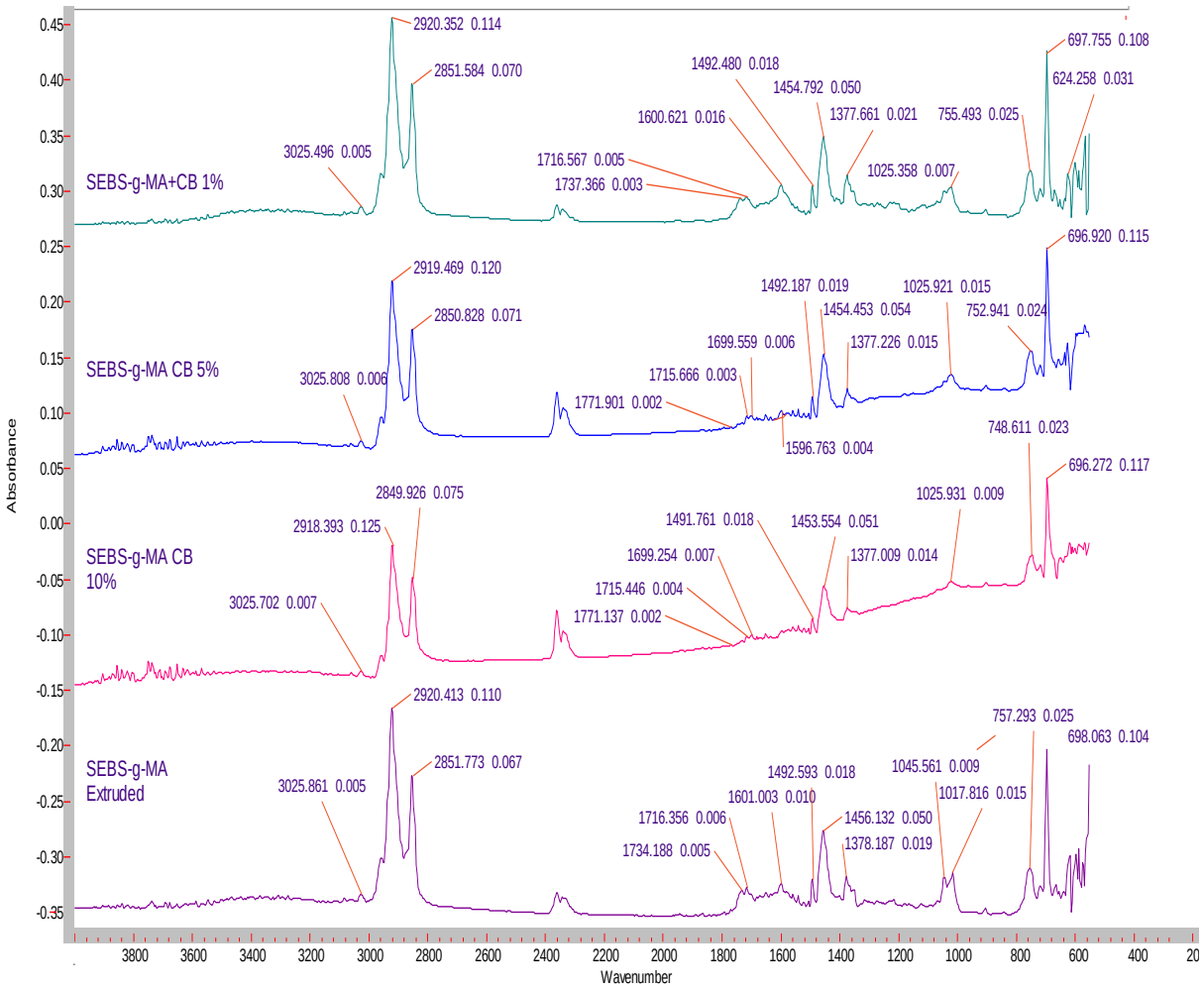

Figure 5.16 FTIR-Spectra of SEBS-g-MA/CB composites

Figure 5.16 shows the FTIR spectra of SEBS-g-MA with CB. SEBS-g-MA shows better interaction with CB than SEBS. The FTIR spectra show CB interacts mainly with Maleic anhydride group. FTIR band shifts and change in intensity, especially in C=O dimers, C-O-C band peaks, and OH peaks demonstrate the interaction of CB with SEBS-g-MA in acidic or other forms. In addition, C=C bond present at 1601 cm^{-1} also showed a similar interaction with CB.

5.2.7 Scanning Electron Microscopy

SEM images of SEBS and SEBS-g-MA-based nanocomposites are presented inFigure 5.17 and Figure 5.18. In SEBS, the dispersion of CB for both nanocomposites was found random as shown in Figure 5.17(a) and Figure 5.17 (b). The orientation of CB on both elastomers was random. 10 wt. % CB tends to make elastomers morphologically different

compared to the virgin elastomer as depicted in Figure 5.17 (a), Figure 5.17 (b) and Figure 5.18. Similar results were reported by different authors based on the morphology analysis from SEM images [217], [218].

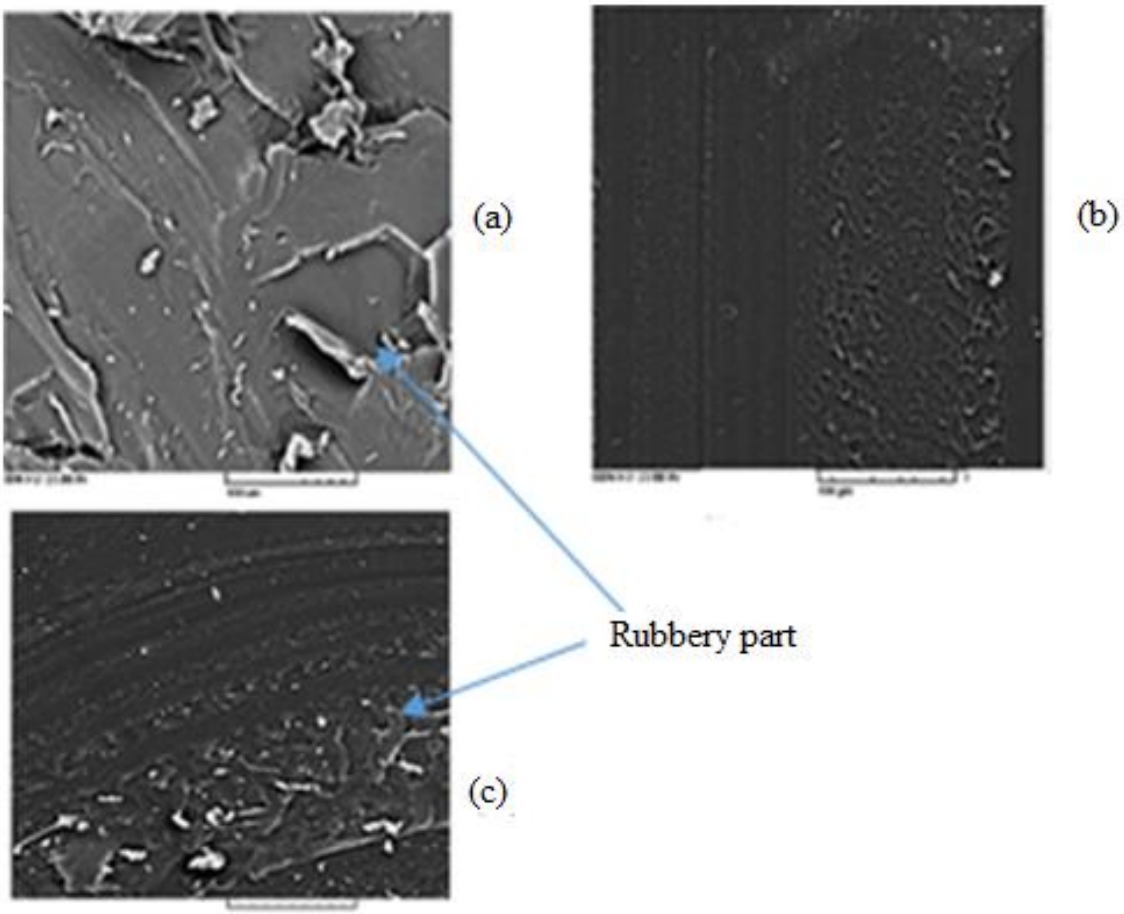

Figure 5.17 SEM images of (a) SEBS (b) SEBS+CB 10% (C) SEBS-g-MA

The concept of distributive and dispersive mixing along with the dispersion of CB in SEBS and SEBS-g-MA under different manufacturing conditions was further analyzed using TEM images in Chapter 6 with page numbers 152 and 164. The change in brittleness behavior of composites was not evident in tensile properties as the samples were only extended up to 200%.

In addition, Figure 5.17 (b) shows the fine distribution of CB in SEBS resulting in the higher mechanical strength of composites transverse to extrusion. For further analysis of dispersion on CB, the element mapping was performed along the thickness of the sample as shown in Figure 5.18.

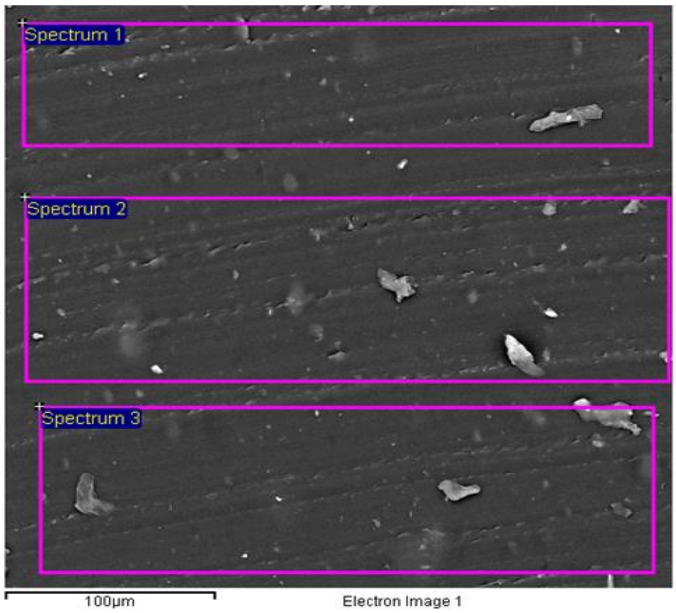

Figure 5.18 Different spectrum range used for element mapping

Table 5.7 Distribution of O and C element along different spectra by wt. %.

Spectrum	C	O
Spectrum 1	94.84	5.16
Spectrum 2	94.82	5.18
Spectrum 3	95.19	4.81
Mean	94.95	5.05
Std. deviation	0.21	0.21
Max.	95.19	5.18

From Table 5.7, it was observed that the distribution of C and O were almost uniform along the thickness of the sample measured. The variation of C and O element is almost uniform with a standard deviation of 0.21% on both elements between three different spectra measaured along the length. Uniform distribution of these elements gave rise to polarization as well as mechanical reinforcement behavior during test conditions.

5.2.8 Conclusion

Polarization enhancement achieved in a non-polarizing (SEBS) triblock as well as polarizing (SEBS-g-MA) triblock using different concentrations of conductive filler materials (carbon black) by using a co-rotating extrusion system suggests high sensitivity and better productivity of materials with an addition of such fillers. It can be further suggested that high dielectric nanocomposites obtained from conductive filler have better suitability for robotic artificial muscle applications. However, compared to other techniques described in the literature, the conventional extrusion technique requires a high amount of CB for percolation threshold hindering its possibility of uses to make conductive composite polymers for strain/stress sensing applications in terms of cost and processibility.

In addition, the high increase in dielectric permittivity was observed for both polymer matrices, dielectric loss was also significant with relative dielectric permittivity at high concentration of carbon black. However, for these nanocomposites to be used as capacity energy harvesters at low frequency remains questionable because of high dielectric loss which is expected to be varied under cyclic loading conditions for energy harvesting.

Young's modulus at 1.5% strain as well as the resilience of SEBS triblock sheet manufactured by twin screw co-rotating extrusion almost remains unchanged upon addition of CB along the axis of extrusion. This result suggests materials manufactured using this process are sensitive enough to the artificial muscle application, but high dielectric loss observed is an issue for these composites to be used as an energy harvester under tensile mode along the direction of extrusion.

In contrast, the stiffness increases in the transverse direction making these nanocomposites insensitive to compression force for stress sensing as well as energy applications which could be further enhanced by swelling the polymer in solvent like paraffin oil. Moreover, from DMA analysis, it was also observed that there are continuous changes in microphase domains in SEBS and SEBS-g-MA nanocomposites giving rise to different loss and storage modulus even with a small change in temperature. This gives rise to the different electrostrictive behavior of nanocomposites over a small range of temperature and hence different actuation and sensing behavior at different temperatures.

5.3 Dielectric Filler Based Thermoplastic Nano-Composites for Electromechanical Applications

5.3.1 Introduction

Although conductive fillers tend to increase the dielectric permittivity of elastomers by several fold as observed in the previous section, low dielectric breakdown strength, as well as a high dielectric loss at high dielectric constant, makes them unsuitable for capacitive energy harvesting applications. Low dielectric breakdown of conductive fillers composites is the result of high electron tunnelling effect in conductive fillers with increase in electrical field. Dielectric filler based thermoplastic composites have huge potential for a variety of electromechanical applications. In this section, the main objective of understanding and evaluation of the thermal, mechanical, morphological and electric behavior of dielectric filler based thermoplastic composites manufactured using twin screw extrusion is discussed. Two thermoplastic elastomers (SEBS and SEBS-g-MA) with one dielectric filler (BT) were selected for evaluating the importance of filler-thermoplastic elastomers interaction. Thermal, morphological, mechanical and electrical techniques were used to understand the interaction between dielectric filler and elastomers and to find out the subsequent effect of dispersion of additives in elastomers on the enhanced polarization of the composite.

5.3.2 Dielectric Studies

The real dielectric permittivity calculated without using any correction factor for SEBS and SEBS-g-MA composites with BT fillers from the Solartron 1296 at a frequency of 1 Hz is shown Table 5.8. These results have not been computed using a correction factor. Similar to results described in section 5.2, the dielectric permittivity obtained for these polymer composites were also systematically smaller by a factor of approximately 100 compared to that reported in the literature [84]. A correction factor was therefore applied by measuring the permittivity of the air at a distance of 1.5-2 mm (depending on thickness of the sample) between two electrodes which is believed to have an absolute value of 1 from 1 Hz to 1 MHz. The correction factor calculation for 1 Hz was calculated to be 72. The dielectric permittivity calculated for SEBS and SEBS-g-MA composites from the

Solartron 1296 at a frequency of 1 Hz at room temperature corrected with correction factor of 72 is shown in Table 5.9.

This correction factor is used to calculate a reference of permittivity of air which is further modified from 72 to 82 for curve smoothing and plotted as shown in Figure 5.19.

Table 5.8 Dielectric permittivity of SEBS and SEBS-g-MA measured Solartron 1296 at a frequency of 1 Hz

Additives	**Real dielectric constant of SEBS ε' (10^{-2})**	**Real dielectric constant of SEBS-g-MA ε' (10^{-2})**
Virgin	3.18	4.49
BT 1%	3.56	5.24
BT 5%	4.07	5.51
BT 10%	3.15	6.17

The real dielectric permittivity calculated for SEBS and SEBS-g-MA composites from the Solartron 1296 at a frequency of 1 Hz at room temperature is presented in Table 5.9.

Table 5.9 Real dielectric permittivity of SEBS and SEBS-g-MA with BT with the correction factor calculated from air

Additives in wt.%	**Dielectric constant of nanocomposite at 1 Hz (ε_r) with percentage changed with additives**			
	SEBS		**SEBS-g-MA**	
	Real ε'	**% Δ**	**Real ε'**	**% Δ**
Virgin	2.29	NA	3.24	NA
BT 1%	2.56	11.76	3.77	14.7
BT 5%	2.93	27.9	3.96	20.5
BT 10%	2.27	-0.88	4.44	34.9

The graph for the real dielectric permittivity of SEBS and SEBS-g-MA composites is shown in Figure 5.19.

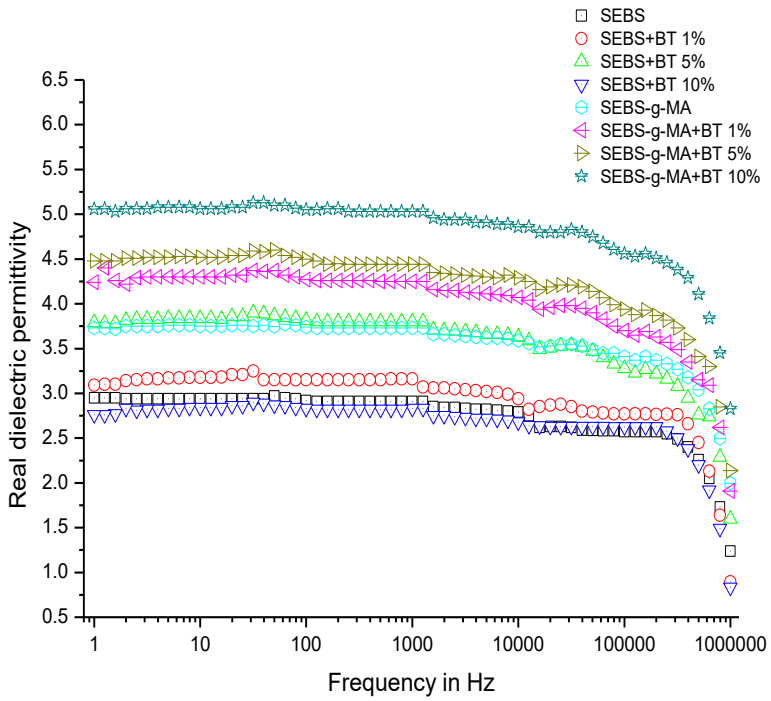

Figure 5.19 Real component of dielectric permittivity of SEBS and SEBS-g-MA composites with different percentages of BT

The dielectric loss tangent (tan delta) was also measured and found to be less than 0.08 below 1 kHz of all composite samples making them suitable for energy storing capacitive applications. However, the loss was observed to increase with an increase in frequency. There was no significant difference between real dielectric permittivity as shown in Figure 5.19 and Table 5.9 and total dielectric permittivity for all samples measured because of the low value of dielectric loss over the range of all frequency measured. However, total dielectric permittivity alone cannot be considered to give the information about the polarization capability of materials for all cases as it is the vector sum of loss factor and real dielectric permittivity. The real dielectric permittivity of the virgin material was increased from 3.24 to 4.44 with the addition of 10 wt. % of BT measured at 1 Hz. Due to the high polarization capability of BT, the addition of BT in SEBS-g-MA shows an increase in the real dielectric permittivity of the overall composite for all cases [219]. Orientation, shape, and dispersion of high dielectric additives in the polymer matrix define the resultant dielectric developed for the nanocomposite [174]. It is suggested that the enhancement of real dielectric permittivity of nanocomposites is the result of interfacial polarization existing between the polymer matrix and the additive particles [184-187].

Similar to the total dielectric permittivity, the real dielectric permittivity of virgin SEBS (2.29 at 1 Hz) also increases with an increase in BT up to a certain percentage (2.93 at 1 Hz with 5 wt.% of BT) and decreases at higher concentrations (2.27 at 1 Hz with10 wt.% of BT). The decrease in dielectric permittivity is probably due to the poor interaction between non-polar SEBS and highly polar BT additives. This type of effect is also found in different epoxy composites by Patsidis *et al*.[220] and Zhang *et al*.[219] . However, the attachment of a maleic anhydride polar molecule enhances the real dielectric permittivity of SEBS even at a higher concentration as shown in Figure 5.19. This positive change in dielectric permittivity is observed when the compatibility is increased between SEBS and BT by attachment of polarizing molecule maleic anhydride (MA) as shown in Figure 5.19 and Table 5.9. Similarly, Stoyanov [108], and Yang and Kofinas [221] also found that the dielectric permittivity increased with an increase in TiO_2 content making SEBS compatible to the additives. This result demonstrates the role of the interaction between additives and polymer molecule for the enhancement of dielectric permittivity. The increase in dielectric permittivity with low dielectric loss optimizes the electroactive properties of different elastomers, thereby, increasing the potential of these elastomers to be used for strain/stress sensors, capacitive energy generators, artificial muscles and flexible charge storing capacitors. The enhanced dielectric permittivity of elastomers composites is a crucial factor for electroactive applications. Mechanical properties (such as Young's modulus and loss factor) and viscoelastic properties are also equally important to determine stiffness, flexibility, hysteresis loss and stability of such composites during their uses.

5.3.3 Mechanical Properties

Table 5.10 shows the secant Young's modulus of different nanocomposites at various strain rates. There was no substantial effect in secant Young's modulus with the addition of additives to elastomers to 1% strain (ca. 100 MPa and 45 MPa for SEBS and SEBS-g-MA composites respectively), but the modulus of SEBS and SEBS-g-MA increases with the increase of BT percentage at the higher extension (3.5MPa, 2.9MPa, 3.9MPa, and 3.2 MPa for SEBS, SEBS-g-MA, SEBS with 10 wt.% BT and SEBS with 10 wt.% BT respectively at 150 % strain).

Table 5.10 Secant Young's modulus of nanocomposites with different stain percentage of BT and percentage change in Young's modulus (% Δ) with respect to virgin polymer

Polymer matrix with wt. % of additives	**Secant Young's modulus (Y) of nanocomposite different strain (MPa)**							
	1%		**50%**		**100%**		**150%**	
	Y	**% Δ**	**Y**	**% Δ**	**Y**	**% Δ**	**Y**	**% Δ**
SEBS	110.0±17.7	NA	8.8±0.44	NA	4.8±0.26	NA	3.5±0.22	NA
SEBS + BT 1%	100.0±16.7	-9.1	6.7±0.24	-23.9	3.9±0.17	-18.8	3.1±0.13	-11.4
SEBS + BT 5%	116.0±6.7	5.4	8.2±0.52	-6.8	4.7 ±0.27	-2.0	3.6±0.19	2.8
SEBS + BT 10%	95.1±16.09	-13.4	8.7±0.68	-1.1	5.0 ±0.46	4.2	3.9 ±0.36	11.4
SEBS-g-MA	45.0±8.8	NA	7.5±0.49	NA	4.0±0.29	NA	2.9±0.23	NA
SEBS-g-MA + BT 1%	47.0±10.2	4	5.0 ±0.52	-33.3	3.0±0.35	-25.0	2.4 ±0.28	-17.24
SEBS-g-MA + BT 5%	40.0±8.0	-11.1	7.6 ±0.59	1.3	4.1 ±2.5	0.25	3.0±1.5	3.4
SEBS-g-MA + BT 10%	47.4±8.6	4	8.2 ±0.8	9.3	4.4±0.39	10	3.2±0.25	10.34

Figure 5.20 and Figure 5.21 show the tensile profile of SEBS and SEBS-g-MA with BT respectively. The stress was measured up to 200 % strain for all samples. After a necking region, stress produces a stronger microstructure leading to the higher amount of energy or stress required for breakage [189].

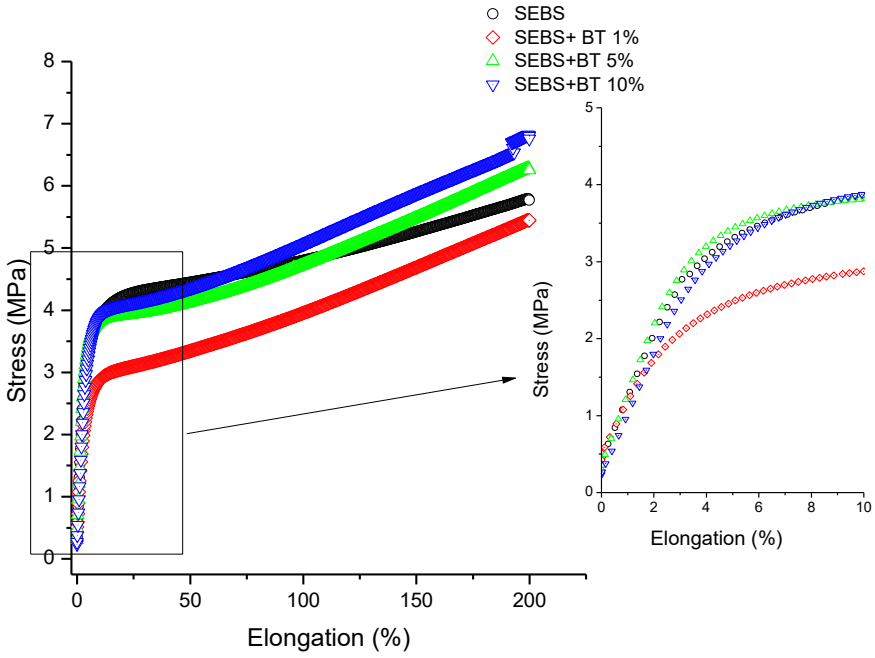

Figure 5.20 Tensile properties of SEBS/BT composites in the parallel to extrusion

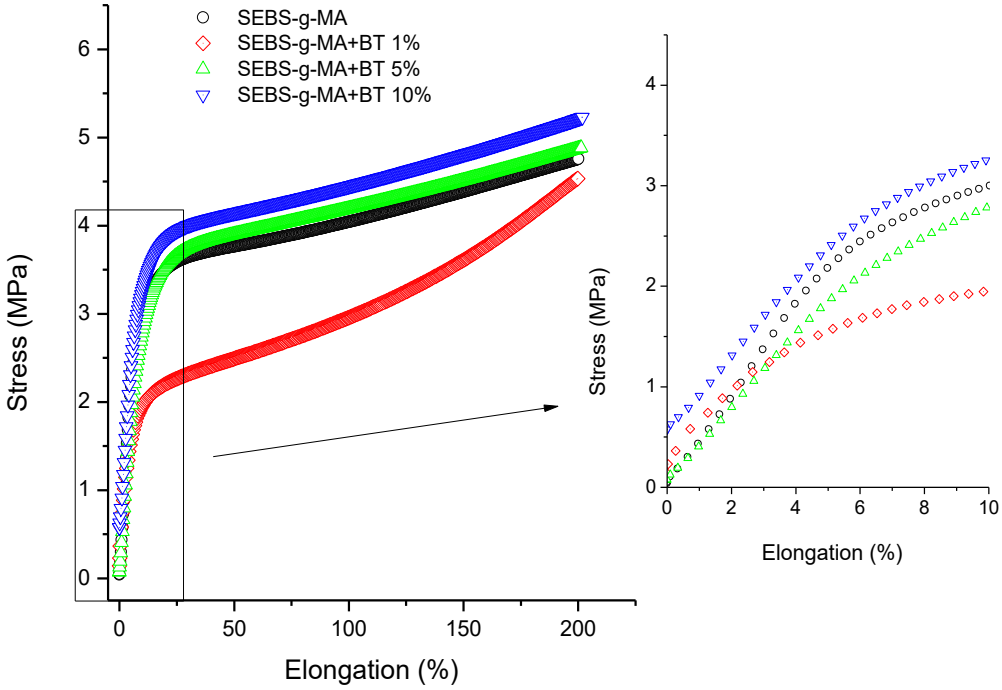

Figure 5.21 Tensile properties of SEBS-g-MA/BT composites in the parallel direction to extrusion

No significant difference was observed in resilience with the addition of 5 wt. % and 10 wt. % BT in the modulus of resilience, however, the modulus of resilience was found to decrease upon addition of 1 wt. % of BT for both polymer matrices, as shown in Table 5.11 . The decrease in modulus of resilience at low concentration of BT can be defined based on the orientation of additives. The orientation of BT additives is not aligned along the direction to the axis of screw speed at which tensile measurement of the extrudate was taken, however, at a high percentage of BT, the mechanical interlocking effects of additives are also seen along the tensile measurement axis giving almost the same modulus of resilience. The energy observed between yield point and breakage defines the modulus of toughness of the material. The modulus of toughness was observed increase with increase in the concentration of additives as shown in Table 5.11.

Table 5.11 Modulus of resilience and modulus of toughness (until 200% strain) of different composites

Composite	**In Parallel direction to the extrusion**	
	Average modulus of resilience of five samples	**Average modulus of toughness at 200 % strain of five samples**
	MPa	**MPa**
SEBS	44.83	912.76
SEBS+BT 1%	31.23	767.99
SEBS+BT 5%	43.05	914.76
SEBS+ BT 10%	45.81	970.45
SEBS-g-MA	47.79	748.35
SEBS-g-MA+BT 1%	32.99	573.812
SEBS-g-MA+BT 5%	47.77	775.21
SEBS-g-MA +BT 10%	50.86	829.67

From Figure 5.20, the addition of 5 wt. % and 10 wt. % BT increases the modulus of toughness of SEBS, but not in the same fashion as 5 % and 10 wt. % of BT in SEBS-g-MA as shown in Figure 5.21. SEBS and SEBS-g-MA with 1 wt. % of BT show a low toughness compared to pure SEBS and SEBS-g-MA respectively, but this result might be

altered if the material is extended to the breaking point as the slope gradient of SEBS as well as SEBS-g-MA with 1 wt. % of BT is higher after the yield point of virgin SEBS and SEBS-g-MA respectively which can be seen from Table 5.10. The percentage change in Young's modulus of SEBS-g-MA with 1 wt. % of BT with respect to unfilled SEBS-g-MA was found to change significantly from 33.2 % to -17.3 % when measured at 50% of strain and 150 % strain respectively. However, SEBS at all concentrations of BT show low values of stress to strain ratio at 50 % strain than virgin SEBS, which suggests a higher drawing region which may be due to lack of reinforcement and low compatibility of SEBS with BT as shown in Table 5.10, but the effect is not observed in SEBS-g-MA. Compared to CB particles, BT has cubic structure which causes low reinforcement compared to CB. The overall results show the poor miscibility of BT (at 5 wt % and 10 wt %) on SEBS when the processing conditions used as described in this section. Generally, manufacturing of highly flexible dielectric composites has huge potential for electroactive applications. However, the incompatibility between additive and elastomer leads to poor mechanical and electrical performance making them not suitable for electroactive applications which require continuous mechanical and electrical deformation.

Figure 5.22 shows the loss factor of different composites under each cycle. The loss factor was found to be 1.40, 1.60, 1.45, and 1.44 for SEBS-g-MA, SEBS-g-MA with 1 wt. % BT, SEBS-g-MA with 5 wt. % BT and SEBS with 10 wt.% BT respectively versus 1.15, 1.75, 1.1, and 1.0 for SEBS, SEBS with 1 wt. % BT, SEBS with 5 wt.% BT and SEBS with 10 wt.% BT respectively. According to Cantournet *et al.*[222], the extension of elastomers occurs due to sliding (after the elastic limit) and non-sliding action (within the elastic limit in the first cycle) between hard and soft blocks. This condition is also observed during the unloading condition. The loss of stiffness during cyclic testing after the first cycle results in stress softening behavior [222] leading to a low loss in consecutive cycles as shown in Figure 5.22. This stress hysteresis or stress softening behavior was first described by Mullins and is known as Mullin's effect [223]. Due to stress softening the effect of dielectric thermoplastic elastomers nanocomposites, the loss factor decreases at least by the factor 3 from first cycle to the second cycle in all cases. Upon addition of 1 wt. % of BT, the loss factor is highly increased in all cycle due to high mechanical interlocking. However, this effect was hindered as the percentage of BT was increased due to the formation of agglomerations. In SEBS with 10 wt. % BT, the loss factor was

found to be lower than virgin SEBS almost for all cycles. This is because of lack of interaction between BT and SEBS and agglomeration of BT in SEBS during the manufacturing procedure. Although this result seems better for electroactive applications, agglomeration of BT hinders overall polarization effects of composites as well as making them mechanically unstable with time. However, SEBS-g-MA shows improved interaction with BT leading to the better dispersion of BT and a continuous loss factor at all concentrations due to the presence of the polar MA molecule.

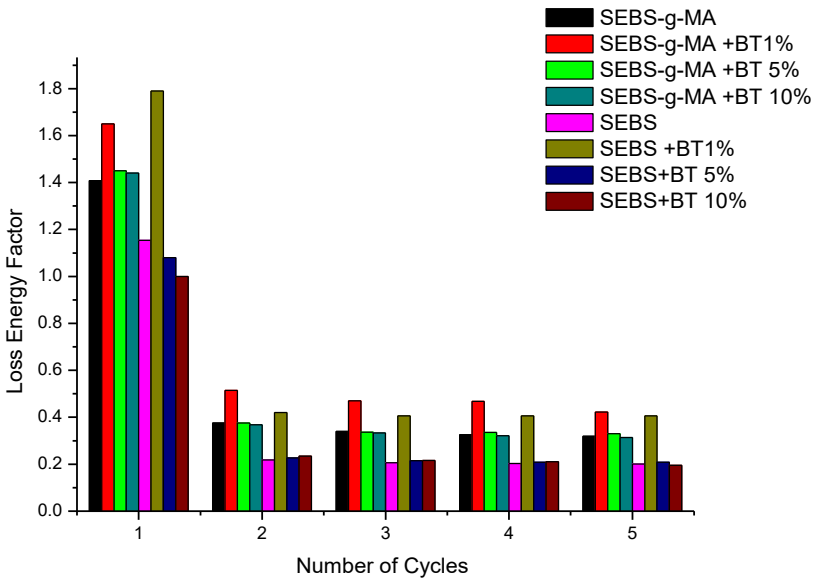

Figure 5.22 Loss factor for each cycle of different composites measured the parallel direction to extrusion

5.3.4 Dynamic Mechanical Analysis

Table 5.12 presents the storage modulus, loss modulus and tan delta of SEBS and SEBS-g-MA with BT measured at a test frequency of 1Hz and 31^{o}C temperature in a transverse and parallel direction to the axis of screw rotation. In the transverse direction of extrusion, the addition of BT demonstrated an increase in moduli and tan delta in both SEBS and SEBS-g-MA-based nanocomposites.

Unlike the high increase in storage modulus and loss modulus observed in the transverse direction, the addition of BT was found to decrease both moduli of the nanocomposites in the parallel direction; except for loss modulus (8.15 MPa) of SEBS with 1 wt. % BT versus 5.19 MPa for virgin SEBS.

Table 5.12 Storage modulus (E'), Loss modulus (E'') and Tan delta of nanocomposites measured at a test frequency of 1 Hz and 31 °C temperature BT and percentage change in of the same (% Δ) with respect to virgin polymer

Polymer matrix with wt. % of additives	**In transverse direction to extrusion**			**In parallel direction to extrusion**		
	E'	**E''**	**Tan Delta**	**E'**	**E"**	**Tan Delta**
	MPa (% Δ)	**MPa (% Δ)**	**NA (% Δ)**	**MPa (% Δ)**	**MPa (% Δ)**	**NA (% Δ)**
SEBS	5.16	0.20	0.039	104.27	5.19	0.049
SEBS + BT 1%	7.65 (38.7)	0.64 (220.0)	0.084 (115.0)	98.29 (-5.7)	8.15 (57.0)	0.083 (69.0)
SEBS + BT 5%	8.94 (73.2)	0.38 (180.0)	0.043 (10.25)	71.39 (-31.5)	4.03(-22.3)	0.056 (14.3)
SEBS + BT 10%	5.84(13.2)	0.24 (20.0)	0.040 (2.5)	75.65 (-27.4)	3.93(-24.3)	0.051 (4.1)
SEBS-g-MA	4.12	0.39	0.095	70.70	6.34	0.047
SEBS-g-MA + BT 1%	12.14 (94.7)	1.10 (182.1)	0.090 (-5.0)	36.27 (-48.6)	3.12 (-50.8)	0.086 (74.4)
SEBS-g-MA + BT 5%	4.60 (11.7)	0.42 (7.7)	0.091 (-4.2)	56.86 (-19.5)	4.65 (-26.7)	0.082 (85.1)
SEBS-g-MA+ BT 10%	4.57 (10.9)	0.41 (5.1)	0.091 (-4.21)	44.05 (-37.6)	3.906 (-8.4)	0.089 (89.3)

The decrease in both moduli observed is due to the presence of low shear stress and high draw ratio due to rollers along the axis of screw rotation during extrusion. The reinforcing effect increases with an increase in the amount of BT from 1 wt. % (storage modulus was 36.27 MPa) to 5 wt. % (storage modulus was 56.86 MPa) with SEBS-g-MA and storage modulus remains comparable with the addition of 10 wt. % of BT (44.05MPa). However, the storage modulus of SEBS decreases when the wt. % of BT was increased from 1% (98.29 MPa) to 5% (71.39 MPa) and remains considerably low (75.65 MPa) with the addition of 10 wt % of BT. In addition, the decrease in the value of tan delta of SEBS-g-MA from 0.95 to 0.91 was observed in a transverse direction with the addition of 5 wt. %

and 10 wt. % BT fillers. On the contrary, this effect was not observed in SEBS composites, where the value of tan delta remains above 0.4 (versus 0.39 for virgin SEBS) polymer with the addition of any concentration of BT. This result also suggests higher compatibility and dispersion of BT fillers with SEBS-g-MA matrix compared to SEBS matrix. Compatibility between filler and polymer matrix is a crucial parameter for sustainable electrical and mechanical property for an electroactive application.

Generally, with the addition of additives to elastomers, they tend to change the stiffness of the material at higher temperatures when they are measured at low strain conditions using DMA. On the other hand, the addition of BT did not improve the storage modulus of SEBS at high temperature as shown in Figure 5.23.

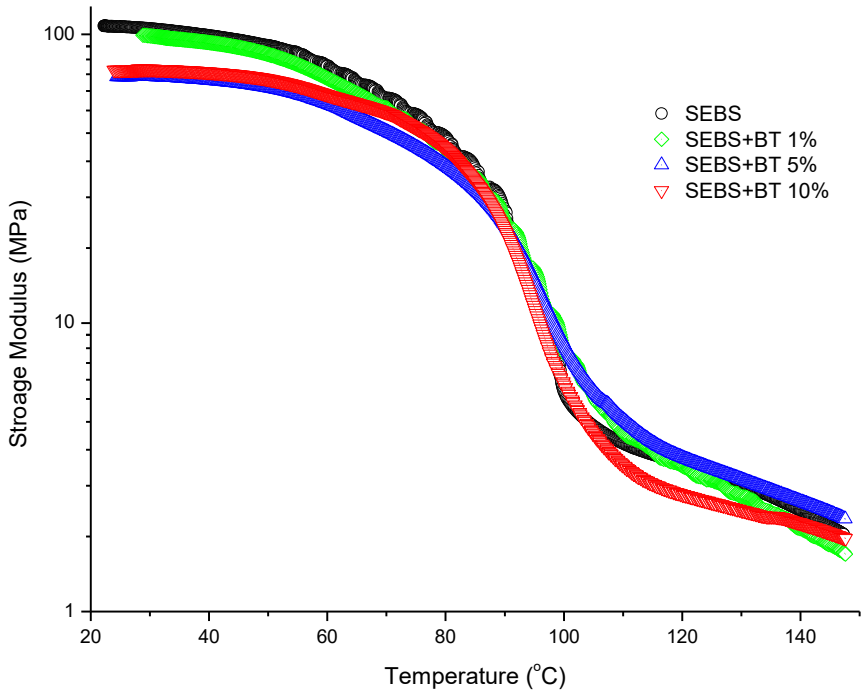

Figure 5.23 Storage modulus of SEBS/BT composites measured in the parallel direction to extrusion

In addition to this, the molecular motion of SEBS starting around 40 °C rise in a similar fashion to higher temperature until 90 °C upon addition of a different percentage of BT shown in Figure 5.24. Moreover, the peak of tan delta also remains almost constant at all concentrations of BT as shown in Figure 5.25. This suggests very less interaction or no interaction between non-polar SEBS with highly polar BT dielectric filler.

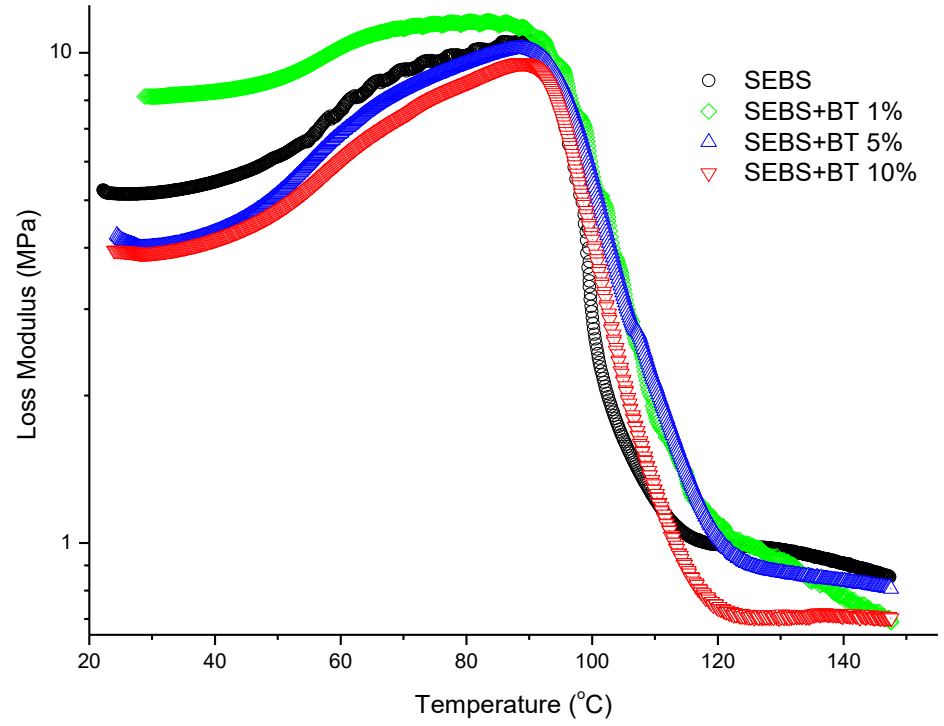

Figure 5.24 Loss modulus of SEBS/BT composites measured in the parallel to extrusion

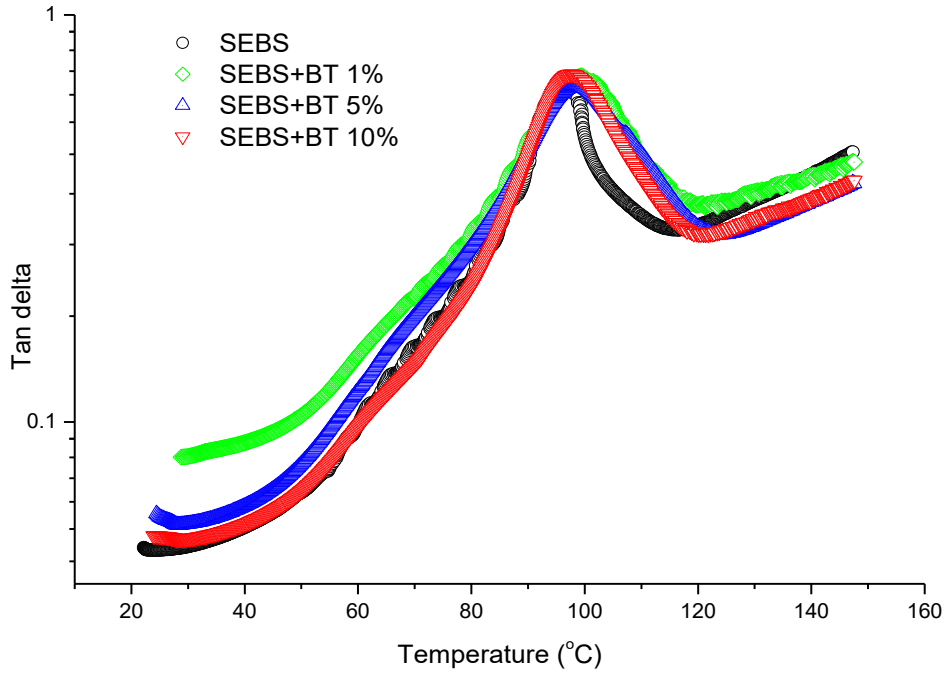

Figure 5.25 Tan delta of SEBS/BT composites in the parallel direction to extrusion

As described in section 5.2.4, a better manufacturing procedure (such as the use of supercritical CO_2 assisted extrusion) allowing better dispersion of additives into polymers, can sometimes readily solve the issue faced in this context [126, 127, 224, 225]. If the Δw is positive and high enough, other techniques like a molecular modification of SEBS (such as the attachment of maleic anhydride with SEBS) will lead to the better dispersion ability of BT in the polymer.

The SEBS-g-MA-BT composites show different behavior compared to SEBS-BT composites based on the storage modulus, loss modulus, and tan delta. Figure 5.26 shows the storage modulus of SEBS-g-MA- BT nanocomposites. The stability or elastic property of SEBS-g-MA- BT nanocomposite increases with an increase in BT content at a higher temperature making it more thermally resistive.

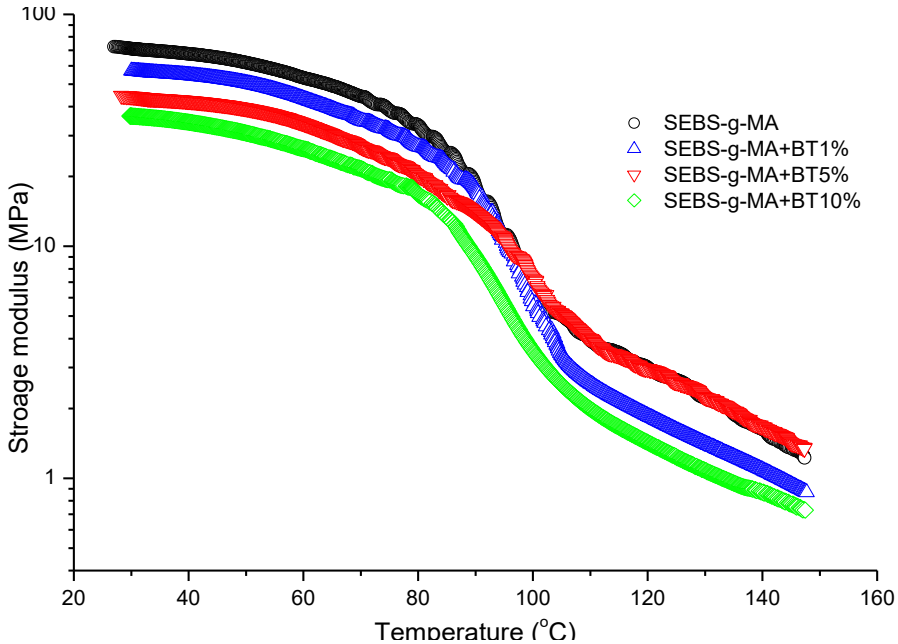

Figure 5.26 Storage modulus of SEBS-g-MA/BT composites in the parallel direction to extrusion

Loss modulus shows a high increase in the width of the peak of loss modulus with an increase in BT. Generally, a broad peak of loss modulus represents the higher damping behavior of the material [226]. However, in the case of Figure 5.27, a broad peak is not due to the higher molecular motion between two segments rather it is because of resistance

to molecular movement segments at higher temperatures due to the high interaction between polar MA molecule of SEBS-g-MA and highly polar dielectric filler BT. Due to the reinforcing nature and high interaction of compatible BT additives, molecules of SEBS-g-MA show only low molecular movement at higher temperature thereby lowering the loss modulus value when measured using DMA under low strain condition. Because of the restriction imposed in molecular movement at a higher temperature when measured at low strain conditions in DMA, the peak appears to be broad rather than a narrow peak. SEBS-g-MA/BT composites show a broader peak compared to virgin SEBS-g-MA as shown in Figure 5.28. In addition, Figure 5.28 also shows a low value of tan delta with the addition of BT fillers at all range of the measured temperatures. This result also suggests the material is still a low loss material although the amount of BT was increased. A temperature shift in the peak of the tan delta was observed on SEBS-g-MA upon addition of BT. Such an effect is likely due to an absolute change in storage and loss modulus under low strain conditions as shown in Figure 5.26 and Figure 5.27. Some authors suggest that these changes observed on the tan delta transition peaks are due to the addition of additives [190], whereas literature suggests a change in time-dependent relaxation of polymers molecules due to the effect of additives [191].

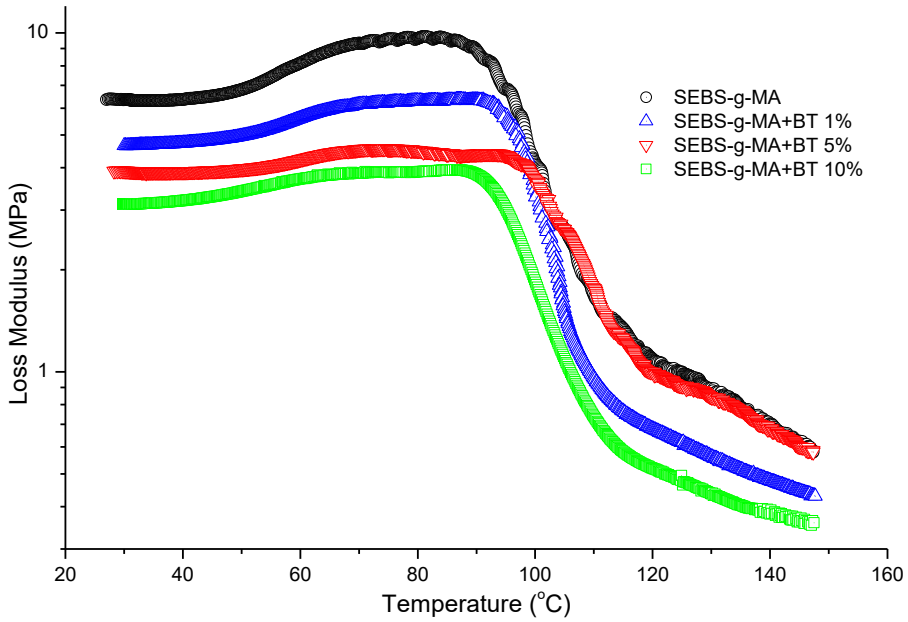

Figure 5.27 Loss Modulus of SEBS-g-MA/BT composites in the parallel direction to extrusion

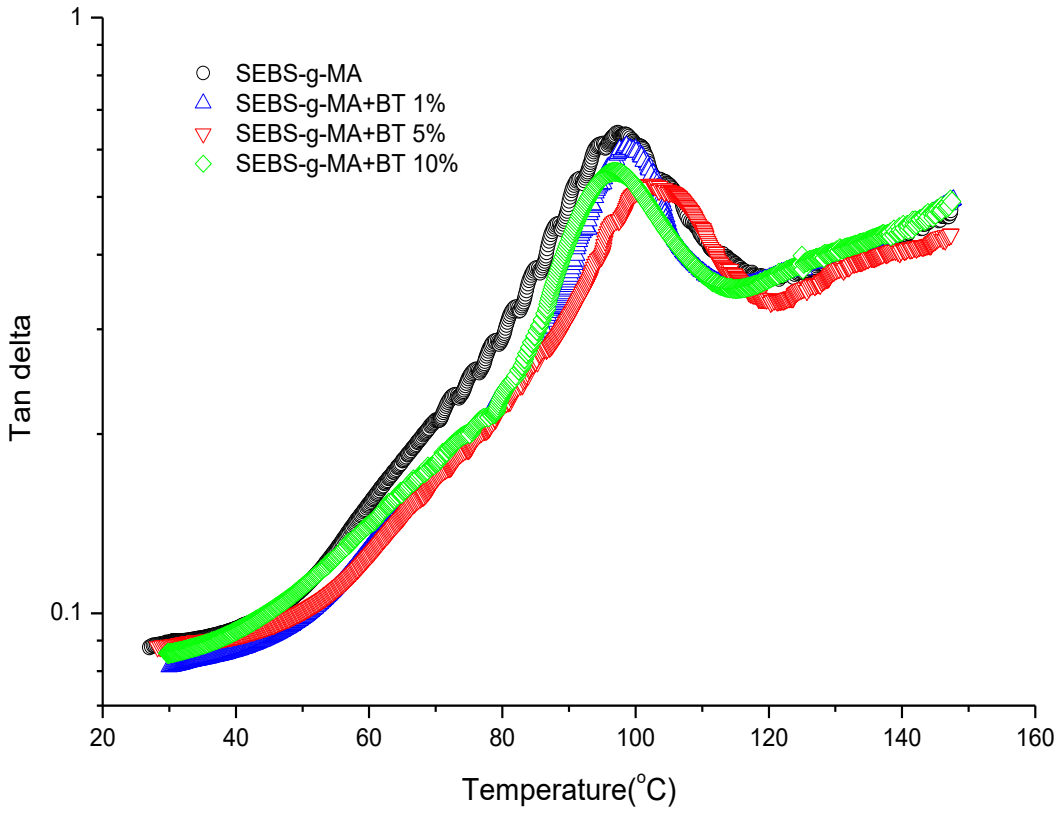

Figure 5.28 Tan delta of SEBS-g-MA/BT composites in parallel direction to extrusion

The temperature shift in the peak of the tan delta was found to be directly proportional to the amount of BT content since when the amount of filler is sufficient; additives form a higher reinforcing effect, thereby overcoming the hydrodynamic effects of polymers. However, this network can be broken down at a high percentage of strain (generally above 0.1% strain range) which is best defined by the Payne effect [193-196]. This effect is not seen when strain % is very low as used in this work. The shift in tan delta (a representation of the glass transition of the hard block) is an essential parameter to study for different nanocomposites as it defines mechanical stability as well as viscoelastic properties of nanocomposites for their all possible applications under different strain/ stress condition for different applications.

5.3.5 Modulated Differential Scanning Calorimetry Analysis

Figure 5.29 and Figure 5.30 presents the heat flow curve, and temperature derivative of reversible specific heat capacity respectively for different BT/polymer matrices. Although the peak of total heat enthalpy around 11 °C was not highly altered upon addition of BT for both triblocks, rearrangement of this peak due to densification of aromatic structure (T_{C1} and T_{C2} in Figure 5.29 and Figure 5.30 respectively) forming multiple interphases with the soft blocks soon after the endothermic peak enthalpy was found to be affected upon addition of BT. This effect is more prominent in SEBS-g-MA than SEBS triblock due to the high interaction of the polar MA molecule attached to the soft block with BT. Similarly, the rate of change of heat enthalpy soon after glass transition (measured in Figure 5.30) in SEBS-g-MA also showed significant change upon addition of BT than in SEBS as shown in Figure 5.29.

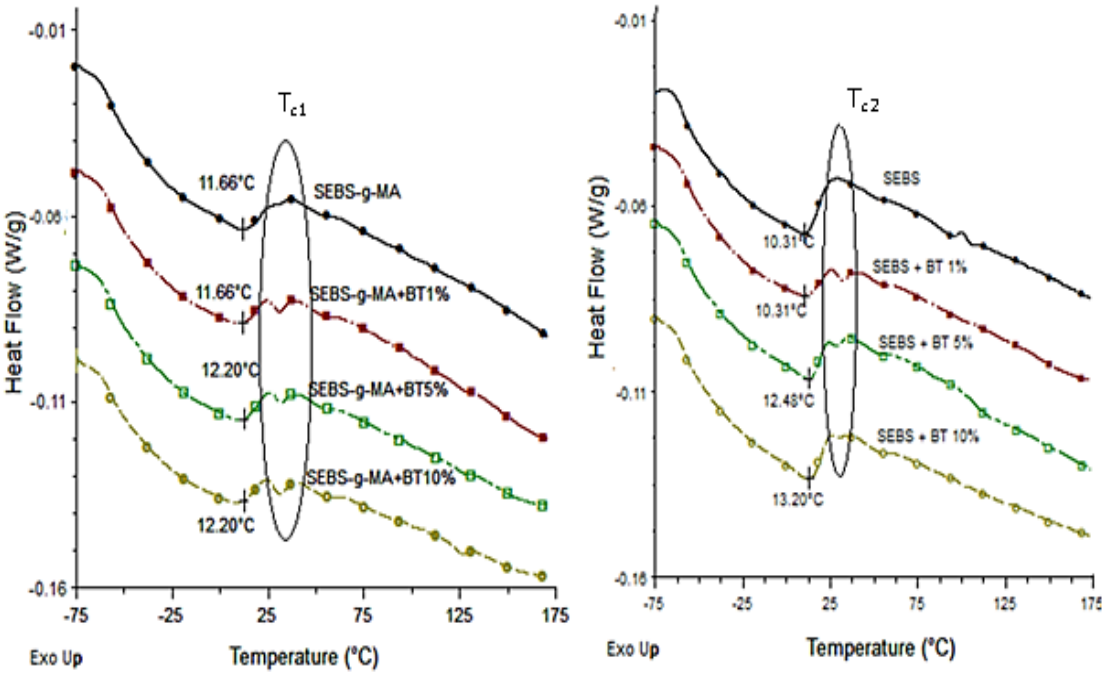

Figure 5.29 Total heat flow curve of SEBS-g-MA/BT composites (left) and SEBS/BT composites (right)

However, the glass transition temperature of different composites (ca. -53°C for SEBS-g-MA composites and -56°C for SEBS composites) calculated by temperature derivative of reversible specific heat capacity were found almost to be constant with the addition of a different amount of BT additives. A slight difference in the glass transition of the soft

block was observed between SEBS-g-MA and SEBS triblock because of the presence of MA, a bulkier molecule, in an ethylene/butylene molecule in SEBS-g-MA. Moreover, the broadening of Tg (ca. 53°C) in SEBS-g-MA compared to SEBS upon addition of BT also confirms the formation of homogenous mixtures of SEBS-g-MA/BT composites than SEBS/BT composites. Also, a sudden change can be observed at around -25 °C in SEBS-g-MA as shown in Figure 5.29 and Figure 5.30 (T1). This sudden change observed around -20°C was found to be altered upon addition of BT additives. In addition, the peak observed around the glass transition temperature of soft block in SEBS-g-MA becomes much smaller and flat compared to SEBS in derivative of Cp curve. It also confirms an interaction of SEBS-g-MA triblock with BT additives.

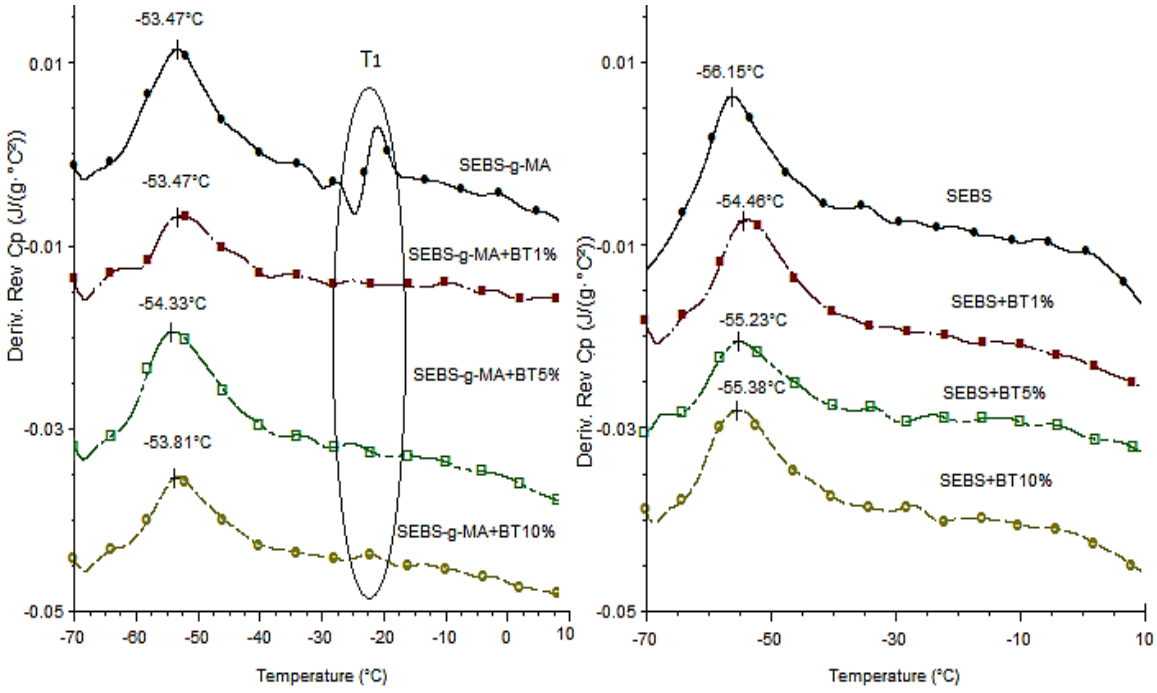

Figure 5.30 Temperature derivative curve of reversible Cp curve of SEBS-g-MA/BT composites (left) and SEBS/BT composites (right)

5.3.6 Attenuated Total Reflectance-Fourier Transfer Infrared Spectroscopy Studies

Figure 5.31 and Figure 5.32 show the ATR-FTIR for SEBS/BT and SEBS-g-MA/BT composites. Similar to CB, BT also shows a slight interaction with SEBS thermoplastic elastomers with the C=C of a benzene ring with a change in wavenumber as shown in

Figure 5.31. The intensity of interaction of BT does not change with C=C bond when BT is changed from 5 wt. % to 10 wt. % (the wavenumber change from 1460 to 1454 cm^{-1} in both cases). In addition, the rocking effect of benzene ring at 758 cm^{-1} wavenumber almost remains constant upon addition of 10 wt.% of BT. Figure 5.32 shows the FTIR graphs of SEBS-g-MA-BT composites.

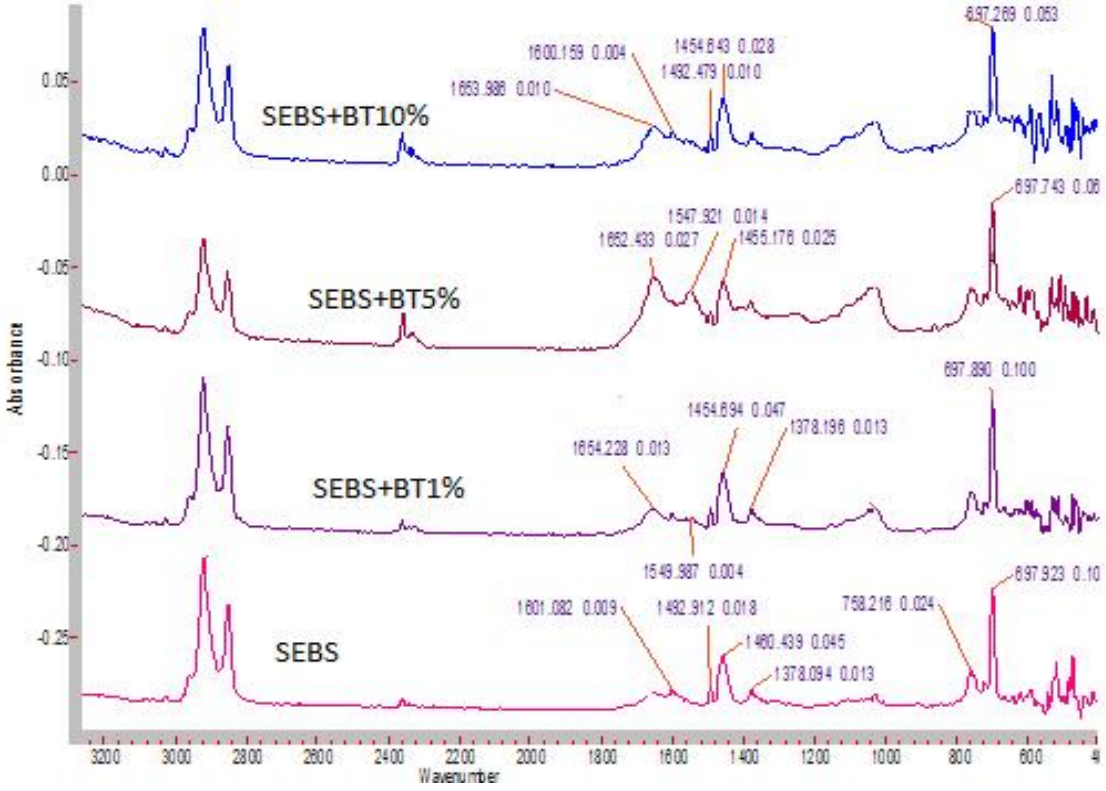

Figure 5.31 ATR-FTIR spectra of SEBS/BT Composites

The graphs show BT interacts mainly with the maleic anhydride group. FTIR band shifts and change in intensity, especially in C=O dimers, C-O-C band peaks, and OH peaks shows the interaction of BT with SEBS-g-MA in acidic or other forms. In addition, change in IR peak band and nature of C=C bond at 1601 cm^{-1} also confirms the interaction of benzene ring of polystyrene with BT. The presence of many other peaks between 1800 cm^{-1} to 1601 cm^{-1} confirms a high interaction of BT with MA molecule together with the benzene ring.

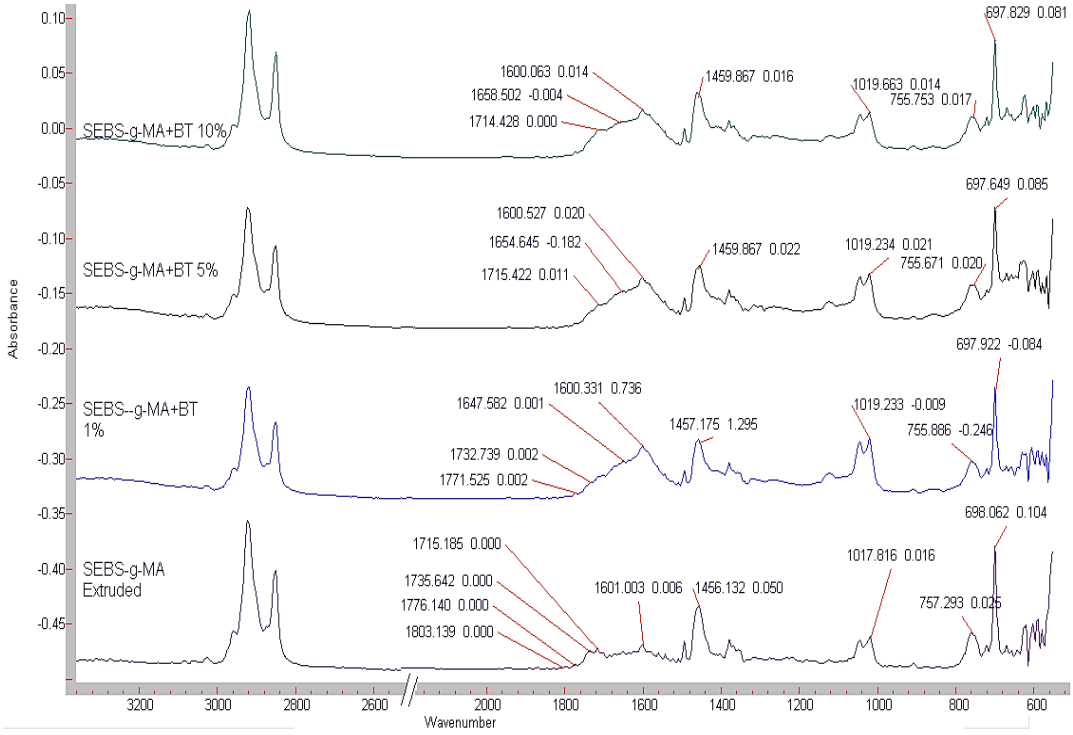

Figure 5.32 ATR-FTIR spectra of SEBS-g-MA/BT Composites

5.3.7 Scanning Electron Microscopy Analysis

Figure 5.33(a) and Figure 5.33(b) show SEM images of SEBS and SEBS-g-MA respectively. SEM images show a slight change in morphological structure between SEBS and SEBS-g-MA. It is suggested that this high glass transition temperature of the soft block of SEBS-g-MA compared to SEBS give rise to the different morphological structure.

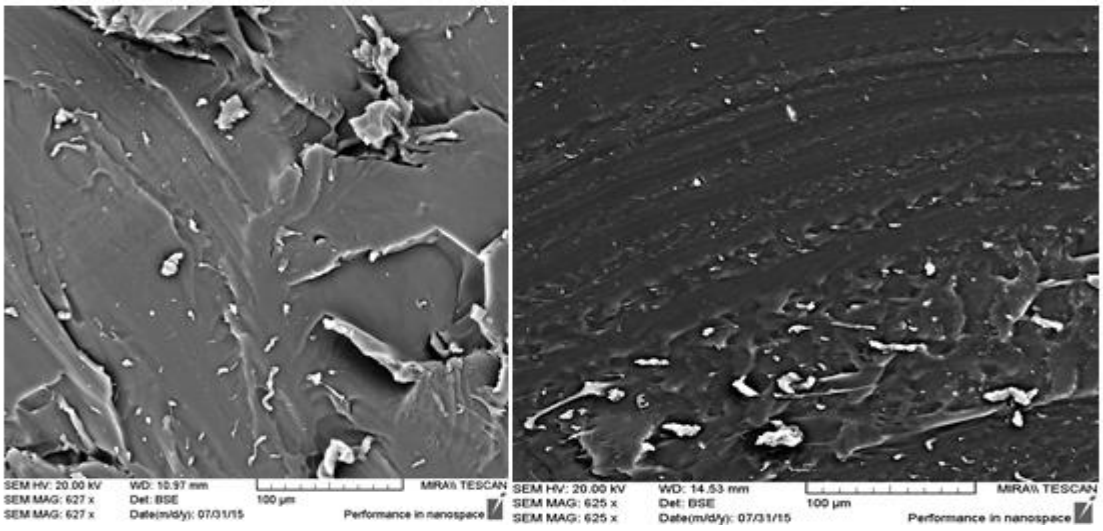

Figure 5.33 SEM images of (a) SEBS left (b) SEBS-g-MA right

Figure 5.34(a) and Figure 5.34(b) show SEM images of SEBS and SEBS-g-MA composites. Comparing Figure 5.33 to Figure 5.34, relatively large morphological changes was observed in SEBS-g-MA nanocomposite compared to SEBS nanocomposite.

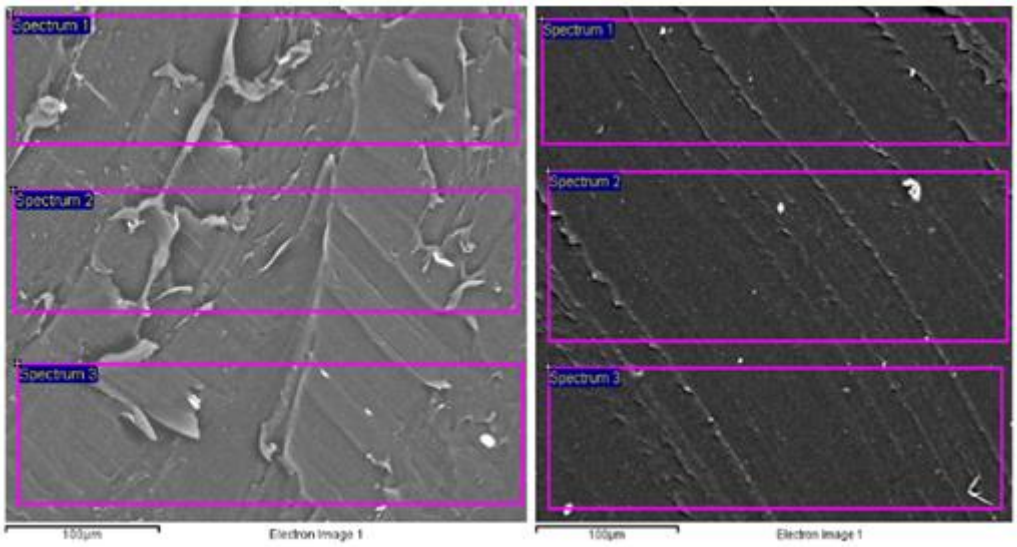

Figure 5.34 Selected area is used for element mapping of (a) SEBS left and (b) SEBS-g-MA Right

For further analysis of dispersion of BT with SEBS and SEBS-g-MA, the element mapping was carried out along the thickness of each sample as shown in Figure 5.34

Table 5.13 Distribution of Ba, Ti, O and C element along different Spectrum on by % weight

Spectrum	SEBS				SEBS-g-MA			
	C	O	Ti	Ba	C	O	Ti	Ba
Spectrum 1	90.50	4.96	1.08	3.46	90.41	5.19	1.06	3.34
Spectrum 2	91.15	4.79	0.98	3.09	90.55	4.97	1.09	3.39
Spectrum 3	91.39	4.75	0.98	2.89	90.47	5.01	1.12	3.40
Mean	91.01	4.83	1.01	3.15	90.48	5.06	1.09	3.38
Std. deviation	0.46	0.11	0.06	0.29	0.07	0.12	0.03	0.03

From Table 5.13, it was observed that the distribution of C, O, Ti and Ba were not uniform along the thickness in SEBS. The percentage weight of Ba element varies from 3.46 to 2.89 by weight making a wide range 0.57 and standard deviation of 0.29 in SEBS. Non-uniform dispersion of these elements gave rise to unexpected polarization as well as mechanical behavior during test conditions. Whereas, from Table 5.13, it can be observed that the dispersion of BT in SEBS-g-MA is uniform with the standard deviation of 0.03 wt % of Ba element between three spectra selected. The addition of a polarization group MA in SEBS was found very useful for increasing dielectric as well as compatibility with different polar materials to optimize dielectric and mechanical properties.

From SEM images of SEBS and SEBS-g-MA, BT was found to be poorly distributed along the thickness of a sample for SEBS compared to SEBS-g-MA. Because of poor dispersion of BT in SEBS, SEBS-BT composite samples can be considered as separate capacitors ($C_1, C_2 ... C_n$) with different dielectric constant (($\varepsilon_1, \varepsilon_2 ... \varepsilon_n$). If we consider graphically as in Figure 5.35 we can develop a model for understanding the overall dielectric permittivity (ε) of the capacitor (C).

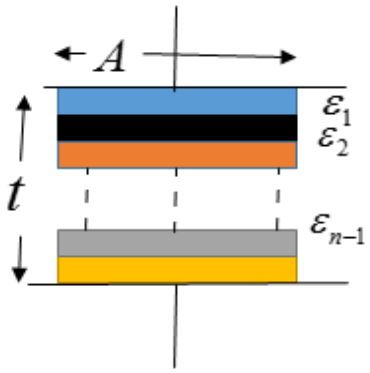

Figure 5.35 Nanocomposite with poor dispersion of additives

$$1/C = 1/C_1 + 1/C_2 ... + 1/C_n \qquad \text{Equation 5.7}$$

$$C = \varepsilon_0 \varepsilon A / t \qquad \text{Equation 5.8}$$

From Equation 5.7 and Equation 5.8

$$t/\varepsilon_0\varepsilon A = t_1/\varepsilon_0\varepsilon_1 A_1 + t_2/\varepsilon_0\varepsilon_2 A_2 ... + t_n/\varepsilon_0\varepsilon_n A_n \quad \text{Equation 5.9}$$

Where $\varepsilon_1, \varepsilon_2 ... \varepsilon_n$ correspond to the dielectric permittivity existing along the sample of capacitance $C_1, C_2 ... C_n$ with thickness $t_1, t_2 ... t_n$ and cross section area $A_1, A_2 ... A_2$ respectively due to poor dispersion of nanofillers into the polymer matrix. For simplicity, thickness and cross section area was constant for all small capacitors within a sample thickness.

Equation 5.9 then reduces to Equation 5.10

$$1/\varepsilon = 1/n(1/\varepsilon_1 + 1/\varepsilon_2 ... + 1/\varepsilon_n) \quad \text{Equation 5.10}$$

If we consider three small capacitors with dielectric permittivity with 2, 5, and 10 arranged in parallel as shown in Figure 5.35, then the average dielectric permittivity measured by an instrument is valued at 3.5 only.

But, as the dispersion level increases, the dielectric permittivity of all small capacitors become almost the same causing an increase in overall dielectric permittivity of composites.

5.3.8 Conclusion

Polarization enhancements with very low dielectric loss were achieved on non-polarising (SEBS) copolymers and polarizing copolymers (SEBS-g-MA) using a variety of concentrations of dielectric filler materials (BT) by using a co-rotating twin screw extrusion system. However, the compatibility and interaction between polymers and additives were found to be crucial for increasing polarization as well as to obtaining better mechanical properties. FTIR, DSC, and DMA results showed an improved interaction of BT with SEBS-g-MA compared to SEBS leading to a highed dispersion of BT in SEBS-g-MA than SEBS polymer matrix. Change in heat enthalpy and rearrangement of micro-molecules upon BT addition on different polymer matrices had led to different thermal, electrical, morphological and mechanical behavior. However, no significant change in the glass transition of polymer matrix was observed upon addition of BT in all composite types.

A high increase in dielectric permittivity with the low dielectric loss with minimal change in loss factor was observed in SEBS-g-MA; this result suggests the potential of these

manufactured nanocomposites to be used not only for stress and strain sensors, robotic artificial muscles applications but also for capacity energy harvesters and charge storing devices.

Minimal changes in mechanical properties (Young's modulus, resilience as well as stiffness in both transverse as well as parallel to extrusion) compared to the high changes in dielectric permittivity in SEBS-g-MA composites also suggests that SEBS-g-MA- BT nanocomposites manufactured using this technology are sensitive to compression force as well as possess high Maxwell stress under an electric field because of higher permittivity and lower stiffness. Moreover, from DMA and DSC analysis, it can be suggested that temperature plays a major role in defining the structural, and mechanical changes of nanocomposite and hence electromechanical properties.

Chapter 6

6 Supercritical Fluid Assisted Extrusion Technology for Manufacturing of Conductive Filler and Dielectric Filler based Thermoplastic Elastomeric Composites for Wide-varying Applications

6.1 Introduction

Development of the exfoliation techniques of conductive as well as dielectric fillers in polymer matrices needs a thoughtful research strategy to reduce cost, production time and scalability of superior composites production for stress/strain sensing and capacitive harvesting applications. Industrial standard supercritical fluid (SCF) technology originally established in the 1970s has huge potential for production as well as exfoliation of conductive fillers and dielectric fillers in different electro-sensitive polymers. However, the use of SCF technology has been limited to extraction due to high initial capital requirement as well as the dearth of combined knowledge of high shear force machines such as extrusion, high pressure chamber equipment used for SCF processing and advanced polymer processing techniques such as extrusion. Among SCFs, it is well known that supercritical carbon dioxide ($scCO_2$) provides good solubility in molten polymers and acts as a plasticizer resulting in a decrease in the viscosity of the molten polymer, the melting point, and the glass transition temperature [126-128]. These changes, in turn, result in the fractionation of polymer, modifying the mechanical, as well as the physical properties of the polymer [126, 128-131]. Although a plethora of work exists in scientific and industrial communities using SCF batch processing techniques, a dearth of knowledge still persists on the use of SCF for continuous industrial standard polymer manufacturing process such as hot melt extrusion. In addition, lack of scientific understanding on how SCF affects the thermal, mechanical, electrical, and morphological properties of different polymers using hot melt extrusion remains unexplored. Therefore, complete use of $scCO_2$ assisted extrusion of polymers is limited for commercial applications.

For better understanding and evaluation of $scCO_2$ processed elastomeric composites for stress/strain sensing and energy harvesting applications, this chapter is further divided into four sections.

6.2 Supercritical Carbon Dioxide Assisted Extrusion of Microphase-Separated SEBS

6.2.1 Introduction

In this section, the microstructural, dielectric, chemical and mechanical effect on SEBS due to $scCO_2$ is highlighted. These analyses are crucial for the scientific understanding of $scCO_2$ assisted extrusion to produce smart composites for different electroactive/smart applications

6.2.2 Thermogravimetric Analysis

The thermal degradation profile of SEBS extruded at different pressures with $scCO_2$ is shown in Figure 6.1.

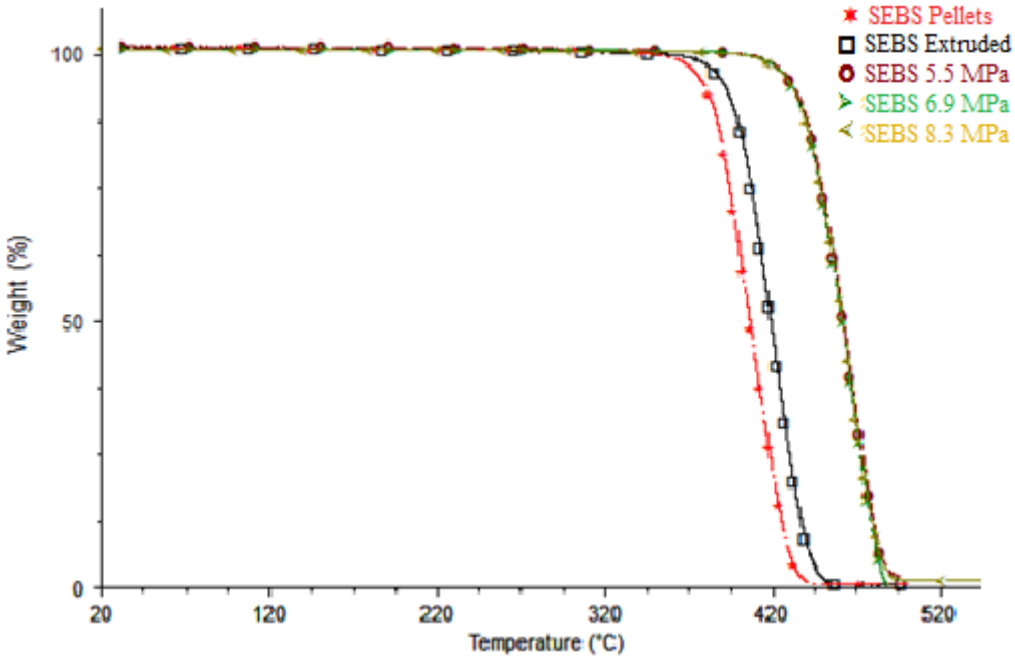

Figure 6.1 Degradation profiles of SEBS extruded under different conditions

Similarly, Table 6.1 shows the overall degradation profile of SEBS processed under set pressures. The overall degradation temperature of virgin SEBS was 405.08 °C, which increased to 419.81°C when extruded. This increase suggests that extruded samples are thermally more stable than their counterparts [227]. The increment of thermal stability after SEBS was extruded suggests that the extrusion had oriented the molecular structure

and decreased the distance between the hard phases. Moreover, thermal degradation of a polymer is a complex phenomenon and is dependent on time, temperature, concentration and migration of molecules within a sample. Small changes in these factors cause a huge change in degradation profile of a polymer [228]. In addition, structural changes caused due to the thermal energy during extrusion leads the material to be more thermally stable than thermally untreated material (pellets). Similarly, the overall degradation temperature of SEBS was found highly enhanced by ca. 62 $^{\circ}$C when extruded with assisted $scCO_2$, as shown in Table 6.1. The increase in degradation temperature of SEBS can be attributed to the restructuring of poly(styrene) (S) hard block around the ethylene/butylene (EB) soft block.

Table 6.1 Degradation profile of SEBS processed under different conditions

Materials	**Degradation Temperature ($^{\circ}$C)**
SEBS	405.08
SEBS extruded	419.81
SEBS 5.50 MPa	467.47
SEBS 6.90 MPa	467.07
SEBS 8.27 MPa	468.07

6.2.3 Modulated Differential Scanning Calorimetry

Modulated differential scanning calorimetry (MDSC) technique was used to analyze all the complex microscopic transitions of SEBS due to its sensitivity towards thermal transitions. Figure 6.2 shows the MDSC thermograms of total heat flow for its first cycle and Figure 6.3 shows the MDSC thermograms of heat capacity for its first cycle. The glass transition of the ethylene-butylene (Tg^{EB}) block was observed at around -55 °C. At higher temperatures, the entanglements are resolved and most of the chain structures take part in thermal motion via break down of the cross-links and rearrangement of the backbone. This relaxation due to entanglement can be observed in the heat flow thermogram at 8.74 °C for untreated SEBS and 12.72 °C for SEBS extruded at 8.27 MPa. This increasing relaxation, when assisted with $scCO_2$, can be attributed to higher temperature requirements to completely resolve the entanglements/break down of

crosslinks and rearrangement of polymer microstructures to behave like a viscous fluid. The Tg of pure styrene (S) rich phase (Tg^S), around 96 °C, is not clearly visible in any of the thermograms. However, small exothermic peaks are evident at 101.74 °C and 100.34 °C for extrudates at 6.90 MPa and 8.27 MPa which shows the formation of phase segregated microstructures or rearrangement process of pure S phase.

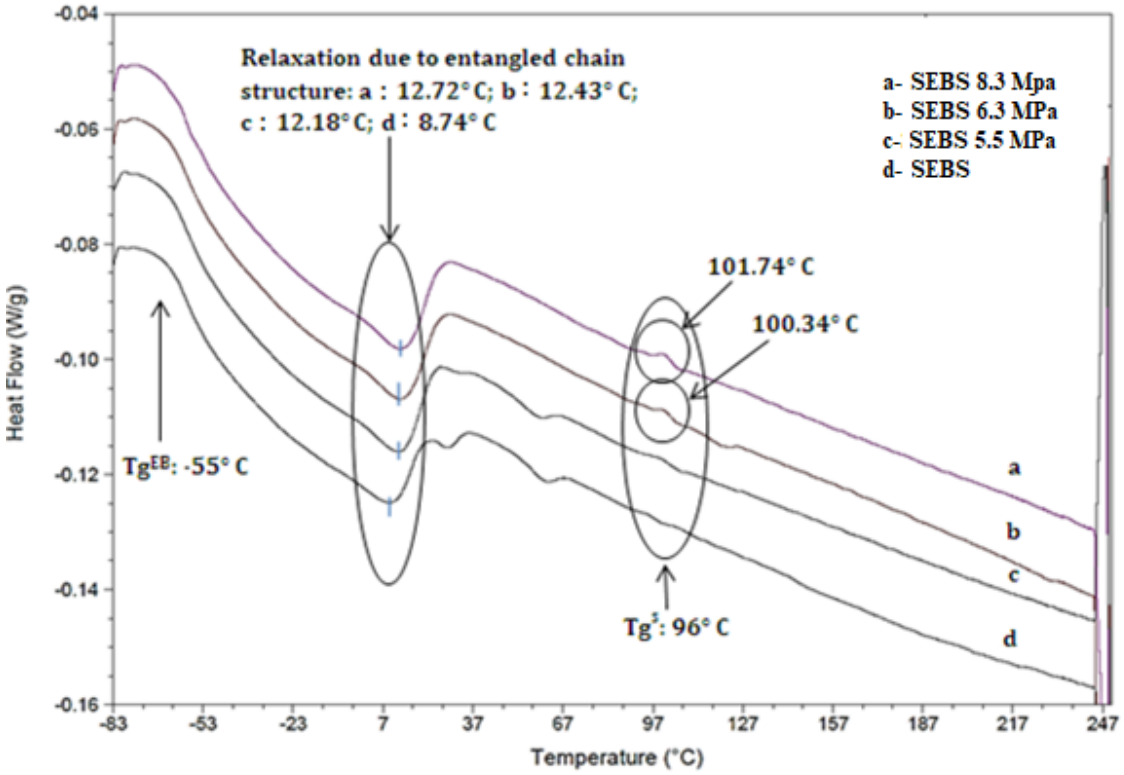

Figure 6.2 Heat flow thermogram of $scCO_2$ assisted extrudates of SEBS for its first cycle

Figure 6.3 shows the first cycle heat capacity thermograms of $scCO_2$ assisted extrudates at various pressures. The breakdown of entanglement rearrangement of microstructures can be observed with increased heat capacity peak. The enthalpic relaxation of EB block is also evident from the untreated and 5.50 MPa SEBS extrudates, however, no evident peaks can be observed for 6.90 MPa and 8.27 MPa SEBS extrudates which may be due to the restructuring of hard phases.

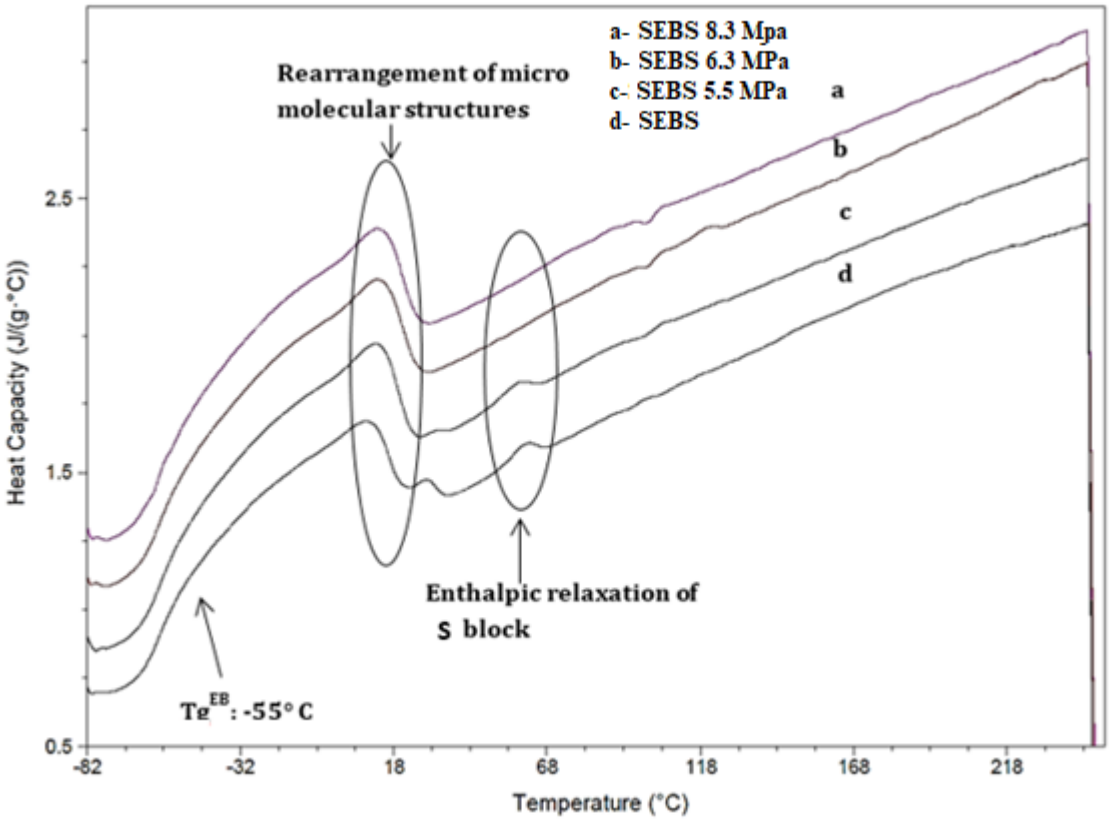

Figure 6.3 Heat capacity thermogram of $scCO_2$ assisted extrudates of SEBS for its first cycle

Many transitions or formation of microphases are not clearly seen directly in the heat capacity curve, however, many transitions are evident from the derivative of the de-convoluted reversing heat capacity curve (Figure 6.4), which otherwise goes undetected by heat flow thermogram of standard DSC. A very clear and single peak can be observed from Figure 6.4 at -55. °C, attributed to Tg of the EB block for virgin, 5.50 MP and 6.90 MPa SEBS extrudates, however, divided peaks were observed at -58.68 °C and -52.59 °C for SEBS extruded at 8.27 MPa. Such division of peaks can be likely due to the formation of new microstructure or increase in the microphase separation within the EB rich phase with its own Tg. The lower temperature peak at -58.63 °C and higher temperature peak at -52.59°C is due to separation of the ethylene and butylene block respectively from the soft EB domain of SEBS triblock. The continuous curvature throughout the cycle represents the formation of phase separation/disordered phases of interfacial domains with its own glass transition temperature (Tg^I). The Tg of S-rich microphase has a slight shift from 97 °C for untreated SEBS to 102 °C for $scCO_2$ treated SEBS. This is also due

to the formation of highly phase separated domains between the soft EB block and the glassy S block.

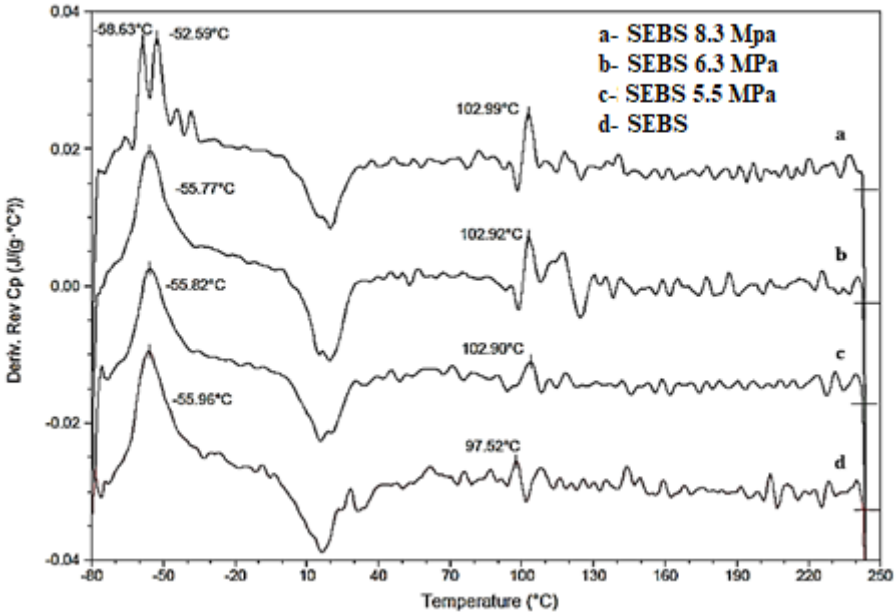

Figure 6.4 Derivative of reversing heat capacity thermogram of $scCO_2$ assisted extrudates of SEBS for its first cycle

6.2.4 Dynamic Mechanical Analysis

The influence of $scCO_2$ on SEBS under different pressure conditions over temperature on storage modulus, and loss modulus is presented in Figure 6.5. In virgin SEBS, the storage modulus is continuously changing starting from 25 °C giving an onset point of 61.88 °C. This temperature can also be compared with the enthalpic relaxation of S domain as seen in the heat capacity thermograph. The pure glassy behavior of polystyrene is evident below this temperature. However, the continuous decrease in storage modulus is observed far below this temperature, which is due to the higher influence of soft block on hard block. This storage modulus becomes stable up to 50 °C when SEBS is extruded with $scCO_2$ at 8.27 MPa. This behavior of S- rich domains also suggests improved phase separation between the hard and the soft domains. In addition, the introduction of $scCO_2$ during extrusion leads to a decrease in modulus (represented by storage modulus) as well as the molecular frictional movements between hard and soft block segments (represented by loss modulus) of the elastomers as shown in Figure 6.5. The influence of $scCO_2$ on

loss and storage modulus SEBS was found to be proportional to the pressure of $scCO_2$. This decrease in storage modulus suggests that the $scCO_2$ treatment has initiated the rearrangement of structure and restructuring of hard domains around the soft block which is also linked to the mechanical properties i.e. the reduction in the modulus. This reduced restriction on movement of molecules due to smaller domain size of both hard and the soft phase results in lowering the viscosity of the polymer and thereby lowering the loss modulus.

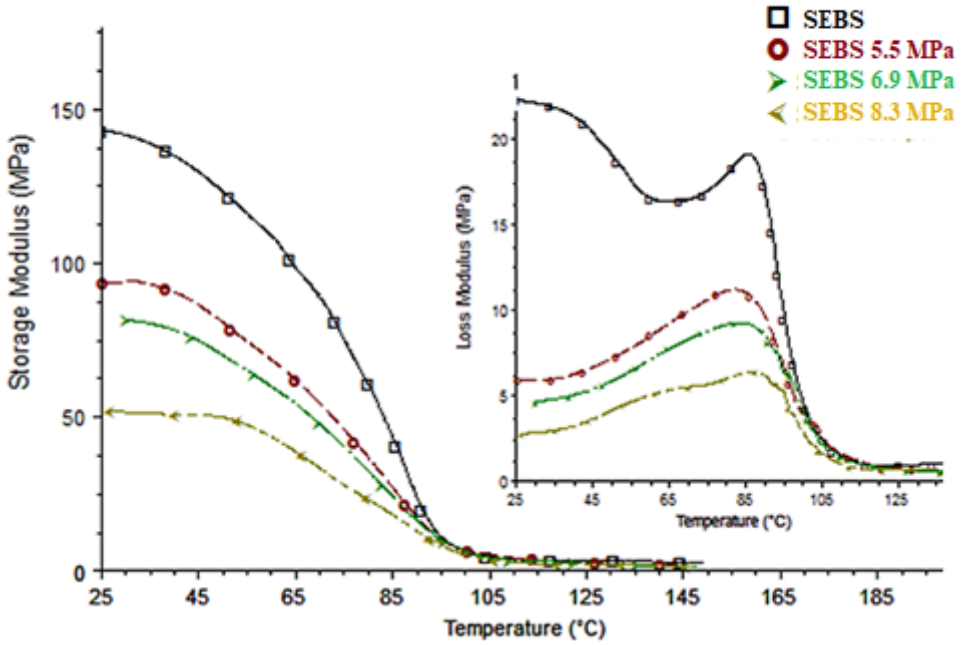

Figure 6.5 Storage and loss moduli of SEBS extruded at different pressure measured in the parallel direction to extrusion

The influence of $scCO_2$ on SEBS under different pressure conditions over temperature on tan delta is presented in Figure 6.6. The change in glass transition temperature of hard block noted using tan delta was found to be 94.68 °C, whereas, a shift in the tan delta was found to be at 97.18 °C, 97.32 °C, and 97.20 °C when SEBS was extruded at 5.50 MPa, 6.90 MPa and 8.27 MPa respectively. Compared to Tg of S-rich phase measured from derivative of Cp reversing curve, the Tg measured using Tan delta of DMA curve has a deviation of 2.68°C, 5.72 °C, 5.62 °C and 5.79 °C for virgin, 5.50 MPa, 6.90 MPa and 8.27 MPa SEBS, respectively. This result was verified using DSC in section 6.2.3. This increase in glass transition temperature of the hard block also suggests that the thermal

incompatibility of hard polystyrene block increases with soft (ethylene- butylene) blocks when extruded with $scCO_2$. Thermal incompatibility refers to two components (hard and soft blocks in SEBS) with wide variation in thermal behaviour due to the different glass transition of soft and hard block. Moreover, the value of tan delta was found to be lower up to 60 °C and the height, as well as broadness of this peak, reduces when SEBS is extruded with an assistance of $scCO_2$. This reducing tan delta peak suggests that the reduced frictional and heating loss as well as damping nature of SEBS at the molecular level, as $scCO_2$ breaks down the microdomains, makes the material behave like a homogeneous network at micro scale. Analysis of such homogenization and thermal incompatibility behavior using DMA has not been reported elsewhere to the best of authors knowledge.

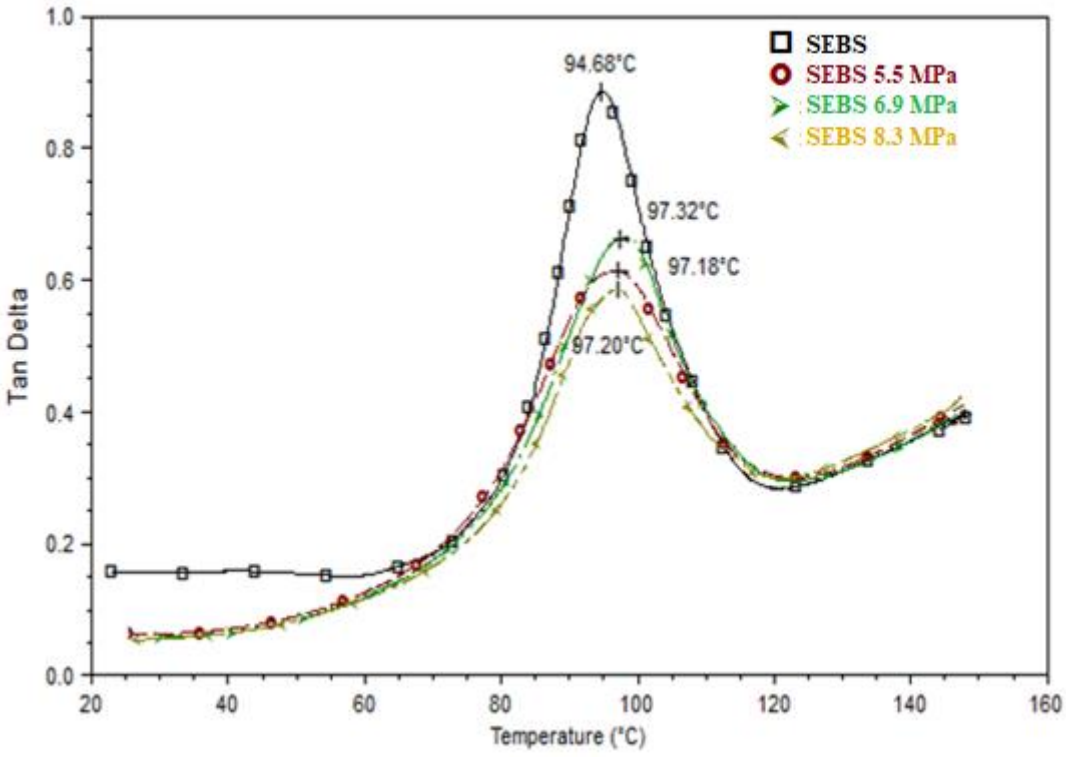

Figure 6.6 Tan Delta of SEBS extruded at different pressure measured in the parallel direction to extrusion

Palakodeti *et al*. [103] and Kombluh *et al*. [35] define the mechanical efficiency of elastomers is dependent on the value of tan delta and is given by Equation 6.1

$$\eta_m = \frac{1}{1 + \Pi \tan \delta_m} \qquad \text{Equation 6.1}$$

From Figure 6.6, SEBS extruded with $scCO_2$ showed 67% reduction in value of tan delta making superior for several applications such as actuation, energy harvesting and stress/strain sensing with 113% enhancement in terms of mechanical performance as derived from Equation 6.1.

6.2.5 Mechanical Testing

The results of the tensile tests are presented in Figure 6.7 and Table 6.2. The Young's modulus shown in Table 6.2 is calculated using the regression method from 0.25 %-1 % extension exhibited by a virgin, 5.50 MPa, 6.90 MPa and 8.27 MPa SEBS. Similar to storage modulus, Young's modulus of SEBS also was found decreased with the introduction of $scCO_2$ from 69.45 MPa to 44.39 MPa when the pressure was increased from 0 psi to 8.27 MPa and this decrease was proportional to the $scCO_2$ pressure. The Young's modulus of extruded SEBS measured in the parallel direction to extrusion in this section is smaller compared to other sections of this whole thesis as the SEBS used here was not reprocessed with haul off system as described in Section 3.3 of Chapter 3.

Table 6.2 Young's Modulus obtained by regression method, modulus of resilience and modulus of toughness of SEBS extruded at a different pressure measured in parallel direction to extrusion

Sample	Young Modulus (MPa)	Modulus of Resilience (MPa)	Modulus of Toughness at 600 % extension (MPa)
Extruded SEBS	69.45±3.77	45.42	3740.44
SEBS 5.50 MPa	67.53±13.4	46.46	3486.52
SEBS 6.9 MPa	46.83±6.3	36.94	3081.10
SEBS 8.27 MPa	44.39± 7.1	28.63	2585.08

According to Cantournet *et al*. [222], the extension of elastomers like SEBS occurs with a combination of sliding and non-sliding action between hard and soft blocks. The non-

sliding behavior is observed in elastomers only within an elastic limit where strain response of an elastomer is directly proportional to applied stress. Table 6.2 also shows the modulus of resilience and modulus of toughness of SEBS extruded with different pressure of $scCO_2$. The modulus of resilience was observed to be almost constant at 5.50 MPa compared to virgin SEBS extrudates, as shown in Table 6.2, as the nature of the curve for virgin and 5.50 MPa SEBS remains constant up to 3% strain as shown in Figure 6.7. This effect of a decrease in modulus of resilience was noted as the pressure of $scCO_2$ was increased to 6.90 MPa and 8.27 MPa; similar to the pattern observed in the storage modulus of the DMA results obtained. The introduction of $scCO_2$ on SEBS has led to high thermal incompatibility between the soft block and hard block as observed in DSC and DMA graphs. This effect suggests a direct impact on sliding behavior of the hard block over soft block making SEBS triblock less resistant to external forces after the elastic linear region.

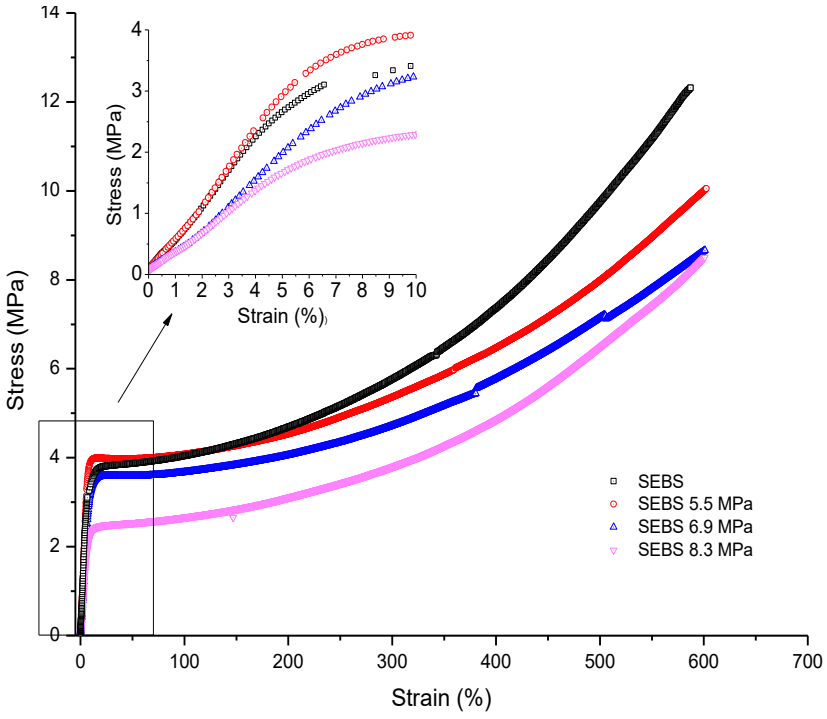

Figure 6.7 Stress - strain response exhibited by extruded SEBS at different pressure measured in the parallel direction to extrusion

6.2.6 Attenuated Total Reflectance-Fourier Transfer Infrared Spectroscopy Studies

ATR-FTIR spectra of transmittance illustrate the effect of supercritical assisted extrusion on SEBS at various critical pressures shown in Figure 6.8. Peaks at 2920 cm^{-1} and 2851 cm^{-1} representing the asymmetrical stretching of $–CH_3$ and $–CH_2$ (the ethylene-butylene block) do not show any shift in the position even when treated at higher critical pressures (8.27 MPa).

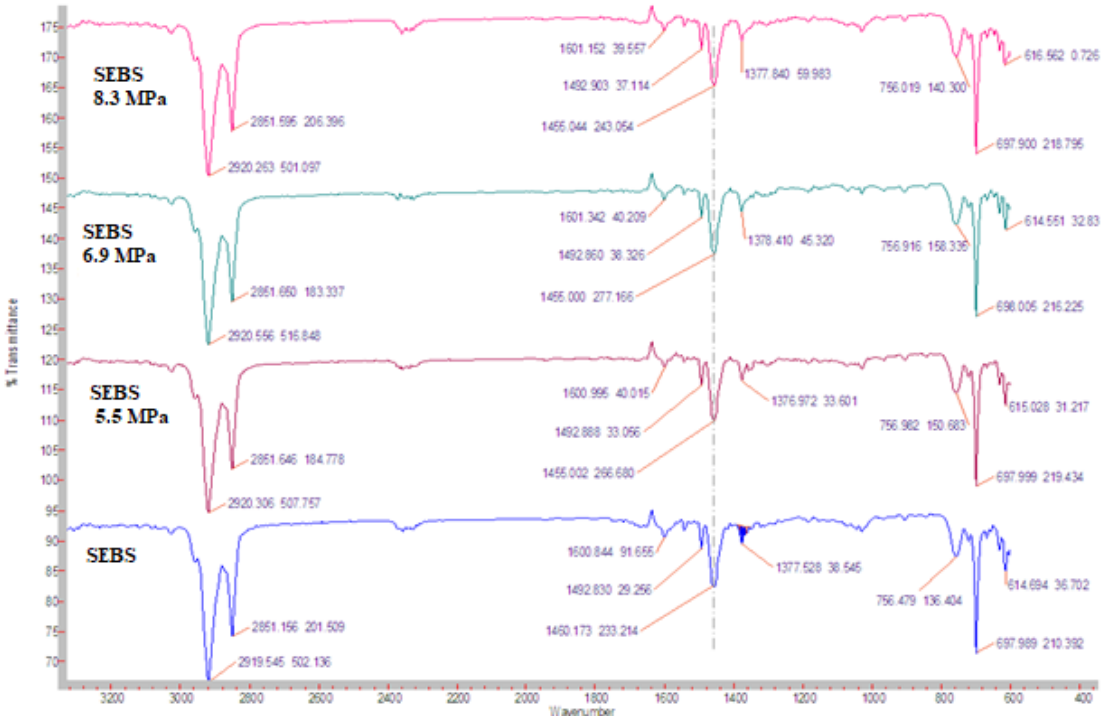

Figure 6.8 ATR-FTIR transmittance spectra of SEBS extruded at different pressure

The aromatic C=C stretching of the aromatic system at peak 1600 cm^{-1} and 1492 cm^{-1} remain in their respective positions for extrudates at all the critical pressures. Peaks 756 cm^{-1} and 697 cm^{-1} are attributed to benzene styrene moiety of SEBS. The peak at 1377 cm^{-1} represents the bending of $-CH_3$. It can be observed from the transmittance spectra that the $scCO_2$ has caused a shift in peak from 1460 cm^{-1} to 1455 cm^{-1}, which was attributed to asymmetric $–CH_2$, bending. These bands are also attributed to stretching vibrations of C=C in the aromatic rings [229] (phenyl rings in polystyrene, C=C pi bond interactions with CO_2). It is suggested that the shifting of 1460 cm^{-1} to 1455 cm^{-1} (near

towards the figure print region 1452 cm^{-1} of virgin polystyrene) is due to the higher thermal incompatibility leading to high phase separation of hard S block with the soft EB block in SEBS [230]. The quadrupole moment of CO_2 allows Lewis acid-base interactions between the polymer matrix and CO_2. Many researchers have observed a similar effect of the CO_2 - phenyl ring interaction [128, 137, 138, 230]. Evident differences in the spectra were not indicative, due to the reason that SEBS is an amorphous polymer with 29% styrene and mostly polyethylene-butylene.

6.2.7 Dielectric Analysis

Figure 6.9 shows the dielectric analysis of SEBS extruded at various critical pressures. The real dielectric permittivity of extruded virgin SEBS, 5.50 MPa, 6.90 MPa and 8.27 MPa was found to be 2.57, 2.46, 2.47, and 2.05 respectively.

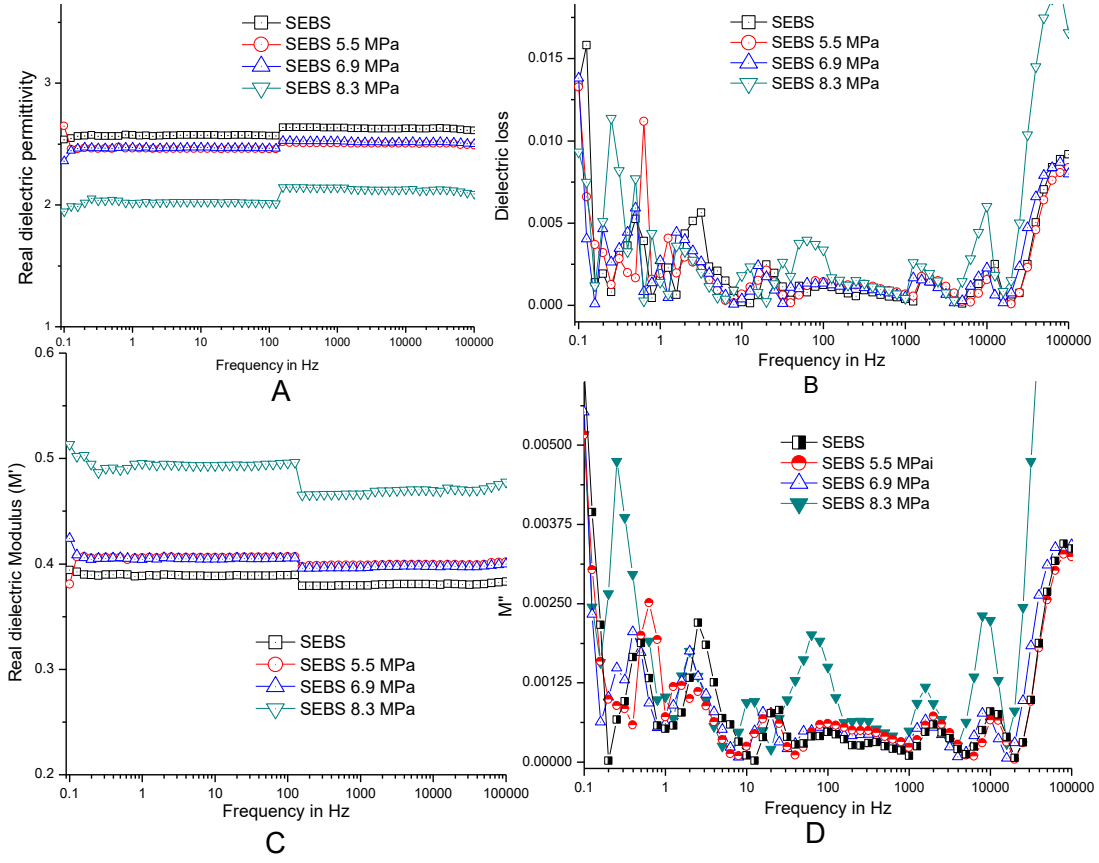

Figure 6.9 A. Real dielectric permittivity, B. Dielectric loss, C. Real dielectric modulus and D. Imaginary dielectric modulus of SEBS extruded at various critical pressures.

Figure 6.9A illustrates the slight decrease in dielectric permittivity of SEBS when extruded with $scCO_2$. This relative decrease in the real dielectric permittivity is attributed to an increase in foaming with an increase in pressure as shown in the morphological images in Figure 6.10. The dielectric loss observed in Figure 6.9B of all extruded SEBS were found to be very low (< 0.02) making them highly electrets in nature. However, the dielectric loss increases with an increase in higher frequency (> 20000Hz). The dielectric relaxation observed in Figure 6.10D as a function of the imaginary electric modulus (M") shows different dielectric relaxation at very low (around 0.1 Hz) and high frequency (around 10^5 Hz) for SEBS 8.27 MPa compared to other counterparts. The change in relaxation process of different domains present in SEBS when extruded with an assistance of $scCO_2$ confirms the change in the microstructure of SEBS. This result along with other analysis performed support the structural changes on SEBS identified when extruded with an assistance of $scCO_2$ This suggests higher microdomain formation leading to higher number of relaxation over the range of measured frequency. This occurs due to the difference in domain size having different conditions of internal dipole polarization within a triblock [231].

6.2.8 Morphology analysis

Figure 6.10 shows the porosity of SEBS extruded under different pressure conditions.

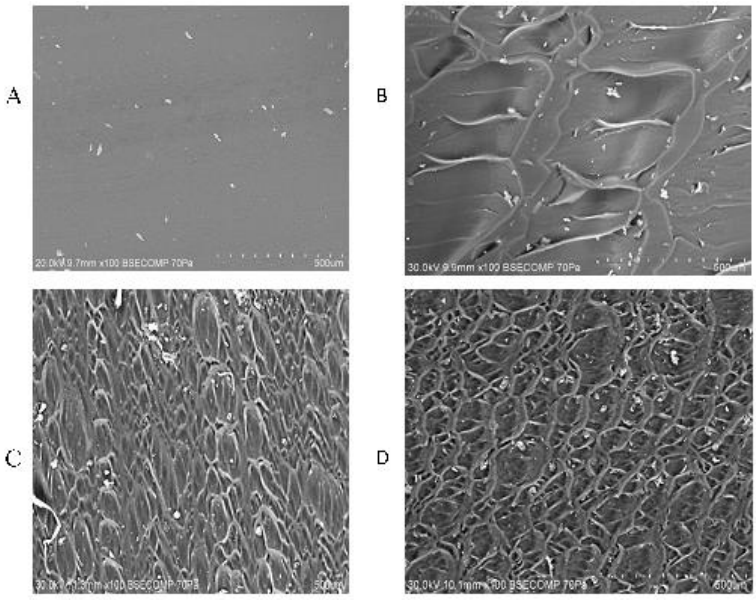

Figure 6.10 SEM images of (A) SEBS (B) SEBS at 5.5MPa (C) SEBS at 6.9 MPa and (D) SEBS at 8.27 MPa

The density of pores at the surface is dependent on the critical pressure of carbon dioxide passed through the extruder. The porosity starts to form at the surface at 5.50 MPa as shown in Figure 6.10 (B), increases at 6.90 MPa as shown in Figure 6.10 (C) and becomes intense at 8.27 MPa as shown in Figure 6.10 (D). The formation of pores is one of the reasons for the decrease in dielectric permittivity and Young's modulus of SEBS at 8.27 MPa.

6.2.9 Conclusion

SEBS was extruded using supercritical carbon dioxide at various critical pressures (5.50 MPa, 6.90 MPa and 8.27 MPa) to investigate its effect on thermal, mechanical, morphological, and dielectric properties. Improvement in homogenization behavior and micro-phase separation and enhancement in mechanical performance due to reduction in tan delta values over the range of temperature of supercritical treated SEBS elastomers was reported in this section for the first time.

The increase in degradation temperature is due to the formation of additional microphases and change in chain length when extruded at different $scCO_2$. The MDSC results confirm that $scCO_2$ assisted extrusion of SEBS at various pressures resulted in increased microphases separations or formation of new microphases, thus producing of the new structure of SEBS. DMTA analysis shows that the introduction of $scCO_2$ during extrusion leads to decrease in modulus (represented by storage modulus) as well as the molecular frictional movements between hard and soft block segments (represented by loss modulus) of the elastomers. The tan delta at 96 °C, shows the actual restructuring of hard and soft domains. Similar decreases in Young's modulus were also observed from the tensile test curves. FTIR spectra of SEBS extruded at various pressures show a significant shift in peak from 1460 cm^{-1} to 1455 cm^{-1} representing the effect of the CO_2 - phenyl ring interaction. Dielectric studies identify a slight decrease in dielectric permittivity due to foaming. In addition, dielectric relaxation over the frequency range concludes the formation of different microphase domain when extruded with 8.27 MPa

6.3 SEBS/CB Composites Manufactured using Supercritical Fluid Assisted Extrusion

6.3.1 Introduction

In this section, the primary objective of enhancing conductivity of thermoplastic elastomers is addressed. In addition, manufacturing conductive flexible composites using $scCO_2$ at very low percentage of CB is also highlighted. Finally, morphological, electrical, mechanical and thermal effects of $scCO_2$ assisted extrusion in dielectric and conductive composites were addressed. These changes might be due to additive- polymer interaction, $scCO_2$ polymer interaction, and $scCO_2$ additive interaction. These interactions are thoroughly discussed in this section

6.3.2 Mechanical Testing

Figure 6.11 and Table 6.3 shows the tensile graphs up to 200% strain and secant Young's modulus of SEBS SCF with different percentage of CB respectively. From Table 6.3, the secant Young's modulus measured at a high percentage of strain along the direction of extrusion show a slight decrease compared to SEBS extruded without $scCO_2$ as described in Chapter 5 in section 5.2.3.

Table 6.3 Secant Young's modulus of SEBS SCF with CB

Nanocomposites	**Young's modulus at several composite different strain (MPa)**			
	1%	**50%**	**100%**	**150%**
SEBS SCF	90.0± 7.69	8.1± 0.30	4.6± 0.24	3.4±0.21
SEBS SCF + CB 1%	98.07± 8.71	8.3± 0.43	4.7±0.32	3.62±0.20
SEBS SCF + CB 2%	97.71± 9.01	8.5± 0.39	4.9±0.29	3.8±0.19
SEBS SCF + CB 5%	87.21± 6.23	8.9± 0.36	5.33±0.31	4.3±0.25
SEBS SCF + CB 10%	107.34±5.38	10.3±0.38	6.6±0.30	5.3±0.28

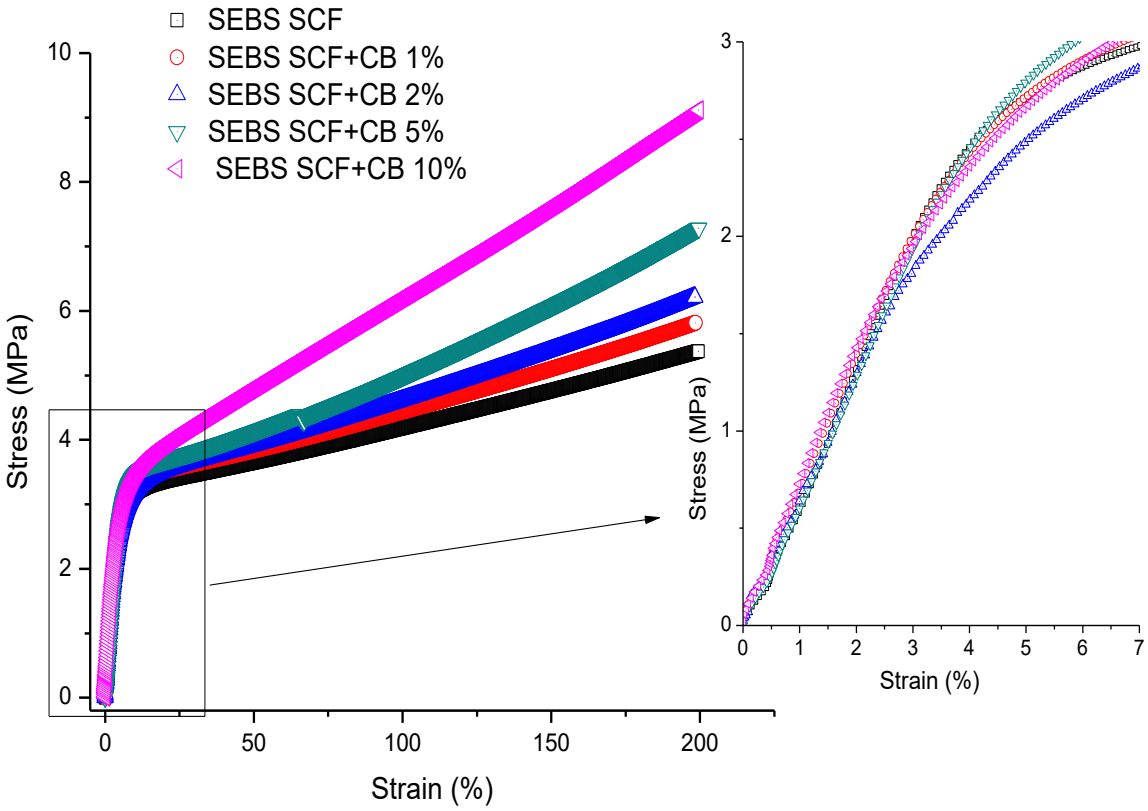

Figure 6.11 Tensile properties of SEBS-scCO$_2$ with CB measured in the parallel direction to extrusion.

This slight decrease in secant Young's modulus was attributed to the dimensional changes in soft and hard domains and the structural change on triblock mainly on chain length, when extruded with an assistance of scCO$_2$ [232].

For the further evaluation of shape memory properties loss factor at 200% strain along the direction was calculated using loss energy factor as described in materials and method Section 3.5.1.

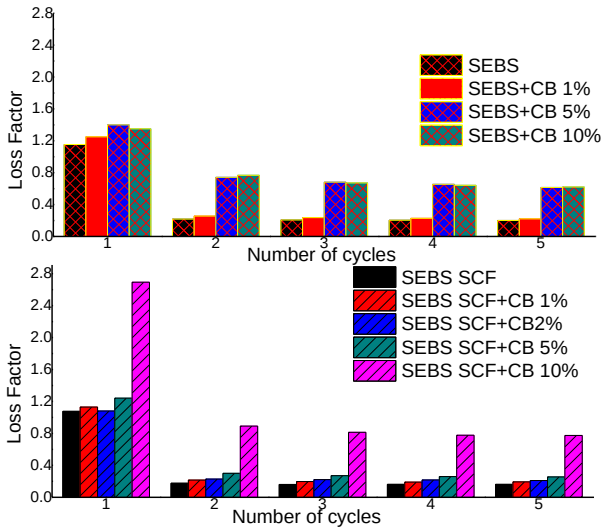

Figure 6.12 Loss energy factor of SEBS extruded parallel to extrusion with/without an assistance $scCO_2$

Figure 6.12 shows the loss energy factor of SEBS extruded with/without an assistance of $scCO_2$. Loss energy factor can be directly correlated with the hysteresis energy loss over elastic energy. From Figure 6.12, SEBS (up to 5 wt. % CB) processed with an assistance of $scCO_2$ show comparatively low mechanical loss for all cycles, thereby enhancing the mechanical performance of the elastomeric composites for stress/strain sensing applications. The microstructural change/shortening of SEBS chains causes enhancement in shape memory properties of SEBS when extruded with $scCO_2$. From section 6.2, it is obvious that $scCO_2$ has a direct impact on the hard block polystyrene of the polymer and also increase in thermal degradation of polymer triblock. Lozano and Barrera [233], claim that the increase in thermal stability is due to breaking down of polymer chains/ domains into small domains. Hence, extrusion of SEBS triblock with an assistance of $scCO_2$ also causes the breakdown of domains which results in small domains size. Due to small domain size, the shape memory property of SEBS is highly improved compared to SEBS extruded without $scCO_2$. However, at a higher percentage of CB (10 wt. %), the loss has increased when extruded with an assistance of $scCO_2$ because of breaking down of CB agglomerates into small domain causing high mechanical movement restriction in shorter chains causing high damage and high loss.

6.3.3 Dynamic Mechanical Analysis

Figure 6.13 and Figure 6.14 show the storage modulus and loss modulus of SEBS-CB composites in a transverse and parallel direction respectively. Under low strain conditions, the addition of CB particles in SEBS tends to show high reinforcement effect in both moduli measured in a transverse direction to extrusion. However, in the parallel direction to the extrusion, the storage, as well as loss modulus of the extrudate, was observed to decrease when the amount of additive is around 1 wt. %, as shown in the value of both moduli, which slowly increases with an increase in the concentration of additives. This effect is seen when the composite is manufactured using twin screw extruder with a roller system. This is because the mechanical properties of nanocomposites are governed by draw ratio, the orientation of additives and polymers chain and dispersion of additives in the polymer matrix

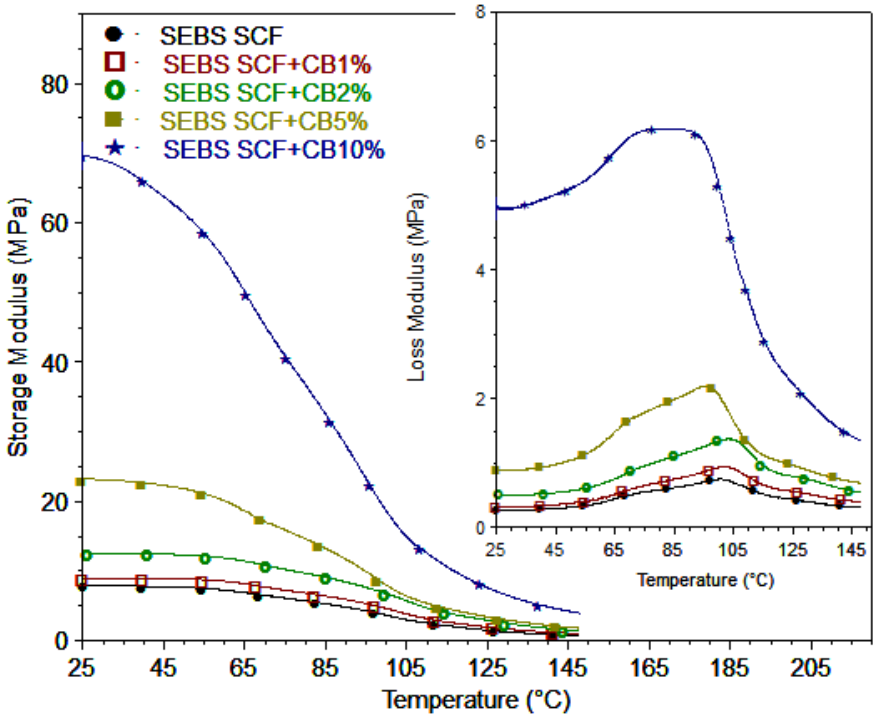

Figure 6.13 Storage modulus and loss modulus of $scCO_2$ processed SEBS in the transverse direction to extrusion

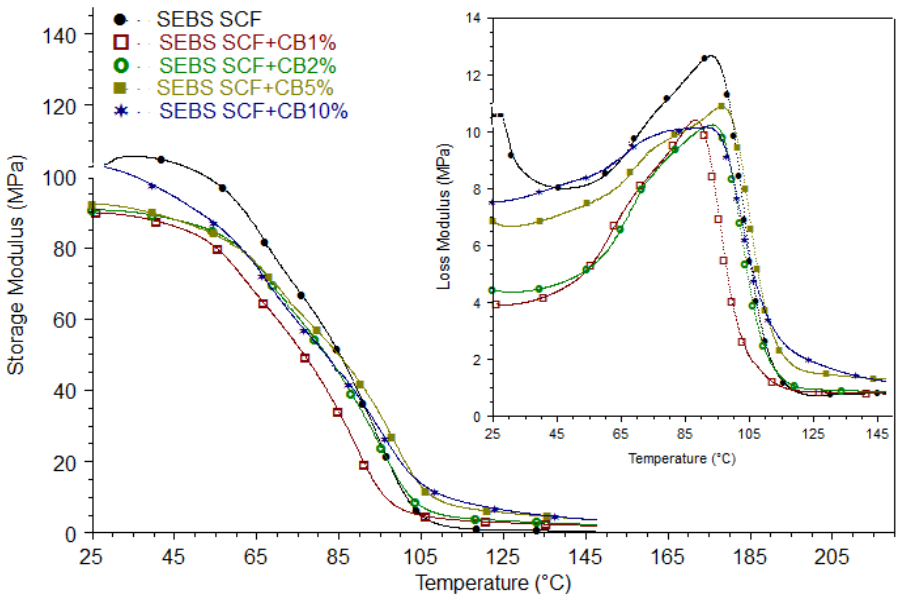

Figure 6.14 Storage modulus and loss modulus of SEBS/CB composites measured in the parallel direction to extrusion

During processing of virgin elastomers, the molten polymer presented in die will be the direction of high shear stress. However, the drawing effect of the rollers gives rise to the high orientation of molecules along the direction of material flow giving a high increase in both moduli in the direction of materials flow[234]. Whereas, in the case of composites, most of the filler particles along with polymer chain will be aligned along the direction of high shear force caused by co-rotating twin screw extruder [234, 235]. During the drawing procedure dispersed particles hinder orientation of elastomers along the drawing direction leading to low moduli of composites along the drawing regions. It is suggested that the viscosity increase in thermoplastic composites due to hindering effects of CB particles dispersed in polymer matrix increases the total viscosity of the composite when extruded with additives. This observation does not hold always true in all composites rather it highly depends on the size of additives [236]. On the other hand, there is a dramatic increase in both moduli of composites with an increase in the amount of CB along the transverse direction to materials flow due to the high alignment of fillers resulting due to high shear force.

Figure 6.15 and Figure 6.16 show tan delta of SEBS SCF/CB composites in transverse and parallel direction respectively. The value of tan delta decreases in both cases at initial

temperature range due to relatively higher percentage change in storage modulus compare to loss modulus.

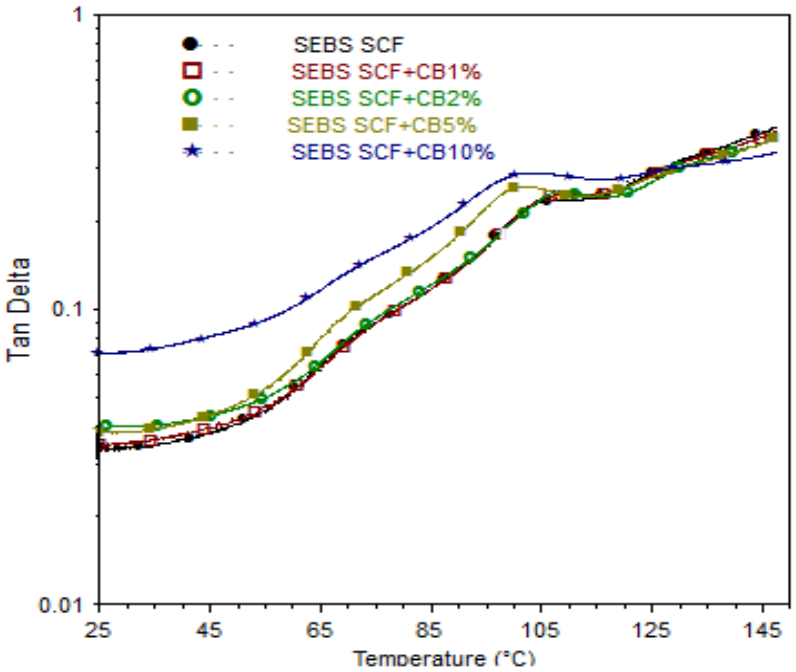

Figure 6.15 Tan delta of $scCO_2$ processed SEBS SCF /CB in the transverse direction to extrusion

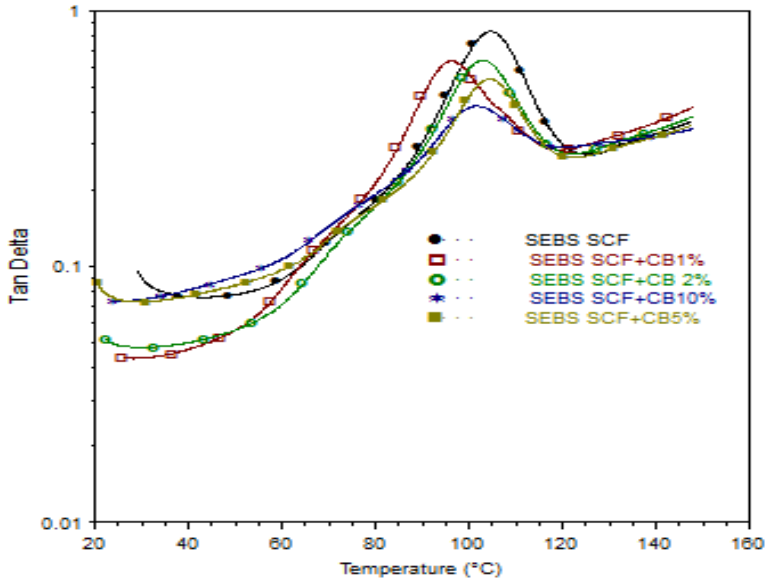

Figure 6.16 Tan delta of $scCO_2$ processed SEBS in the parallel direction to extrusion

According to Table 6.4, comparing SEBS and SEBS/CB composites processed with/ without $scCO_2$, storage and loss moduli were found greater in SEBS and SEBS/CB when processed with $scCO_2$ than their counterparts. The slight increase in storage modulus of virgin SEBS processed with $scCO_2$ compared to SEBS processed without $scCO_2$ is attributed to better intermixing of the soft EB block and hard S block. It is suggested that the increase in moduli in these composites compared to their counterparts processed without $scCO_2$ is the result of reduction in particle size of CB (TEM images as described in Section 6.3.7) as well as the better dispersion of CB in EB and S segment as well as in the interface between EB and S block (DSC curve as described in Section 6.3.5). This reduction in value of tan delta over all the measured temperatures as well as reduction of tan delta height also suggests improved dispersion of CB at all different phases of polymer matrix when the elastomer is processed with $scCO_2$

Table 6.4 Storage modulus and loss modulus of $scCO_2$ processed SEBS in the parallel and transverse direction to extrusion

Additives	**In transverse direction to extrusion**			**In parallel direction to extrusion**		
	Storage modulus	**Loss Modulus**	**Tan Delta**	**Storage Modulus**	**Loss Modulus**	**Tan Delta**
	MPa	**MPa**	**NA**	**MPa**	**MPa**	**NA**
SEBS	5.16	0.20	0.039	104.27	5.19	0.049
SEBS+CB 1%	6.50	0.30	0.046	66.39	3.14	0.047
SEBS +CB 5%	15.84	1.54	0.097	80.20	4.10	0.051
SEBS + CB 10%	45.79	2.88	0.063	91.97	4.35	0.047
SEBS SCF	7.87	0.26	0.033	106.24	8.92	0.083
SEBS SCF +CB 1%	9.01	0.31	0.034	89.56	3.92	0.043
SEBS SCF +CB 2%	12.55	0.50	0.038	90.51	4.37	0.048
SEBS SCF +CB 5%	23.14	0.89	0.040	91.88	6.67	0.072
SEBS SCF +CB 10%	69.06	4.9	0.071	102.1	7.58	0.074

In the transverse direction, the tan delta of SEBS and SEBS/CB processed with $scCO_2$ were found to have much lower value than SEBS processed without $scCO_2$. The value of tan delta measured on SEBS processed with $scCO_2$ in the parallel direction was found to increase to 0.085 from 0.049 of SEBS processed without $scCO_2$.as observed in Table 6.4. This value 0.085 decreases to 0.075 when the temperature in increased from 20 °C to 45 °C as shown in Figure 6.16. SEBS with 1 wt. % and 2 wt. % of CB showed a decrease in tan delta maintaining almost same storage modulus in a parallel direction even below 45 °C. As the percentage of CB increases the tan delta increases but does not reach higher than 0.074 at 25 °C. SEBS processed with $scCO_2$ with an addition 1 wt. % and 2 wt. % CB showed a decrease in tan delta maintaining higher storage modulus in the transverse direction. As the percentage of CB increases, the tan delta increases but does not get higher than 0.071 at 25 °C even when the percentage of CB reaches 10 wt.%. These results suggest three measures of improvement during the process (i) high dispersion of CB at all phases (the soft EB domain, the interphase domain and the hard S domain) of triblock (DSC curves) (ii) lower viscosity of CB/SEBS as the storage modulus in parallel direction to the extrusion remains also unchanged when SEBS is extruded with an assistance with $scCO_2$ (change in tan delta value) and (iii) small particle size of carbon particle (TEM images) when extruded with an assistance with SEBS as very small agglomerates of particles provides low viscosity [236] and high reinforcement effects.

Table 6.5 features the different glass transition based on the structure of different composites measured using DMA at 1 Hz.

Table 6.5 Glass transition temperature measured using DMA observed on different composites

Composites	**Tg -storage modulus**			**Tg –loss modulus**	**Tg- tan delta**
	Onset point	**Inflection point**	**Cut-off point**		
SEBS SCF	68.85	94.37	103.82	93.00	104.21
SEBS SCF +CB1%	64.34	88.83	97.68	88.23	96.33
SEBS SCF +CB2%	67.14	95.18	104.08	90.70	102.22
SEBS SCF +CB5%	72.61	98.45	106.96	93.38	104.22
SEBS SCF + CB10%	62.14	95.37	103.82	96.28	101.49

Glass transition measured using storage modulus, loss modulus and tan delta, it is observed that SEBS (from tan delta measurement) extruded with $scCO_2$ was found to have higher glass transition than all composites. It is suggested that these increases in glass transition temperature are due to the high microphase separation of the hard block with the soft block. However, the glass transition of SEBS-1% CB processed with $scCO_2$ show slight decrease in glass transition temperature. This result suggests that most of the energy and interaction of supercritical fluid during extrusion occurs with CB leading to particle formation of CB as well as exfoliation of CB in SEBS. This highly exfoliated CB tends to hinder the relaxation of elastomeric materials as it is found that the glass transition constantly increases when it is increased up to 5 wt. %. However, at a higher percentage of CB (10 wt. %) the peak of loss modulus becomes nearly flat due to a heterogeneous mixture of CB with SEBS. This leads to an increase in storage modulus to 69 MPa and 102 MPa in a transverse and parallel direction respectively. However, as agglomeration starts at higher percentage CB no significant change in glass transition was observed. The decrease in the peak of the tan delta with CB additives can be attributed to the carbon particles network formation with SEBS.

6.3.4 Dielectric and Conducting Properties

Figure 6.17 shows the real dielectric modulus, dielectric loss, real electric modulus (M') and loss electric modulus (M") of SEBS $scCO_2$, SEBS-CB1%, and SEBS-CB2%. The real dielectric permittivity of SEBS- $scCO_2$ was found to increase over all the frequency range. The real dielectric permittivity of SEBS-$SCCO_2$ at 1 Hz was found to be 2.66, which increases to 3.47 and 3.9 upon addition of 1 wt. % and 2 wt.% of CB respectively. This 30 % and 47 % increase in dielectric permittivity with the addition 1 and 2% of CB was found to have much improvement in the percentage of dielectric permittivity (15.6 %) compared to SEBS with 1 % of CB processed without $scCO_2$. Similarly, the dielectric loss measured of SEBS with 1 % CB processed with and without $scCO_2$ was found to be 0.0001 and 0.006 respectively.

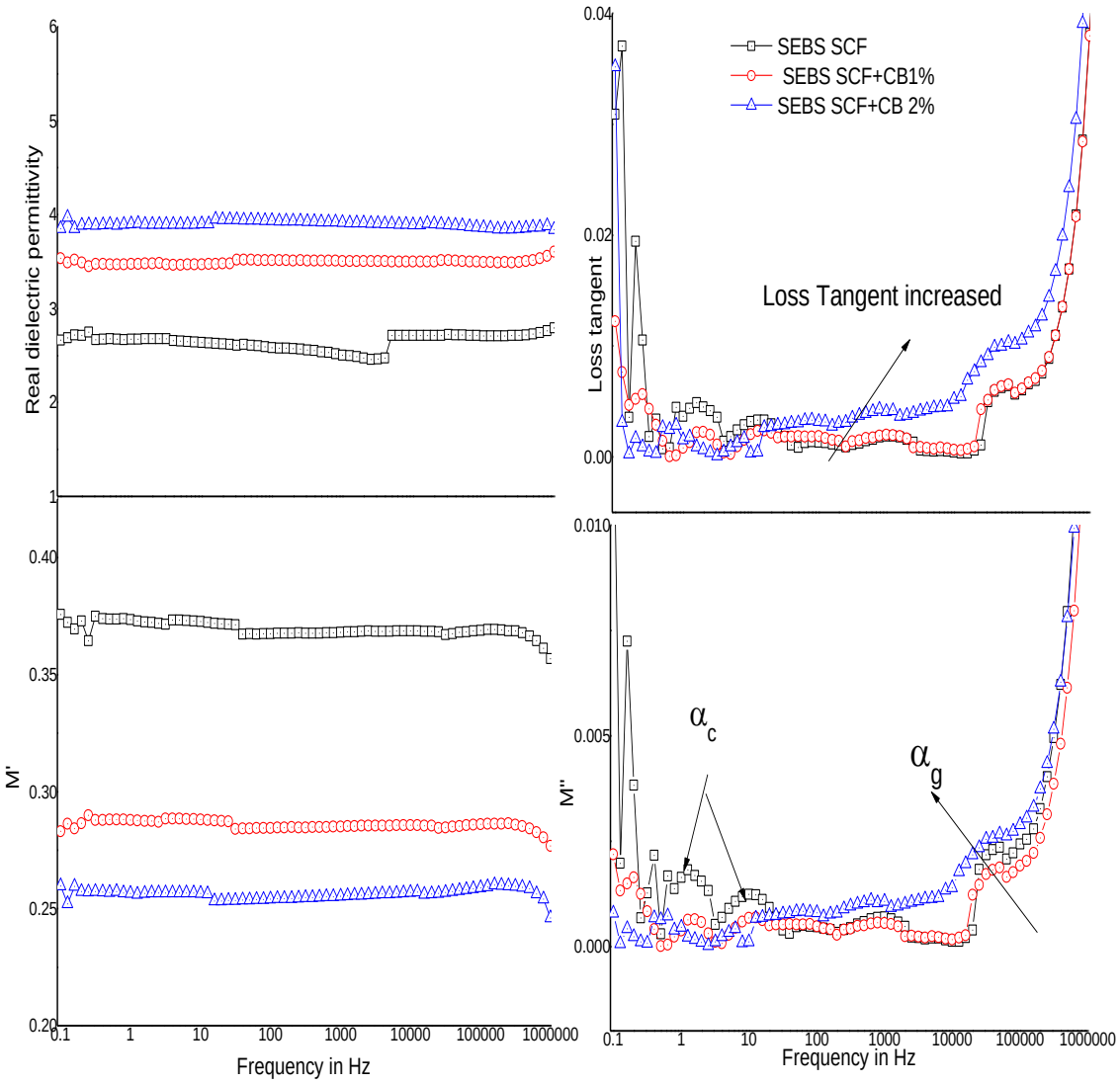

Figure 6.17 Real dielectric permittivity, loss tangent, real electric modulus and loss electric modulus of SEBS/CB below percolation threshold

As per Equation 2.18 and Table 6.4, the enhancement in the electrical and mechanical efficiency of the SEBS/CB composites manufactured using $scCO_2$ assisted extrusion technology was observed compared to their counterparts (below percolation threshold) for actuation like applications. In addition, this also enhances the efficiency of SEBS/CB composites manufactured using $scCO_2$ compared to their counterparts manufactured without using $scCO_2$. However, it is suggested that the conductive filler based nano-

composites are not suitable for capacitive applications because of their low electric breakdown.

The real dielectric permittivity of SEBS at different percentage of CB was found to be almost constant over the range of frequencies measured from 0.1 Hz to 1 MHz as referred to Figure 6.17. However, the dielectric loss with CB was found to increase after 10 Hz. Real electric modulus does not show any significant relaxation of SEBS and SEBS/CB composites. M" shows the initial two prominent relaxations denoted at α_s at 1 and 10 Hz due to different domains present in the triblock. These two relaxation phenomena were found to suppressed by the addition of carbon black. Suppression of this relaxation suggests a change in the structure of triblock with the addition of CB M" and loss tangent show another prominent relaxation at high frequency denoted at α_g. This relaxation is mainly due to the backbone movement of the polymer. The relaxation at 10^5 Hz was found to have almost no change with the addition of 1 wt. % of carbon black. However, this relaxation shifts to lower frequency with the addition of 2 wt. % of carbon black. Early relaxation of the backbone of triblock with 2 wt. % CB suggests a different structure with the addition of carbon black and is also the function of electrostatic attraction between CB particles and SEBS.

Figure 6.18, Figure 6.19 and Figure 6.20 show the total dielectric permittivity, loss tangent and conductivity of SEBS with 5 wt. % and 10 wt. % CB extruded with $scCO_2$ respectively. The dielectric permittivity and conduction of SEBS/CB processed with $scCO_2$ demonstrated a high improvement in conducting behavior compared to SEBS/CB processed without $scCO_2$ (which is discussed in Chapter 5 at page 73). It is suggested that the improvement of dielectric permittivity and conducting behaviour of SEBS/CB is attributed to change in (i) viscoelastic properties of SEBS when processed with $scCO_2$ as observed in DMA curve as high viscous materials tend to have low percolation threshold energy [237] (ii) structural change in polystyrene block due to $scCO_2$ as shown by FTIR graphs and change in polymer chains structure as shown by DMA, TGA and DSC observation in section 6.1 from page 121-134 (iii) high exfoliation of CB particles [238] in SEBS elastomers as shown in TEM graphs in Figure 6.26.

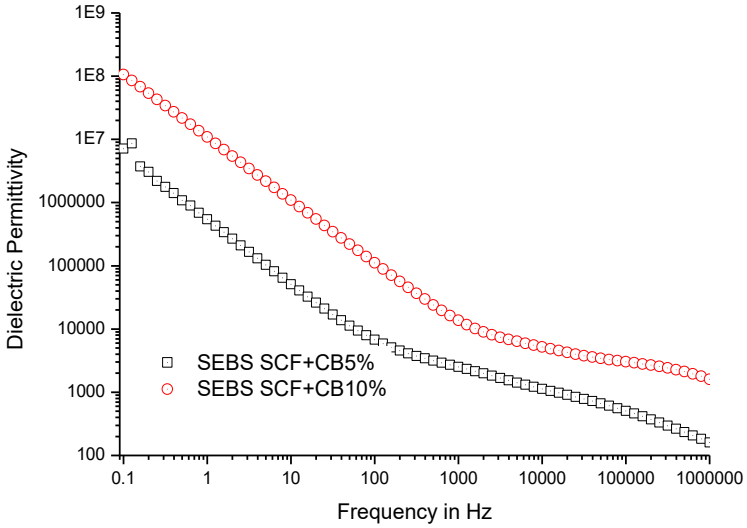

Figure 6.18 Total dielectric permittivity of SEBS SCF with 5% and 10% of CB

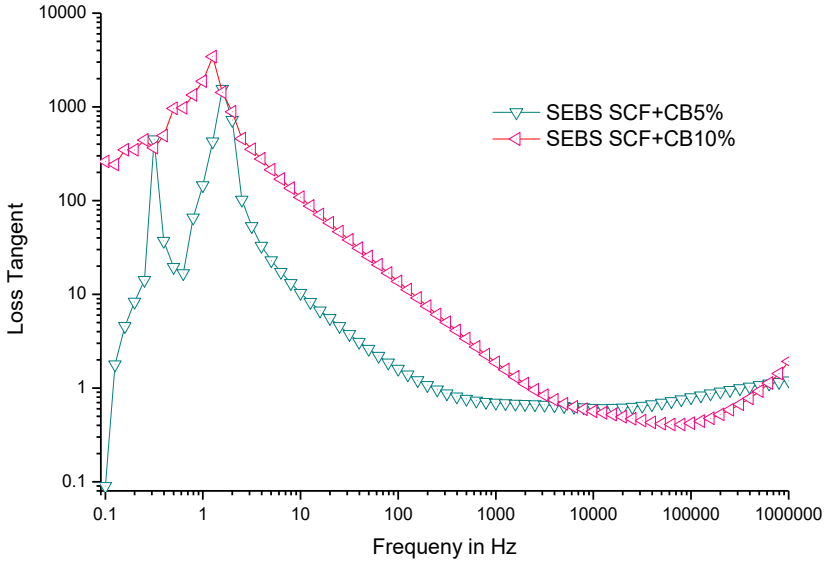

Figure 6.19 loss tangent of SEBS with 5% and 10% CB

The conductivity, as well as total dielectric permittivity, was also enhanced when the percentage of CB changes from 5 wt. % to 10 wt. %. From Figure 6.20, the conductivity of SEBS/CB composites with 5 wt. % and 10 wt. % with CB has two distinct features over frequency (i) the conductivity independent of frequency up to 100 Hz for SEBS/CB

5 wt. % and up to 2000 Hz for SEBS/CB 10 wt. %, and (ii) the frequency dependent conductivity.

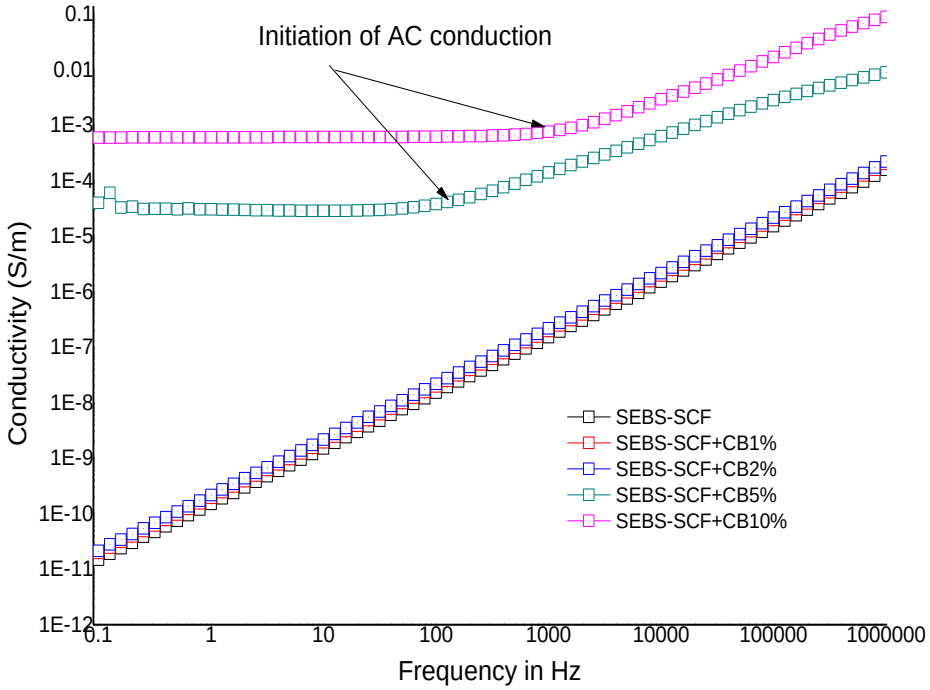

Figure 6.20 AC conductivity measurement of SEBS-SCF with 1%, 2%, 5% and 10% of CB

This transition/relaxation frequency at which AC current start to triggers is generally observed in conducting nanocomposites and is dependent on a different number of sites for conduction and polarization [239]. MWS relaxation is the result of relaxation in the diffusion of charge carriers or electrons between charge particles in nanocomposites [240]. As SEBS/CB 10 wt. % has more conducting sites compared to SEBS/CB 5 wt. %, the relaxation frequency of SEBS/CB 10 wt. % is higher when compared to SEBS/CB 5 wt. %. In most cases of conductive nanocomposites, the imaginary electric modulus was used to determine the relaxation frequency for MWS. Figure 6.21 confirms that the MWS of SEBS/CB 10 wt. % has higher MWS relaxation frequency than SEBS/CB 5 wt. %.

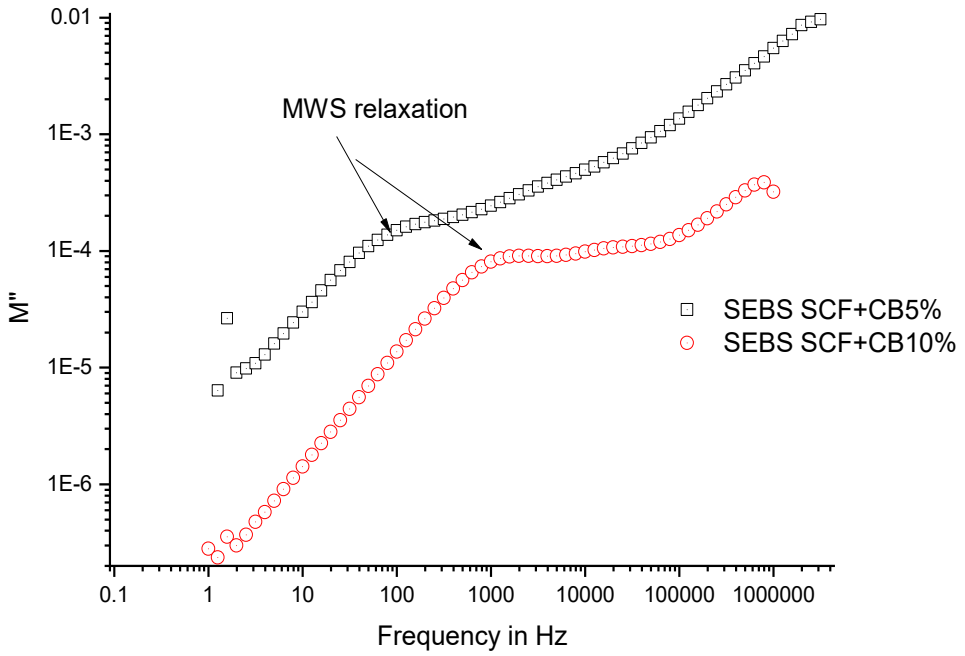

Figure 6.21 Imaginary electric modulus of SEBS-SCF with 5% and 10% of CB

6.3.5 Differential Scanning Calorimetry

Figure 6.22 shows the heat flow thermogram for SEBS-scCO_2/CB composites at various CB percentages. Thermodynamically, incompatibility between the polystyrene and poly (ethylene-co-1-butene) results in phase separated microstructures bringing about changes with respect to the physical and morphological characteristics of SEBS. The amorphous ethylene-butylene (EB) block (–(CH_2-CH_2)–$_n$) relaxation peak is in the range of -20 to 30 °C. The glass transition temperature of ethylene butylene is at (Tg) –55 °C and the glass transition of S block around 96 °C along with heat enthalpic relaxation of styrene block at 60 °C

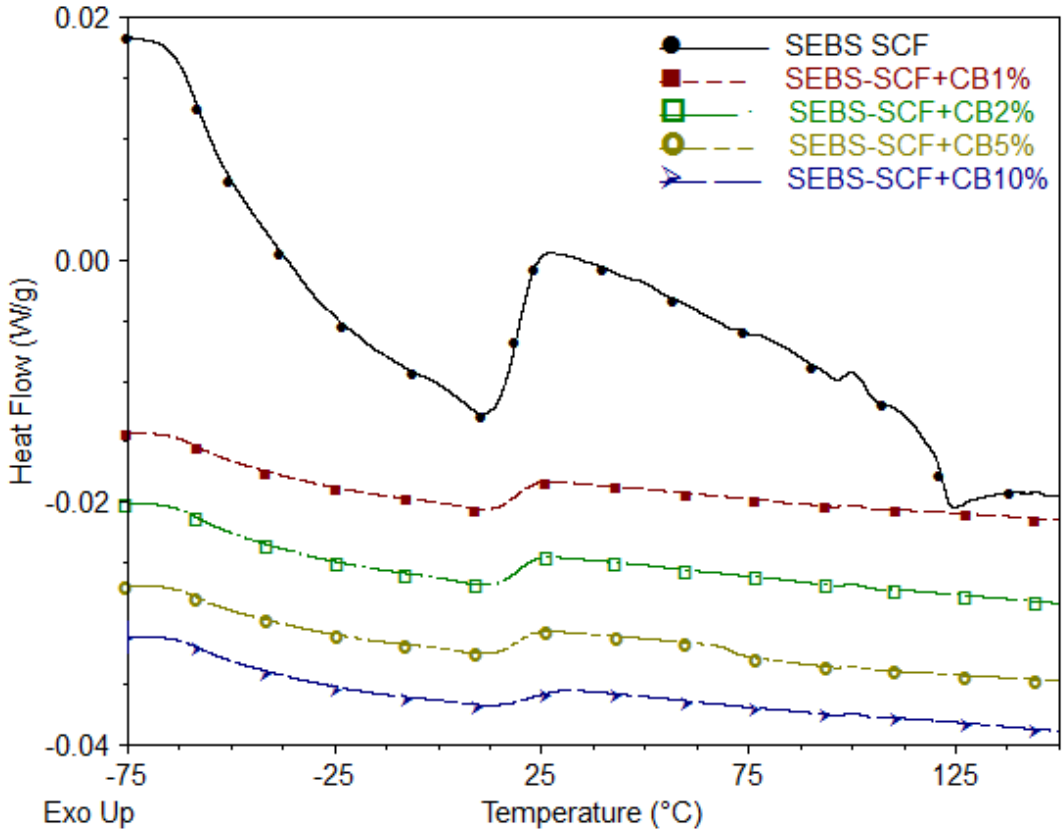

Figure 6.22 Heat flow of SEBS-SCF with different percentages of CB

It is evident from the heat flow thermogram in Figure 6.22 that the heat of enthalpy of the endothermic region of amorphous EB block reduces in accordance with carbon percentage ratio. This also shows that addition of CB reduced the free flow or rearrangement of the EB block. This shows that the addition of carbon particles further restricts the further flow or relaxation of EB block after its Tg.

Although it is not so evident to know the dispersion of CB particle using TEM graphs, DSC analysis clearly shows the high dispersion of CB particle in this EB phase, hence causing high restriction in movement of EB block in SEBS when extruded with an assistance of $scCO_2$

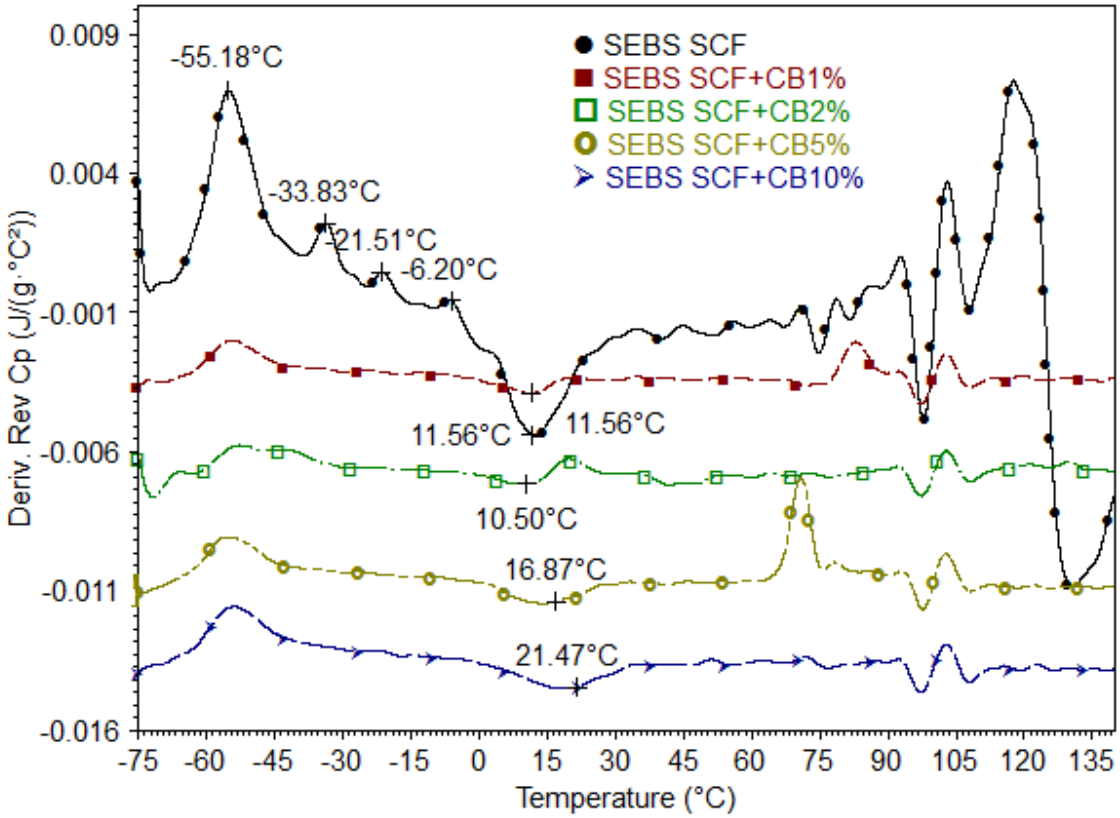

Figure 6.23 Derivative of reversible specific heat capacity of SEBS SCF/CB composites

Figure 6.23 shows the derivative of reversing heat capacity for SEBS/CB composites using supercritical fluid assisted extrusion. The long polymer chains are oriented randomly and have more freedom to move which results in change in the microstructure of the material, resulting in higher specific heat capacity after the glass transition temperature at -55 °C. The specific heat capacity, which is also called as the measure of molecular motion, reduces its specific heat capacity between -30 to 25 °C (almost becomes flat) upon addition of CB restricting the free movement. This is not only evident on the relaxation after the Tg but the Tg of EB also subsequently reduces with respect to heat of fusion. This shows that addition of carbon hinders the molecular movement or rearrangement of interphase domains. It can also be observed that the maximum relaxation after Tg of EB block evident at 11.56 °C gradually decreases and shifts towards 21.47 °C upon incremental addition of carbon black. This demonstrates that $scCO_2$ treated carbon composites at higher filler concentrations slow down the relaxation process (longer time is taken for styrene to aggregate on the surface of melt). The Tg of styrene-

rich phase is also clearly seen on the reversing heat capacity curve at around 103 C. It is evident that the dispersion of CB in SEBS extruded with an assistance of $scCO_2$ has better dispersion in all phases of the triblock compared to SEBS treated extruded without $scCO_2$ described in section 5.2.

6.3.6 Attenuated Total Reflectance-Fourier Transfer Infrared Spectroscopy Studies

Figure 6.24 shows the ATR-FTIR spectra of SEBS/ CB composites. The change in the baseline is obvious in all composites with the addition of CB fillers due to the high negativity of CB particles compared to SEBS triblock. The continuous shift in 2851cm^{-1} (symmetrical stretching vibration of CH_2 in EB units) and 1491 cm^{-1} (stretching vibration of carbons in aromatic ring) can be observed upon addition of CB filler, the intensity of 1491 cm^{-1} (wagging of CH_2 in EB units of SEBS) decreases with increase in filler content and becomes negligible when the CB percentage reaches 10 wt. %.

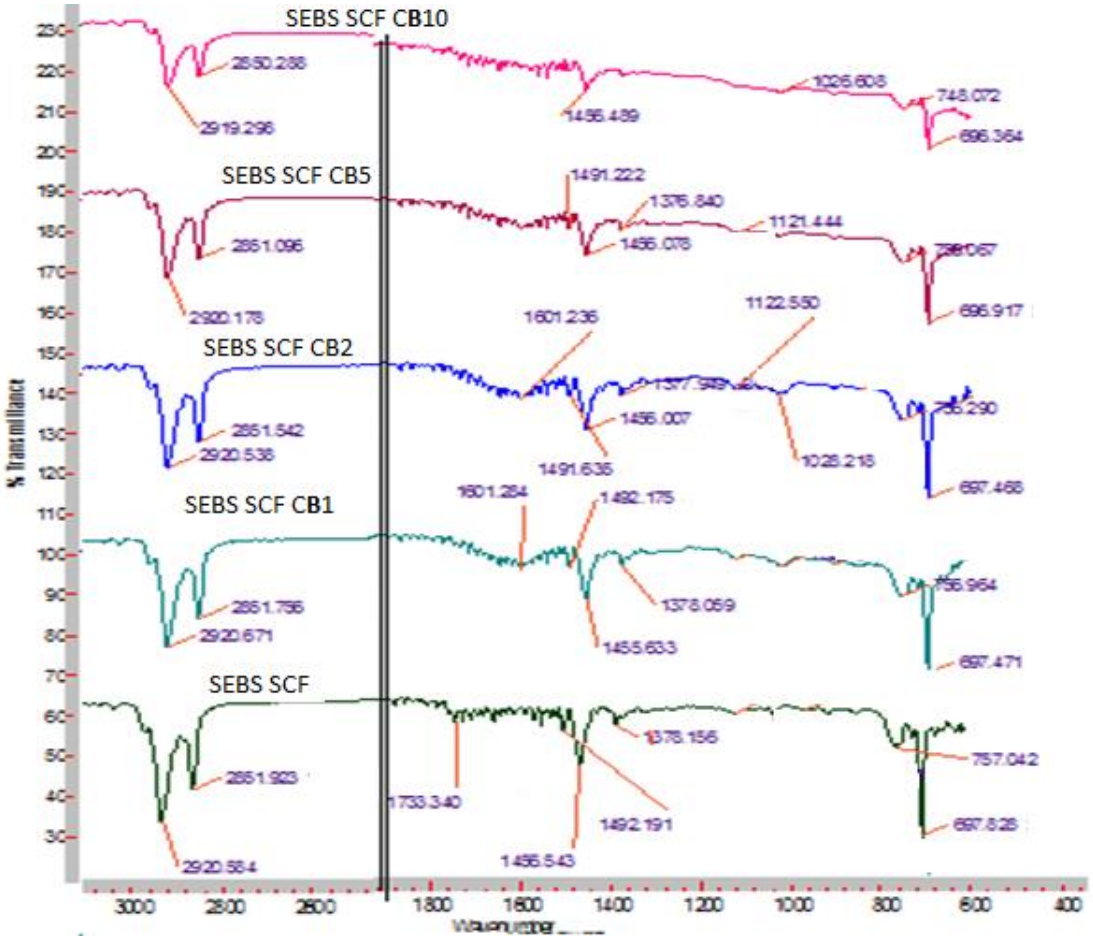

Figure 6.24 FTIR spectra of SEBS SCF/CB composites

Similarly, interaction is observed at 1378 cm^{-1}. A similar shift is observed in 697 cm^{-1} and 757 cm^{-1} (Deformation vibration of CH groups in aromatic ring in PS units), where 757 cm^{-1} shows the most prominent shift in wavelength upon addition of fillers. The FTIR results also suggest a high level of dispersion as well as interaction to all the phases present in SEBS.

6.3.7 Transmission Electron Microscopy

Figure 6.25 shows the morphology of SEBS/CB composites with the orientation of molecules. Polymer molecules are more oriented towards the longitudinal flow and have shown high modulus along the axis of screw rotation. However, the CB particles were found to be randomly oriented or more aligned along the shear force of the screw as suggested by DMA analysis.

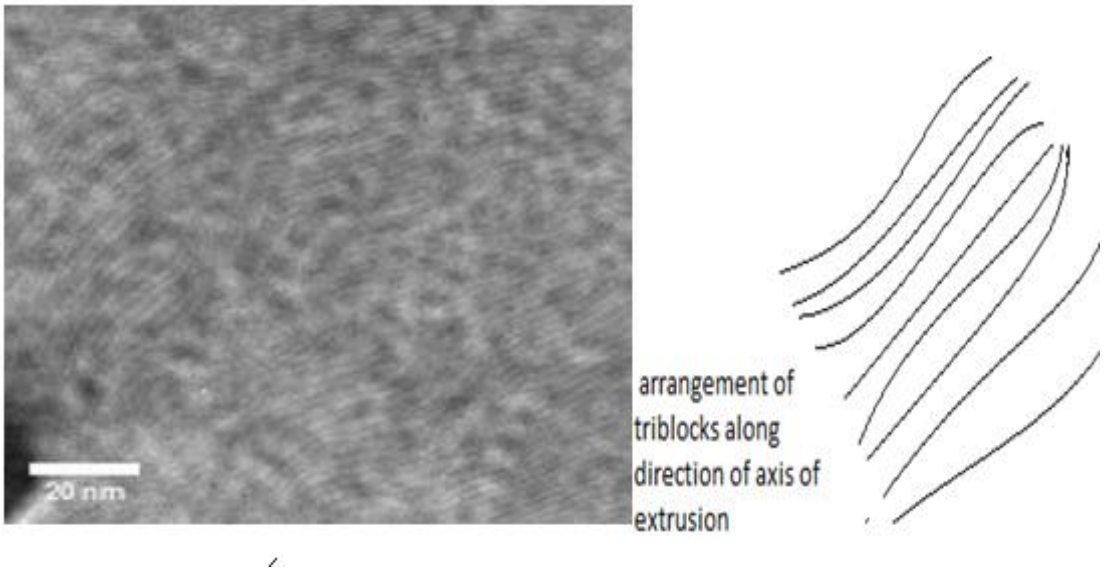

Figure 6.25 Alignment of SEBS and additives polymers during extrusion

Figure 6.26 shows TEM images of SEBS/CB composites extruded with and without an assistance of $scCO_2$. Although it is very hard to define the domain at which dispersion of CB takes place, the figure shows improved dispersion of CB. In addition to better dispersion, the CB particles in SEBS were found be smaller in size compared to CB particles extruded without $scCO_2$ Due to improved dispersion and the presence of high surface area of CB particles in SEBS when extruded with an assistance of $scCO_2$, the

conductivity as well as dielectric permittivity and mechanical properties at all concentration levels were highly enhanced.

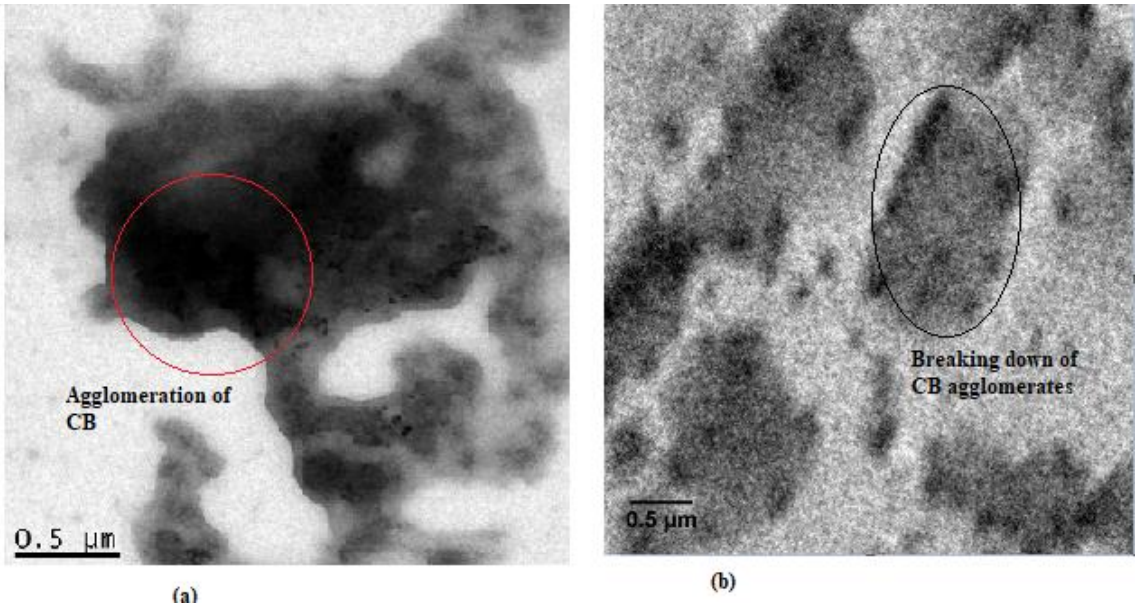

Figure 6.26 TEM images of SEBS/CB composites manufactured using extruder (a)without and (b) with an assistance of SCF

6.3.8 Conclusion

TEM images obtained show the high dispersion of CB additives in SEBS with supercritical fluid assisted extrusion resulting in better dispersive and distributive mixing. Due to high dispersion, as well as the distribution of CB in SEBS, the mechanical properties like storage modulus in transverse direction were highly enhanced making these composites highly isotropic in nature. Due to the formation of small domains size when processed with $scCO_2$ assisted extrusion provides low loss tangent and low cyclic loss properties making them suitable for wide range of electro-active applications. In addition, the high exfoliation of CB in SEBS provides high dielectric permittivity with a low dielectric loss at low concentration. At higher percentage of CB, $scCO_2$ assisted extruded SEBS/CB provides better conductivity and low percolation threshold which has huge applications in strain sensing applications.

6.4 Supercritical Fluid Extrusion of SEBS-g-MA/BT Composites

6.4.1 Introduction

The primary objective of this section is to address the issue of enhancing dielectric permittivity of thermoplastic elastomers while maintaining dielectric loss even at low-frequency range. In addition, manufacturing dielectric flexible composites using $scCO_2$ at very low percentage of BT is also highlighted. The elastomer selected for this study was SEBS-g-MA. Finally, morphological, electrical, mechanical and thermal properties of extruded composites with an assistance of $scCO_2$ were compared with conventional extruded composites

6.4.2 Mechanical and Cyclic Analysis

Figure 6.38 and Table 6.6 show the tensile properties and Young's modulus of SEBS-g-MA/BT composites extruded with an assistance of $scCO_2$. Compared to SEBS-g-MA extruded without an assistance of $scCO_2$ as described in section 5.3.3 Young's modulus has increased from 45 MPa to 59 MPa at one percentage of strain However, due to enhanced microphase separation and shorter chain lengths as illustrated in section 6.2, the SEBS-g-MA/BT extruded with an assistance of $scCO_2$ show low secant modulus above the elastic limit as hard domains can easily slide one over another. BT fillers have shown a slight reinforcement effect in SEBS-g-MA. The enforcement effect increases with increase in the concentration of BT fillers as suggested by secant modulus at different percentages of strain. This low mechanical reinforcement effect was attributed to the low volume concentration of BT fillers and low reinforcing structure of BT (cubic - the structure of BT).

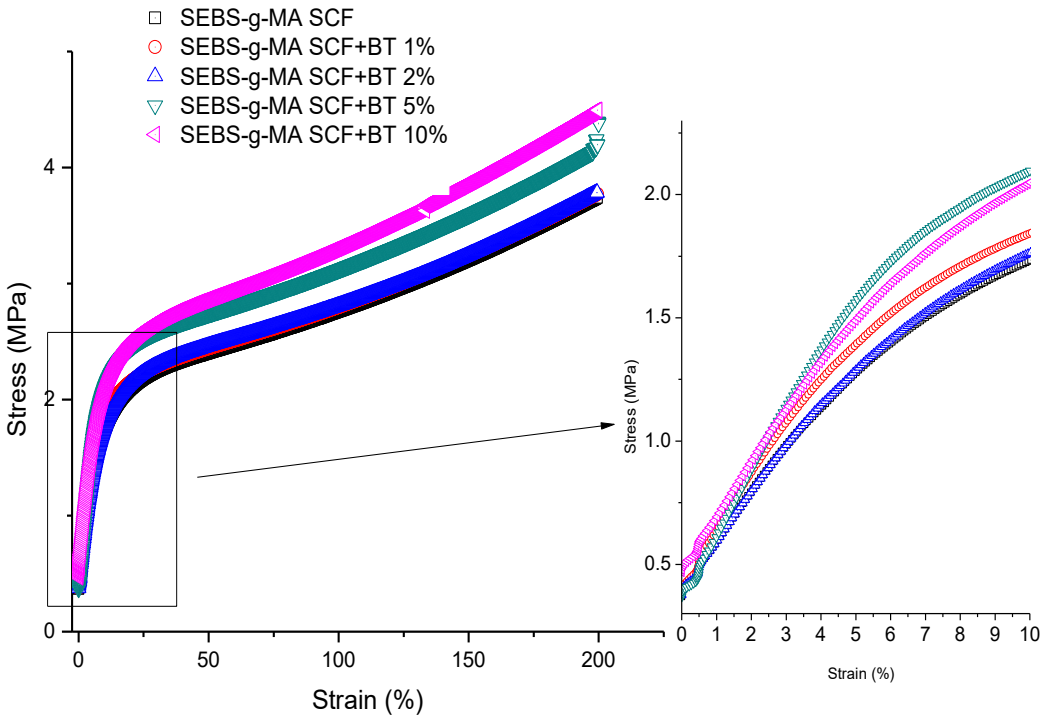

Figure 6.27 Tensile test of SEBS-g-MA/BT composites extruded with an assistance of $scCO_2$ measured in the parallel direction to extrusion

Table 6.6 Secant Young's modulus of SEBS- SCF with BT

Nanocomposites	**Young's modulus at several composite different strain (MPa)**			
	1% **(Std. dev.)**	**50%** **(Std. dev.)**	**100%** **(Std. dev.)**	**150%** **(Std. dev.)**
SEBS-g-MA SCF	57.94 (±5.9)	4.8 (±0.3)	2.76 (±0.1)	2.14 (±0.1)
SEBS-g-MA SCF + BT-1%	61.23 (±3.8)	4.88 (±0.8)	2.79 (±0.4)	2.16 (±0.3)
SEBS-g-MA SCF + BT-2%	62.50 (±2.1))	4.92 (±0.4)	2.81 (±0.2)	2.17 (±0.1)
SEBS-g-MA SCF + BT-5%	59.10 (±8.4)	5.46 (±0.3)	3.11 (±0.1)	2.39 (±0.1)
SEBS-g-MA SCF + BT-10%	68.0 (±7.0)	5.73 (±0.1)	3.31 (±0.1)	2.58 (±0.1)

Figure 6.28 presents the loss energy of SEBS-g-MA processed with $scCO_2$ as described by Equation 3.2. A slight decrease in loss energy factor was found when extruded with an

assistance of $scCO_2$ compared to SEBS-g-MA/BT extruded without $scCO_2$ as described in Section 5.3.3. This decrease in loss energy factor or increase in elastomeric properties of SEBS-g-MA under large extension is a result of a decrease in domain size when extruded with $scCO_2$.

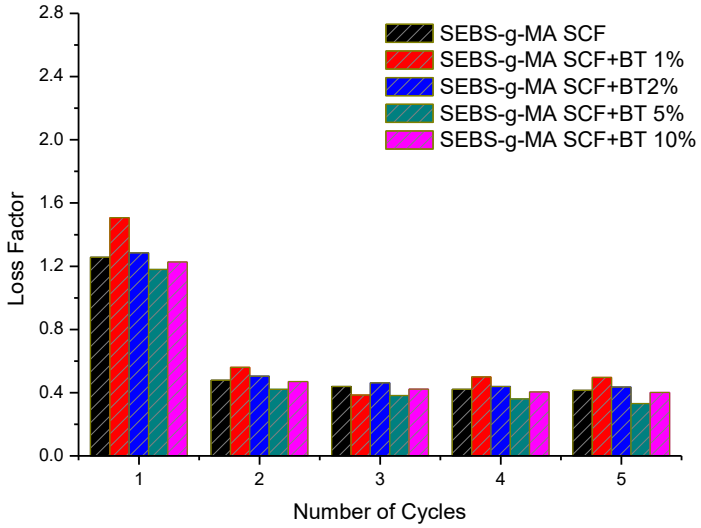

Figure 6.28 Loss energy factor for SEBS-g-MA SCF/BT composites measured in the parallel direction to extrusion

6.4.3 Dielectric Properties

Figure 6.29 shows the real dielectric permittivity of SEBS-g-MA/BT composites. The result obtained in this section is comparatively much lower than that of SEBS-g-MA processed without $scCO_2$. This difference in dielectric permittivity is attributed to the difference in measurement and dielectric calculation procedure. In Chapter 5 in page 73, the dielectric measurement was performed and general correction factor calculated from the open cell electrode for different frequencies was used, whereas, for this section, correction factor was applied during the measurement procedure by using normalization methods described in the datasheet of Solartron with dielectric interface 1926. There was no significant difference or error between the two measurement techniques. Relative changes with the addition of additives have been shown to be identical.

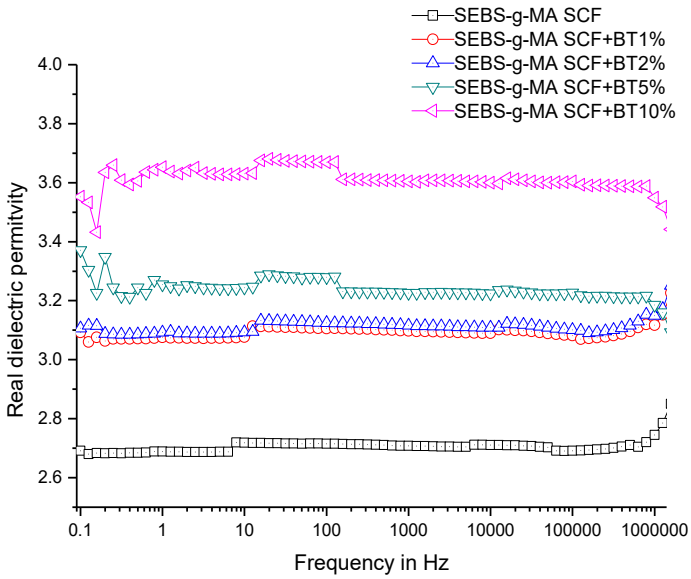

Figure 6.29 Real dielectric permittivity of SEBS-g-MA SCF/BT composites

The percentage of dielectric permittivity increase of SEBS-g-MA was found to be 14 %, 15%, 21% and 35% upon addition of 1 wt. %, 2 wt. %, 5 wt. % and 10 wt. % of BT. Figure 6.30 shows the loss tangent of SEBS-g-MA/BT composites. The dielectric loss of all composites remains below 0.005 at all concentration of SEBS-g-MA/BT processed with $scCO_2$.

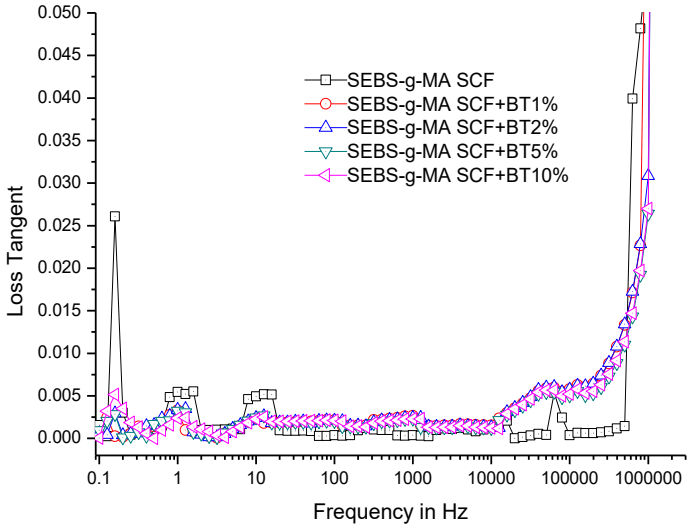

Figure 6.30 Dielectric loss of SEBS-g-MA SCF/BT composites

A comparison of dielectric permittivity and dielectric tangent loss SEBS-g-MA/BT using this method manufactured with/without an assistance of $scCO_2$ is shown in Figure 6.31 and Figure 6.32 respectively. Figure 6.31 and Figure 6.32 show the dielectric measurement was taken from a Solartron 1260 impedance analyzer with 1296 dielectric interface using correction factor as described in the datasheet which show high dielectric loss and high dielectric permittivity at a low frequency of SEBS-g-MA/BT 10% compared to SEBS-g-MA/BT 10% processed with $scCO_2$. However, the real dielectric permittivity as well as the loss tangent sharply drops along the frequency range from 1 mHz to 1 Hz. This phenomena of dielectric drop over the range of frequencies is further described in section 7.2 In addition, compared to SEBS-g-MA/BT 10% processed without an assistance of $scCO_2$, the SEBS-g-MA/BT10 processed with an assistance of $scCO_2$ show highly stable dielectric permittivity over the range of frequency measured. The main reason for this variation in dielectric permittivity is observed due to (i) improved dispersion of BT in different phases triblock (described in thermal analysis of SEBS-g-MA/BT composites, (ii) change in microstructure of the triblock, and (iii) possibility of reduction in size of BT agglomerates when extruded with an assistance of $scCO_2$. The effect on dielectric properties of SEBS-g-MA/BT composites, when extruded with and without an assistance of $scCO_2$, is further detailed in section 7.2.

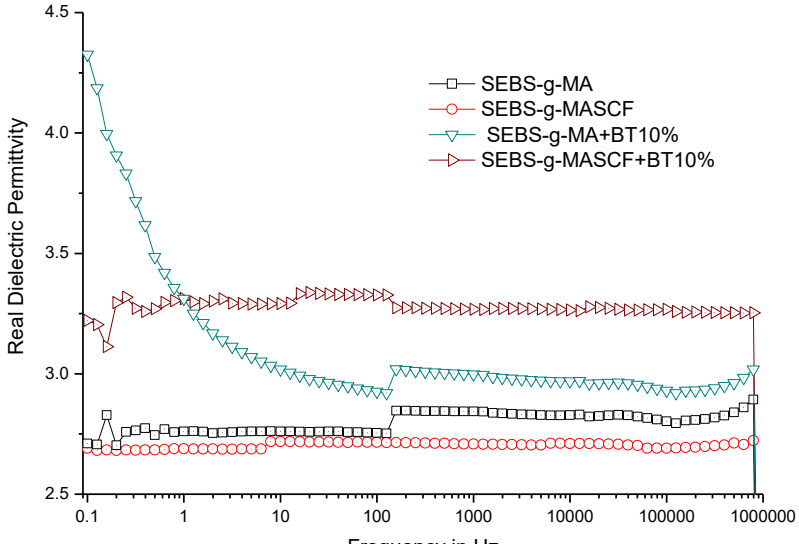

Figure 6.31 Frequency dependence real dielectric permittivity of SEBS-g-MA and SEBS-g-MA/BT 10 % processed with/without an assistance of $scCO_2$ measured using Solartron impedance analyzer with dielectric interface 1926.

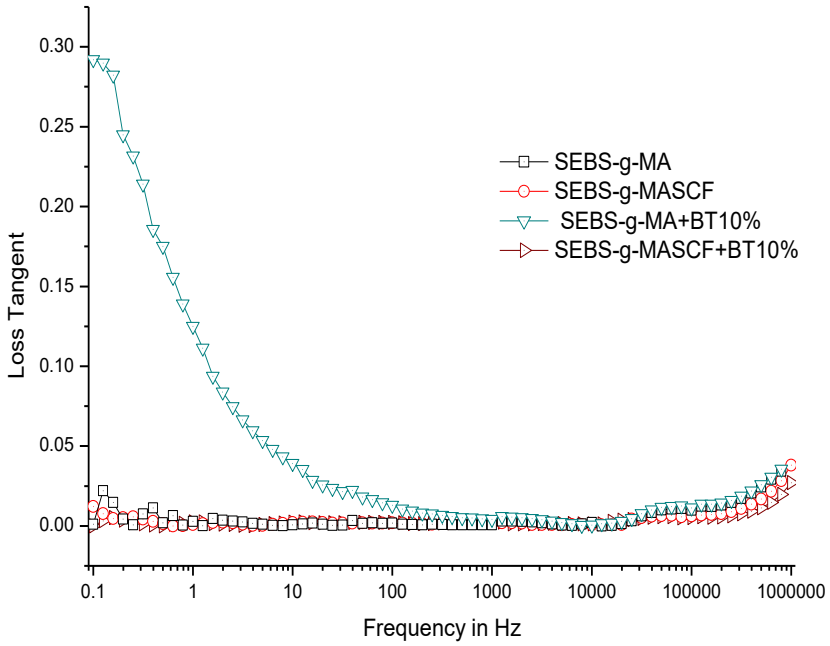

Figure 6.32 Frequency dependence dielectric loss tangent of SEBS-g-MA and SEBS-g-MA/BT 10% processed with/without an assistance of $scCO_2$ measured using Solartron impedance analyzer with dielectric interface 1926.

In addition, the dielectric loss measured over frequency also shows high dielectric loss of SEBS-g-MA/BT10% processed without $scCO_2$ compared to SEBS-g-MA/BT10 % processed $scCO_2$ respectively.

Figure 6.33 depicts the dielectric relaxation phenomenon of SEBS-g-MA/BT composites. At low frequency, two low-frequency relaxations at 1 Hz and 10 Hz can be observed on SEBS-g-MA triblock. The intensity of relaxation was found to decrease upon addition of BT and lowers with higher BT percentage. However, at higher frequencies above 10 kHz, the early intensity of relaxation occurs in all BT composites compared to virgin SEBS-g-MA.

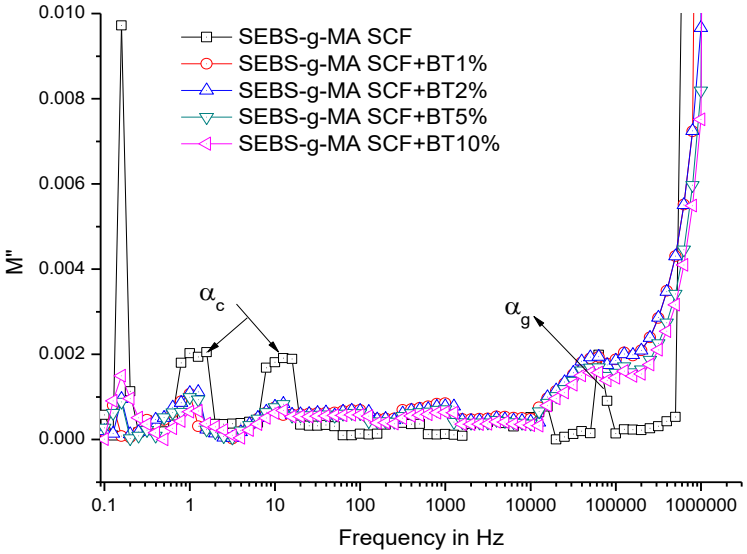

Figure 6.33 Imaginary electric modulus of SEBS-g-MA SCF/ BT composites.

6.4.4 Differential Scanning Calorimetry

Figure 6.34 presents the derivative of reversing heat capacity for SEBS-g-MA/BT using supercritical fluid assisted extrusion. It is evident that heat capacity is reduced for both Tg of EB block at -55 °C and enthalpic relaxation at 13.86 °C. This occurs mainly due to the restriction imposed upon adding BT as filler for free movement of polymer chains. The endothermic relaxation melting observed after Tg of the EB block shifts from 13.86 °C to 19.72 °C depending on the amount of BT filler. This shows that $scCO_2$ treatment increases the enthalpic relaxation for an extended temperature even with the highest BT filler concentration. This may be attributed to the breaking of the polymer chain and the BT filler particles which prolong the relaxation process to higher temperatures. A similar reduction in heat capacity is also evident at 103 °C upon gradual increase of BT filler percentage, which occurs mainly due to increased BT filler restrictions. However, no additional formation of microphases can be observed as all the thermograms produced are smooth.

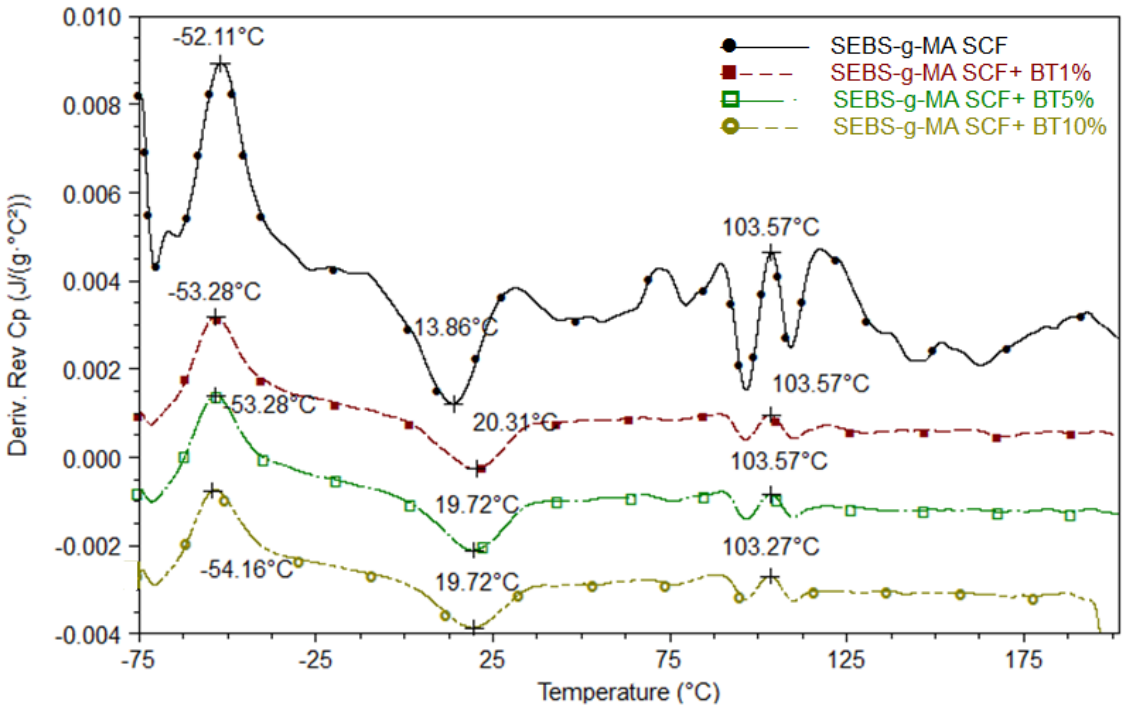

Figure 6.34 Derivative of reversible Cp of SEBS-g-MA SCF/BT composites

The reduction in the peak of reversible Cp of SEBS-g-MA upon addition of BT fillers suggests a heterogeneous network is formed between the soft EB block and BT fillers. Prolonged relaxation process resulted due to the restriction of movement of EB soft block confirms the dispersion of BT particles in EB block. In addition, enthalpic relaxation of hard block observed around 60 °C is highly altered upon addition of fillers. This confirms the interaction and dispersion of BT particles in hard S domain as well when extruded with $scCO_2$. In contrast, a negligible interaction of BT with different phases of SEBS-g-MA as well as a low dispersion can be noticed when the extrusion was carried out without $scCO_2$ as described in Section 5.3.5 at page 112.

6.4.5 Attenuated Total Reflectance-Fourier Transform Infrared Studies

Figure 6.35 presents the ATR-FTIR of SEBS-g-MA/BT composites. A slight shift in 2920 cm^{-1} and 2851 cm^{-1} was observed on addition of BT on SEBS-g-MA. Major shift and change in intensity were observed on 1732 cm^{-1} on SEBS-g-MA upon addition of BT fillers. Similarly, 1456 cm^{-1} and 1378 cm^{-1} also shows a shift in wavenumber to 1456 and 1378 upon addition of BT fillers. The 1112 cm^{-1} wavenumber in SEBS-g-MA spectra diminishes and new peaks were observed around 1028 cm^{-1}. Moreover, the 756 cm^{-1}

wavenumber shows a slight shift to 767 cm^{-1} wavenumber upon addition of BT The observation in shifting in FTIR peaks shows the interaction of BT with SEBS-g-MA.

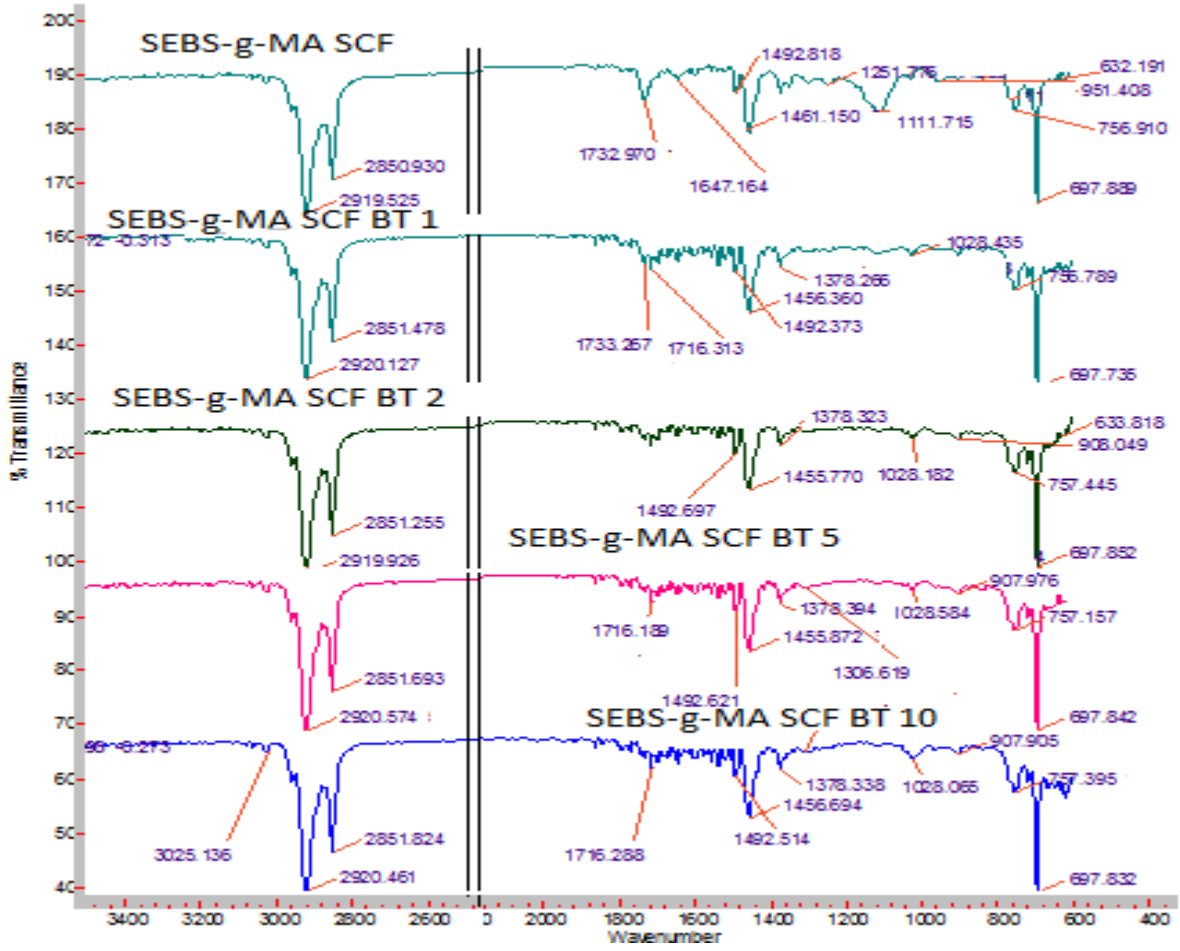

Figure 6.35 ATR-FTIR for the SEBS-g-MA SCF/BT composites

6.4.6 Transmission Electron Microscopy

Figure 6.36 shows the TEM images of SEBS-g-MA/BT wt.5% extruded with an assistance of $scCO_2$. Although it is very hard to separate the domains of SEBS-g-MA which interact with BT fillers, it shows a uniform distribution of BT filler in SEBS-g-MA when extrusion was carried out with an assistance of $scCO_2$. As domain size of the hard and soft block of SEBS-g-MA are much larger than BT particles it is very hard to clearly distinguish the domain of interaction from the TEM images.

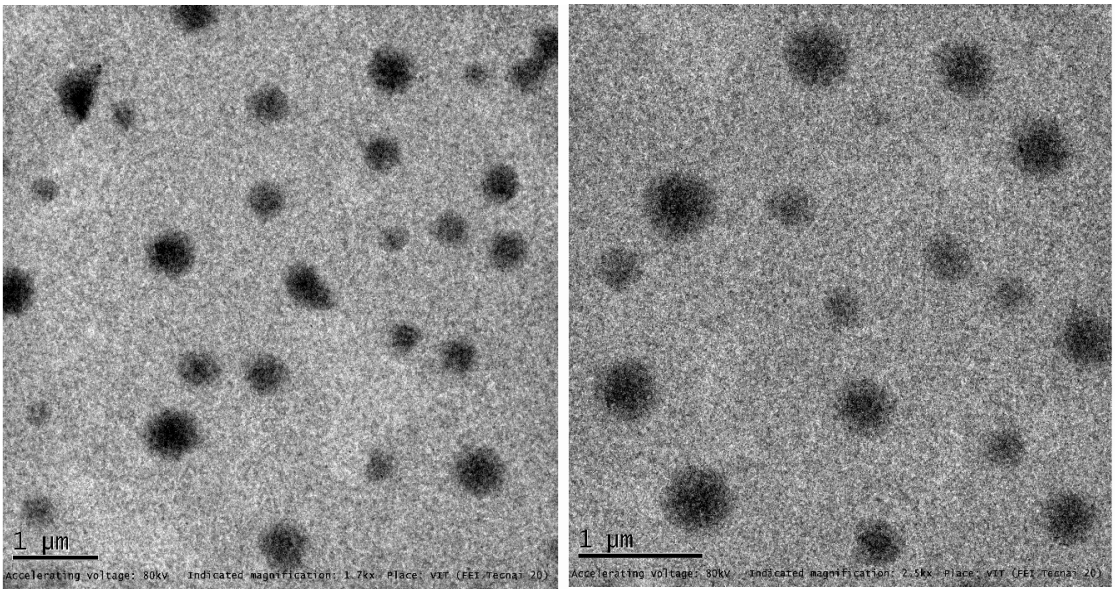

Figure 6.36 TEM images of SEBS SCF/BT 5 wt. % composite

6.4.7 Conclusion

DSC and DMA results show the enhanced interaction of BT in SEBS-g-MA when extruded with an assistance of $scCO_2$ leading to the improved dispersion of BT in SEBS-g-MA. The enhanced distributive dispersion of BT particles in SEBS-g-MA as observed in TEM images leads to uniform polarization capability with very low dielectric tangent loss over the range of frequencies (1 mHz to 1 MHz) as well as low hysteresis loss during mechanical loading and unloading conditions This uniform polarization mechanism with low dielectric loss over the range of frequencies, obtained in nanocomposites manufactured using $scCO_2$ assisted manufacturing process broadens the application horizon of nanocomposites for capacitive energy harvesting applications. The application is further enhanced by shape memory properties of the elastomeric composites. The better dispersion phenomena in all domains of SEBS-g-MA can also be seen in $scCO_2$ assisted extrudates due to the better molecular interaction as detected by FTIR-spectra.

6.5 Thermal, Mechanical and Dielectric Properties Analysis of SEBS-g-MA/CB Composites Manufactured using Supercritical Fluid Assisted Extrusion

6.5.1 Introduction

This section is similar to section 6.4. In this section, the dielectric, morphological, mechanical, and thermal effects of CB on SEBS-g-MA is described. Section 6.4 has all nanocomposites either just above the percolation threshold or below the percolation threshold. In addition, the ability to disperse the additives in polymer matrix depends on nature of polymer as well as additives and the interaction of both is highlighted here. In this section, a nanocomposite very near to the conductive threshold is described. From this section, a composite of near percolation threshold is further selected for thermoelectrical analysis.

6.5.2 Transmission Electron Microscopy

Figure 6.36 shows TEM images of SEBS-g-MA/CB composites extruded without/with an assistance of $scCO_2$. Twin screw extruder is well known for different mixing capability in the context of dispersive, distributive and extensional mixing. The twin screw with kneading block has a high tendency to provide high shear force for distribution mixing of additives in polymers, but it still provides low dispersion mixing as shown in Figure 6.37 as well as in the literature [241].The twin screw extruder shows a high distributive mixing with some effects of dispersive mixing of CB agglomerates in polymers as shown in Figure 6.36. This effect is attributed to high shear dominated flow for distributive mixing with the small longitudinal flow. The dispersion of CB agglomerates demonstrated a marked increase in the context of both dispersive with reduction in agglomerates size and distributive mixing with well distributed CB agglomerates when extrusion was carried out with an assistance of $scCO_2$

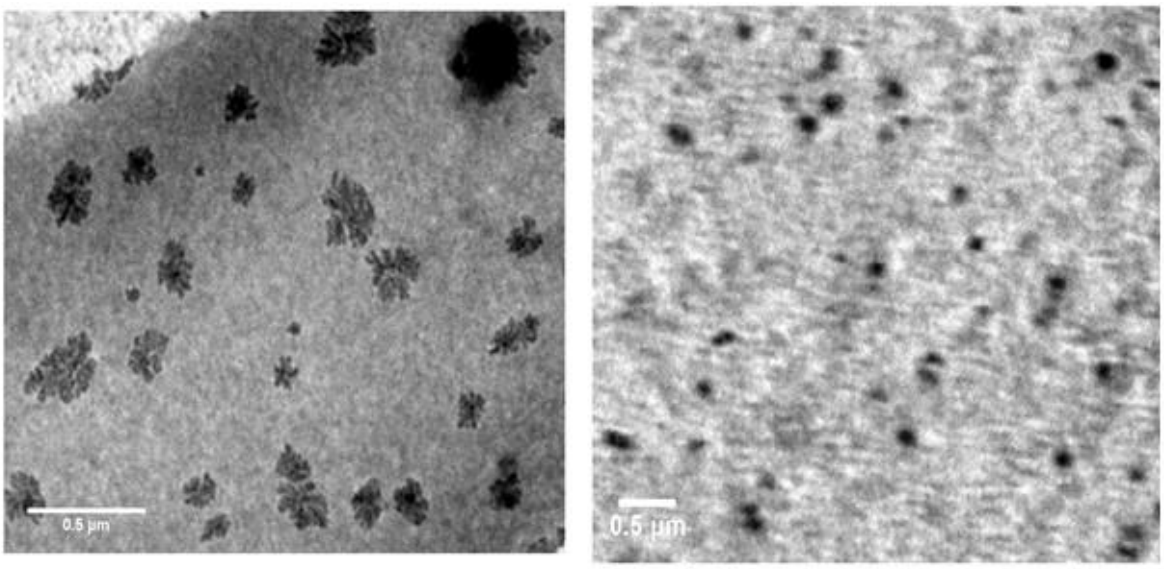

Figure 6.37 TEM images of SEBS/CB wt. 1% composite extruded (a) without and (b) with an assistance of supercritical fluid CO_2

6.5.3 Tensile and Cyclic Properties

Figure 6.38 and Table 6.7 show the tensile properties and Young's modulus of SEBS-g-MA/CB composites extruded with an assistance of $scCO_2$ respectively. Compared to SEBS-g-MA/CB extruded without an assistance of $scCO_2$, similar results in secant Young's modulus were observed at one percentage of strain. Similar to SEBS-g-MA/BT extruded with an assistance of $scCO_2$ described in section 6.2 in page 154, due to enhanced microphase separation and shorter chain lengths, the SEBS-g-MA/CB extruded with an assistance of $scCO_2$ shows a low Secant Modulus at a higher percentage of strain as hard S domains easily can slide over soft EB domain.

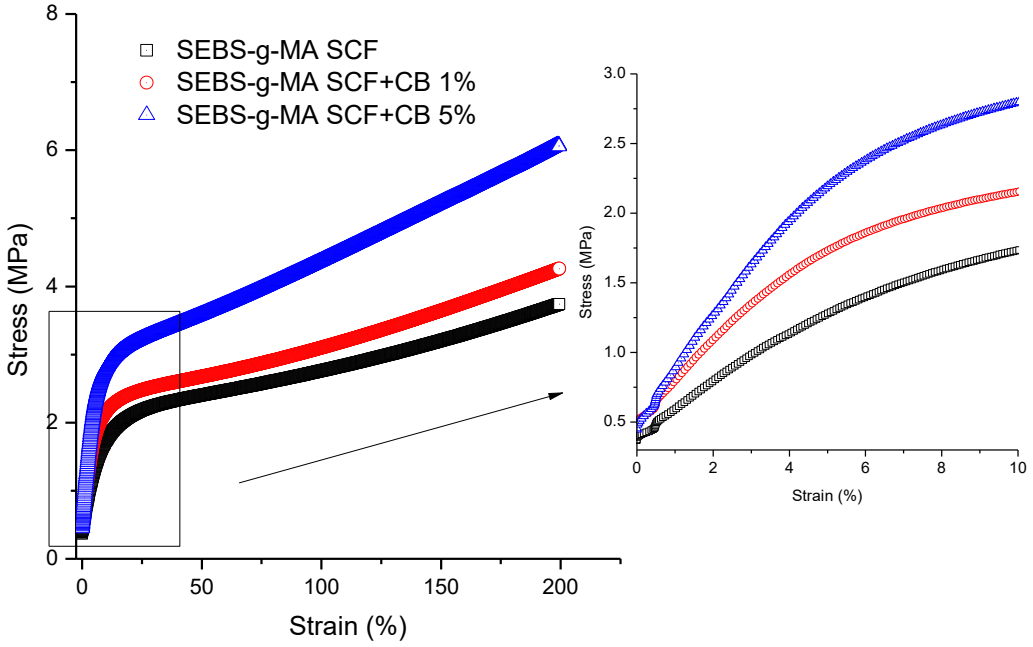

Figure 6.38 Tensile graphs of SEBS-g-MA/CB composites extruded with an assistance of $scCO_2$ measured in the parallel direction to extrusion

Compared to SEBS-g-MA/BT extruded with an assistance of $scCO_2$ described in section 6.2 in page 154, the reinforcement effect of CB was found to be much higher because of (i) small particle sizes of CB particles compared to BT, (ii) inherent mechanical properties of CB, and (iii) high level of interaction and dispersion of CB in SEBS-g-MA matrix.

Table 6.7 Secant Young's modulus of SEBS-g-MA SCF/CB composites

Nanocomposites	**Young's modulus at several composite different strain (MPa)**			
	1% (Std. dev.)	50% (Std. dev.)	100% (Std. dev.)	150% (Std. dev.)
SEBS-g-MA-SCF	57.94 (±5.9)	4.8 (±0.3)	2.76 (±0.1)	2.14 (±0.1)
SEBS-g-MA SCF + CB-1%	77.62 (±4.6)	5.34 (±0.5)	3.10 (±0.3)	2.42(±0.2)
SEBS-g-MA SCF + CB-5%	87.47 (±7.9)	7.16 (±0.6)	4.37 (±0.4)	3.48 (±0.3)

The loss energy factor of SEBS-g-MA/CB composites extruded with/without an assistance of $scCO_2$.is presented in Figure 6.39. This increase in shape memory properties was again attributed to reduction in domain size of soft and hard block

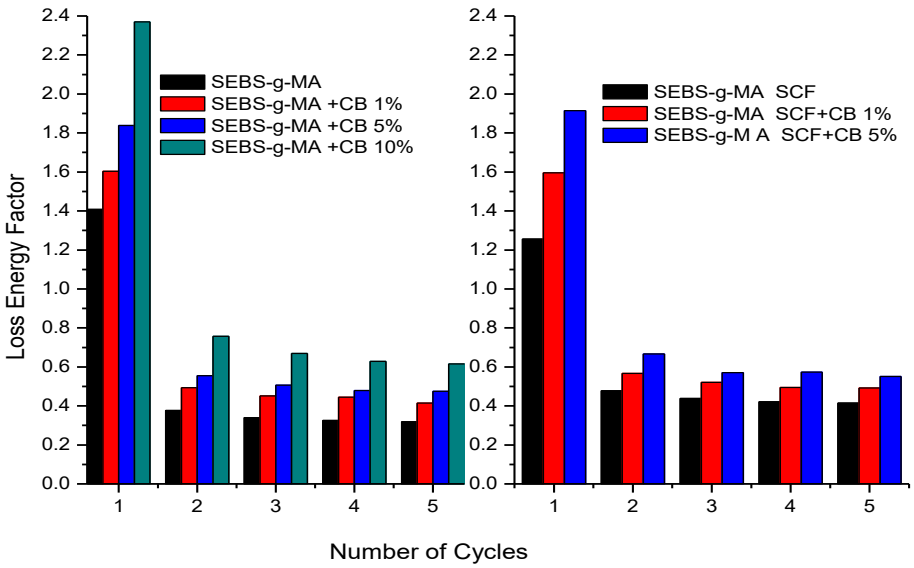

Figure 6.39 Loss energy factor of SEBS-g-MA SCF/CB composites with/without $scCO_2$ measured in the parallel to extrusion

6.5.4 Dielectric Properties

Figure 6.40, Figure 6.41, and Figure 6.42 and show the dielectric permittivity, dielectric loss tangent, and conductivity of SEBS-g-MA/CB composites manufactured using $scCO_2$ respectively The percentage of dielectric permittivity increase for SEBS-g-MA was found to be higher with the addition of CB when extruded with $scCO_2$ as shown in Figure 6.40 compared to the percentage of dielectric permittivity increased without the addition as described in section 5.1. In addition, when the percentage of CB was below 2 %, the dielectric loss was also found to decrease when the composites were manufactured using an assistance of $scCO_2$ then their counterparts processed without $scCO_2$. When the percentage of CB is 5 % the total conductivity, total dielectric permittivity, as well as dielectric loss, was highly increased as it starts to become conductive.

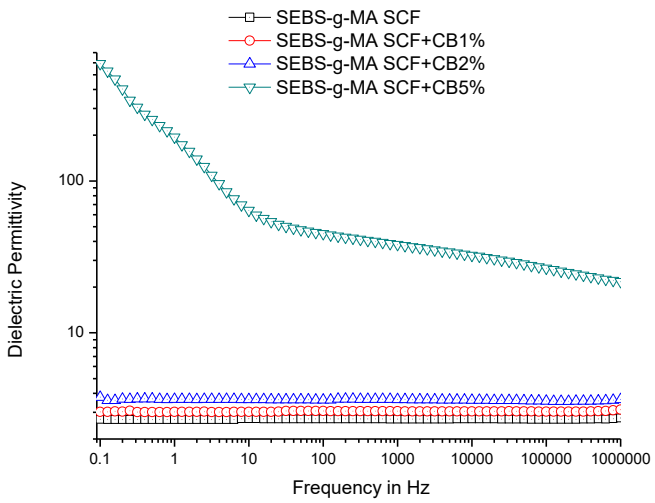

Figure 6.40 Dielectric permittivity of SEBS-g-MA SCF/CB composites

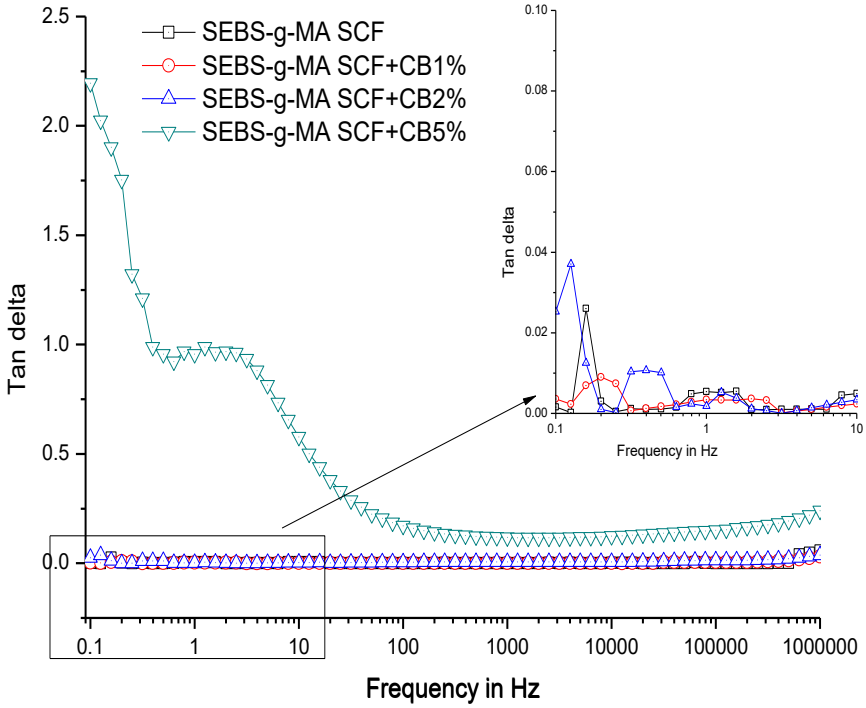

Figure 6.41 Dielectric loss of SEBS-g-MA SCF/CB composites

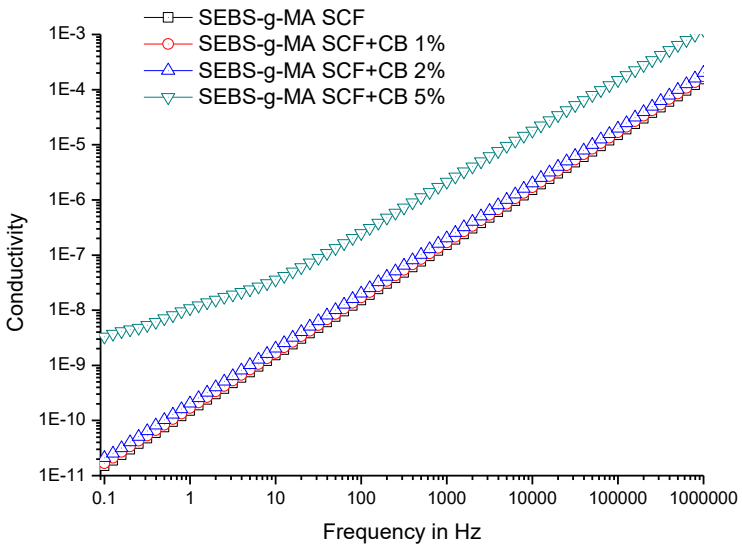

Figure 6.42 Conductivity of SEBS-g-MA SCF/CB composites

From Figure 6.42, it can be noted that at low frequency the conductivity is highly dependent on frequency. However, when the percentage of CB reaches 5%, at low frequency the total conductivity starts to show the frequency dependent and frequency independent behavior. The CB frequency independent behavior was more prominent in SEBS when the percentage of CB reached 5%, and it is attributed to different viscoelastic properties of SEBS/SEBS-g-MA. Some literature claim that the viscoelastic properties of the polymer matrices determine the percolation threshold of additive fillers in them [242]. From Figure 6.43, it can be observed that the relaxation of movement of the backbone of a triblock denoted by α_g decreases with an increase in the percentage of CB. At low frequency, MWS relaxation was found to be present only in SEBS-g-MA with 5 wt. % of CB at 10 Hz when the lowest frequency of measurement was 0.1 Hz

The high-frequency relaxation observed in SEBS-g-MA-SCF/CB composites can also be attributed due to the low glass transition (range -55℃ to 13℃) temperature of EB block present in SEBS-g-MA. Presence of early relaxation of a main chain upon addition of CB is attributed to enhanced restriction in molecular movement with high dispersion achieved upon addition of CB all phases of SEBS [243].

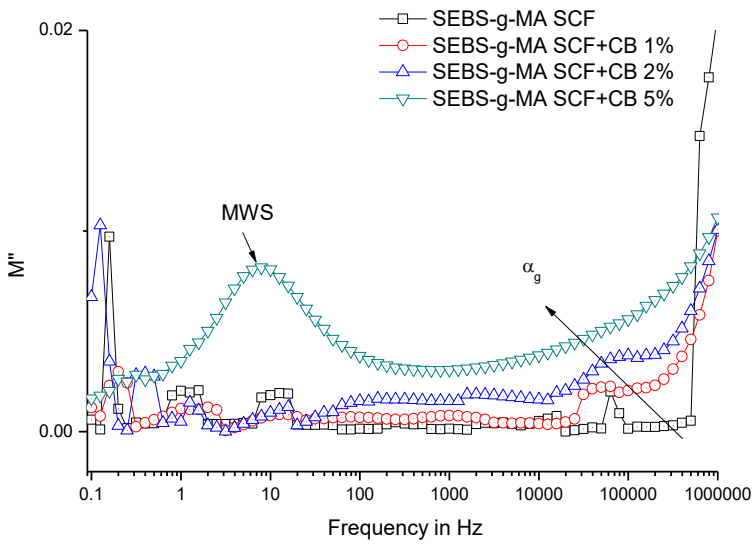

Figure 6.43 Electric modulus of SEBS-g-MA SCF/CB composites

6.5.5 Attenuated Total Reflectance-Fourier Transform Infrared Studies

Figure 6.44 shows the ATR-FTIR for SEBS-g-MA/CB composites extruded with an assistance of $scCO_2$. Like SEBS/CB composites extruded with $scCO_2$, SEBS-g-MA /BT spectra also shows the change in baseline. Similar to SEBS-g-MA/BT Composites, a slight shift in 2920 cm^{-1} 2851 cm^{-1} and 1456 cm^{-1} observed on addition of CB in SEBS-g-MA and a major shift and change in intensity was observed on 1732 cm^{-1} on SEBS-g-MA upon addition of SEBS-g-MA. As observed in SEBS-g-MA/BT composites, the 1112 cm^{-1} wavenumber in SEBS-g-MA spectra diminishes and a new spectrum was observed around 1028 cm^{-1} with the addition of CB. These observations show the interaction of CB of SEBS-g-MA with the highest interaction related to C=O polar bone of the triblock.

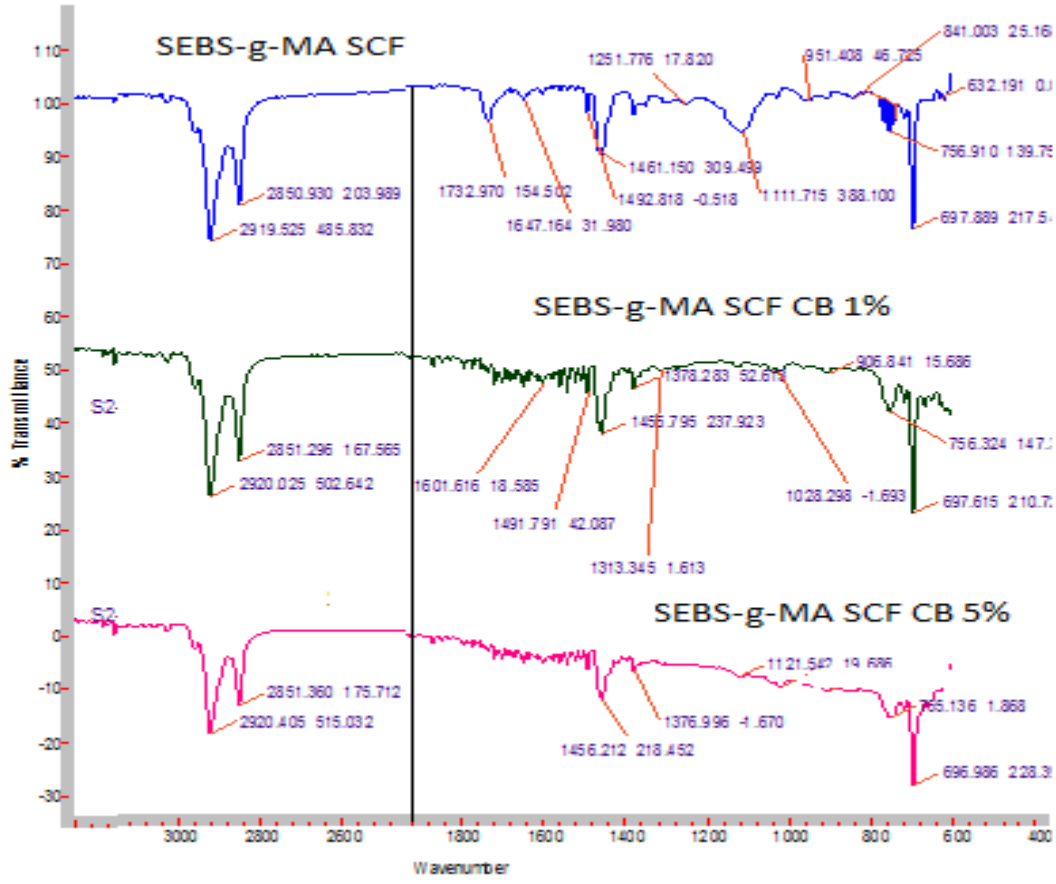

Figure 6.44 ATR-FTIR spectra of SEBS-g-MA SCF/CB composites

6.5.6 Differential Scanning Calorimetry

The derivative of reversing heat capacity for SEBS-g-MA- scCO$_2$-CB 1 wt.% and 5 wt.% using supercritical fluid assisted extrusion is presented in Figure 6.45. It is evident that the heat capacity Tg of the EB block reduces upon addition of carbon black particles as carbon particles restrict polymer movement. This restriction is also evident at the heat enthalpic relaxation peak at 13.89 °C with reduced heat capacity and prolonged heat enthalpic temperature. Compared to CB diserpersion and interaction with SEBS-g-MA extrusion without scCO$_2$, high level of structural changes confirm the dispersion and interaction.of CB in the EB soft domains and interphase domains between the polystyrene hard domains and the EB soft domains of SEBS-g-MA. For further analysis of CB particles dispersion in the hard domain, DMA analysis was performed. In addition, 5 wt.%, the addition of CB on SEBS-g-MA confirms the formation of microphases illustrated with multiple smaller peaks. This shows that higher percentages of CB within the SEBS-g-MA matrix increased the thermodynamic incompatibility between the EB

block and the filler, thereby resulting in multiple interphase domains with its own Tg, specifically during the Tg^{EB} and the melting relaxation of the EB block.

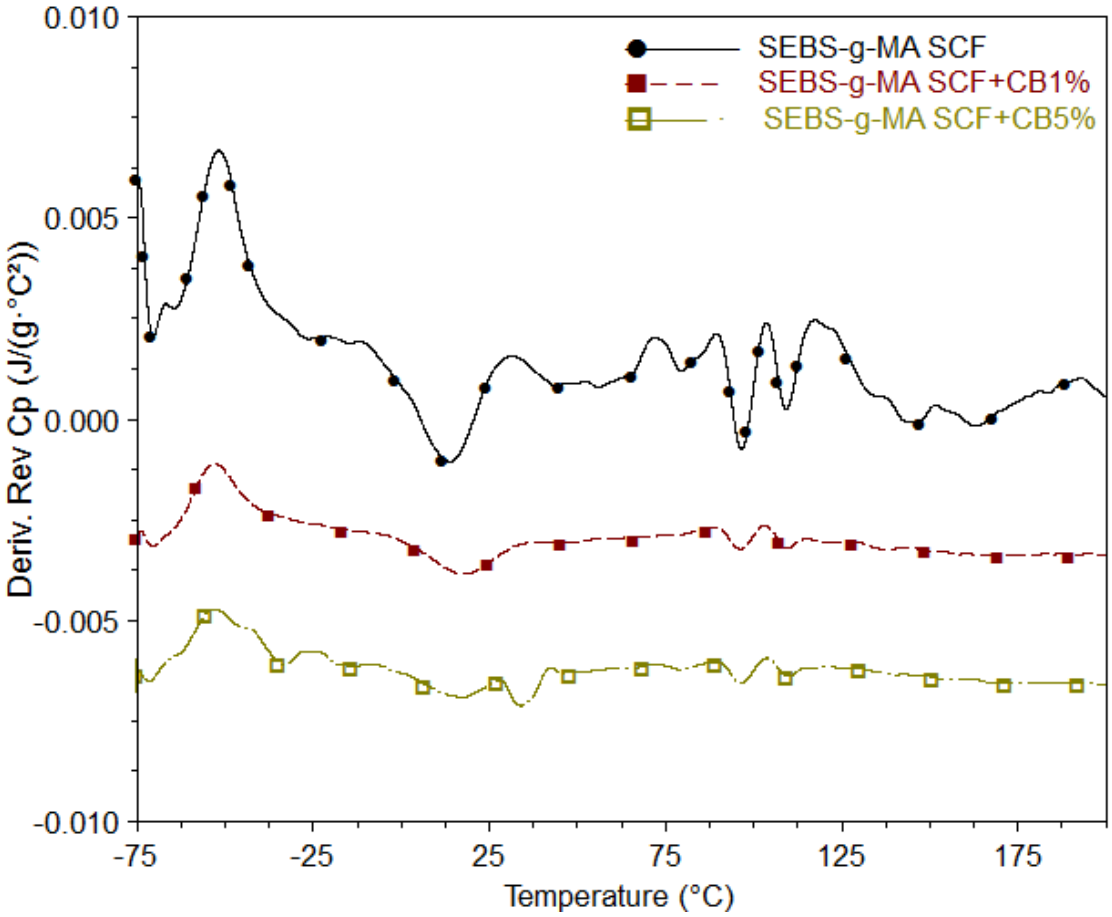

Figure 6.45 Derivative of rev. specific heat capacity of SEBS-g-MA SCF/CB composites

6.5.7 Dynamic Mechanical Analysis

Figure 6.46 shows the tan delta of SEBS-g-MA/CB composites extruded with an assistance of $scCO_2$. A slight shift was observed in onset point of transition with the addition of CB fillers. The onset transition of the tan delta was shifted from 72.83 °C to 73.89 °C and 78.76 °C. In addition to shift in onset tan delta transition, a huge reduction

of tan delta peak and minimum change in the peak of the tan delta was illustrated in the graphs with the addition of CB fillers.

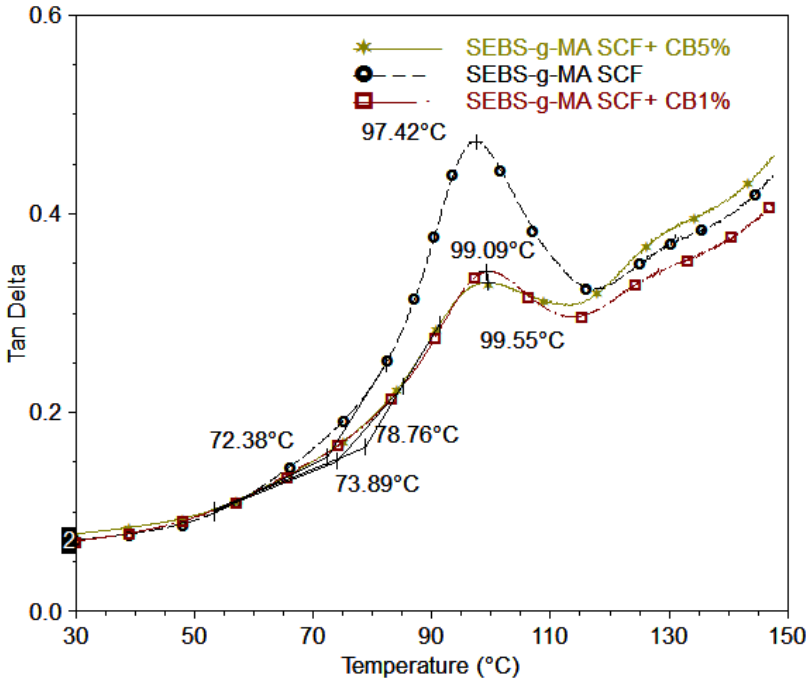

Figure 6.46 Tan delta of SEBS-g-MA SCF/CB composites

The change in onset transition, as well as reduction in tan delta peak, is the representation of heterogeneous network formation with hard block polymer showing interaction to polystyrene domain of hard block.

In addition, the decrease in tan delta signifies the enhanced mechanical performance of the elastomers for stress/strain sensing applications. Similar results were obtained for SEBS/CB composites processed with $scCO_2$ as described in section 6.3.

6.5.8 Conclusion

TEM images show supercritical fluid assisted extrusion with screw consisting of kneading blocks can substantially increase the dispersion as well as distributive mixing capability of extrusion. Major improvements were seen for mechanical as well as dielectric properties is due to (i) high exfoliation of CB particles when extruded with an assistance of $scCO_2$ compared to agglomerated CB particles when the extrusion was carried out without an assistance of $scCO_2$, (ii) reduction in the size of CB agglomerates, and (iii)

high interaction of CB particles on SEBS-g-MA due to small particle size with larger surface area as suggested by ATR-FTIR, DSC and DMA results. The high mechanical, electrical and thermal performance enhancement observed makes SEBS-g-MA/CB composites more sensitive for stress/strain sensing applications. In addition, the uniform distributive and dispersive dispersion of CB in SEBS-g-MA enhances repeatability and reproducibility of micro device applications

Chapter 7

7 Thermo-Electrical Properties of Dielectric Fillers and Conductive Filler Based Thermoplastic Elastomers Manufactured using Supercritical Fluid Extrusion

7.1 Introduction

This chapter is further divided into two sections for (i) the evaluation of dielectric change of dielectric fillers based thermoplastic elastomer/composites and (ii) dielectric relaxation phenomena of conductive composites near the percolation threshold over a range of temperature.

7.2 Dielectric Fillers Based Thermoplastic Nanocomposites

7.2.1 Introduction

Supercritical fluid assisted processing technique can be used for processing of these kinds of thermoplastic elastomers for improved dielectric properties providing better intermixing of different domains and fillers for the design of better electrical products for insulation, actuation, and energy harvesting applications. However, there is the lack of knowledge about the processing and their understanding of electrical properties in different frequency/temperature range of these polymers and polymer- additives with/without $scCO_2$ in co-rotating twin screw extruder.

This work presents the scientific understanding of tailoring of dielectric, and thermal properties of SEBS-g-MA processed with/without $scCO_2$ over a range of frequency and temperature. Specifically, this work addresses the following issues (i) comparison and enhancement of dielectric properties of SEBS-g-MA and SEBS-g-MA/BT manufactured with twin screw hot melt extrusion with and without assistance of $scCO_2$ and (iii) the effect on dielectric properties of BT/polymer composites due to the dispersion of additives in the polymer matrix.

7.2.2 Thermo-dielectric Analysis

Figure 7.1 depicts the real dielectric permittivity of SEBS-g-MA extruded with and without $scCO_2$ measured at different frequencies over a range of temperatures (40-120

°C). SEBS-g-MA extruded without $scCO_2$ shows a higher positive change in polarization effect as temperature increases at all frequencies compared to SEBS-g-MA extruded with $scCO_2$.The standard deviation of real dielectric permittivity measured 40°C to 120 °C at 10 kHz was found to 3.56% and 0.98% for SEBS-g-MA processed without and with $scCO_2$ as shown in Table 7.1. This result can be correlated with change in specific heat capacity of the material as shown in Figure 7.2. Specific heat capacity shows sensitivity to the change in molecular motion with a copolymer.

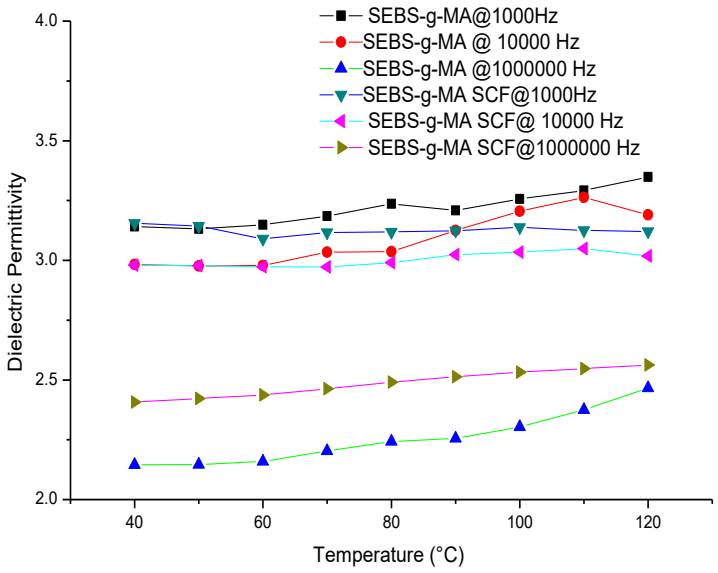

Figure 7.1 Real dielectric permittivity of SEBS-g-MA (manufactured with/without $scCO_2$ assisted extrusion) at different temperature and frequency

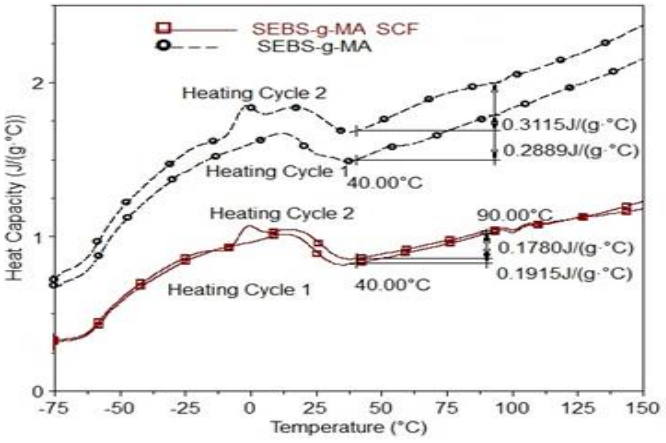

Figure 7.2 Change in specific heat capacity of SEBS-g-MA manufactured with/ without $scCO_2$ assisted extrusion

Figure 7.2 further shows the higher change in specific heat capacity of SEBS-g-MA (0.2889 J/g °C) extruded without $scCO_2$ compared to SEBS-g-MA (0.1915 J/g °C) extruded with $scCO_2$ over the range of temperature (40 °C to 90 °C). The stability effect observed in SEBS-g-MA extruded with the assistance of $scCO_2$ is attributed to a change in triblock chain length. These observations are consistent with the literature which claims shorter chain has higher thermal stability and vice versa [233].

Although SEBS-g-MA extruded with/without an assistance of $scCO_2$ shows a negligible difference in real dielectric permittivity (ca. 3.0) below 20 kHz; above 20 kHz, SEBs-g-MA extruded without $scCO_2$ shows a slight decrease in real dielectric permittivity compared to SEBS-g-MA extruded with $scCO_2$, as shown in Figure 7.3.

Table 7.1 Average real dielectric permittivity of SEBS-g-MA and SEBS-g-MA/BT processed under different conditions

Materials	**Average real dielectric permittivity from 40-120 °C**	
	At 10 kHz	**At 20 kHz**
SEBS-g-MA	3.09±0.110	3.06±0.12
SEBS-g-MA SCF	3.00±0.029	2.97±0.04
SEBS-g-MA +BT 5%	3.96±0.064	3.89±0.062
SEBS-g-MA SCF+BT 5%	4.78±0.047	4.77±0.087

The linear slope measured from 20 kHz to 1MHz was found to be $-4.6*10^{-7}$ and $-2.0*10^{-7}$ for SEBS-g-MA extruded with and without $scCO_2$ respectively. With an increase in frequency, the mobility of the molecular chain of a polar molecule becomes slow to respond to higher frequency showing a high dielectric loss and low polarization capability. In SEBS-g-MA, the SEBS-g-MA triblock consists of ethylene-butylene-grafted-maleic anhydride soft block and polystyrene hard block. The mobility of molecules is not only the function of the movement of a single molecule within a copolymer but also the polymer chain length of triblock as well as the interaction between the soft block and hard block [48]. A small particle or small phase size means a higher surface area for interaction. Here, the higher surface area of interaction contributed by

polystyrene during extrusion with $scCO_2$ is due to higher swelling of two separated blocks due to the effect of the supercritical fluid, followed by better infusion of hard and soft blocks [225, 244]. The increase in phase separation of each triblock leads to higher sensitivities at higher frequencies as small strands can respond faster than big strands of polymers and higher thermal stability of polymers. However, the results in Figure 7.3 do not agree with this theory.

When SEBS-g-MA is treated with $scCO_2$, the phase size of polystyrene decreases leading to the higher surface area for interaction between the soft block and the hard blocks. In addition, it is suggested $scCO_2$ affects the structure of polystyrene in polymer blends helping for better mixing of different polymers, thereby causing the high reinforcement effects due to polystyrene on the soft polymer [126]. Hence, the overall movement of the triblock is decreased due to a high reinforcement effect of the hard block to the soft block. However, the phase size of each block has decreased, which can respond to the frequency easily compared to the bigger block.

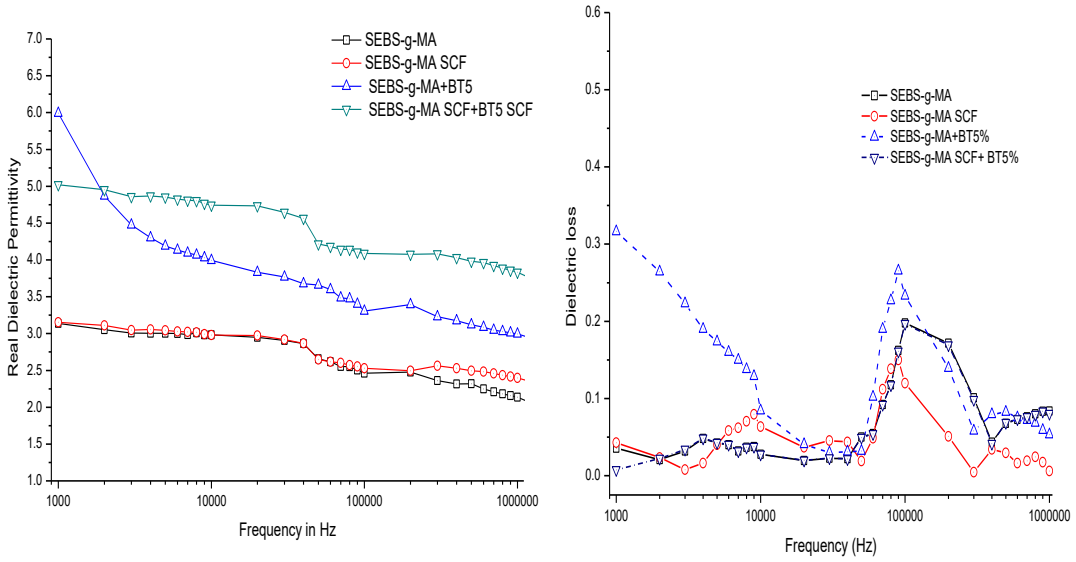

Figure 7.3 Real dielectric permittivity (Left) of SEBS-g-MA/ BT composite and Dielectric loss (right) manufactured with and without $scCO_2$ assisted extrusion over different frequency

The increase in specific heat capacity with an increase in temperature causes the overall movement of a triblock, whereas frequency response causes only the molecular segmental movement within a triblock. Hence, SEBS-g-MA extruded with $scCO_2$ shows a higher

sensitivity to the oscillating electrical field at a higher frequency than SEBS-g-MA extruded without $scCO_2$.

A significant difference was observed in the real dielectric property of SEBS-g-MA/BT composites processed with/without $scCO_2$ over a range of frequencies as shown in Figure 7.3. The dielectric composites manufactured with $scCO_2$ show a low rate of change for dielectric properties over a range of frequency. Similarly, at low-frequency range, the dielectric loss tangent of the SEBS-g-MA/BT composites manufactured using $scCO_2$ was found to be very low (<0.005) compared to SEBS-g-MA /BT (0.3) composite manufactured without using $scCO_2$. This result can also be discussed based on the dispersion of BT materials in polymer composites. When BT fillers are highly dispersed into the polymer matrix, the nanocomposite manufactured consists of small particles/ aggregates of BT particles which can show high polarization effect over a range of frequencies. However, the formation of agglomerates leads to high dielectric loss due to heat generation over frequency as well as the slow response of such dielectric fillers in nanocomposites. Similarly, polymer shell thickness also affects the dielectric property of the material [245].

Due to higher molecular movement over the range of temperature measured at 10 kHz and 20 kHz frequency, the dielectric permittivity of SEBS/BT manufactured without $scCO_2$ fluctuates over the range of temperature with a standard deviation of 1.61% as shown in Table 7.1.

On the other hand, in SEBS-g-MA processed with $scCO_2$, the real dielectric permittivity over the range of temperature varies by 1.8% at 20 kHz compared to 0.98% at 10 kHz. This is because temperature aids in the polarization of dispersing additives in SEBS-g-MA processed with $scCO_2$ compared to agglomerated BT particles in SEBS-g-MA processed without $scCO_2$. Hence SEBS-g-MA processed with $scCO_2$ is marked constant over the range of frequency measured from 10 kHz and 20 kHz. The change in specific heat capacity from 40℃ to 90 °C was 0.2889M J/g. °C and 0.03654J/g. °C for SEBS-g-MA extruded with and without $scCO_2$ respectively, for the first heating cycle, and 0.2708 J/g. °C and 0.03654 J/g. °C for SEBS-g-MA extruded with and without $scCO_2$ respectively, for the second heating cycle. Figure 7.4 shows the real dielectric permittivity of SEBS-g-MA/BT composites over the range of temperature at 5kHz, 10 kHz and 20 kHz.

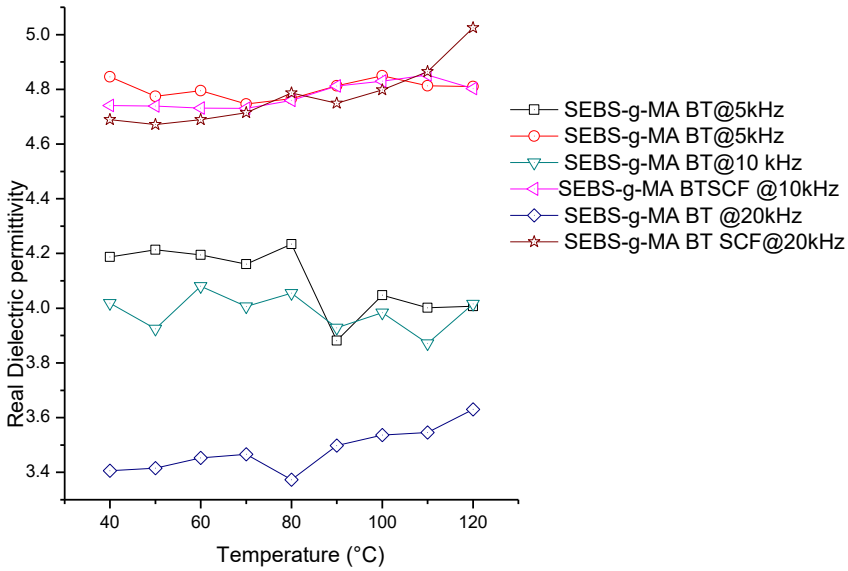

Figure 7.4 Temperature dependency of SEBS-g-MA /BT composite processed with/without at 5kHz, 10 kHz and 20 kHz

At 5 kHz, SEBS-g-MA/BT composites processed without $scCO_2$ showed a sudden decrease in real dielectric permittivity around 90 °C near the glass transition temperature of polystyrene. This is because of high swelling behaviour of polymers near glass transition making BT additives increase the distance from each other. However, this effect was not seen due to small shell size of polymers and high dispersion of BT additives when treated with $scCO_2$ because the dipoles can response very well at higher frequencies compared to immediate relaxation on the non- $scCO_2$ processed SEBS-g-MA (Figure 7.3).

7.2.3 Conclusion

In the present work, dielectric thermoplastic elastomer and nanocomposites were manufactured with/without an assistance of $scCO_2$ and their dielectric properties were investigated in the frequency domain as a function of temperature. The interfusion of the soft block and the hard block was found to change the dielectric properties of same thermoplastic elastomer over the range of frequency and temperature. Similarly, the dispersion of fillers also has a high influence on the dielectric properties of composites manufactured. The relative change in dielectric properties of SEBS-g-MA extruded without $scCO_2$ with an increase in temperature was due to higher segmental movement present in a triblock. However, this effect did not prevail in SEBS-g-MA-treated with

$scCO_2$ due to a high reinforcement effect of polystyrene in the ethylene-butylene block. On the contrary, the breaking down of polystyrene phases into smaller phases makes SEBS-g-MA when extruded with $scCO_2$ more sensitive to higher frequency because of easier movement of a polar group within a molecule. Similarly, SEBS-g-MA/BT composites manufactured with $scCO_2$ were found to be sensitive to frequencies, making constant dielectric properties over a range of temperature. Therefore, based on these observations, the exfoliating and reacting nature of $scCO_2$ with elastomer causes structure changes and increases micro phase separation of the elastomer. In addtion, $scCO_2$ also provides better dispersion of additives in the elastomeric matrix, thereby making elastomer/composites equally sensitive to a wide range of frequencies and temperature for capacitive energy harvesting techniques.

7.3 SEBS-g-MA/CB Composites near the Electrical Percolation Threshold

7.3.1 Introduction

This work presents the least understood dimension of dielectric relaxation phenomena and energy dissipation over temperature of multiphase thermoplastic conductive network near percolation threshold (Poly(styrene-b-ethylene-butylene-styrene)-grafted-maleic anhydride (SEBS-g-MA) with CB 5 wt. %) processed with $scCO_2$ assisted extrusion over a range of frequency from temperature 40 °C to 120 °C. The aim of the work is to investigate the effect of temperature on dielectric/conducting relaxation phenomena of thermoplastic elastomers composites above room temperature and its correlation with viscous and molecular processes. Specifically, this work addresses following issues (i) investigation of the dielectric response of SEBS-g-MA/CB composites over a range of frequencies and temperatures (ii) dielectric property variation of SEBS-g-MA/CB manufactured below and above the range of glass transition of hard block and (iii) difference in different types of relaxation frequency with temperature.

7.3.2 Dynamical Mechanical Analysis

Figure 7.5 shows the dynamical mechanical analysis of SEBS-g-MA/CB 5% composite extruded with an assistance of $scCO_2$. From the storage modulus curve, a measure of the mechanical stiffness of the material, it can be noted the onset of the glass transition of the

hard block starts around 57.68 °C. A sharp drop of storage modulus is observed from 80 to 110 °C. At 96.85 °C, a point of inflection was observed. In the literature, this is considered as a glass transition temperature [246]. The drop in mechanical strength becomes almost constant after 110 °C. All these transitions are highly controlled by the molecular motion of the triblock. The loss modulus, a direct measure of molecular motion, of a triblock, starts as early as 40 °C. At ca. 70 °C, the increase in loss modulus almost becomes flat. The peak of loss modulus was observed at 80.53 °C, which represents a maximum frictional/heating effect produced due to the highest molecular motion of the hard S segment of the triblock. This is also pronounced as a glass transition temperature measured due to molecular motion [246, 247], as the rotation of C-C bond of S-segment of a triblock becomes much easier. The peak tan delta is also generally considered a good measure of glass transition temperature of the materials as it directly signifies the ratio of stiffness to viscous nature of the triblock[248, 249]. The peak of tan delta was observed at 104.62 °C in this case.

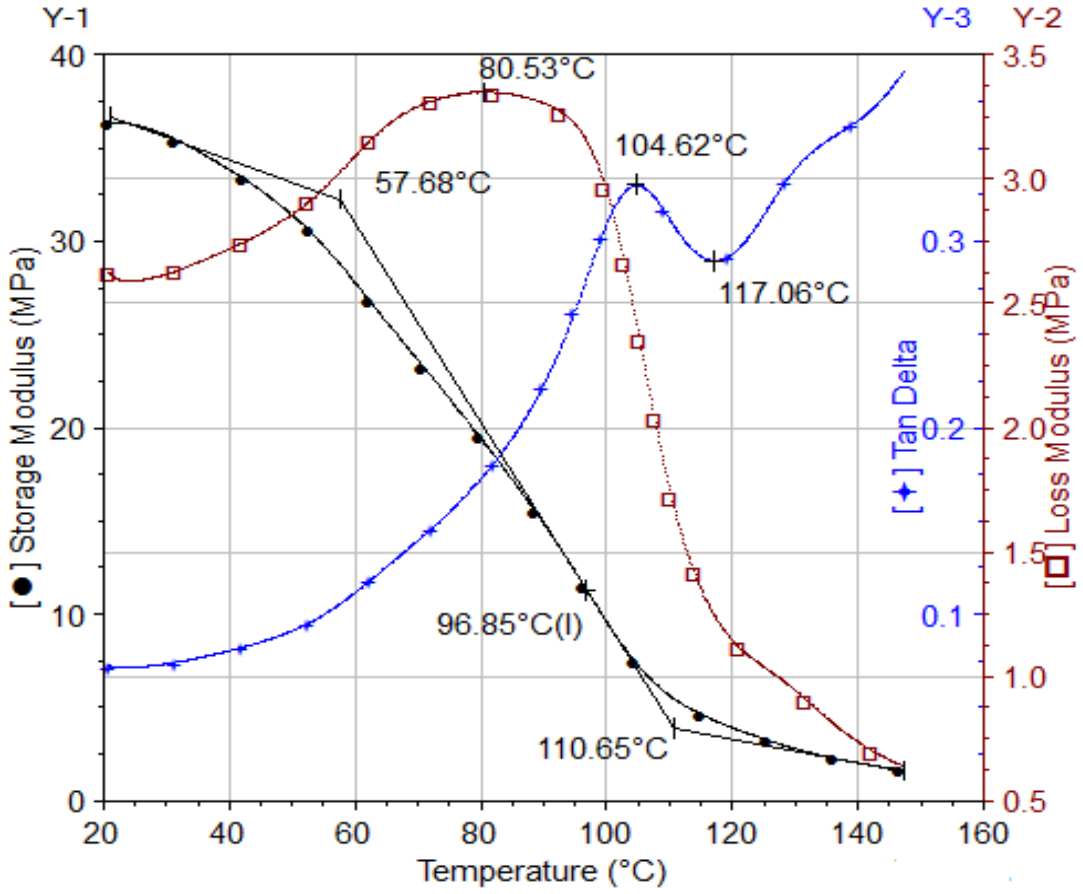

Figure 7.5 DMA curve of SEBS-g-MA SCF/CB 5 wt. % composite

7.3.3 Electrical Characterization

Figure 7.6 and Figure 7.7 show the dielectric permittivity (ε^*) of SEBS-g-MA /CB at 40-80 °C and 90-120 °C respectively from 1 kHz to 1 MHz. It is observed that dielectric permittivity of composites decreases with an increase in frequency at all temperature ranges. However, the dielectric permittivity of SEBS-g-MA/CB 5% is constant at different temperatures above 10^5 Hz. The decrease in polarization effect over frequency is because of relaxation phenomenon of the polymer-additive interface.

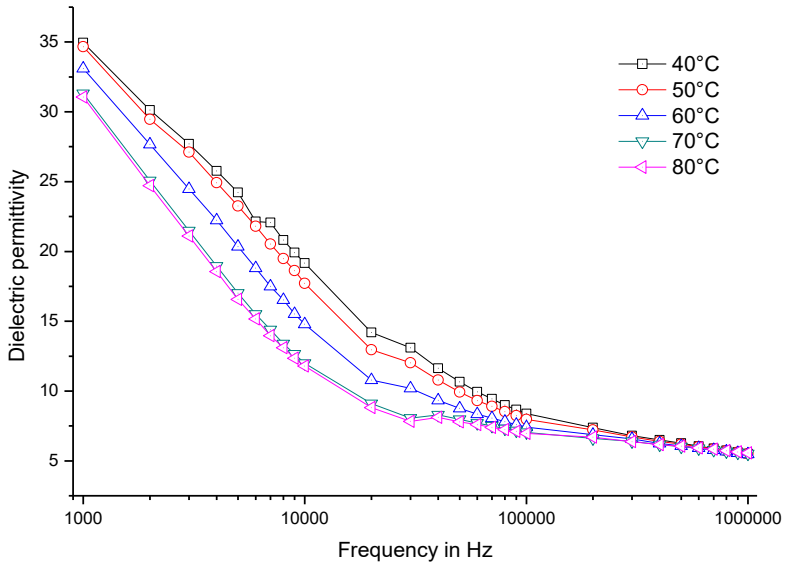

Figure 7.6 Dielectric permittivity of SEBS-g-MA SCF/CB 5 wt. % composite

Highly conductive CB particles when in contact with an insulating polymer surface from an imbalance of charge resulting in high polarization at the interface. The frequency relaxation phenomenon differs with amount/structure/surface area/dispersion of additive in polymers, as well as environmental conditions including, but not limited to pressure and temperature as these variables change the distance between two CB particles within a polymer matrix. The polarization behavior was found to be more pronounced at low frequencies as all dipoles resulting from the polymer- additive interface have sufficient time for polarization of dipole present in the composites. In addition, the dielectric permittivity of the SEBS-g-MA/CB composite was found to decrease with temperature from 40-80 °C, whereas, from 80-120 °C, the dielectric permittivity of the composites

was found to increase below 2*10^5 Hz. After 2*10^5 Hz, the dielectric permittivity becomes almost constant. The resultant polarization (dielectric permittivity) occurs due to (i) movement of conductive charges giving rise to dc conductivity (σ_{dc}) and (ii) interfacial polarization. Both phenomena tend to relax at their own respective frequencies.

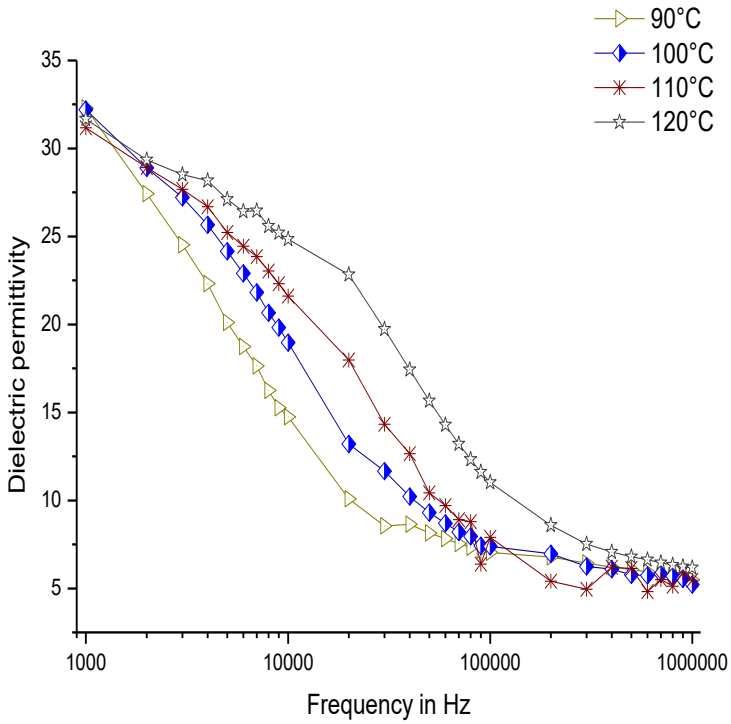

Figure 7.7 Dielectric properties of SEBS-g-MA SCF/CB 5 wt. % composite

This change in dielectric permittivity over temperature at a frequency lower than 2*10^{5}Hz can be correctly evaluated using the loss modulus curve of the DMA graph as shown in Figure 7.5. Below 70 °C, the hard S segment in the triblock does not show enough mobility for the movement of molecules in the triblock, however, it does show the continuous swelling effect by the SEBS triblock as a whole as the result of continuous decrease and increase in stiffness and viscous nature of hard block. The continuous decrease in storage modulus also demonstrates the continuous increase in linear expansion coefficient of the polymer as shown in the literature [250]. This also resists the polarization mobility of CB entrapped between the soft- hard domain and the hard- hard domains. From 80 °C, the triblock has higher swelling effects as the steepness of storage modulus curve increases. In contrast, it also shows better mobility of molecules as shown

by loss modulus graphs of DMA leading to faster escaping of charges being entrapped between different domains leading to high polarizing effect. The interfacial polarization is accurately defined by the real dielectric permittivity (ε') of the composites as shown in Figure 7.8 and Figure 7.9.

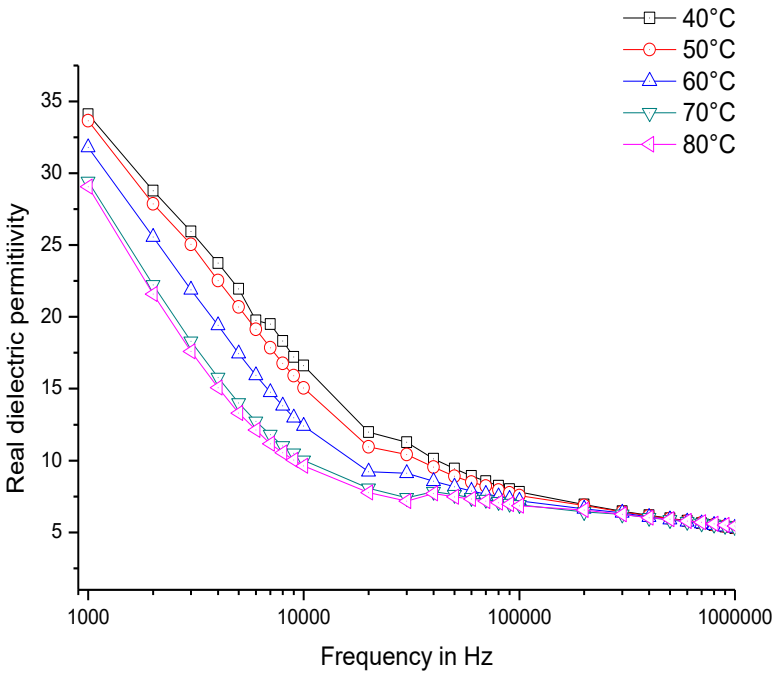

Figure 7.8 Real dielectric permittivity SEBS-g-MA SCF/CB 5 wt. % composite

The frequency profile of real dielectric property for SEBS-g-MA/CB composites at different temperature presents a similar pattern of dielectric permittivity of SEBS-g-MA/CB composites. The real dielectric relaxation also decreases with an increase in temperature from 40 °C to 70 °C from $7*10^4$ Hz to $1*10^4$. This result confirms that the temperature decreases the real polarization effects on SEBS-g-MA/CB composites from 40-70 °C above 1000Hz, where the overall dielectric strength (Δε) can be measured using Harvriliak-Negarmi (HN) modeling. This effect can be attributed towards insufficient mobility of hard domains above 1 kHz, but noticeable swelling behavior in the triblock exists from 40-70°C. However, above 10 kHz, the effect is reversed above 70°C as temperature enhances higher conducting behavior of carbon fillers as well as the mobile nature of the hard block present in SEBS-g-MA. High conductive nature of fillers

increases high interfacial polarization between polymers and additives even at high frequency, whereas the swelling nature of the triblock creates longer electrical distance between conductive CB aggregates.

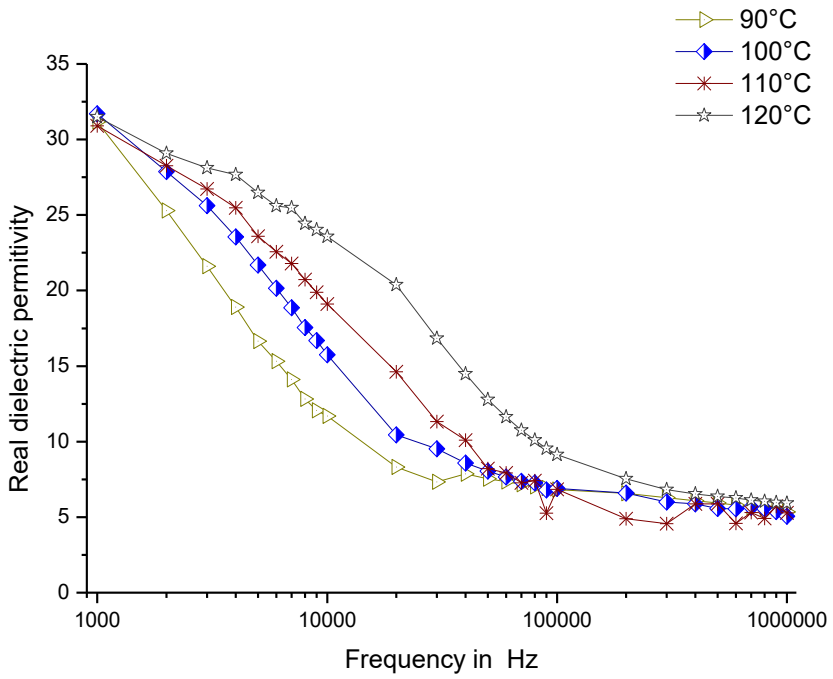

Figure 7.9 Real dielectric permittivity of SEBS-g-MA SCF/CB 5 wt. % composite

The imaginary part of dielectric permittivity (ε'') generally defines the total loss due to movement of electrons/ protons and the heating/frictional loss during movement of dipoles created within polymer-filler interface. The loss tangent, a ratio of imaginary dielectric permittivity to real dielectric permittivity, defines accurately the electrical loss behavior of the composites.

The loss tangent of SEBS-g-MA SCF/CB composites is frequency as well as temperature dependent as shown in Figure 7.10 and Figure 7.11. Conductive fillers when exfoliated in thermoplastic elastomers like SEBS-g-MA form domains between the polymer and carbon black, which tend to polarize as well as conduct due to the semiconducting nature of carbon black. This conducting behavior of the composite relaxes at low frequencies. The peak of loss tangent also denotes the dissipation factor of polymer CB composites. At 40 °C, the dissipation relaxation frequency resulted due to the glassy polystyrene block

of the triblock is found at 20 kHz. This relaxation frequency decreases with an increase in temperature and reaches around 6 kHz at 80 °C.

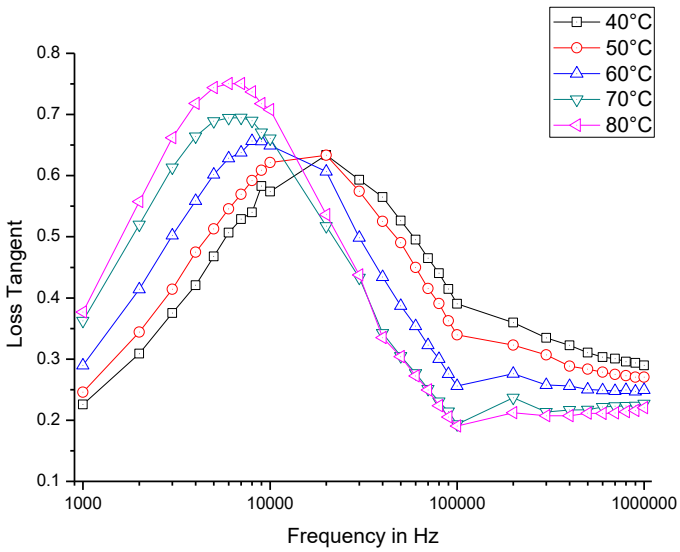

Figure 7.10 Loss tangent of SEBS-g-MA SCF/CB 5 wt. % composite

This dissipation relaxation frequency can also be explained using the molecular motion and stiffness of the tri-block observed in DMA curves. The CB entrapped between different domains need more time to move from one point to another as it goes from 40 to 80 °C because of the spectroscopically noticeable swelling effect of the tri-block which increases the distance between agglomerates of CB within a polymer. However, after 80°C, the agglomerates of carbon particles trapped between the hard domains and between hard and the soft domains have the easier mobility to the electric field applied leading to higher relaxation frequency and better response at higher frequencies. This dissipation relaxation frequency again increases to 60 kHz when the temperature is increased from 80 to 120 °C. Similar result of an increase in relaxation frequency above the glass transition temperature of polycarbonate was observed by Alegria *et al* [243]. The highest peak of loss tangent, 0.78, was observed at 20 kHz, 30 kHz, and 40 kHz at temperature 90, 100 and 110 °C respectively. The region between 80 to 110 °C is also considered to be the glass transition temperature of the hard domain, polystyrene, of SEBS-g-MA. This result also coincides with the results obtained from DMA curve. Before dissipation relaxation frequency of SEBS-g-MA/CB composites, the dielectric loss increases from 40 °C to 80 °C and decreases until 120 °C as shown in Figure 7.10.

This increase from 40 °C to 80 °C is due to the positive temperature of CB filler materials where their hard domain is still in glassy phase [251], however, it requires a longer time for carbon particles to transfer an electron from one point to another as the glassy domain is immobile and the tri-block is continuously swelling from 40-80 °C. This relaxation frequency occurs due to restriction in movement of charges. It is also due to irregular expansion and mobility facilitated by the hard block before and after the glass transition.

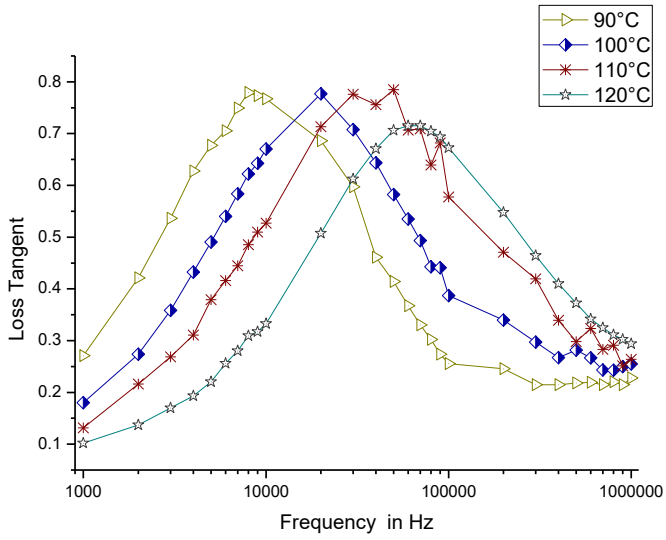

Figure 7.11 Loss tangent of SEBS-g-MA SCF/CB 5 wt. %

Figure 7.12 shows the dielectric modeling of using HN equation which is generally represented by Equation 7.1 [252].

$$\varepsilon^* = \varepsilon_\infty + (\varepsilon_0 - \varepsilon_\infty) \times \frac{1}{[1+(i\omega\tau)^{1-\alpha_{HN}}]^{\beta_{HN}}} - \frac{i\sigma_{dc}}{\varepsilon_0 \omega^s} \qquad \text{Equation 7.1}$$

Where ε_∞ and ε_0 represent the total dielectric permittivity of nanocomposites at high frequency and low frequency respectively, i is the characteristic complex number $\sqrt{-1}$, ω is the angular frequency (where $\omega = 2\pi f$), τ is the relaxation time and is given by $1/2\pi f_{max}$, f_{max} is the peak frequency of loss modulus and α_{HN} and β_{HN} are shaped characteristics of the fitted curve which describe width and asymmetry of loss peak respectively where $0 \leq \alpha_{HN}, \beta_{HN} \leq 1$. The fitting parameters become 1 for purely ohmic conductivity and decrease with electrode polarization. The parameter $\varepsilon_0 - \varepsilon_\infty$ denotes the dielectric strength ($\Delta\varepsilon$) of nanocomposites. For the Equation 7.2, where $\alpha_{HN}=0$ the HN model reduces to the Cole –

Davidson model

The real and imaginary parts of the complex dielectric permittivity are given by Equation 7.2 and Equation 7.3 respectively.

$$\varepsilon' = \varepsilon_\infty + (\varepsilon_0 - \varepsilon_\infty) \times \frac{\cos(\beta_{HN}\theta)}{\left[1 + 2(\omega\tau_{HN})^{1-\alpha_{HN}} \sin\left(\frac{\alpha_{HN}\pi}{2}\right) + (\omega\tau)^{2(1-\alpha)}\right]^{\frac{\beta}{2}}} \qquad \text{Equation 7.2}$$

$$\varepsilon'' = (\varepsilon_0 - \varepsilon_\infty) \times \frac{\sin(\beta_{HN}\theta)}{\left[1 + 2(\omega\tau_{HN})^{1-\alpha_{HN}} \sin\left(\frac{\alpha_{HN}\pi}{2}\right) + (\omega\tau)^{2(1-\alpha)}\right]^{\frac{\beta}{2}}} \qquad \text{Equation 7.3}$$

with

$$\theta = \tan^{-1} \frac{(\omega\tau)^{1-\alpha_{HN}} \cos\left(\frac{\alpha_{HN}\pi}{2}\right)}{1 + (\omega\tau)^{1-\alpha_{HN}} \sin\left(\frac{\alpha_{HN}\pi}{2}\right)} \qquad \text{Equation 7.4}$$

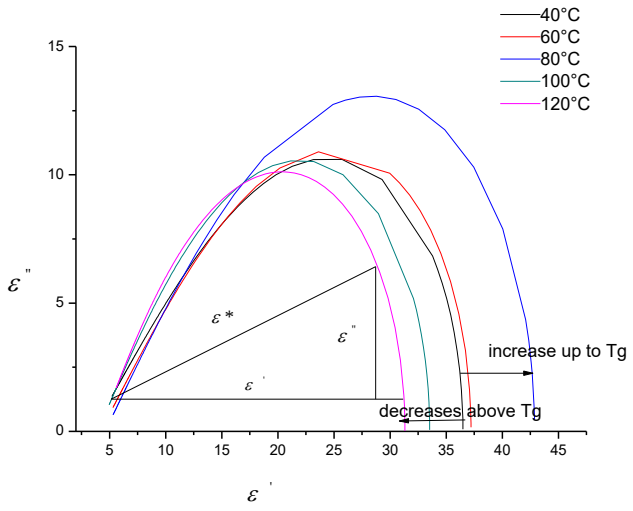

Figure 7.12 HN modeling of SEBS-g-MA SCF/CB 5 wt. % at different temperature

Table 7.2 shows parameters with the standard deviation extracted by fitting the HN model. As the value of α_{HN} equals to zero, this composite can be best fitted modeled using the

Cole-Davidson model. The value of β_{HN} increases with increase in temperature. The increase in temperature from 40 to 80 °C of composites shifts the relaxation frequency, f_o, to the lower value indicating the more conducting behavior of the composites. However, shifting of the relaxation frequency to higher values indicates more polarizing behaviour of the composites when measurement was carried out from 80 to 120 °C. Increase in temperature from 40 to 80 °C also increase the dielectric strength of the composites, however, above 80 °C the dielectric strength decreases due to high swelling effect from 80 to 120 °C of the triblock. The high dielectric strength obtained is the result of high polarizing capabilities of nanocomposites at low frequencies. This variation in polarization capacity of a nanocomposite between two relaxation frequency (as measured using tan delta and HN relaxation) is due to the difference in relaxation HN frequency (low) and tan delta relaxation frequency (high).

Table 7.2 Different parameters obtained from HN modelling

Parameters	Temperature (°C)				
	40	60	80	100	120
α_{HN}	0 ± 0	0 ± 0	0 ± 0	0 ± 0	0 ± 0
β_{HN}	0.426 ± 0.008	0.447 ± 0.019	0.469 ± 0.0309	0.5095 ± 0.0138	0.54775 ± 0.02419
f_0	1746.046 ± 22.169	911.497 ± 194.940	397.634 ± 285.952	2675.615 ± 208.429	10489.731 ± 846.923
$\Delta\varepsilon$ (ε_o-ε_ω)	33.007 ± 0.623	33.008± 2.196	38.281 ± 10.347	29.576 ± 0.681	27.209 ± 0.567
ε_∞	3.486± 0.154	4.20 ± 0.279	4.596 ± 0.359	3.950 ± 0.18	4.115 ± 0.306
τ (sec.)	0.573	1.097	2.51487	0.374	0.095

Below the glass transition of the hard block and above HN relaxation frequency, most of the molecules of the hard block are immobile and resist the movement of dipole formed between the polymer matrix and CB trapped in between hard and soft blocks leading to low polarization effects. However, at low frequencies, below 80 °C, the electrons of CB particles have enough time to escape from the valance band leading to high dielectric loss of SEBS-g-MA/CB. SEBS-g-MA/CB remains stable with less swelling effect below 80 °C compared to highly mobile and highly swelled SEBS-g-MA/CB at 120 °C. Similarly, below HN relaxation frequency, the dipoles formed have enough time to respond to the electric field leading to high polarisation effect

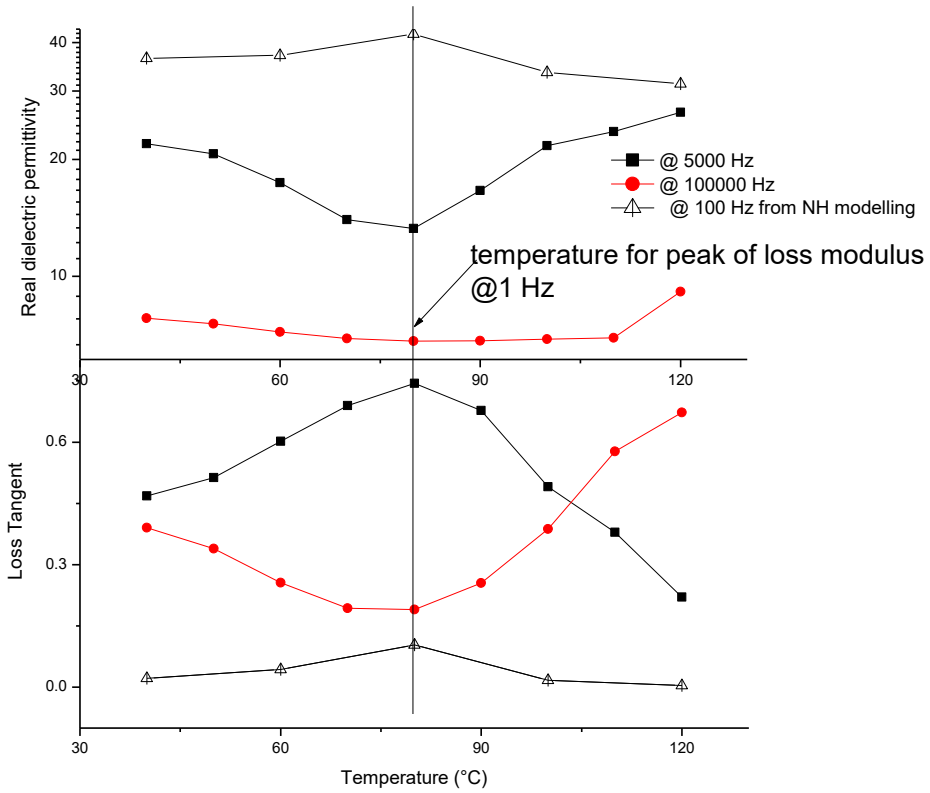

Figure 7.13 Dielectric permittivity and loss tangent as a function of temperature above and below the tan delta relaxation frequency.

At 100 Hz (below HN relaxation frequency), the polarization increases the transition temperature (peak) of loss modulus and decreases above this temperature. However, At 5 kHz (below tan delta relaxation frequency and above HN relaxation frequency), Figure 7.13 shows the polarization of SEBS-g-MA/CB nanocomposites near the percolation threshold decreases as the temperature increases up to the transition temperature measured by peak of loss modulus in Figure 7.13 and continues to increase above that temperature regardless of measurement taken above and below the dissipation relaxation frequency. On the contrary, at 100 Hz as well as at 5 kHz, the conduction phenomena due to electron tunneling effect increases up to the glass transition temperature and decrease above the glass transition if the measurement is taken below dissipation relaxation frequency and vice versa if the measurement is taken above the peak of tan delta

7.3.4 Conclusion

Dielectric thermoplastic elastomeric nanocomposites were manufactured with an assistance of $scCO_2$ and their dielectric properties over frequency were investigated in different temperature domains. The dielectric properties of SEBS-g-MA/CB 5 wt. % were found to be highly dependent on the glass transition temperature of hard block polymers measured from loss modulus peak of DMA curve. From 40°C, at frequency between HN relaxation and tan delta relaxation, the dielectric permittivity initially decreases up to the glass transition temperature of the hard domain of the triblock (measured by the peak of loss modulus) of the hard block in the triblock, then increases with an increase in temperature due to higher segmental movement of hard block present in a triblock. However, the total dielectric strength of the nanocomposite was found to be increasing up to the glass transition temperature followed by a decrease in total dielectric strength as temperature increases above the glass transition. Before tan delta relaxation frequency, the dielectric tangent loss measured was found to be increasing up to the glass transition temperature and decreases after glass transition temperature of the hard block as measured for the peak of loss modulus. Similarly, after tan delta relaxation frequency, the dielectric loss of the triblock was found to decrease from 40 to 80 °C and again increase when the temperature is increased from 80 to 120 °C. This change is attributed to the difference in higher swelling behavior of triblock effect by the glass transition temperature of the hard domain together with positive temperature coefficient behavior of CB filled materials having a total impact on the frequency based conduction and dielectric relaxation processes.

This section fills the knowledge gaps regarding the scientific understanding of the different types of relaxation frequencies, conductive properties, the dielectric strength and dielectric permittivity of microphase separated SEBS based conductive nano-composites over range of temperatures and frequencies which are dependent on viscoelastic factors, glass transition of domains for stress/strain sensors and artificial muscles like applications.

Chapter 8

8 Electrical Behaviour of Different Thermoplastic Composites under Tensile Conditions as a Potential for Different Strain/Stress Sensing and Energy Harvesting Applications

8.1.1 Introduction

The additions of different dielectric and conductive fillers into thermoplastic elastomers have shown great impact in the electrical, mechanical, thermal, and morphological structure of elastomers. Dielectric fillers and conductive fillers have their own advantages and disadvantages depending on their applications. Conductive fillers tend to increase the conductive properties of a polymer leading its high-end application in different strain/strain sensing technology, however, this technology does not show any advantage on elastomeric capacitive energy harvesting applications because of its low breakdown strength.

The use of different polymer based nanocomposites under different mechanical conditions has shown great promise in the field of energy harvesting applications from different mechanical vibration sources. Similarly, conductive filler based nanocomposites have the potential for several civil infrastructural sensing applications. This work presents the conduction behavior as well as dielectric relaxation phenomena of dielectric thermoplastic elastomers with conductive and dielectric fillers under different strain conditions. In addition, this work also confirms the enhanced sensitivity of SEBS/CB (with slightly higher than percolation threshold) for stress/strain sensing applications. Similarly, the energy harvesting model confirms the greater amount of energy harvested using composites (SEBS-g-MA/BT) than dielectric elastomers on its own

8.1.2 Dielectric Permittivity under Tensile Mode

The dielectric permittivity of SEBS and SEBS/CB 2 wt. % under the different percentage of strain measured from 0.1 Hz to 1 MHz in a log manner, 10 points per decade as presented in Table 8.1. It is observed that the dielectric permittivity of SEBS almost remains constant with the range from 2.66 to 2.61 when stretched from 0 to 5%. Similarly, no significant changes in loss tangent, as well as electric loss modulus, were observed when the elastomer is kept under constant strain conditions, although a slight change in

relaxation can be observed around 10 Hz as shown in Figure 8.1, which diminishes when the elastomer is kept under strain conditions. In addition, the low-frequency relaxation (ca. 10 Hz and 1000 Hz) resulted due to glassy block polystyrene was diminished under strain condition. This phenomenon was attributed to the alignment of glassy polymer domains along the force applied (opposite to measurement taken).

Table 8.1 Average dielectric permittivity under different uniaxial tensile strain of SEBS and SEBS/CB 2% over the frequency range of 0.1Hz to 1 MHz

Composites	**Average dielectric permittivity at different percentage of strain from 0.1Hz to 1 MHz**				
	0	**0.25**	**1**	**2.5**	**5**
SEBS –SCF	2.66 (±0.02)	2.62 (±0.04)	2.61 (±0.01)	2.63 (±0.05)	2.61 (±0.04)
SEBS-SCF-CB2 %	3.89 (±0.02)	4.08 (±0.06)	3.94 (±0.06)	3.96 (±0.06)	4.18 (±0.06)

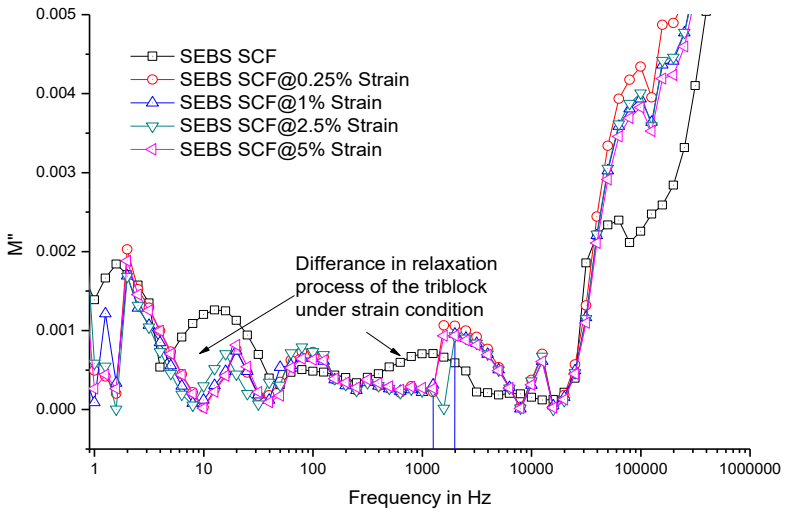

Figure 8.1 Loss electric moduli of SEBS SCF measured under different strain conditions

The dielectric permittivity SEBS/CB 2 wt. % processed with an assistance of supercritical fluid shows a slight increase under stretching. Similar to an increase in dielectric permittivity, the backbone relaxation phenomena of the triblock was also altered when composite was kept under the stretch condition as shown in Figure 8.2. This change in dielectric permittivity and relaxation phenomena under stretch conditions can be

attributed to changes in construction and destruction of dielectric domains under stress conditions. According to Houwink [253], when the elastomer is extended, one molecule segment slips over another molecule or over the surface of the filler resulting in the formation of new bonds along the chains. The nature of the new bond formed will be similar to the original ones but would appear at different locations along the rubbery molecule. The formation of different dielectric and conductive domains under strain conditions is further analysed at a higher weight percentage of CB in the following section.

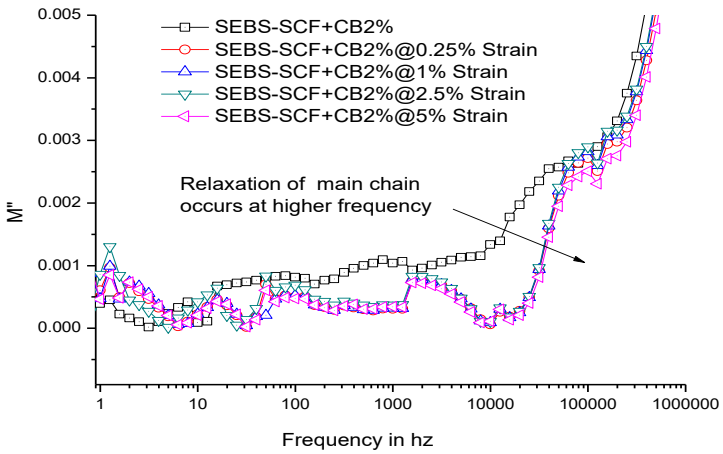

Figure 8.2 Electric modulus of SEBS SCF/CB2 wt.% with different percentage of strain

Figure 8.3, Figure 8.4, and Figure 8.5 show the total dielectric permittivity, total conductivity and imaginary electric modulus of SEBS/CB 5 wt. % extruded with an assistance of $scCO_2$ respectively. From Figure 8.3, and Figure 8.4, at low strain up to 5% strain, the total dielectric permittivity and the total conductivity of the elastomeric composites increases up to certain frequency. This increase in conductivity behavior is attributed to the difference in elastic modulus of difference between CB particles and SEBS triblock similar to the description given by authors in similar work [254], where easily deformable triblock triggers CB particles to come together allowing new conduction pathways. However, total dielectric permittivity, as well as total conductivity, decreases after certain frequency/relaxation frequency. At higher frequency, the total dielectric permittivity as well as the conductivity of relaxed SEBS/CB 5 wt. % nanocomposite is higher than that of stretched polymers.

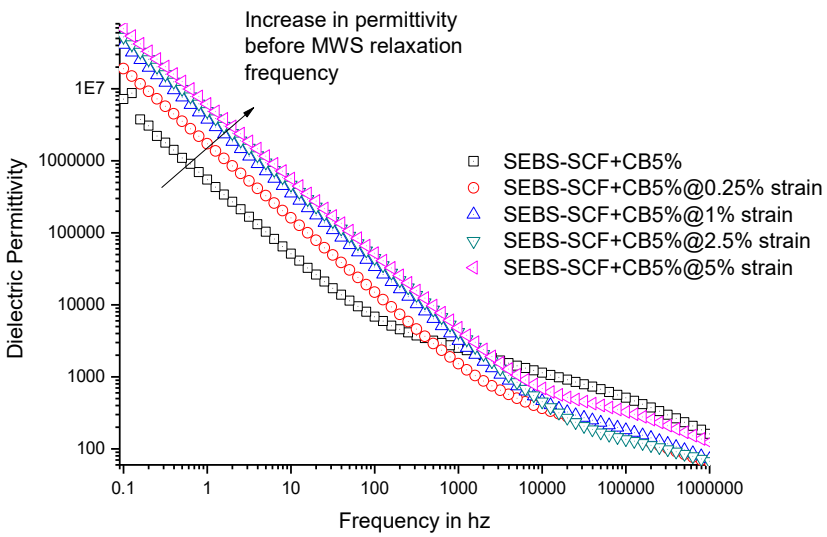

Figure 8.3 Dielectric permittivity of SEBS SCF/CB 5 wt.% at different percentage of strain

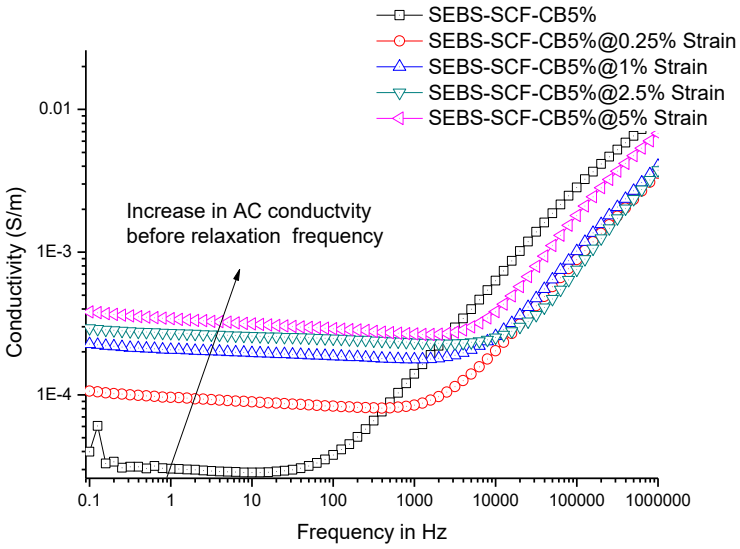

Figure 8.4 Conductivity of SEBS-SCF/CB 5 wt. % at different percentage of strain

In most cases, M" is used to determine the relaxation frequency. Figure 8.5 shows that the relaxation frequency of elastomeric composites, which increases with increase in strain (up to 5% strain). The relaxation frequency of the virgin composite was found to be around 100 Hz. This relaxation frequency in the elastomeric composites increases to ca. 1 kHz, 7 kHz, and 10 kHz upon 0.25%, 1% and 2.5% strain. However, the relaxation frequency was found to be ca. 5 kHz on 5% strain. This relaxation frequency is slightly

lowered compared to the relaxation frequency of nanocomposites under 1% and 2.5% strain. The relaxation frequency is also considered as AC conduction starting frequency from where AC conductivity starts to dominate the DC conductivity. The total conduction in the polymer-CB composite is a result of polarization as well as pure DC conduction. The interfacial polarization is mainly attributed to polarization phenomena of polymer/CB interface, whereas unbound CB leads to pure DC conduction. This change in relaxation behavior can be better explained using the tensile curve of the elastomeric composites and dispersion phenomena of CB particles in the elastomers. According to Cantournet *et al*. [222], the extension of elastomers occurs due to sliding (after the elastic limit) and non-sliding action (within the elastic limit in the first cycle) between hard and soft blocks. Within an elastic point or at low strain, each CB particle remains very close to each other. Early relaxation of virgin polymers occurs compared to polymer under strain, as most polymer chains are free for polarization, hence early AC conduction starts. As the strain increases, the polymer chains experience more stress opposite to the measurement taken and become highly aligned per the force applied making less number of polymer-additive interface domains available for polarization. However, the result also shows the polymer under high strain conditions beyond the elastic limit, has low relaxation frequency compared to elastomeric nanocomposites under strain within an elastic limit.

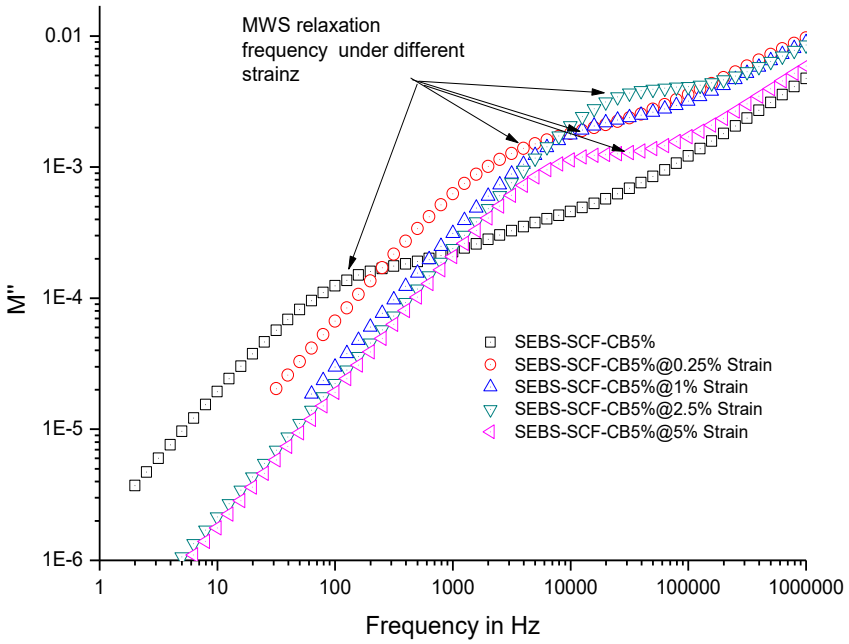

Figure 8.5 Imaginary electric modulus of SEBS-SCF/CB5 % with different of strain

Because of this high conducting behavior of SEBS/CB 5 wt. % composites, SCF-assisted extrusion technology shows huge potential for manufacturing of strain/stress sensors.

Similar to SEBS, SEBS-g-MA also does not show a major change in its dielectric properties as shown in Table 8.2. The dielectric permittivity with very low dielectric loss remains very similar between stretched and un-stretched polymers and has high mechanical compliance, whereby there is a possibility of energy harvesting from these polymers. However, it is suggested that the energy harvested will be very low (because of low dielectric permittivity. The total energy harvested will only depend on the square of relative thickness change of a capacitor.

Table 8.2 Average dielectric permittivity under different uniaxial tensile strain of SEBS and SEBS/CB 2% over the frequency range of 0.1Hz to 1 MHz

Composites	Average dielectric permittivity at different percentage of strain from 0.1Hz to 1 MHz in a log manner, 10 points per decade					Average dielectric permittivity at different percentage of strain at 1 kHz (std. dev was observed in 3 decimal places)				
	0	0.25	1	2.5	5	0	0.25	1	2.5	5
SEBS-g-MA-SCF	2.70 (±0.01)	2.76 (±0.01)	2.74 (±0.01)	2.71 (±0.01)	2.66 (±0.01)	2.7	2.77	2.75	2.71	2.66
SEBS-g-MA SCF-BT 2%	3.17 (±0.01)	3.19 (±0.02)	3.18 (±0.02)	3.19 (±0.02)	3.20 (±0.02)	3.18	3.22	3.21	3.22	3.21
SEBS-g-MA SCF-BT 10%	3.43 (±0.03)	3.47 (±0.06)	3.50 (±0.05)	3.51 (±0.05)	3.55 (±0.05)	3.43	3.54	3.57	3.58	3.59

SEBS-g-MA/BT 2 wt.% shows a slight increase in the dielectric permittivity under strain. This effect was found to be highly enhanced when the percentage of BT is 10 wt.%. Average dielectric permittivities of composites measured from 0.1 Hz to 1 MHz and at 1 kHz were found to be highest when composites were under 5 % strain. The dielectric permittivity (at 1 kHz) increases upon an increase in the strain. The increase in dielectric permittivity under strain condition was attributed to the inherent piezoelectric property of BT due to which BT exhibits higher dielectric permittivity under stress conditions. In addition, SEBS-g-MA/BT composites have dielectric loss less than 0.02 when the measurement was taken from 0.01 to 10^6 Hz frequency range which makes them highly suitable for energy harvesting applications.

8.1.3 Energy Harvesting Capabilities with Compliant Electrode

The amount of energy harvested (U) under applied stress (σ_s) and relative change in capacitance under relaxed (C_s) and stretched (C_r) conditions is given by Equation 8.1 under the biasing voltage

$$U = 0.5(C_s - C_r)V_b^2 \qquad \text{Equation 8.1}$$

Consider a thermoplastic dielectric elastomer made up of an elastomeric material of real dielectric permittivity, ε', with negligible loss tangent, length, L, breadth, W and thickness, t. The dielectric permittivity was found to be ε_s when the elastomer stretched by λ in bi-direction of length and breadth. Considering an elastomer being incompressible, the total energy harvested can be written as following Equation 8.2

$$Energy\ harvested = 0.5C_1(k\lambda^4 - 1)V_b^2 \qquad \text{Equation 8.2}$$

Where k is the ratio of dielectric permittivity under stretch and relaxed condition.

Biasing voltage of dielectric thermoplastic elastomers has a major role in harvesting energy from the elastomers. As stated in the literature, the dielectric breakdown strength of elastomers is lowered with the addition of conductive fillers [84], making them unsuitable for energy harvesting applications. However, the addition of dielectric fillers like BT, tend to increase the dielectric breakdown strength. Literature suggests that the breakdown voltage of similar SEBS-g-MA (Kraton-FG 1924) was found ca. 125±15 V/μm [84].With the addition of BT, the dielectric strength is generally enhanced. Under voltage conditions, the percentage of energy harvested is given by Equation 8.3.

$$\%Energy\ harvested = (k\lambda^4 - 1)*100\% \qquad \text{Equation 8.3}$$

The amount of energy harvested depends on the initial capacitance of the elastomers. It was shown in Chapter 6 that the cyclic loss energy factor and mechanical performance was given by tan delta factor of elastomers extruded without the assistance of $scCO_2$ is significantly inferior to the elastomers processed with the assistance of $scCO_2$. In addition, SEBS-g-MA processed without $scCO_2$ tends to alter its dielectric permittivity over the range of temperature, as discussed in Chapter 7. For this reason, there was no basis for comparative energy harvesting performance in Figure 8.6 and Figure 8.7

The percentage of energy harvested changes with the change in relative permittivity. Considering the same change in dielectric permittivity when the elastomer is stretched uniaxially and bi-axially from 0-5%, the percentage of energy harvesting can be estimated as shown in Figure 8.6.

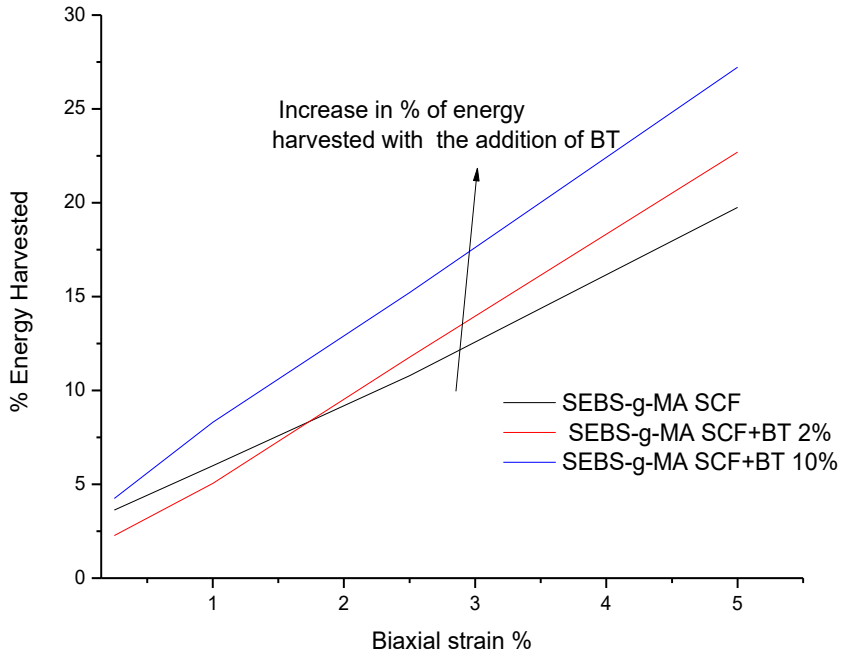

Figure 8.6 Estimation of % of energy harvestable using compliant electrode under constant voltage calculated from dielectric permittivity under strain measured at 1kHz.

From Figure 8.6, The percentage of energy harvested was calculated using Equation 8.3. Similarly, Equation 8.2 was used to calculate the total energy harvested form thermoplastic dielectric elastomers based on SEBS-g-MA/BT with area of 1*1 m^2, and thickness of 100μm and biasing voltage of 5 kV (dielectric ultimate strength that can be applied is 12.5 kV), the energy harvested can be estimated as shown in Figure 8.7

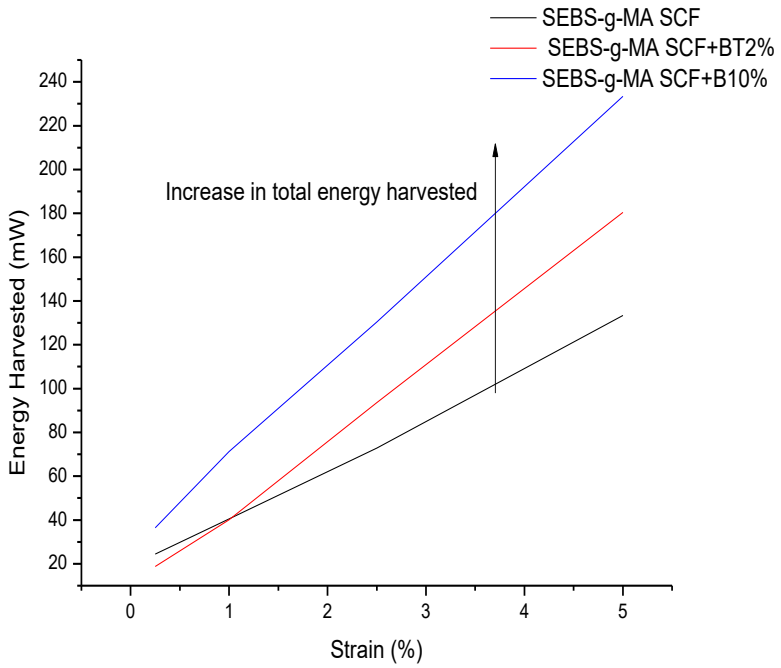

Figure 8.7 Estimation of Energy harvesting capacity of SEBS-g-MA with BT fillers with an area of 1*1m^2, and thickness of 100µm and biasing voltage of 5 kV.

8.1.4 Conclusion

The dielectric permittivity of SEBS and SEBS-g-MA under different stretch conditions remains almost constant. However, with the addition of CB above the percolation threshold, significant changes in AC relaxation frequency, dielectric permittivity and conductivity were observed under constant strain conditions making them suitable for strain/stress sensors. Thermoplastic nano-composites with conductive fillers (CB) at low percentage manufactured using SCF processing technique show low dielectric loss under strain conditions, however, low dielectric breakdown strength as stated many authors hinders their application as energy harvesters. Thermoplastic composites based on different dielectric fillers (BT) manufactured using $scCO_2$ showed huge potential as energy harvesters with their relative change in dielectric permittivity with very low dielectric under different strain conditions. With all geometrical dimensions constant and a biasing voltage of 5 kV, the energy harvested at 5% biaxial strain from SEBS-g-MA/BT wt 10% processed with an assistance of $scCO_2$ increased by 100% compared to the virgin

SEBS-g-MA processed under the same condition, as shown in Figure 8.7. This finally meets the aim of this thesis.

Chapter 9

9 Conclusion and Future Work

SEBS-g-MA and SEBS composites manufactured using twin screw extruder under different conditions were studied for the suitability of their applications in energy harvesting and sensing applications. Their elastomeric properties due to superior morphological structure, low dielectric loss, and ability to sustain mechanical stress up to 60°C with large extension has huge potential for actuator, capacitive energy harvester, and stress/strain sensor applications. The addition of fillers (dielectric and conductive) was used to enhance the electrical mechanical and thermal performance of these elastomers of specified applications.

In Chapter 4, various thermoplastic elastomers were selected to evaluate the suitability of dielectric elastomers for capacitive energy harvesting applications and stress/stress sensing applications These selected thermoplastic elastomers are well known for their flexibility because of their morphology. The total dielectric investigation was carried out on extruded PU, PEBAX, SEBS and SEBS-g-MA in the broadband frequency (0.1Hz to 1MHz) to evaluate the feasibility of these thermoplastic polymers as capacitive energy harvesters for different low frequency mechanical sources as a novel part of this work. The literature states that different mechanical energy sources such as seawaves involve low complex frequency (<0.5) profile [180, 181], which means that PU and PEBAX are inappropriate to be used for capacitive energy harvesting applications and flexible capacitors. In addition, conductive nanocomposites are more sensitive than PU and PEBAX for stress/stress applications. The low loss tangent of SEBS and SEBS-g-MA makes them suitable for capacitive energy generators. However, the low dielectric permittivity of these polymers must be enhanced for better power generation using capacitive methods. Furthermore, the addition of conductive fillers can make them improved for stress/strain sensing applications by making them conductive/piezoresistive in nature.

In Chapter 5, the dielectric properties and conductivity of SEBS and SEBS-g-MA were successfully enhanced using dielectric filler (BT) and conductive filler (CB) using a twin screw extruder. For the capacitive energy harvesting and stress sensing applications of thermoplastic elastomers, the microstructure formed and the mechanical morphological alteration during the manufacturing process was found to play an important role to change the conductivity and dielectric permittivity of elastomers.

In section 5.2, thermoplastic elastomers with conductive fillers were manufactured using a twin screw extruder with an aim and objective of enhancing the electrical conductivity and dielectric permittivity around the percolation threshold for stress/strain sensing, flexible capacitors, and artificial muscle applications as a novel part of the work. However, compared to other techniques described in the literature [84], the extrusion technique requires a high amount of CB to reach the percolation threshold thereby hindering its possibility to be used as conductive composites for strain/stress sensing applications in terms of cost and processibility. In addition, the stiffness and tan delta increase in the transverse direction made these nanocomposites insensitive to compression force for stress sensing and reduced the mechanical performance of the composites. Moreover, FTIR and DSC studies show the very slight interaction of CB with SEBS and SEBS-g-MA in all phases (soft, hard and interphases) present in the elastomers. This finding compared with literature reviews suggests a requirement for an improved manufacturing process for better dispersion of CB in elastomers for enhancing the electrical properties of the polymer matrices at low carbon content to make them feasible for stress/strain sensing applications.

Investigation of the interaction of dielectric filler (BT) with SEBS and SEBS-g-MA form a novel part of the work in section 5.3. DSC, FTIR and DMA techniques have shown that the interaction between polymer and additive plays an important role in dielectric phenomena. The decrease in dielectric permittivity in SEBS with BT was suggested to be due to the poor interaction between non-polar SEBS and highly polar BT additives. The high increase in dielectric permittivity with the low dielectric loss with minimal change in loss factor was observed on SEBS-g-MA; this result suggests the potential of these manufactured nanocomposites can be used not only for stress and strain sensors, robotic artificial muscles applications but also for capacitive energy harvesters and charge storing devices. Minimal changes in mechanical properties (Young's modulus, resilience as well as stiffness in both transverse as well as parallel to extrusion) compared to the high changes in dielectric permittivity in SEBS-g-MA composites also suggests that SEBS-g-MA/BT nanocomposites manufactured using this technology are highly sensitive to compression force as well as possessing high Maxwell stress under an electric field. Moreover, from DMA and DSC analysis, it can be stated that temperature plays a major role in defining the structural and mechanical changes of nanocomposite and hence electromechanical properties. This leads to further studies of dielectric phenomena within

a temperature range of operation. In addition, SEM images show that high shear flow can help in better distributive mixing of additives to some extent, but compatibility remains still critical.

For further dielectric analysis below 1 Hz for SEBS-g-MA/BT composites in Chapter 6 section 4, they showed a high dielectric tangent loss (0.3) making these nanocomposites poor choices for capacitive energy generators low-frequency sources.

With an aim to use supercritical fluid technology as an exfoliating agent for dispersion of additives in elastomers, at first, the effect of supercritical fluid carbon dioxide ($scCO_2$) assisted extrusion on thermal, mechanical, electrical, and morphological properties of microphase separated Poly(styrene-ethylene/butylene-styrene) [SEBS] triblock was investigated at various critical pressures. The extrusion of thermoplastic elastomer, SEBS showed an increase in degradation temperature which is due to the formation of additional microphases and changes in chain length. The MDSC results confirm that scCO2 assisted extrusion of SEBS at various pressures resulted in increased microphase separations or formation of new microphases, thus producing of the new structure of SEBS. DMA analysis shows that the introduction of $scCO_2$ during extrusion leads to a decrease in modulus (represented by storage modulus) as well as the molecular frictional movements between hard and soft block segments (represented by loss modulus) of the elastomers. The tan delta at 96 °C, shows the actual restructuring of hard and soft domains. In addition, reduction in value of tan delta showed high sensitivity and mechanical performance of these elastomers for energy harvesting, artificial muscles, and stress/strain sensing applications. Similarly, a decrease in Young's modulus was also observed from the tensile test curves. FTIR spectra of SEBS extruded at various pressures identifies CO_2-phenyl ring interaction. Dielectric studies identify a slight decrease in dielectric permittivity due to foaming. In addition, dielectric relaxation over the frequency range concludes the formation of different microphase domain when extruded with 8.27 MPa

From section 6.3 and 6.5, the potential of supercritical fluid carbon dioxide ($scCO_2$) assisted extrusion for making highly thermally, mechanically and electrically suitable composites with CB leading to high dispersed and distributed additives for sensing and energy harvesting applications were explored. TEM results identified high dispersion and dispersive mixing of CB on SEBS and SEBS-g-MA. Due to high dispersion, as well as the distribution of CB in SEBS and SEBS-g-MA, the mechanical properties such as

storage modulus in the transverse direction were highly enhanced. Due to the formation of small domain sizes when processed with $scCO_2$ assisted extrusion provides high shape memory properties and low tan delta as measured by DMA making them suitable for a wide range of electroactive applications. In addition, ATR-FTIR, DMA as well as DSC showed the high interaction of CB with all domains of both triblock. In addition, the high exfoliation of CB in SEBS and SEBS-g-MA matrix provides high dielectric permittivity with a low dielectric loss at a low concentration compared to other literature. At higher percentage of CB, $scCO_2$ assisted extruded SEBS/CB provides better conductivity and low percolation threshold which has huge applications in artificial muscles, flexible capacitor below the percolation threshold and strain/stress sensor above the percolation threshold. The main different in a threshold amount of CB required for SEBS and SEBS-g-MA was attributed to different in viscosity of SEBS and SEBS-g-MA.

In section 6.4, the primary objective of enhancing dielectric permittivity of thermoplastic elastomer while maintaining dielectric loss even at the very low-frequency range was successfully accomplished. DSC results identified the high dispersion of BT in all phases of SEBS-g-MA (the soft phase, interphases and hard phases). The enhanced distributive dispersion of BT particles in SEBS-g-MA as observed in TEM images leading to uniform polarization capability with very low dielectric loss tangent (enhanced electrical performance) over the range of frequency from 1 mHz to 1 MHz, low dynamic mechanical tangent loss (enhanced mechanical performance) and shape memory loss of the range of frequency. Thermo-dielectric studies reveal that the stability of the electrical property of virgin SEBS-g-MA, as well as nanocomposites over temperature and frequency range, was highly enhanced when processed with $scCO_2$. Thermal, ATR-FTIR and DMA analysis prove high interaction, and better dispersion of BT fillers in all domains (hard, soft and interphase domains) of SEBS-g-MA. In addition, low mechanical loss (highly flexible) during each cycle during the cyclic testing was also found to be reduced compared to the composites manufactured without an assistance of $scCO_2$. The better dispersion phenomena in all domains of SEBS-g-MA can also be seen in $scCO_2$ assisted extrudates due to the better molecular interaction as detected by FTIR-spectra.

Section 7.2 presented the scientific understanding of tailoring the dielectric and thermal properties of SEBS-g-MA composites processed with/ without an assistance of $scCO_2$ over a range of frequencies and temperature. The interfusion of the soft block and the hard block was found to change the dielectric properties of the same thermoplastic elastomer

over the range of frequency and temperature. Similarly, the dispersion of fillers also has a high influence on the dielectric properties of composites manufactured. The large change in dielectric properties of SEBS-g-MA extruded without $scCO_2$ with an increase in temperature was due to higher segmental movement present in a triblock. However, this effect did not prevail in SEBS-g-MA-treated with $scCO_2$ due to a high reinforcement effect of polystyrene in the ethylene-butylene block. On the contrary, the breaking down of polystyrene phases into smaller phases makes SEBS-g-MA when extruded with $scCO_2$ more sensitive to higher frequency because of easier movement of a polar group within a molecule. Similarly, SEBS-g-MA/BT composites manufactured with $scCO_2$ were found to be sensitive to frequency, making constant dielectric properties over a range of temperatures. This investigation confirms the suitability of such elastomeric composites manufactured using $scCO_2$ over a range of temperatures for energy harvesting applications.

In section 7.3, the dielectric relaxation and energy dissipation phenomena of multiphase thermoplastic conductive network near percolation threshold SEBS-g-MA/CB 5 wt. % processed with $scCO_2$ assisted extrusion over a range of frequencies from temperature 40 °C to 120 °C was examined. The dielectric properties of SEBS-g-MA/CB 5 wt. % were found to be highly dependent on the glass transition temperature of a hard block of SEBS-g-MA measured from loss modulus peak of DMA curve. From 40°C, at frequency between HN relaxation and tan delta relaxation, the dielectric permittivity initially decreases up to the glass transition temperature of the hard domain of the triblock (measured by the peak of loss modulus) of the hard block in the triblock, then increases with an increase in temperature due to higher segmental movement of hard block present in a triblock. However, the total dielectric strength of the nanocomposite was found to be increasing until glass transition temperature followed by a decrease in total dielectric strength after glass transition temperature. Before tan delta relaxation frequency, the dielectric tangent loss measured was found to be increasing up to the glass transition temperature and decreases after glass transition temperature of the hard block as measured for the peak of loss modulus. Similarly, after tan delta relaxation frequency, the dielectric loss of the triblock was found to decrease from 40 to 80 °C and again increase when the temperature is increased from 80 to 120 °C. This change is attributed to the difference in higher swelling behavior of triblock effect by the glass transition temperature of the hard domain together with positive temperature coefficient behavior of CB filled materials

having a total impact on the frequency based conduction and dielectric relaxation processes

Chapter 8 presented the enhanced sensitivity of SEBS/CB (with slightly higher than percolation threshold) for stress/strain sensing applications. Similarly, the energy harvesting model confirms the greater amount of energy harvested using composites (SEBS-g-MA/BT) than dielectric elastomers on their own. The dielectric permittivity of SEBS and SEBS-g-MA under different stretch conditions remained almost constant. However, addition of CB above the percolation threshold yielded a significant change in DC relaxation frequency, where dielectric permittivity and conductivity was observed under strain conditions making them suitable for strain/stress sensors. BT filler based elastomeric composites manufactured show huge potential as energy harvesters with their relative change in dielectric permittivity with low dielectric loss under different strain conditions, which finally meets the main aim of this thesis.

In conclusion, supercritical fluid assisted extrusion shows huge potential for making elastomeric composites conductive and very low loss dielectric nanocomposites at low percentage of CB and BT fillers due to (i) high dispersion/ distribution mixing, (ii) high interaction of polymers and CB particles and (iii) enhancing phase separation on the base polymer leading to high flexibility and elastomeric properties making them suitable of stress/strain sensing applications

A part of this research also finds superior technology to enhance mechanical, thermal and electrical properties of the composites with high dispersion and distribution mixing of additives in polymers using the industrial standard system in the context of cost, production, and scalability. This research shows great potential for capacitive energy generators using this technology. However, issues prevail in different sectors including processing, mechanical and electrical testing, which are highlighted as follows.

9.1 Processing of Elastomeric-Based Composites

Supercritical fluid carbon dioxide ($scCO_2$) assisted extrusion technology shows conceivable potential for fine dispersion of CB in polymers to attain uniform dispersion/distributive mixing as well as to promote percolation threshold at low concentration of CB in polymers. The percentage of additive required to obtain the conductive percolation threshold can further be enhanced if multiwall carbon nanotubes

and graphene are used due to their inherent conductive properties. However, graphene and carbon nanotubes might increase the stiffness and deteriorate the shape memory properties of elastomers because of their high aspect ratio.

In addition, $scCO_2$ was found to disperse the high dielectric filler when the wt. % is up to 10 %. Future research needs to be carried out for dispersion of a high amount of dielectric fillers in elastomers and to observe the consequent effect on the dielectric, and shape memory properties and their potential for energy harvesting as a function of relative dielectric permittivity change at different strain (unidirectional and bi-directional).

9.2 Long Term Mechanical Testing

This thesis does groundwork in the context of mechanical testing of these composites. However, a long-term test including, but not limited to fatigue test (stress cycles (S-N curves), and strain cycles), creep test (master curve), damage models under the cyclic stress of manufactured composites should be taken into consideration.

9.3 Dielectric Breakdown Strength Test

One of the major parameters that define the energy harvesting capabilities from a dielectric elastomer is an applied voltage. The energy harvested is directly proportional to the square of the amount of voltage applied. The dielectric breakdown strength sets the amount of voltage that can be applied to elastomers before it is electrically broken down (becomes conductive). Hence, this dielectric strength test is one of the crucial tests that is not addressed in this thesis and remains the work for future studies.

9.4 Design and Manufacturing of Highly Compliant Electrodes

Apart from the mechanical compliance of elastomers, a highly compliant electrode is essential for capacitive energy harvesters [254]. A lot of work has to be carried out in this content for manufacturing of compliant electrodes made up of silver nanowires, carbon black, graphene, single/multi-wall carbon nanotubes etc. However, a feasible manufacturing technique for making a compliant electrode for dielectric elastomers still requires a considerable amount of work to be carried out to know the feasibility of such as compliant electrode. Investigation on compliant conductive paints for electroactive elastomers for large extension also remains a major part for future studies to harvest the energy using capacitive methods from mechanical energy sources such as sea waves.

9.5 Design of Protocols to Harvest Energy

It is suggested that capacitive harvesting energy from mechanical sources using simple techniques with voltage and diodes may act only as a power booster. More work on energy harvesting techniques and its circuitry must be carried out for high energy power generation.

References

[1] A. D. Price, Berndt, C. S., Deluca, J. M., Farra, N., Gillies, A. G., Kopec, M. O. and Naguib, H. E. , "Synthesis and evaluation of ionic electroactive polymer actuators," in *10th International Workshop on Smart Materials and Structures*, 2007, pp. pp. 197–206.

[2] M. Shahinpoor and K. J. Kim, "Ionic polymer-metal composites: I. Fundamentals," *Smart Materials and Structures,* vol. 10, p. 819, 2001.

[3] K. J. Kim and M. Shahinpoor, "Ionic polymer–metal composites: II. Manufacturing techniques," *Smart Materials and Structures,* vol. 12, p. 65, 2003.

[4] N. A. Vandesteeg, P. A. Anquetil, Peter G. A. Madden, A. Takshi, R. Z. Pytel, S. R. Lafontaine, *et al.*, "Artificial muscle technology: physical principles and naval prospects. ," *IEEE Journal of Oceanic Engineering,* vol. 29, pp. 706-728, 2004.

[5] Y. Bar-Cohen, *EAP history, current status, and infrastructure in :Electroactive Polymer (EAP) Actuators as Artificial Muscles: Reality, Potential and Challenges*, 2nd ed. vol. PM136. Bellingham: SPIE Press, 2004.

[6] A. H. Barber, S. R. Cohen, and H. D. Wagner, "External and internal wetting of carbon nanotubes with organic liquids," *Physical Review B,* vol. 71, p. 115443, 2005.

[7] Y. Bar-Cohen, *Electroactive Polymer (EAP) Actuators as Articial Muscles - Reality, Potential and Challenges.* , 2 ed.: SPIE Press, 2004.

[8] P. K. Chu and X. Liu, *Biomaterials fabrication and processing handbook*: CRC press, 2008.

[9] F. C. a. E. Smela, in *Electroactive Polymers as SmartMaterials for Actuation: in Biomedical Applications of Electroactive Polymer Actuators*, ed: John Wiley & Sons, Ltd, 2009, pp. i-xx.

[10] K. A. a. K. Oguro, *IPMC Actuators: Fundamentals: in Biomedical Applications of Electroactive Polymer Actuator*. UK: John Wiley and Sons, Ltd., 2009.

[11] T. Shiga, "Deformation and viscoelastic behavior of polymer gels in electric fields.," *Advances in Polymer Science,* pp. 131-134, 1997.

[12] B. Tondu, R. Emirkhanian, S. Mathé, and A. Ricard, "A pH-activated artificial muscle using the McKibben-type braided structure," *Sensors and Actuators A,* vol. 150, pp. 124-130, 2009.

[13] K. J. Kim and M. Shahinpoor, "A novel method of manufacturing three-dimensional ionic polymer–metal composites (IPMCs) biomimetic sensors, actuators and artificial muscles," *Polymer,* vol. 43, pp. 797-802, 2// 2002.

[14] S. Nemat-Nasser, "Micromechanics of actuation of ionic polymer-metal composites," *Journal of Applied Physics,* vol. 92, pp. 2899-2915, 2002.

[15] M. Shahinpoor and K. J. Kim, "Ionic polymer–metal composites: IV. Industrial and medical applications," *Smart Materials and Structures,* vol. 14, p. 197, 2005.

[16] J.-S. Plante, "Dielectric elastomer actuators for binary robotics and mechatronics," Doctor of Philoshophy Department of Mechanical Engineering, Massachusetts Institute of Technology, Massachusetts, 2006.

[17] B. Gaihre, G. Alici, G. M. Spinks, and J. M. Cairney, "Synthesis and performance evaluation of thin film PPy-PVDF multilayer electroactive polymer actuators," *Sensors and Actuators A: Physical,* vol. 165, pp. 321-328, 2// 2011.

[18] J. D. W. Madden, N. A. Vandesteeg, P. A. Anquetil, P. G. A. Madden, A. Takshi, R. Z. Pytel, *et al.*, "Artificial muscle technology: physical principles and naval prospects," *Oceanic Engineering, IEEE Journal of,* vol. 29, pp. 706-728, 2004.

[19] K. J. Kim and S. Tadokoro, "Electroactive polymers for robotic applications," *Artificial Muscles and Sensors (291 p.), Springer: London, United Kingdom,* 2007.

[20] Q. Pei and O. Inganäs, "Electrochemical applications of the bending beam method. 1. Mass transport and volume changes in polypyrrole during redox," *The Journal of Physical Chemistry,* vol. 96, pp. 10507-10514, 1992.

[21] Q. Pei and O. Inganäs, "Electrochemical applications of the bending beam method; a novel way to study ion transport in electroactive polymers," *Solid State Ionics,* vol. 60, pp. 161-166, 1993.

[22] T. Mirfakhrai, J. D. W. Madden, and R. H. Baughman, "Polymer artificial muscles," *Materials Today,* vol. 10, pp. 30-38, 4, 2007.

[23] R. Baughman, "Conducting polymer artificial muscles," *Synthetic metals,* vol. 78, pp. 339-353, 1996.

[24] G. M. Spinks, G. G. Wallace, J. Ding, D. Zhou, B. Xi, and J. Gillespie, "Ionic liquids and polypyrrole helix tubes: bringing the electronic Braille screen closer to reality," 2003, pp. 372-380.

[25] A. Della Santa, A. Mazzoldi, and D. De Rossi, "Steerable microcatheters actuated by embedded conducting polymer structures," *Journal of intelligent material systems and structures,* vol. 7, pp. 292-300, 1996.

[26] R. H. Baughman, A. A. Zakhidov, and W. A. de Heer, "Carbon nanotubes--the route toward applications," *Science,* vol. 297, pp. 787-792, 2002.

[27] R. H. Baughman, C. Cui, A. A. Zakhidov, Z. Iqbal, J. N. Barisci, G. M. Spinks, *et al.*, "Carbon nanotube actuators," *Science,* vol. 284, pp. 1340-1344, 1999.

[28] A. E. Aliev, J. Oh, M. E. Kozlov, A. A. Kuznetsov, S. Fang, A. F. Fonseca, *et al.*, "Giant-stroke, superelastic carbon nanotube aerogel muscles," *science,* vol. 323, pp. 1575-1578, 2009.

[29] Y. Takase, J. Lee, J. Scheinbeim, and B. Newman, "High-temperature characteristics of nylon-11 and nylon-7 piezoelectrics," *Macromolecules,* vol. 24, pp. 6644-6652, 1991.

[30] Q. Gao, J. I. Scheinbeim, and B. A. Newman, "Ferroelectric properties of nylon 11 and poly (vinylidene fluoride) blends," *Journal of Polymer Science Part B: Polymer Physics,* vol. 37, pp. 3217-3225, 1999.

[31] C. Huang, R. Klein, F. Xia, H. Li, Q. M. Zhang, F. Bauer, *et al.*, "Poly(vinylidene fluoride-trifluoroethylene) based high performance electroactive polymers," *Dielectrics and Electrical Insulation, IEEE Transactions on,* vol. 11, pp. 299-311, 2004.

[32] Q. Zhang, J. Zhao, T. Shrout, N. Kim, L. Cross, A. Amin, *et al.*, "Characteristics of the electromechanical response and polarization of electric field biased ferroelectrics," *Journal of applied physics,* vol. 77, pp. 2549-2555, 1995.

[33] Z. Suo, "Theory of dielectric elastomers," *Acta Mechanica Solida Sinica,* vol. 23, pp. 549-578, 2010.

[34] R. Pelrine, R. Kornbluh, J. Joseph, R. Heydt, Q. Pei, and S. Chiba, "High-field deformation of elastomeric dielectrics for actuators," *Materials Science and Engineering: C,* vol. 11, pp. 89-100, 2000.

[35] R. D. Kornbluh, R. Pelrine, Q. Pei, S. Oh, and J. Joseph, "Ultrahigh strain response of field-actuated elastomeric polymers," in *SPIE's 7th Annual International Symposium on Smart Structures and Materials,* 2000, pp. 51-64.

[36] P. Brochu and Q. Pei, "Advances in Dielectric Elastomers for Actuators and Artificial Muscles," *Macromolecular Rapid Communications,* vol. 31, pp. 10-36, 2010.

[37] M. Li, A. Brulet, P. Davidson, P. Keller, and J. Cotton, "Observation of hairpin defects in a nematic main-chain polyester," *Physical review letters,* vol. 70, p. 2297, 1993.

[38] D. L. Thomsen, P. Keller, J. Naciri, R. Pink, H. Jeon, D. Shenoy, *et al.*, "Liquid crystal elastomers with mechanical properties of a muscle," *Macromolecules,* vol. 34, pp. 5868-5875, 2001.

[39] W. Lehmann, H. Skupin, C. Tolksdorf, E. Gebhard, R. Zentel, P. Krüger, *et al.*, "Giant lateral electrostriction in ferroelectric liquid-crystalline elastomers," *Nature,* vol. 410, pp. 447-450, 2001.

[40] W. Lehmann, L. Hartmann, F. Kremer, P. Stein, H. Finkelmann, H. Kruth, *et al.*, "Direct and inverse electromechanical effect in ferroelectric liquid crystalline elastomers," *Journal of applied physics,* vol. 86, pp. 1647-1652, 1999.

[41] H. Finkelmann and M. Shahinpoor, "Electrically controllable liquid crystal elastomer-graphite composite artifical muscles," in *SPIE's 9th Annual International Symposium on Smart Structures and Materials*, 2002, pp. 459-464.

[42] C. M. Spillmann, B. R. Ratna, and J. Naciri, "Anisotropic actuation in electroclinic liquid crystal elastomers," *Applied physics letters*, vol. 90, pp. 021911-021911-3, 2007.

[43] S. V. Ahir, A. R. Tajbakhsh, and E. M. Terentjev, "Self-assembled shape-memory fibers of triblock liquid-crystal polymers," *Advanced Functional Materials*, vol. 16, pp. 556-560, 2006.

[44] Z. Yu, W. Yuan, P. Brochu, B. Chen, Z. Liu, and Q. Pei, "Large-strain, rigid-to-rigid deformation of bistable electroactive polymers," *Applied Physics Letters*, vol. 95, p. 192904, 2009.

[45] S. Bauer, "Piezo-, pyro- and ferroelectrets: soft transducer materials for electromechanical energy conversion," *Dielectrics and Electrical Insulation, IEEE Transactions on*, vol. 13, pp. 953-962, 2006.

[46] D. Lovera, H. Ruckdäschel, A. Göldel, N. Behrendt, T. Frese, J. K. W. Sandler, *et al.*, "Tailored polymer electrets based on poly(2,6-dimethyl-1,4-phenylene ether) and its blends with polystyrene," *European Polymer Journal*, vol. 43, pp. 1195-1201, 4// 2007.

[47] S. Bauer, R. Gerhard-Multhaupt, and G. M. Sessler, "Ferroelectrets: Soft electroactive foams for transducers," *Physics Today*, vol. 57, pp. 37-43, 2004.

[48] Z. Ahmad, *Polymer Dielectric Materials*, 2012.

[49] S. O. Nelson, "Fundamentals of dielectric properties measurements and agricultural applications," *Journal of Microwave power and electromagnetic energy*, vol. 44, pp. 98-113, 2010.

[50] O. Tereshchenko, F. Buesink, and F. Leferink, "An overview of the techniques for measuring the dielectric properties of materials," in *Proceedings of the General Assembly and Scientific Symposium, Istambul, Turquia*, 2011, p. 14.

[51] U. Kaatze and Y. Feldman, "Broadband dielectric spectrometry of liquids and biosystems," *Measurement Science and Technology*, vol. 17, p. R17, 2005.

[52] C. Chanmal and J. Jog, "Dielectric relaxation spectroscopy for polymer nanocomposites," *Characterization Techniques for Polymer Nanocomposites*, pp. 167-184, 2012.

[53] V. Ranjan, L. Yu, M. B. Nardelli, and J. Bernholc, "Phase equilibria in high energy density PVDF-based polymers," *Physical review letters*, vol. 99, p. 047801, 2007.

[54] A. Wickenheiser, Ed., *Analysis of Energy Harvesting Using Frequency Up-Conversion by Analytic Approximations* (Small-Scale Energy Harvesting. Intech, 2012 p.^pp. Pages.

[55] C. Putson, "Energy conversion from electroactive materials and Modeling of behaviour on these materials," Doctor of Philosophy, Department of Electrical Engineering, LGEF Laboratory, Lyon, 2010.

[56] S. Chalasani and J. M. Conrad, "A Survey of Energy Harvesting Sources for Embedded Systems," presented at the Southeastcon, IEEE 2008.

[57] D. Davino, A. Giustiniani, and C. Visone, "Effects of hysteresis and eddy currents in magnetostrictive harvesting devices," *Physica B,* vol. 407, pp. 1433–1437, 2012.

[58] F. Cottone, "Introduction to vibration energy harvesting," *NiPS Energy Harvesting Summer School,* 2011.

[59] S. Saadon and O. Sidek, "A review of vibration-based MEMS piezoelectric energy harvesters," *Energy Conversion and Management,* vol. 52, pp. 500-504, 2011.

[60] Z. Houqlng, L. Jlanguo, W. Xmrong, X. Yanhong, and Z. Hongping, "Applications of Terfenol-D in China," *Journal of Alloys and Compounds,* vol. 258, pp. 49-52, 1997.

[61] C. M. Koo. (2012). *Electroactive Thermoplastic Dielectric Elastomers as a New Generation Polymer Actuators*.

[62] A.-G. Olabi and A. Grunwald, "Design and application of magnetostrictive materials," *Materials & Design,* vol. 29, pp. 469-483, 2008.

[63] J. Engel, J. Chen, Z. Fan, and C. Liu, "Polymer micromachined multimodal tactile sensors," *Sensors and Actuators A,* vol. 117 pp. 50–61, 2005.

[64] S. Laflamme, M. Kollosche, J. J. Connor, and G. Kofod, "Soft capacitive sensor for structural health monitoring of large-scale systems," *Struct. Control Health Monit.,* vol. 19, pp. 17-81, 2012.

[65] M. B. Rao, M. R. Bhat, C. R. L. Murthy, K. V. Madhav, and S. Asokan, "Structural Health Monitoring (SHM) Using Strain Gauges, PVDF Film and Fiber Bragg Grating (FBG) Sensors: A Comparative Study," in *Proc. National Seminar on Non-Destructive Evaluation*, Hyderabad, 2006.

[66] Y. Zhang, M. G. Lloyd, and M. L. Wang, *Random Vibration Response Testing of PVDF Gages for LOng-span Bridge Monitoring*. Pennsyrvannia: DEStech Publications Inc., 2003.

[67] M. C. Carrozza, B. Massa, P. Dario, M. Zecca, S. Micera, and P. Pastacaldi, "A two DoF finger for a biomechatronic artificial hand," *Technology and Health Care 10 (2002) 77–89,* vol. 10, pp. 77-89, 2002.

[68] F. Gao, H. Deng, and Y. Zhang, "Hybrid actuator combining shape memory alloy with DC motor for prosthetic fingers," *Sensors and Actuators A: Physical,* vol. 223, pp. 40-48, 2015.

[69] D. Sangian, S. Naficy, G. M. Spinks, and B. Tondu, "The effect of geometry and material properties on the performance of a small hydraulic McKibben muscle system," *Sensors and Actuators A: Physical,* vol. 234, pp. 150-157, 2015.

[70] Y. K. Lee and I. Shimoyama, "A Micro Rubber Artificial Muscle Driven by a Micro Compressor for Artificial Limbs," presented at the In: Actuator 2000, 7th International Conference on New Actuator, Germany 2000

[71] H. Tzou, *Piezoelectric shells: distributed sensing and control of continua* vol. 19: Springer Science & Business Media, 2012.

[72] J. L. Pons, H. Rodríguez, A. Duarte, A. R. Jiménez, I. Luyckx, D. Reynaerts, *et al.*, "High torque ultrasounic motors or hand prosthetics : current status and trends.," presented at the In: Actuator 2000, 7th International Conference on New Actuator, Germany 2000.

[73] D. Xu, Y. Liu, J. Liu, and W. Chen, "A crossbeam linear ultrasonic motor using bending vibrations," in *Applications of Ferroelectric, International Symposium on Integrated Functionalities and Piezoelectric Force Microscopy Workshop (ISAF/ISIF/PFM), 2015 Joint IEEE International Symposium on the*, 2015, pp. 13-16.

[74] K. L. Delaurentis and C. Mavroidis, "Developementof a shape memory alloy actuated hand " presented at the In: Actuator 2000, 7th International Conference on new actuators, Germany, 2000.

[75] D. L. Brock. (1994). *Review of Articial Muscle based on Contractile Polymers*.

[76] T. F. Otero and J. G. Martinez, "Physical and chemical awareness from sensing polymeric artificial muscles. Experiments and modeling," *Progress in Polymer Science,* vol. 44, pp. 62-78, 2015.

[77] A. A. A. Moghadam, A. Kouzani, K. Torabi, A. Kaynak, and M. Shahinpoor, "Development of a novel soft parallel robot equipped with polymeric artificial muscles," *Smart Materials and Structures*, vol. 24, p. 035017, 2015.

[78] M. Y. Sakamoto, E. A. R. Duck, C. A. C. Zavaglia, and J. A. Cliquet, "A myoelectric hand prothesis driven by polymers," Brazil, 1994.

[79] M. Rajagopalan, J.-H. Jeon, and I.-K. Oh, "Electric-stimuli-responsive bending actuator based on sulfonated polyetherimide," *Sensors and Actuators B: Chemical,* vol. 151, pp. 198-204, 2010.

[80] R. Pelrin, R. Kornbluh, Q. Pei, and J. Joseph. High-Speed Electrically Actuated Elastomers with Strain Greater Than 100%. [Online].

[81] R. Shankar, T. K. Ghosh, and R. J. Spontak, "Electromechanical Response of Nanostructured Polymer Systems with no Mechanical Pre-Strain," *Macromolecular rapid communication*, vol. 28, pp. 1142–1147, 2007.

[82] S. Laflamme, M. Kollosche, J. Connor, and G. Kofod, "Soft capacitive sensor for structural health monitoring of large-scale systems," *Structural Control and Health Monitoring*, vol. 19, pp. 70-81, 2012.

[83] T. McKay, B. O'Brien, E. Calius, and I. Anderson, "Realizing the potential of dielectric elastomer generators," in *SPIE Smart Structures and Materials+ Nondestructive Evaluation and Health Monitoring*, 2011, pp. 79760B-79760B-8.

[84] H. Stoyanov, D. Mc Carthy, M. Kollosche, and G. Kofod, "Dielectric properties and electric breakdown strength of a subpercolative composite of carbon black in thermoplastic copolymer," *Applied physics letters*, vol. 94, p. 232905, 2009.

[85] C. Zhang, Q. Chi, J. Dong, Y. Cui, X. Wang, L. Liu, *et al.*, "Enhanced dielectric properties of poly (vinylidene fluoride) composites filled with nano iron oxide-deposited barium titanate hybrid particles," *Scientific Reports*, vol. 6, 2016.

[86] Q. Pei, "Artificial Muscles based on Synthetic Dielectric Elastomers," presented at the Engineering in Medicine and Biology Society, 2009. EMBC 2009. Annual International Conference of the IEEE, Minnesota, 2009.

[87] E. Biddiss and T. Chau, "Dielectric elastomers as actuators for upper limb prosthetics: Challenges and opportunities," *Medical Engineering & Physics*, vol. 30, pp. 403–418, 2008.

[88] S. Kharroub, S. Laflamme, S. Madbouly, and F. Ubertini, "Bio-based soft elastomeric capacitor for structural health monitoring applications," *Structural Health Monitoring*, vol. 14, pp. 158-167, 2015.

[89] S. C. B. Mannsfeld, B. C.-K. Tee, R. M. Stoltenberg, C. V. H.-H. Chen, S. Barman, B. V. O. Muir, *et al.*, "Highly sensitive flexible pressure sensors with microstructured rubber dielectric layers," *Natural materials*, vol. 9, pp. 859-864, 2010.

[90] P. Brochu, H. Stoyanov, X. Niu, and Q. Pei, "All-silicone prestrain-locked interpenetrating polymer network elastomers: free-standing silicone artificial muscles with improved performance and robustness," *Smart Mater. Struct.*, vol. 22, 2013.

[91] T. Someya, T. Sekitani, S. Iba, Y. Kato, H. Kawaguchi, T. Sakurai, *et al.*, "A Large-Area, Flexible Pressure Sensor Matrix with Organic Field-Effect Transistors for Artificial Skin Applications," presented at the Proceedings of the National Academy of Sciences of the United States of America, 2004.

[92] S. Wan, Y. Li, J. Peng, H. Hu, Q. Cheng, and L. Jiang, "Synergistic Toughening of Graphene Oxide–Molybdenum Disulfide–Thermoplastic Polyurethane Ternary Artificial Nacre," *ACS nano*, vol. 9, pp. 708-714, 2015.

[93] K. E. Kear, "Structure of Thermoplastic Elastomers," in *Developments in Thermoplastic Elastomers* vol. 10, ed: Smithers Rapra, 2003, pp. 3-6.

[94] K. Chatterjee and K. Naskar, "Development of thermoplastic elastomers based on maleated ethylene propylene rubber (m-EPM) and polypropylene (PP) by dynamic vulcanization," *Express Polym Lett,* vol. 1, pp. 527-534, 2007.

[95] M. Rajagopalan, i.-H. Jeo, and I.-K. Oh, "Electric-stimuli-responsive bending actuator based on sulfonated polyetherimide," *Sensors and Actuators B: Chemical,* vol. 151, pp. 198–204, 2010.

[96] H. Okuzaki, S. Takagi, F. Hishiki, and R. Tanigawa, "Ionic liquid/polyurethane/PEDOT: PSS composites for electro-active polymer actuators," *Sensors and Actuators B: Chemical,* vol. 194, pp. 59-63, 2014.

[97] T. Chen, L. Pan, M. Lin, B. Wang, L. Liu, Y. Li, *et al.*, "Dielectric, mechanical and electro-stimulus response properties studies of polyurethane dielectric elastomer modified by carbon nanotube-graphene nanosheet hybrid fillers," *Polymer Testing,* vol. 47, pp. 4-11, 2015.

[98] C. M. Koo. (2012). *Electroactive Thermoplastic Dielectric Elastomers as a New Generation Polymer Actuators*.

[99] B. Kim, Y. D. Park, K. Min, J. H. Lee, S. S. Hwang, S. M. Hong, *et al.*, "Electric Actuation of Nanostructured Thermoplastic Elastomer Gels with Ultralarge Electrostriction Coeffi cients," *Adv. Funct. Mater,* vol. 21, pp. 1-8, 2011.

[100] J. G. Drobny, "Testing of Electrial Properties of Polymers," in *Polymers for Electricity and Electronics : Materials, Properties, and Applications.*, ed: Johns Wiley & Sons, Inc., 2012.

[101] R. Shankar, T. K. Ghosh, and R. J. Spontak, "Electromechanical Response of Nanostructured Polymer Systems with no Mechanical Pre-Strain," *Macromol. Rapid Commun.,* vol. 28, pp. 1142–1147, 2007.

[102] O. Van den Berg, W. G. F. Sengers, W. F. Jager, S. J. Picken, and M. Wubbenhorst, "Dielectric and Fluorescent Probes To Investigate Glass Transition, Melt,and Crystallization in Polyolefins," *Macromolecules*, vol. 37, pp. 2460-2470, 2003.

[103] R. Palakodeti and M. R. Kessler, "Influence of frequency and prestrain on the mechanical efficiency of dielectric electroactive polymer actuators," *Materials Letters,* vol. 60, pp. 3437–3440, 2006.

[104] M. Molberg, Y. Leterrier, C. J. G. Plummer, C. Walder, C. Löwe, D. M. Opris, *et al.*, "Frequency dependent dielectric and mechanical behavior of elastomers for actuator applications," *JOURNAL OF APPLIED PHYSICS* vol. 106, 2009.

[105] C. Putson, L. Lebrun, D. Guyomar, N. Muensit, P.-J. Cottinet, L. Seveyrat, *et al.*, "Effects of copper filler sizes on the dielectric properties and the energy harvesting capability of nonpercolated polyurethane composites," *Journal of Applied Physics* vol. 109, 2011.

[106] J. Nunes-Pereira, V. Sencadas, V. Correia, J. G. Rochad, and S. Lanceros-Méndez, "Energy harvesting performance of piezoelectric electrospun polymer fibers and polymer/ceramic composites," *Sensors and Actuators A: Physical*, vol. 196, pp. 55– 62, 2013.

[107] P. A. Brochu, "Dielectric Elastomers for Actuation and Energy Harvesting," Doctor of Philosophy, Materials Science and Engineering, University of California,, Los Angeles, 2012.

[108] H. Stoyanov, "Soft nanocomposites with enhanced electromechanical response for dielectric elastomer actuators," Doctor of Natural Sciences Doctoral Thesis, Faculty of Mathematics and Natural Sciences, University of Potsdam, Patsdam, 2011.

[109] S. Zulfiqar, Z. Ahmad, M. Ishaq, S. Saeed, and M. I. Sarwar, "Thermal and mechanical properties of SEBS-g-MA based inorganic composite materials," *Journal of Material Science* vol. 42, pp. 93-100, 2007.

[110] A. Pustak, M. Denac, M. Leskovac, I. Švab, V. Musil, and I. Šmit, "Morphology and Mechanical Properties of iPP/Silica Composites Modified with (Styrene-b-ethylene-co-butylene-b-styrene) Grafted with Maleic Anhydride," *Polymer-Plastics Technology and Engineering*, vol. 54, pp. 647-660, 2015.

[111] Z. Ghallabi, M. Arous, A. Kallel, I. Royaud, G. Boiteux, and G. Seytre, "Giant Permittivity in three-phase PVDF Composites," presented at the International Conference on Solid Dielectrics, Potsdam, Germany, 2010.

[112] M. Kollosche, H. Stoyanov, S. Laflamme, and G. Kofod, "Strongly enhanced sensitivity in elastic capacitive strain sensors," *J. Mater. Chem.*, vol. 21, pp. 8292-8294, 2010.

[113] C. M. Koo, *Electroactive Thermoplastic Dielectric Elastomers as a New Generation Polymer Actuators*: INTECH Open Access Publisher, 2012.

[114] L. He and S. C. Tjong, "Low percolation threshold of graphene/polymer composites prepared by solvothermal reduction of graphene oxide in the polymer solution," *Nanoscale research letters*, vol. 8, p. 1, 2013.

[115] Z. Wang, J. K. Nelson, J. Miao, R. J. Linhardt, L. S. Schadler, H. Hillborg, *et al.*, "Effect of high aspect ratio filler on dielectric properties of polymer composites: a study on barium titanate fibers and graphene platelets," *Dielectrics and Electrical Insulation, IEEE Transactions on*, vol. 19, pp. 960-967, 2012.

[116] M. H. Kim, S. M. Hong, and C. M. Koo, "Electric actuation properties of SEBS/CB and SEBS/SWCNT nanocomposite films with different conductive fillers," *Macromolecular Research,* vol. 20, pp. 59-65, 2012.

[117] W. Li, A. Dichiara, and J. Bai, "Carbon nanotube–graphene nanoplatelet hybrids as high-performance multifunctional reinforcements in epoxy composites," *Composites Science and Technology,* vol. 74, pp. 221-227, 2013.

[118] Y. J. Kim, T. S. Shin, H. Do Choi, J. H. Kwon, Y.-C. Chung, and H. G. Yoon, "Electrical conductivity of chemically modified multiwalled carbon nanotube/epoxy composites," *Carbon,* vol. 43, pp. 23-30, 2005.

[119] M. El Achaby and A. Qaiss, "Processing and properties of polyethylene reinforced by graphene nanosheets and carbon nanotubes," *Materials & Design,* vol. 44, pp. 81-89, 2013.

[120] E.-C. Cho, J.-H. Huang, C.-P. Li, C.-W. Chang-Jian, K.-C. Lee, Y.-S. Hsiao, *et al.*, "Graphene-based thermoplastic composites and their application for LED thermal management," *Carbon,* vol. 102, pp. 66-73, 2016.

[121] F. d. C. Fim, N. R. Basso, A. P. Graebin, D. S. Azambuja, and G. B. Galland, "Thermal, electrical, and mechanical properties of polyethylene–graphene nanocomposites obtained by in situ polymerization," *Journal of Applied Polymer Science,* vol. 128, pp. 2630-2637, 2013.

[122] Z. Spitalsky, D. Tasis, K. Papagelis, and C. Galiotis, "Carbon nanotube–polymer composites: chemistry, processing, mechanical and electrical properties," *Progress in polymer science,* vol. 35, pp. 357-401, 2010.

[123] C. J. Rauwendaal, "Screw extruder with independently adjustable groove depth," ed: Google Patents, 1999.

[124] H. Kim, K. Kim, S. Lee, J. Joo, H. Yoon, S. Cho, *et al.*, "Charge transport properties of composites of multiwalled carbon nanotube with metal catalyst and polymer: application to electromagnetic interference shielding," *Current Applied Physics,* vol. 4, pp. 577-580, 2004.

[125] P. Pötschke, A. R. Bhattacharyya, and A. Janke, "Carbon nanotube-filled polycarbonate composites produced by melt mixing and their use in blends with polyethylene," *Carbon,* vol. 42, pp. 965-969, 2004.

[126] S. Kazarian, "Polymer processing with supercritical fluids," *POLYMER SCIENCE SERIES CC/C OF VYSOKOMOLEKULIARNYE SOEDINENIIA,* vol. 42, pp. 78-101, 2000.

[127] M. Sauceau, J. Fages, A. Common, C. Nikitine, and E. Rodier, "New challenges in polymer foaming: A review of extrusion processes assisted by supercritical carbon dioxide," *Progress in Polymer Science,* vol. 36, pp. 749-766, 6// 2011.

[128] O. S. Fleming and S. G. Kazarian, "Polymer Processing with Supercritical Fluids," in *Supercritical Carbon Dioxide*, ed: Wiley-VCH Verlag GmbH & Co. KGaA, 2006, pp. 205-238.

[129] J. W. Tom and P. G. Debenedetti, "Particle formation with supercritical fluids—a review," *Journal of Aerosol Science,* vol. 22, pp. 555-584, // 1991.

[130] S. P. Nalawade, F. Picchioni, and L. P. B. M. Janssen, "Supercritical carbon dioxide as a green solvent for processing polymer melts: Processing aspects and applications," *Progress in Polymer Science,* vol. 31, pp. 19-43, 1// 2006.

[131] G. K. Serhatkulu, C. Dilek, and E. Gulari, "Supercritical CO2 intercalation of layered silicates," *Journal of Supercritical Fluids,* vol. 39, pp. 264-270, Dec 2006.

[132] F. Cansell, C. Aymonier, and A. Loppinet-Serani, "Review on materials science and supercritical fluids," *Current Opinion in Solid State and Materials Science,* vol. 7, pp. 331-340, 8// 2003.

[133] J. R. Combes, S. Kumar, L. S. Smith, H. K. Mahabadi, and P. G. Odell, "Supercritical fluid processes," ed: Google Patents, 2000.

[134] A. I. Cooper, "Polymer synthesis and processing using supercritical carbon dioxide," *Journal of Materials Chemistry,* vol. 10, pp. 207-234, 2000.

[135] V. Goodship and E. Ogur, *Polymer Processing with Supercritical Fluids*. Shrewsbury, GBR: Smithers Rapra, 2004.

[136] S. R. Marre, Y.; Aymonier, C, "Supercritical microfluidics: Opportunities in flow-through chemistry and materials science,". *J. Supercrit. Fluids,* 2011.

[137] S. G. Kazarian, M. F. Vincent, F. V. Bright, C. L. Liotta, and C. A. Eckert, "Specific Intermolecular Interaction of Carbon Dioxide with Polymers," *Journal of the American Chemical Society,* vol. 118, pp. 1729-1736, 1996/01/01 1996.

[138] S. P. Nalawade, F. Picchioni, J. H. Marsman, and L. Janssen, "The FT-IR studies of the interactions of CO 2 and polymers having different chain groups," *The Journal of supercritical fluids,* vol. 36, pp. 236-244, 2006.

[139] E. Kiran, "Supercritical fluids and polymers–The year in review–2014," *The Journal of Supercritical Fluids,* vol. 110, pp. 126-153, 2016.

[140] S. Costeux, "CO2-blown nanocellular foams," *Journal of Applied Polymer Science,* vol. 131, 2014.

[141] Y. Haldorai, J.-J. Shim, and K. T. Lim, "Synthesis of polymer–inorganic filler nanocomposites in supercritical CO 2," *The Journal of Supercritical Fluids,* vol. 71, pp. 45-63, 2012.

[142] F. Yang, M. Manitiu, R. Kriegel, and R. M. Kannan, "Structure, permeability, and rheology of supercritical CO 2 dispersed polystyrene-clay nanocomposites," *Polymer,* vol. 55, pp. 3915-3924, 2014.

[143] A. Y. Shalyapina, A. Y. Solov'eva, M. Zaporozhets, E. Khokhlov, V. Plotnichenko, S. Savilov, *et al.*, "Zinc oxide nanoparticles immobilized on graphene flake," *Russian Journal of Inorganic Chemistry*, vol. 58, pp. 354-360, 2013.

[144] N. Farhangi, Y. Medina-Gonzalez, R. R. Chowdhury, and P. A. Charpentier, "Growing TiO2 nanowires on the surface of graphene sheets in supercritical CO2: characterization and photoefficiency," *Nanotechnology*, vol. 23, p. 294005, 2012.

[145] Y. Haldorai, B.-K. Kim, Y.-L. Jo, and J.-J. Shim, "Ag@ graphene oxide nanocomposite as an efficient visible-light plasmonic photocatalyst for the degradation of organic pollutants: A facile green synthetic approach," *Materials Chemistry and Physics*, vol. 143, pp. 1452-1461, 2014.

[146] J. Zhao, H. Yu, Z. Liu, M. Ji, L. Zhang, and G. Sun, "Supercritical deposition route of preparing Pt/graphene composites and their catalytic performance toward methanol electrooxidation," *The Journal of Physical Chemistry C*, vol. 118, pp. 1182-1190, 2014.

[147] S. Xu, H. Yang, K. Wang, B. Wang, and Q. Xu, "Effect of supercritical CO 2 on fabrication of free-standing hierarchical graphene oxide/carbon nanofiber/polypyrrole film and its electrochemical property," *Physical Chemistry Chemical Physics*, vol. 16, pp. 7350-7357, 2014.

[148] M.-T. Lee, C.-Y. Fan, Y.-C. Wang, H.-Y. Li, J.-K. Chang, and C.-M. Tseng, "Improved supercapacitor performance of MnO 2–graphene composites constructed using a supercritical fluid and wrapped with an ionic liquid," *Journal of Materials Chemistry A*, vol. 1, pp. 3395-3405, 2013.

[149] Y. Xiang, S. Lu, and S. P. Jiang, "Layer-by-layer self-assembly in the development of electrochemical energy conversion and storage devices from fuel cells to supercapacitors," *Chemical Society Reviews*, vol. 41, pp. 7291-7321, 2012.

[150] L. Chen, X. Wang, X. Zhang, and H. Zhang, "3D porous and redox-active prussian blue-in-graphene aerogels for highly efficient electrochemical detection of H 2 O 2," *Journal of Materials Chemistry*, vol. 22, pp. 22090-22096, 2012.

[151] C.-H. Wu, C.-H. Wang, M.-T. Lee, and J.-K. Chang, "Unique Pd/graphene nanocomposites constructed using supercritical fluid for superior electrochemical sensing performance," *Journal of Materials Chemistry*, vol. 22, pp. 21466-21471, 2012.

[152] X. Dong, X. Wang, L. Wang, H. Song, H. Zhang, W. Huang, *et al.*, "3D graphene foam as a monolithic and macroporous carbon electrode for electrochemical sensing," *ACS applied materials & interfaces*, vol. 4, pp. 3129-3133, 2012.

[153] G. Yang, J. Su, J. Gao, X. Hu, C. Geng, and Q. Fu, "Fabrication of well-controlled porous foams of graphene oxide modified poly (propylene-carbonate) using

supercritical carbon dioxide and its potential tissue engineering applications," *The Journal of Supercritical Fluids,* vol. 73, pp. 1-9, 2013.

[154] V. Eswaraiah, V. Sankaranarayanan, and S. Ramaprabhu, "Functionalized graphene–PVDF foam composites for EMI shielding," *Macromolecular Materials and Engineering,* vol. 296, pp. 894-898, 2011.

[155] H. Huang, P. Chen, X. Zhang, Y. Lu, and W. Zhan, "Edge-to-edge assembled graphene oxide aerogels with outstanding mechanical performance and superhigh chemical activity," *Small,* vol. 9, pp. 1397-1404, 2013.

[156] J. Zhao, L. Zhang, T. Chen, H. Yu, L. Zhang, H. Xue, *et al.*, "Supercritical carbon-dioxide-assisted deposition of Pt nanoparticles on graphene sheets and their application as an electrocatalyst for direct methanol fuel cells," *The Journal of Physical Chemistry C,* vol. 116, pp. 21374-21381, 2012.

[157] B.-K. Kim, Y.-L. Jo, and J.-J. Shim, "Preparation and antibacterial activity of silver nanoparticles-decorated graphene composites," *The Journal of Supercritical Fluids,* vol. 72, pp. 28-35, 2012.

[158] S. Padmajan Sasikala, P. Poulin, and C. Aymonier, "Prospects of Supercritical Fluids in Realizing Graphene-Based Functional Materials," *Advanced Materials,* 2016.

[159] P. Maiti, P. H. Nam, M. Okamoto, N. Hasegawa, and A. Usuki, "Influence of crystallization on intercalation, morphology, and mechanical properties of polypropylene/clay nanocomposites," *Macromolecules,* vol. 35, pp. 2042-2049, 2002.

[160] H. M. Tiggemann, V. F. Ribeiro, F. Celso, and S. M. Nachtigall, "Effect of commercial clays on the properties of SEBS/PP/oil thermoplastic elastomers. Part 1. Physical, mechanical and thermal properties," *Applied Clay Science,* vol. 109, pp. 151-156, 2015.

[161] J. Z. Kovacs, B. S. Velagala, K. Schulte, and W. Bauhofer, "Two percolation thresholds in carbon nanotube epoxy composites," *Composites Science and Technology,* vol. 67, pp. 922-928, 2007.

[162] P. Russo, M. Lavorgna, F. Piscitelli, D. Acierno, and L. Di Maio, "Thermoplastic polyurethane films reinforced with carbon nanotubes: The effect of processing on the structure and mechanical properties," *European Polymer Journal,* vol. 49, pp. 379-388, 2013.

[163] U. Tayfun, Y. Kanbur, U. Abaci, H. Y. Guney, and E. Bayramli, "Mechanical, Flow and Electrical Properties of Thermoplastic Polyurethane/Fullerene Composites: Effect of Surface Modification of Fullerene," *Composites Part B: Engineering,* 2015.

[164] H. Tang, X. Chen, and Y. Luo, "Studies on the PTC/NTC effect of carbon black filled low density polyethylene composites," *European polymer journal,* vol. 33, pp. 1383-1386, 1997.

[165] I. A. Estrada Moreno, A. Díaz Diaz, M. E. Mendoza Duarte, and R. Ibarra Gómez, "Strain effect on the electrical conductivity of CB/SEBS and GP/SEBS composites," in *Macromolecular symposia*, 2009, pp. 361-368.

[166] J. E. Kennedy and C. L. Higginbotham, *Synthesis and characterisation of styrene butadiene styrene based grafted copolymers for use in potential biomedical applications*: INTECH Open Access Publisher, 2011.

[167] Y. V. Kolen'ko, K. A. Kovnir, I. S. Neira, T. Taniguchi, T. Ishigaki, T. Watanabe, *et al.*, "A novel, controlled, and high-yield solvothermal drying route to nanosized barium titanate powders," *The Journal of Physical Chemistry C,* vol. 111, pp. 7306-7318, 2007.

[168] M. d. C. B. López, G. Fourlaris, B. Rand, and F. L. Riley, "Characterization of barium titanate powders: barium carbonate identification," *Journal of the American Ceramic Society,* vol. 82, pp. 1777-1786, 1999.

[169] A. J. Moulson and J. M. Herbert, *Electroceramics: materials, properties, applications*: John Wiley & Sons, 2003.

[170] E. A. Cherney, "Silicone rubber dielectrics modified by inorganic fillers for outdoor high voltage insulation applications," *Dielectrics and Electrical Insulation, IEEE Transactions on,* vol. 12, pp. 1108-1115, 2005.

[171] H. Zhao, Y. J. Xia, Z. M. Dang, J. W. Zha, and G. H. Hu, "Composition dependence of dielectric properties, elastic modulus, and electroactivity in (carbon black-BaTiO3)/silicone rubber nanocomposites," *Journal of Applied Polymer Science,* vol. 127, pp. 4440-4445, 2013.

[172] J. G. Speight and J. Speight, *Handbook of petroleum product analysis* vol. 233: Wiley-Interscience New Jersey, 2002.

[173] O. A. Al-Hartomy, F. Al-Solamy, A. Al-Ghamdi, N. Dishovsky, M. Ivanov, M. Mihaylov, *et al.*, "Influence of carbon black structure and specific surface area on the mechanical and dielectric properties of filled rubber composites," *International Journal of Polymer Science,* vol. 2011, pp. 1-8, 2011.

[174] M. B. Heaney, "Measurement and interpretation of nonuniversal critical exponents in disordered conductor–insulator composites," *Physical Review B,* vol. 52, p. 12477, 1995.

[175] D. J. Hourston, M. Song, A. Hammiche, H. M. Pollock, and M. Reading, "Modulated differential scanning calorimetry: 6. Thermal characterization of multicomponent polymers and interfaces," *Polymer,* vol. 38, pp. 1-7, 1// 1997.

[176] E. J. Donth, *Relaxation and Thermodynamics in Polymers: Glass Transition*: Wiley, 1993.

[177] Y. Zhang, M. Zuo, Y. Song, X. Yan, and Q. Zheng, "Dynamic rheology and dielectric relaxation of poly (vinylidene fluoride)/poly (methyl methacrylate) blends," *Composites Science and Technology,* vol. 106, pp. 39-46, 2015.

[178] M. Jomaa, L. Seveyrat, L. Lebrun, K. Masenelli-Varlot, and J. Cavaille, "Dielectric properties of segmented polyurethanes for electromechanical applications," *Polymer,* vol. 63, pp. 214-221, 2015.

[179] A. North and J. Reid, "Dielectric relaxation in a series of heterophase polyether polyurethanes," *European Polymer Journal,* vol. 8, pp. 1129-1138, 1972.

[180] E. Tedeschi, M. Carraro, M. Molinas, and P. Mattavelli, "Effect of control strategies and power take-off efficiency on the power capture from sea waves," *IEEE Transactions on Energy Conversion,* vol. 26, pp. 1088-1098, 2011.

[181] P. Izquierdo and C. G. Soares, "Analysis of sea waves and wind from X-band radar," *Ocean Engineering,* vol. 32, pp. 1404-1419, 2005.

[182] R. Khazaka, M. Locatelli, S. Diaham, P. Bidan, L. Dupuy, and G. Grosset, "Broadband dielectric spectroscopy of BPDA/ODA polyimide films," *Journal of Physics D: Applied Physics,* vol. 46, p. 065501, 2013.

[183] R. H. Boyd, "Relaxation processes in crystalline polymers: molecular interpretation—a review," *Polymer,* vol. 26, pp. 1123-1133, 1985.

[184] K. Sau, T. Chaki, and D. Khastgir, "Conductive rubber composites from different blends of ethylene-propylene-diene rubber and nitrile rubber," *Journal of materials science,* vol. 32, pp. 5717-5724, 1997.

[185] M. E. Achour, C. Brosseau, and F. Carmona, "Dielectric relaxation in carbon black-epoxy composite materials," *Journal of Applied Physics,* vol. 103, p. 094103, 2008.

[186] M. El Hasnaoui, A. Triki, M. E. Achour, and M. Arous, "Modelling of dielectric relaxation processes of epoxy-resin filled with carbon black particles," *Physica B: Condensed Matter,* vol. 433, pp. 62-66, 2014.

[187] M. El Hasnaoui, J. Belattar, M. Achour, L. Costa, and F. Lahjomri, "Electrical transport properties of CB/epoxy polymer composites," *Optoelectron Adv Mater-Rapid Commun,* vol. 6, pp. 610-613, 2012.

[188] V. L. Rao, T. Shekharam, T. M. Kumar, and M. Nagabhushanam, "Effect of copper on impedance and dielectric studies of Cu x Zn 1− x S mixed semiconductor compounds," *Materials Chemistry and Physics,* vol. 159, pp. 83-92, 2015.

[189] D. Roylance, "Stress-strain curves," *Massachusetts Institute of Technology study, Cambridge,* 2001.

[190] G. Tsagaropoulos and A. Eisenberg, "Dynamic mechanical study of the factors affecting the two glass transition behavior of filled polymers. Similarities and differences with random ionomers," *Macromolecules,* vol. 28, pp. 6067-6077, 1995.

[191] C. G. Robertson, C. Lin, M. Rackaitis, and C. Roland, "Influence of particle size and polymer− filler coupling on viscoelastic glass transition of particle-reinforced polymers," *Macromolecules,* vol. 41, pp. 2727-2731, 2008.

[192] C. R. Szczepanski, C. S. Pfeifer, and J. W. Stansbury, "A new approach to network heterogeneity: polymerization induced phase separation in photo-initiated, free-radical methacrylic systems," *Polymer,* vol. 53, pp. 4694-4701, 2012.

[193] A. R. Payne, "The dynamic properties of carbon black-loaded natural rubber vulcanizates. Part I," *Journal of Applied Polymer Science,* vol. 6, pp. 57-63, 1962.

[194] D. Kohls and G. Beaucage, "Rational design of reinforced rubber," *Current opinion in solid state and materials science,* vol. 6, pp. 183-194, 2002.

[195] P. Cassagnau, "Payne effect and shear elasticity of silica-filled polymers in concentrated solutions and in molten state," *Polymer,* vol. 44, pp. 2455-2462, 4// 2003.

[196] K. Tananuwong and D. S. Reid, "Differential scanning calorimetry study of glass transition in frozen starch gels," *Journal of agricultural and food chemistry,* vol. 52, pp. 4308-4317, 2004.

[197] Z. Wang and T. J. Pinnavaia, "Nanolayer reinforcement of elastomeric polyurethane," *Chemistry of Materials,* vol. 10, pp. 3769-3771, 1998.

[198] P. S. Gill, S. R. Sauerbrunn, and M. Reading, "Modulated differential scanning calorimetry," *Journal of Thermal Analysis,* vol. 40, pp. 931-939, 1993/09/01 1993.

[199] G. W. I.R. Harrison, T.C. Hsu, "A Differential Scanning Calorimetry Study of Asphalt Binders," National Research Council, Washington, DC1992.

[200] K. J. Jones, I. Kinshott, M. Reading, A. A. Lacey, C. Nikolopoulos, and H. M. Pollock, "The origin and interpretation of the signals of MTDSC," *Thermochimica Acta,* vol. 304–305, pp. 187-199, 11/3/ 1997.

[201] P. Claudy, J. Letoffe, G. King, J. Planche, and B. Brule, "Characterization of paving asphalts by differential scanning calorimetry," *Fuel Science & Technology International,* vol. 9, pp. 71-92, 1991.

[202] P. Claudy, J. M. Letoffe, G. N. King, and J. P. Plancke, "Characterization of asphalts cements by thermomicroscopy and differential scanning calorimetry: Correlation to classic physical properties," *Fuel Science and Technology International,* vol. 10, pp. 735-765, 1992/01/01 1992.

[203] D. J. Hourston, F.-U. Schäfer, M. H. S. Gradwell, and M. Song, "TMXDI-based poly(ether urethane)/polystyrene interpenetrating polymer networks: 2. Tg

behaviour, mechanical properties and modulus-composition studies," *Polymer,* vol. 39, pp. 5609-5617, 11// 1998.

[204] D. Hourston, M. Song, A. Hammiche, H. Pollock, and M. Reading, "Modulated differential scanning calorimetry: 6. Thermal characterization of multicomponent polymers and interfaces," *Polymer,* vol. 38, pp. 1-7, 1997.

[205] J. Wen, "Heat Capacities of Polymers," in *Physical Properties of Polymers Handbook*, J. Mark, Ed., ed: Springer New York, 2007, pp. 145-154.

[206] E. Donth, "Characteristic length of glass transition: Impossibility of a sharp critical kinetic temperature T c > T g," *Physica Scripta,* vol. 1993, p. 223, 1993.

[207] I. M. Kalogeras and H. E. Hagg Lobland, "The nature of the glassy state: structure and glass transitions," *Journal of Materials Education,* vol. 34, p. 69, 2012.

[208] B. Wunderlich, I. Okazaki, K. Ishikiriyama, and A. Boller, "Melting by temperature-modulated calorimetry," *Thermochimica acta,* vol. 324, pp. 77-85, 1998.

[209] B. Wunderlich, "A classification of molecules, phases, and transitions as recognized by thermal analysis," *Thermochimica Acta,* vol. 340–341, pp. 37-52, 12/14/ 1999.

[210] B. Wunderlich, Y. Jin, and A. Boller, "Mathematical description of differential scanning calorimetry based on periodic temperature modulation," *Thermochimica Acta,* vol. 238, pp. 277-293, 6/15/ 1994.

[211] A. Boller, C. Schick, and B. Wunderlich, "Modulated differential scanning calorimetry in the glass transition region," *Thermochimica Acta,* vol. 266, pp. 97-111, 1995.

[212] B. H. Stuart, *Infrared Spectroscopy: Fundamentals and Applications*: Wiley, 2004.

[213] R. Liu, J. Farinha, and M. Winnik, "Preparation and spectroscopic properties of phenanthrene-labeled SEBS triblock copolymers," *Macromolecules,* vol. 32, pp. 3957-3963, 1999.

[214] S. Munteanu and C. Vasile, "Spectral and thermal characterization of styrene-butadiene copolymers with different architectures," *Journal of Optoelectronics and Advanced materials,* vol. 7, p. 3135, 2005.

[215] M. Pracella, M. M.-U. Haque, and V. Alvarez, "Functionalization, compatibilization and properties of polyolefin composites with natural fibers," *Polymers,* vol. 2, pp. 554-574, 2010.

[216] Y. Cao, Z. Lai, J. Feng, and P. Wu, "Graphene oxide sheets covalently functionalized with block copolymers via click chemistry as reinforcing fillers," *Journal of Materials Chemistry,* vol. 21, pp. 9271-9278, 2011.

[217] G. Matzeu, A. Pucci, S. Savi, M. Romanelli, and F. Di Francesco, "A temperature sensor based on a MWCNT/SEBS nanocomposite," *Sensors and Actuators A: Physical,* vol. 178, pp. 94-99, 5// 2012.

[218] X. Fan, Z. Wang, K. Wang, H. Deng, F. Chen, and Q. Fu, "Acid-modified carbon nanotubes distribution and mechanical enhancement in polystyrene/elastomer blends," *Polymer Engineering & Science,* vol. 52, pp. 964-971, 2012.

[219] Z.-F. Zhang, X.-F. Bai, J.-W. Zha, W.-K. Li, and Z.-M. Dang, "Preparation and dielectric properties of BaTiO3/epoxy nanocomposites for embedded capacitor application," *Composites Science and Technology,* vol. 97, pp. 100-105, 2014.

[220] A. Patsidis, K. Kalaitzidou, and G. Psarras, "Dielectric response, functionality and energy storage in epoxy nanocomposites: Barium titanate vs exfoliated graphite nanoplatelets," *Materials Chemistry and Physics,* vol. 135, pp. 798-805, 2012.

[221] T.-I. Yang and P. Kofinas, "Dielectric properties of polymer nanoparticle composites," *Polymer,* vol. 48, pp. 791-798, 2007.

[222] S. Cantournet, R. Desmorat, and J. Besson, "Mullins effect and cyclic stress softening of filled elastomers by internal sliding and friction thermodynamics model," *International Journal of Solids and Structures,* vol. 46, pp. 2255-2264, 2009.

[223] L. Mullins, "Effect of stretching on the properties of rubber," *Rubber Chemistry and Technology,* vol. 21, pp. 281-300, 1948.

[224] H. Karanth, V. S. Shenoy, and R. R. Murthy, "Industrially feasible alternative approaches in the manufacture of solid dispersions: a technical report," *AAPS PharmSciTech,* vol. 7, pp. E31-E38, 2006.

[225] M. D. Elkovitch and D. L. Tomasko, "Effect of supercritical carbon dioxide on morphology development during polymer blending," *Polymer Engineering & Science,* vol. 40, pp. 1850-1861, 2000.

[226] D. Klempner, *Advances in interpenetrating polymer networks* vol. 4: CRC Press, 1994.

[227] S. Thomas and G. Zaikov, *Recent advances in polymer nanocomposites*: CRC Press, 2009.

[228] H. Jeske, A. Schirp, and F. Cornelius, "Development of a thermogravimetric analysis (TGA) method for quantitative analysis of wood flour and polypropylene in wood plastic composites (WPC)," *Thermochimica Acta,* vol. 543, pp. 165-171, 2012.

[229] M. Avram and G. D. Mateescu, *Infrared spectroscopy: applications in organic chemistry*: Krieger Pub Co, 1978.

[230] A.-Y. León-Bermúdez and R. Salazar, "Synthesis and characterization of the polystyrene-asphaltene graft copolymer by FT-IR spectroscopy," *CT&F-Ciencia, Tecnología y Futuro,* vol. 3, pp. 157-167, 2008.

[231] N. A. Nikonorova, A. L. Didenko, V. V. Kudryavtsev, and R. A. Castro, "Dielectric relaxation in segmented copolyurethane imides," *Journal of Non-Crystalline Solids,* vol. 447, pp. 117-122, 2016.

[232] P. Myerscough, *Nuclear Power Generation: Incorporating Modern Power System Practice*: Elsevier, 2013.

[233] K. Lozano and E. Barrera, "Nanofiber-reinforced thermoplastic composites. I. Thermoanalytical and mechanical analyses," *Journal of Applied Polymer Science,* vol. 79, pp. 125-133, 2001.

[234] X.-L. Xie, Y.-W. Mai, and X.-P. Zhou, "Dispersion and alignment of carbon nanotubes in polymer matrix: a review," *Materials Science and Engineering: R: Reports,* vol. 49, pp. 89-112, 2005.

[235] Q. Zhang, Y. Wang, and Q. Fu, "Shear-induced change of exfoliation and orientation in polypropylene/montmorillonite nanocomposites," *Journal of Polymer Science Part B: Polymer Physics,* vol. 41, pp. 1-10, 2003.

[236] S. Jain, J. G. Goossens, G. W. Peters, M. van Duin, and P. J. Lemstra, "Strong decrease in viscosity of nanoparticle-filled polymer melts through selective adsorption," *Soft Matter,* vol. 4, pp. 1848-1854, 2008.

[237] K. Abazine, H. Anakiou, M. El Hasnaoui, M. Graça, M. Fonseca, L. Costa, *et al.*, "Electrical conductivity of multiwalled carbon nanotubes/polyester polymer nanocomposites," *Journal of Composite Materials,* p. 0021998315618249, 2015.

[238] G. Chen, W. Weng, D. Wu, C. Wu, J. Lu, P. Wang, *et al.*, "Preparation and characterization of graphite nanosheets from ultrasonic powdering technique," *Carbon,* vol. 42, pp. 753-759, 2004.

[239] P.-C. Ma, M.-Y. Liu, H. Zhang, S.-Q. Wang, R. Wang, K. Wang, *et al.*, "Enhanced electrical conductivity of nanocomposites containing hybrid fillers of carbon nanotubes and carbon black," *ACS applied materials & interfaces,* vol. 1, pp. 1090-1096, 2009.

[240] G. Psarras, E. Manolakaki, and G. Tsangaris, "Electrical relaxations in polymeric particulate composites of epoxy resin and metal particles," *Composites Part A: Applied Science and Manufacturing,* vol. 33, pp. 375-384, 2002.

[241] S. O. Carson and J. M. Maia, "EXTENSIONAL MIXING ELEMENTS FOR TWIN-SCREW EXTRUSION: EFFECTIVENESS AT DISPERSIVE MIXING OPERATIONS IN COMPOSITES," presented at the SPE ANTEC™ Indianapolis, 2016.

[242] G. Wu, J. Lin, Q. Zheng, and M. Zhang, "Correlation between percolation behavior of electricity and viscoelasticity for graphite filled high density polyethylene," *Polymer,* vol. 47, pp. 2442-2447, 2006.

[243] A. Alegría, O. Mitxelena, and J. Colmenero, "On the molecular motions originating from the dielectric γ-relaxation of bisphenol-A polycarbonate," *Macromolecules,* vol. 39, pp. 2691-2699, 2006.

[244] M. D. Elkovitch, D. L. Tomasko, and L. J. Lee, "Supercritical carbon dioxide assisted blending of polystyrene and poly (methyl methyacrylate)," *Polymer Engineering & Science,* vol. 39, pp. 2075-2084, 1999.

[245] D. R. Dreyer, S. Park, C. W. Bielawski, and R. S. Ruoff, "The chemistry of graphene oxide," *Chemical Society Reviews,* vol. 39, pp. 228-240, 2010.

[246] G. Li, P. Lee-Sullivan, and R. Thring, "Determination of activation energy for glass transition of an epoxy adhesive using dynamic mechanical analysis," *Journal of thermal analysis and calorimetry,* vol. 60, pp. 377-390, 2000.

[247] Y. Sun, Z. Zhang, K. S. Moon, and C. Wong, "Glass transition and relaxation behavior of epoxy nanocomposites," *Journal of Polymer Science Part B: Polymer Physics,* vol. 42, pp. 3849-3858, 2004.

[248] J. Fidelus, E. Wiesel, F. Gojny, K. Schulte, and H. Wagner, "Thermo-mechanical properties of randomly oriented carbon/epoxy nanocomposites," *Composites Part A: Applied Science and Manufacturing,* vol. 36, pp. 1555-1561, 2005.

[249] P. Xiao, M. Xiao, and K. Gong, "Preparation of exfoliated graphite/polystyrene composite by polymerization-filling technique," *Polymer,* vol. 42, pp. 4813-4816, 2001.

[250] J. Thomason and L. Yang, "Temperature dependence of the interfacial shear strength in glass–fibre epoxy composites," *Composites Science and Technology,* vol. 96, pp. 7-12, 2014.

[251] C. Zhang, C.-A. Ma, P. Wang, and M. Sumita, "Temperature dependence of electrical resistivity for carbon black filled ultra-high molecular weight polyethylene composites prepared by hot compaction," *Carbon,* vol. 43, pp. 2544-2553, 2005.

[252] I. M. Kalogeras, "Contributions of dielectric analysis in the study of nanoscale properties and phenomena in polymers," *Polymer Nanocomposite Recent Advances, Nova Science,* 2008.

[253] R. Houwink, "Slipping of molecules during the deformation of reinforced rubber," *Rubber Chemistry and Technology,* vol. 29, pp. 888-893, 1956.

[254] R. Soltani and A. Katbab, "The role of interfacial compatibilizer in controlling the electrical conductivity and piezoresistive behavior of the nanocomposites based on RTV silicone rubber/graphite nanosheets," *Sensors and Actuators A: Physical,* vol. 163, pp. 213-219, 2010.